Cranfield Institute of Technology.
School of Mechanical Engineering.

Ph.D. Thesis

1993

K.J.YOUNG

"SOOT FORMATION IN TURBULENT, VAPORISED KEROSINE / AIR JET FLAMES AT ELEVATED PRESSURE."

Supervisor: Prof.J.B.MOSS

February 1993

This thesis is submitted for the degree of Doctor of Philosophy.

To Jane.

ABSTRACT

The objective of this thesis is to develop and validate a model of soot formation which is capable of being applied to a computational fluid dynamic (CFD) simulation of gas turbine combustion. The work follows previous research by Moss and Co-workers (Moss et al.1987, Syed 1990, Stewart et al.1991)

The concept of the study is to generate a detailed set of experimental data in turbulent flames of kerosine in which the complicating factors of gas turbine combustion - that is 3D geometry and droplet combustion - are removed. This allows more confidence in the computational simulation of the flames and therefore more insight into the soot formation process.

There are two components to the work: the experimental and theoretical studies. The first involves the compilation of an experimental dataset of key variables in ethylene and vaporised kerosine jet flames at elevated pressure, the second with the simulation of two of the experimentally studied flames using CFD methods.

The main achievement of the study is the generation of a formidable and detailed experimental database for flames at a variety of pressures and conditions. The unexpected finding is the extremely large conversion of carbon to soot found in the flames even at low pressure. This results in high radiant heat losses and measurement difficulties.

From the data, it is possible to assess the pressure dependence of soot growth in kerosine flames. Although, at the higher pressures, high soot levels created uncertainties in the measurements, in absolute terms growth rate is shown to be independent of pressure up to 6atm pressure. Above this it increases significantly.

The soot model of Moss et al.1988 - originally developed in laminar ethylene flames - was shown to give excellent agreement in turbulent situations. However, owing to the large radiant heat loss and soot levels, its application to the kerosine flames was more problematic since the assumptions that soot is a perturbation to the gaseous field and that temperature may be accurately described by a single perturbed flamelet were no longer valid. Further models to deal with such situations are proposed and tested.

Aside from the obvious relevance of this study to the field of gas turbine combustion, the large radiant heat loss and high soot levels observed in the flames studied here imply a further significance for the study of fire hazards. That a laboratory scale flame may be made to behave in a similar manner to a much larger pool fire flame is a very useful finding.

ACKNOWLEDGEMENTS

I am extremely grateful to my supervisor, Prof.J.B.Moss, for sharing with me his vast experience and knowledge. His patience and support throughout the period of this study are greatly appreciated.

Many thanks are also due to my other research colleagues in Cranfield. In particular Cecil Stewart, Khawar Syed and Nigel Tait for their lighthearted but invaluable assistance over the past three years.

In addition, I am indebted to the sponsors of this research - the Science and Engineering Research Council, the Defense Research Agency and Rolls Royce plc. - for their support and interest.

Finally, I would like to thank my family for their continued encouragement and support (and personal computer, Dad!). Most of all my wife, Jane, for keeping me on the straight and narrow and for understanding.

NOMENCLATURE

C	Cunningham drag coefficient
C	general constant
C_α, C_β, C_γ, C_δ	constants in the soot formation model
C_{g1}, C_{g2}	constants in the source term of mixture fraction fluctuation
$C_{\epsilon 1}$, $C_{\epsilon 2}$	constants in the source term of eddy dissipation rate
C_μ, C_v, C_d	constants in the turbulence model
C_1, C_2	Plank's first and second constants
D	diameter
e	electronic charge
f_v	soot volume fraction
F_c	fraction of carbon in the solid phase
g	gravitational constant
h	specific enthalpy
I	intensity of radiation
I_o	unattenuated light intensity
k	turbulent kinetic energy
K_a	absorption coefficient (cf. Q_{abs})
K_s	stimulated emission coefficient
L	length
m	complex refractive index ($= \eta - i\kappa$)
m	soot mass density ($=\rho_{soot} f_v$)
n	particle number density
N	Normalised number density ($=n/N_o$)
N_o	Avogadros number (6.023×10^{23})
p	pressure
P	Probability density function
Pr	Prandtl number
Q_{abs}	absorption extinction efficiency
Q_{ext}	total extinction efficiency
Q_{sca}	scattering extinction efficiency
Q	heat flux
R	gas constant
R_o	universal gas constant
Re	Reynolds number
s	position along laser path
Sc	Schmidt number
t	time
T	temperature
u	velocity
w	reaction rate
W	molecular mass

x	position
Y	species mass fraction
Z	conserved scalar
Z_p	electrical mobility of particle p

Greek Symbols

α, β	exponents in the beta function
α, δ	nucleation terms in the soot formation model
β	coagulation term in the soot formation model
γ	surface growth term in the soot formation model
ϵ	emissivity
ϵ	eddy dissipation rate
ϵ	constant in soot oxidation model
ϵ_g	equivalent grey body emissivity
η	probability density function of number
η	real component of complex refractive index
θ	angle
κ	imaginary component of complex refractive index
λ	wavelength of radiation
μ	dynamic viscosity
ν	kinematic viscosity
ξ	mixture fraction
ρ	density
ρ_s	density of soot
σ_ϕ	Prandtl/Schmidt number of ϕ
τ	turbidity
ϕ	general variable
ϕ_m	soot mass fraction (=m/ρ)
ϕ_n	soot number density per unit mass of gas (=N/ρ)
Ω	solid angle

Subscripts

a, abs	absorption
b	black body
ext	extinction
λ	spectral property
mass	fraction by mass
rad	radiation

s	soot
sca	scattering
T	turbulent
th	thermocouple
v, vol	fraction by volume

Superscripts

$\bar{}$	Reynolds (time) average
'	Reynolds (time) fluctuation
$\tilde{}$	Favre (density weighted) average
"	Favre (density weighted) fluctuation

Abbreviations

DMPS	Differential Mobility Particle Sizer
DWEE	Distribution Weighted Extinction Efficiency
PDF	Probability Density Function
RTE	Radiative Transfer Equation

CONTENTS

FIGURE LIST

CHAPTER 1 INTRODUCTION

Solid carbon or soot generated during the process of combustion of hydrocarbon fuels is of great concern to the combustion engineer for a number of reasons. Firstly, soot plays a very important role in the process of radiative exchange of thermal energy to the surrounding environment. Although in most practical devices the concentration of soot is far lower than that of the main gaseous species such as H_2O or CO_2, unlike the gaseous species, it has the ability to emit radiation over a wide frequency range. This makes a large impact on the radiative properties of flames and hence, whether radiative exchange is desirable or not, the knowledge of soot levels is obviously of great use.

Secondly, with the exception of carbon black furnaces, the presence of smoke in the exhaust of all practical devices is undesirable since it is a recognised pollutant emission which is controlled and legislated against. Such factors are of particular concern to the sponsors of the present research, Rolls Royce plc., since strategies that are often adopted to reduce the level of other pollutant species - most notably the oxides of nitrogen, NO_x - in gas turbine engines tend to increase the level of smoke (Lefebvre 1983).

Finally, for the case of military engines for which pollutant emissions are not of primary concern, exhaust smoke is undesirable from the standpoint of stealth. A visible smoke plume in any application could compromise detectability greatly.

In all cases, the ability to predict the levels of smoke that would be formed in a combustor in its design phase would be a very powerful and economic tool. It is towards the development of such a capability that the present study is directed.

Although the understanding of soot formation has increased in recent years leading to a number of very detailed and useful review papers (eg. Glassman 1988, Kent and Wagner 1984, Calcote 1981), this still lags far behind that of the main thermochemistry of flames. This lack hinders the development of robust and generally applicable sub-models to be used in the computational fluid dynamic (CFD) simulation of flames.

This difficulty is further compounded by the timescales associated with soot chemistry. Due to its heterogeneous nature and the complicated chemical routes by which it is formed the chemistry of soot is slow compared with the main heat releasing reactions in flames and,

combustion modelling approaches that have been developed for and applied to practical combustor modelling rely on the assumption of fast chemistry. Such models are, therefore, not directly applicable to soot modelling and hence further strategies are necessary.

However, arguably one of the most important hindrances to the development of any model for the prediction of soot is the lack of suitable and sufficiently detailed experimental data for the purposes of model validation. Detailed soot measurements have been made in many different situations, but often the data is reported in the absence of any other vector or scalar information which would further aid the simulation (eg. Charalampopoulos and Felske 1989, Bard and Pagni 1981, Wood and Samuelson 1985).

Other studies which do contain such information (eg. Mitchell et al. 1980, Smyth et al. 1985, Nishida and Mukohara 1982) are for flames supported by a gaseous, pure fuels of simple molecular structure at atmospheric pressure. Although of relevance and interest, such studies cannot be directly related to gas turbine combustion which, for an aero engine at full power, may be maintained at 40 bar pressure with the highly complex, blended fuel, kerosine.

Studies which have been conducted on kerosine fuel, with the notable exception of that of Stewart and Moss 1989, have tended to focus on either phenomenological aspects of sooting propensity (eg. Hurley 1982) or on more general issues such as fuel characterisation (eg. Blazowski 1979)

Stewart et al. 1991 report detailed flowfield measurements of soot volume fraction and other key variables in kerosine fuelled laminar Wolfhard Parker flat flames and propose a model suitable for CFD application based on that first proposed by Moss et al. 1988 which fits their observations. However, such simple, laminar flames are still a significant step away from practical, turbulent geometries. Further validation is vital.

It was therefore the principal aim of the present study to address this shortfall by the compilation of a further detailed experimental database but in a more realistic, turbulent flame environment. Such an experiment was devised and conducted and is reported herein.

In all experiments it is expedient to remove as many uncertainties as possible from the analysis in order to focus unambiguously on that which is of interest. For this reason complicating factors of gas turbine combustion such as complex three dimensional geometry and liquid spray combustion were removed by selecting the turbulent, round jet of pre-vaporised kerosine for study.

Such a geometry has a number of benefits from a modelling and experimental viewpoint. It has extremely good optical and probe access, it is very well documented for other fuels and also inert jets (eg. Liew 1983, Kent and Honnery 1987, Nishida and Mukohara 1982, Becker et al. 1967) and it has a symmetrical flowfield which is of the boundary layer or parabolic type which greatly reduces modelling effort.

In order to keep conditions closer to those within the gas turbine, a pressure vessel rig was built to contain the flames up to the site limit air supply pressure of 17.5bar. Of further concern, mindful of the experience of Stewart and Moss 1989, were the expected levels of soot formation and, as a result, thermal radiation loss from the flames. The pressure vessel was therefore designed with a reflective radiation shield to reflect radiation back to its source.

The second aim of the study was to implement the soot model of Moss and co-workers (Moss et al. 1988, Stewart et al. 1991, Syed 1990) to the turbulent jet flame cases in order to assess the further assumptions necessary and to make adjustments and assessments to the model based upon the findings. In particular, the effects of turbulence on the highly mixture fraction specific soot source terms were of interest since it is in this area that the model is least satisfactory.

Chapter 2 begins by reviewing the various combustion and turbulence modelling strategies that are available at the present time focusing principally on those used in the present study, namely the k-e, two equation model of turbulence and the laminar flamelet / conserved scalar model of diffusion flame combustion. The mechanisms of soot growth and radiation are then reviewed and their effects on the local flame chemistry discussed.

The relevant experimental methods which have been applied to combustion systems are then reviewed and the advantages and disadvantages of each assessed.

Chapter 3 describes in detail the experimental methods that were adopted to study the kerosine jet flames and also a pilot study of an ethylene jet flame. The configurations of each experiment is discussed and the application, implementation and error analysis of each adopted measurement technique reviewed.

In chapter 4 are reported the experimental results for both ethylene and kerosine jet flames at a variety of pressures. Comparisons between different flames are made and some important findings described.

Chapter 5 is devoted to the computational modelling of two of the flames. The chapter begins with a detailed description of the governing equations to the fluid flow and the models and model parameters used. It proceeds to describe their application to the experimental cases.

Chapter 6 concludes by summarising all the important findings of and points raised during the research and gives suggestions for future work.

CHAPTER 2:

SIMULATION AND MEASUREMENT OF TURBULENT REACTING FLOWS

This work involves aspects of both computational modelling and experimental measurement of turbulent jet flames of ethylene and vaporised kerosine. This chapter provides a review of the techniques that have been adopted in the study for this purpose. Modelling and experimentation are dealt with in the two main sections 2.1 and 2.2 respectively.

2.1 SIMULATION OF TURBULENT REACTING FLOWS

The conservation of mass and momentum for a low Mach number flow may be described for a fluid element by the Navier Stokes equations. If the flow is also reacting, provided thermal and mass diffusion are adequately described by the laws of Fourier and Fick respectively, the same principle may also be applied to enthalpy and species concentration in order to yield the energy and species conservation equations.

The resulting expressions take the form. (Libby and Williams, 1980).

Mass Continuity

$$\frac{\partial \rho}{\partial t} + \frac{\partial}{\partial x_k}(\rho u_k) = 0 \qquad (2.1)$$

Momentum Conservation

$$\frac{\partial}{\partial t}(\rho u_i) + \frac{\partial}{\partial x_k}(\rho u_k u_i) = - \frac{\partial p}{\partial x_k} + F_i + \frac{\partial}{\partial x_k}\tau_{ik} \qquad (2.2)$$

Energy Conservation (assuming unity Lewis number)

$$\frac{\partial}{\partial t}(\rho h) + \frac{\partial}{\partial x_k}(\rho u_k h) = \frac{\partial p}{\partial t} + \frac{\partial}{\partial x_k}\left[\frac{\mu}{\sigma}\frac{\partial h}{\partial x_k}\right] - Q_r \tag{2.3}$$

Conservation of Species, Y_i, (i = 1,2,....,N)

$$\frac{\partial}{\partial t}(\rho Y_i) + \frac{\partial}{\partial x_k}(\rho u_k Y_i) = \frac{\partial}{\partial x_k}\left(\frac{\mu}{S_c}\frac{\partial Y_i}{\partial x_k}\right) + \dot{w}_i \tag{2.4}$$

Where τ_{ik} is the viscous stress tensor:

$$\tau_{ij} = \mu\left(\frac{\partial u_i}{\partial x_j} + \frac{\partial u_j}{\partial x_i} - \frac{2}{3}\delta_{ij}\frac{\partial u_k}{\partial x_k}\right)$$

$$\delta_{ij} = \begin{cases} 1 : i = j \\ 0 : i \neq j \end{cases} \tag{2.5}$$

Two further state equations are necessary in order to link enthalpy, species fraction and density:

The equation of state assuming ideal gas behaviour,

$$\rho = \frac{p}{R_o T \sum_{i=1}^{N} \frac{Y_i}{W_i}} \tag{2.6}$$

and the calorific equation of state,

$$h_i = \int_{T_o}^{T} C_{p_i} dT + \Delta H_{f_i}$$

$$h = \sum_{i=1}^{N} Y_i h_i \tag{2.7}$$

Chemical reaction is embodied in the balance equations through the chemical source term,

w_i. It is generally accepted that this reaction rate takes the form of an Arhennius rate expression (Williams, 1985). For a one step reaction of species α and β with stoichiometric integers ν_α and ν_β, the reaction rate is expressed:

$$\dot{w}_i = \rho A T^m C_\alpha^{\nu_\alpha} C_\beta^{\nu_\beta} \exp(-T_a/T) \tag{2.8}$$

Where $C_{\alpha,\beta}$ are species mass fractions and A is a reaction specific pre-exponential factor.

The highly non-linear form of this equation coupled with the fact that reacting flows are characterised by time scales far shorter than those exhibited by the mixing process result in large localised variations in reaction rates. Such systems of equations are notoriously difficult to solve and termed "stiff".

It is possible to solve the exact set of equations directly using computational fluid dynamic methods (eg. Patankar 1980). However, for problems involving combustion in which, even for relatively simple hydrocarbon fuels, 30 species and 100 reactions may be involved, the solution becomes extremely time consuming and expensive. For example, Smooke et al. 1989, required 150 hours of supercomputer time to converge a direct numerical simulation (DNS) of a steady two dimensional laminar methane flame with a detailed reaction scheme.

The added dimension of time in a turbulent situations creates yet further demands and, at present, prevents the application of DNS to anything but the simplest of geometries.

Obviously, it makes sense to rationalise the detailed chemical kinetics in order to simplify the problem. Semi global reaction schemes have been developed for a variety of fuels (eg. Paczko et al. 1986, Leung et al. 1991) which ease the load considerably at the expense of 'stiffness'. However, even this extends the practical applicability of DNS techniques to only moderate to high Reynolds number flows.

At higher Reynolds numbers, such as those in any practical combustion device where length and time scales vary by orders of magnitude, DNS, at present, is beyond the capability of current computer technology and is likely to remain so for some time.

In view of this, alternative strategies have been adopted to simplify the problem further. Averaging the conservation equations over time has been used for this purpose with great success.

2.1.1 TIME AVERAGED EQUATIONS

In most engineering situations, it is only the mean value of any given property with perhaps some indication of the level of fluctuation with time that is of interest. In this sense, DNS techniques might be considered to supply far too much information. The instantaneous detail of all variables in time and space is simply not necessary for design purposes. It is this and the resulting simplifications to the solution procedure (providing certain assumptions are made) that has led to the success and development of time averaging techniques.

The property under consideration is decomposed into two components, its mean and its fluctuation about the mean. These are then substituted into the instantaneous conservation equation of that quantity which is time averaged. Ensemble averaging is necessary if the mean flow varies with time, but for the present application to statistically stationary jet flames, conventional time averaging is sufficient.

Two forms of time averaging are used most frequently, unweighted or Reynolds averaging and density weighted or Favre averaging (Tennekes and Lumley, 1972).

The Reynolds average of any property, ϕ, may be calculated:

$$\overline{\phi} = \frac{1}{t^*}\int_t^{t+t^*}\phi\,dt \qquad \lim\, t^* \to \infty \tag{2.9}$$

The fluctuating component, ϕ', with relation to the Reynolds mean is defined,

$$\phi = \overline{\phi} + \phi' \tag{2.10}$$

The Favre average may be calculated,

$$\tilde{\phi} = \frac{1}{t^*\,\overline{\rho}}\int_t^{t+t^*}\rho\phi\,dt = \frac{\overline{\rho\phi}}{\overline{\rho}} \qquad \lim\, t^* \to \infty \tag{2.11}$$

The fluctuating component, ϕ", with relation to the Favre mean is defined,

$$\phi = \tilde{\phi} + \phi'' \tag{2.12}$$

By definition,

$$\overline{\phi'} = \overline{\rho\phi''} = 0 \qquad (2.13)$$

Taking the example of the equation of conservation of momentum (eq.2.1) for a constant density fluid, the above procedure results in the Reynolds averaged form below:

$$\frac{\partial}{\partial x_k}\rho\,\overline{u_i}\,\overline{u_k} = \frac{\partial \overline{P}}{\partial x_k} + \overline{F_i} + \frac{\partial \overline{\tau_{ik}}}{\partial x_k} - \frac{\partial}{\partial x_k}\rho\,\overline{u_i' u_k'} \qquad (2.14)$$

This averaged equation is exact but contains cross correlations between the fluctuating quantities, u_i'. These cross correlations are termed Reynolds stresses and similar terms arise as a result of averaging any conservation equation - those from the scalar equations are termed turbulent scalar fluxes.

For situations in which the fluid has variable density such as in combustion or high Mach number flows, further correlations with the fluctuating component of density arise. In this case Favre averaging is more desirable since the inclusion of density in the mean form of the variable leads to a reduction in the number of correlation terms over conventional Reynolds averaging.

In all cases, since the mean equation can only provide mean property information, further equations are needed in order to close the system.

It is indeed possible to construct such equations for the new terms by multiplying the appropriate instantaneous equation by the fluctuating component and again averaging. The resulting equations, however, include yet higher order correlations and the problem remains. If repeated for the new terms, the process would yield even higher order correlations, ad infinitum. This is known as the closure problem and an implication of it is that some modelling assumption will always be necessary if the advantages of time averaging are to be exploited.

2.1.2 TURBULENCE MODELLING

For the application of computational fluid dynamics (CFD) to engineering problems, there is no tractable alternative to time averaging. However the closure problem remains. It is in

response to this impasse that turbulence models have been developed. Since, due to the nature of the equations, any model which revolves around averaging will inevitably require assumptions, they all are the result of intuition and empiricism to varying degrees.

Models are generally of two forms, first and second order closures. The order of the closure refers to the moment of the equations beyond which the modelling assumptions are made. It is perfectly feasible to consider third or even higher order closures but, at present, none exist. A feature of the equation set is the proliferation of Reynolds stress terms as the order of the closure increases. Since the same number of conservation equations would also be required, higher order closures soon become impractical.

The simplest and most widely used turbulence models are the first order closures. These all stem from the concept of turbulent viscosity first postulated by Boussinesq 1877. He considered that Newton's viscosity law may be equally applicable to turbulent flow and that the turbulent correlations may be represented as a product of turbulent viscosity, μ_T, and the gradient of mean velocity.

The Reynolds stresses may then be represented as follows

$$- \rho\overline{u_i' u_k'} = \mu_T\left\{\frac{\partial \overline{u_k}}{\partial x_i} + \frac{\partial \overline{u_i}}{\partial x_k} - \frac{2}{3}\delta_{ik}\frac{\partial \overline{u_k}}{\partial x_k}\right\} \qquad (2.15)$$

Further, assuming a linear relationship between Reynolds stresses and scalar fluxes, they may be written

$$- \rho\overline{u_i' \phi'} = \frac{\mu_T}{\sigma_T}\frac{\partial \overline{\phi}}{\partial x_k} \qquad (2.16)$$

Where ρ_T is the turbulent Prandtl / Schmidt number for the scalar under consideration.

The only remaining unknown in the equations is then the turbulent viscosity, μ_T which unlike its molecular counterpart is a function of the flowfield rather than a physical property of the fluid itself.

By analogy with molecular diffusion, Prandtl 1925 hypothesised that turbulent diffusion might

be similar in nature to molecular diffusion and was formed from a product of the density, a length scale, l_T, and a random velocity associated with the turbulence, v_T.

Such an approach proved very successful and a great deal of subsequent research concentrated on the application and development of these so called eddy viscosity models in order that velocity and length scales could be accurately prescribed. Launder and Spalding, 1972 provide an excellent review of the evolution of these models and beyond.

The most developed eddy viscosity models are the two equation models such as the k - ϵ model of Jones and Launder, 1972. Two further conservation equations are constructed for kinetic energy of turbulence, k, and its dissipation rate, ϵ. The turbulent velocity and length scale may be inferred from these in order to define turbulent viscosity.

$$\mu_T = \bar{\rho} C_\mu \frac{k^2}{\epsilon} \tag{2.17}$$

where C_μ is an empirical constant. The balance equations for these two equations and the values of the empirical constants used are given in chapter 5.

The principle advantages of the eddy diffusion based models are their simplicity and ease of implementation. They do, however, suffer an important drawback. Implicit in the original concept is the assumption that turbulence is isotropic in nature. This allows the prescription of a unique value of turbulent viscosity at any given point for all directions and aids model simplicity. However, no account is taken for situations in which the turbulence has a strong directional preference - for example highly swirling flows. In such situations the concept is inappropriate and a more sophisticated higher order turbulence model is necessary.

As described above, the proliferation of correlation terms makes it impractical to consider any higher than a second order closure but many of these exist eg. Chou 1945, Chen and Rodi 1975, Launder and Spalding 1972. The modelling assumptions are made one order more remote from the averaged momentum equations than for the eddy viscosity models, and conservation equations of the Reynolds stresses themselves are constructed.

The fixed relationship between the Reynolds stresses is now broken allowing more generality and a physically more accurate model. However, this is at the expense of model complexity. Due to the increased number of conservation equations necessary, (6 Reynolds stresses in recirculating flow, Launder and Spalding 1972) these techniques are more complex and

require much greater computer resources.

Launder et al. 1972 assessed the performance of the numerous available turbulence models to the simulation of the non reacting jet issuing into stagnant surroundings. They made a comparison of six different models - ranging from the simplest eddy viscosity models through to the most highly developed Reynolds stress closure - with experimental measurements. For this simple geometry, the k-ϵ model proved to be one of the most accurate.

Since this geometry is also studied here and the k-ϵ model has been further proven in reacting jet cases (eg. Liew 1983, Syed 1990) it has again been utilised throughout the present study where computer time was of the essence. For information on the exact form of the equations and constants used the reader is referred to chapter 5.

2.1.3 MEAN CHEMICAL SOURCE TERM CLOSURE

The last section briefly described the modelling assumptions necessary to estimate the Reynolds stresses and scalar fluxes in the averaged conservation equations. However, one remaining term must be calculated before the complete set of governing equations may be solved - the mean chemical source term, w_i.

Libby and Williams, 1980, illustrate the problems associated with evaluation of mean reaction rate very clearly. Taking the example of the simple, irreversible one step reaction, $M_1 + 2M_2 \rightarrow M_3$, they expand the mean reaction rate based on an Arhennius expression (cf. eq(2.7)). The expansion includes 9 individual terms with cross correlations between species concentration, reaction rate and density of up to third order. The number of similar correlations for a practical reaction scheme including close to one hundred reversible reactions would be enormous.

Some simplification is possible if the degree of fluctuation is small and the temperature is not large compared with the activation temperature (Borghi 1975). Alternatively the correlations may be ignored completely and mean reaction rate calculated purely on the basis of mean property information. However, such methods are only valid for extremely specific cases and cannot be generalised to all combustion systems. Clearly, an alternative strategy is required which enables the mean source term to be evaluated accurately and simply.

A method that has proved very valuable for this purpose arises from the concept of the conserved scalar. A consequence of assuming the diffusivity of all species to be the same -

the unity Lewis number assumption - is the resulting possibility of defining a single conserved scalar property which characterises the mixing field. Under this assumption, the balance equations of chemical elements, Schvab Zeldovich coupling functions (Bilger 1980) and, if the system is adiabatic, enthalpy have no source. For modelling purposes, a new conserved scalar, mixture fraction ξ, may then be defined which is normalised between 0 and 1 such that,

$$\xi = \frac{Z - Z_2}{Z_1 - Z_2} \tag{2.18}$$

where Z is any conserved scalar property and the subscripts 1 and 2 refer to the uniform composition in the two streams. By convention, 2 refers to the oxidant, 1 to the fuel.

The instantaneous balance equation for this new scalar also has no source and may be written (Bilger 1980).

$$\frac{\partial}{\partial t}(\rho\xi) + \frac{\partial}{\partial x_k}(\rho u_k \xi) = \frac{\partial}{\partial x_i}\left(\frac{\mu}{\sigma}\frac{\partial \xi}{\partial x_k}\right) \tag{2.19}$$

Favre averaging of this equation with the eddy viscosity closure of the turbulent scalar flux yields a closed equation which describes the mean mixture state of the flow. A further equation may be constructed for Favre mixture fraction variance - see chapter 5.

The further assumption that the combustion chemistry is infinitely fast results in a second very important simplification. For diffusion flames, under this condition, the local chemistry is not affected by the flowfield. The rate of diffusion of fresh fuel and oxidant is now the limiting step with the flame existing at the contour of stoichiometric mixture fraction, Bilger 1980. The value of any chemistry dependent scalar may then be algebraicly related to the instantaneous mixture state and hence mixture fraction.

$$\phi = \phi(\xi) \tag{2.20}$$

Provided that this state relationship is known for the scalar of interest, all information relating to the combustion chemistry may be gained directly from knowledge of mixture

fraction. Thus, since the balance equation of mixture fraction does not contain any chemical source term, the closure problem is completely circumvented. Except for the remaining link with density, the chemistry calculation is effectively removed from the flow calculation and may be performed a priori.

The remaining problem with the technique lies with the requirement of instantaneous information of mixture fraction in a combustion simulation in which this is not computed. Moments of all scalars may only be calculated from the state relationships if the probability density function (PDF) of the mixture fraction, $P(\xi)$, is known.

$$\tilde{\phi}(x) = \frac{1}{\bar{\rho}} \int_0^{\infty} \rho(\xi)\, \phi(\xi)\, P(\xi;x)\, d\xi = \int_0^{\infty} \phi(\xi)\, \tilde{P}(\xi;x)\, d\xi \qquad (2.21)$$

$$\phi''^2 = \int_0^{\infty} (\phi(\xi) - \tilde{\phi}(x))^2\, \tilde{P}(\xi;x)\, d\xi \qquad (2.22)$$

Where:

$P(\xi;x)$ is the probability of mixture fraction, ξ, at location x

$\tilde{P}(\xi;x) = \rho P(\xi;x)/\bar{\rho}$

Calculation of these moments requires knowledge of the form of the PDF which initially appears to be a very limiting condition. However the constraints imposed by assuming a standard form of the PDF - being prescribed by its first and second moments - is sufficient to limit the error even for the most arbitrary assumed PDF (Bilger 1980).

In view of this, the normalised beta function PDF is used in the present study for simplicity. A more detailed description of the present application of the laminar flamelet technique, including the definition of the beta function, is given in chapter 5.

Regarding the prescription of the scalar state relationships, eq.(2.20), many have been considered. The simplest is the Burke Schuman flame sheet approximation where a one step irreversible reaction is considered, Williams 1985. This obviously has limited validity to flames where reversible reactions are possible and many species exist. It also may be considered to be unnecessarily simplified. Since the unique state relationships are generated

outside the CFD calculation, chemistry of arbitrary complexity may be incorporated without greatly increasing computational expense.

The effects of fast, reversible chemistry including intermediate species are embodied in chemical equilibrium calculations. A computer program which is capable of performing such a calculation is that of Gordon and McBride 1971. Chemical equilibrium calculations are used by Priddin 1992 in 3D simulations of the gas turbine combustion chamber.

However, the legitimacy of the equilibrium assumption is also questionable. Each mixture state is considered in isolation of others and no diffusional processes which exist in the diffusion flame are embraced. Combustion simulations using equilibrium thus tend to greatly overestimate the concentration of reaction intermediates - such as CO and H_2 on the rich side of stoichiometric (Liew 1983) - since the smoothing effects of diffusion are not present.

Liew et al. 1981 addressed this issue by considering the turbulent flame to consist of a multitude of microscopic laminar flamelets which are stretched and distorted with the flowfield. The state relationships may then be taken from laminar flame simulation or alternatively measurement.

This approach has been adopted widely (Liew 1983, Peters 1984, Fairweather et al 1992) and has led to the development of computer programs which solve the full set of balance equations (eqs.(2.1-5)) for greatly simplified laminar flame simulations to generate the flamelet relationships - eg. the stagnation streamline of a counterflow burner, Warnatz 1981 or the diffusion of fuel and oxidant, initially apart, into one another, Liew 1983.

A further advantage of the laminar flamelet technique is that state relationships may be taken directly from measurements in laminar diffusion flames (Syed 1990, Sivanathu and Faeth 1990). This technique has been used again in the present study and avoids uncertainties in flamelet calculations if the exact chemical kinetics are uncertain.

This section has described the essential features of the laminar flamelet model of non premixed combustion and the reasons for its emergence. In many cases it has proved to be adequate for this purpose and has been successfully applied to turbulent flames (Liew 1983, Fairweather et al 1992, Young et al. 1991, Sivanathu and Faeth 1990). There are, however, three commonplace situations in combustion systems of practical interest when the model breaks down.

The first is for situations in which the enthalpy loss from the system by radiation or conduction is significant. In this case, the state relationship can no longer be approximated by a single function of mixture fraction. Instead, they will be a joint function of mixture fraction and the local level of heat loss, $T=T(\xi,h)$.

The second case is for situations where the chemistry of a particular scalar is slow with relation to the flowfield. Then, the fast chemistry assumption implicit in the laminar flamelet model is no longer valid and the formation of that scalar will be affected by the local turbulence structure and flowfield.

The final case is for situations where the reactants are, somehow, bound in some relatively unreactive phase - eg. fuel droplets or soot. In this situation, the model will indicate scalar properties appropriate to local mixture state whilst, in reality, although the reactants are indeed present, they may not take part in reaction.

Unfortunately, the kerosine jet flames in the present study are subject to each of these effects to varying degrees. They radiate strongly and they produce significant amounts of soot, which has slow chemistry. Part of the present work was concerned with the development of methods to overcome these difficulties (see chapter 5). They are reviewed in more detail in the subsequent sections.

2.1.4 RADIATION HEAT TRANSFER

Heat transfer by thermal radiation is an inevitable mechanism in any device in which combustion is present. It is caused by high temperature molecules or solid particles emitting electromagnetic radiation in random directions in order to lower themselves from an excited state to a less excited state.

The radiation by combustion gases is very different in nature than that by solid particles such as soot or fly ash which may also be present. Gaseous radiation, predominantly from species such as CO_2, H_2O and CO (Siegel and Howell 1981), results from transitions between specific molecular rotational and vibrational energy levels. For this reason, the resulting non-luminous radiation only occurs at very specific wavelength regions corresponding to these lines. Such radiation is highly dependent upon gas temperature and partial pressure. Solids, however, are capable of emitting radiation in a continuum across all wavelengths and hence, when present, contribute greatly to the total radiative exchange.

In order to incorporate radiative transfer into a combustion calculation the so called radiation transfer equation (RTE) must be solved (Siegel and Howell 1981). This describes the conservation of radiative energy on an elemental volume taken along the direction of a pencil of rays confined within an elementary solid angle for an elementary time.

The necessary idealising assumptions are that:

1) the absorbing/emitting medium is homogeneous and isotropic,
2) the state of polarization is neglected,
3) the medium is in local thermodynamic equilibrium.

Then the RTE may be expressed (Siegel and Howell 1981):

$$(\Omega \cdot \nabla) I_\lambda(r,\Omega) = (-K_{a_\lambda} + K_{s_\lambda}) I_\lambda(r,\Omega) + K_{a_\lambda} I_{b_\lambda}(r) + K_{s_\lambda} \int_{\omega = 4\pi} I_\lambda(r,\omega) P(\Omega,\omega) d\omega \qquad (2.23)$$

The three terms represent: 1) absorption and stimulated emission, 2) emission, 3) scattering, where r is the position, Ω and ω are solid angles, $K_{a\lambda}$ is the absorption coefficient, $K_{s\lambda}$, is the scattering coefficient, $I_{b\lambda}$ is the Planck black body function (eq.2.24) and P_λ is the scattering phase function

$$I_{b_\lambda} = \frac{c_1}{\pi \lambda^5 (e^{\left(\frac{c_2}{\lambda T}\right)} - 1)} = \frac{E_{b_\lambda}}{\pi} \qquad (2.24)$$

C_1 and C_2 - Planck's first and second constants .

Although exact solution of the integro-differential equation in this form is possible, it is extremely expensive in computer time given the necessity to consider all wavelengths and solid angles. Such a technique would be intractable for a combustion calculation.

Various simplifications are possible. These include Monte Carlo statistical approaches (Steward and Cannon 1971) and zonal methods (Hottel and Sarofim 1967). These techniques, although useful in calculating radiative transfer are still not directly suited to CFD application since they use different solution procedures which are not directly compatible.

It is for this reason that flux models have had increased popularity in recent years. One great problem with the RTE is its angular dependence. Flux models assume radiation to be constant for given intervals of solid angle. The RTE, cast in an Eulerian coordinate system, may then be solved for each direction using the same techniques as CFD (Viskanta and Menguc 1987). The number of fluxes chosen (typically 2 to 6) are dependent upon the complexity of the problem. Obviously, the higher the number of fluxes, the more realistic the model but at the expense of computational effort.

Many other simplifications are possible with some hybrid schemes also used. They are reviewed extensively by Viskanta and Menguc 1987.

2.1.4.1 DETERMINATION OF THE ABSORPTION COEFFICIENT

Given that the appropriate simplification to the RTE has been chosen, the second major difficulty in assessing the radiation from flames is the absorption coefficient, $K_{a\lambda}$. Especially in situations where gaseous radiation is important, $K_{a\lambda}$ is extremely wavelength specific corresponding to spectral lines.

The number of bands involved is huge and so simplification is necessary in engineering applications. Narrow band models are available which split the range over which radiation is important, 0 - 10,000cm^{-1} (deRis 1978) into many small intervals of 5 - 25cm^{-1}. Each band is then considered in turn for all gases present. As can be imagined, this is an extremely computationally expensive technique and has only been applied to a combustion calculation as a post process (Gore and Faeth 1988, Syed 1990).

Simplifications to the narrow band models are desirable. Edwards and Balakrishnan (1973) have developed the exponential wide band model which is based upon the fact that gaseous infra red radiation occurs as groups of spectral rotational lines centred around up to six vibrational levels. The rotational lines are then approximated by a Gaussian distribution about each vibrational level.

Grey gas assumptions are also widely used. Hottel and Sarofim 1967, supply charts of the equivalent or grey gas emissivity, ϵ_g for systems of H_2O and CO_2 at various compositions.

The usefulness of such techniques is however limited by the tabulated grey gas emissivity

$$\epsilon_g = \frac{\int_0^\infty K_{a_\lambda} E_{\lambda_b} d\lambda}{\int_0^\infty E_{\lambda_b} d\lambda} = \frac{\int_0^\infty K_{a_\lambda} E_{\lambda_b} d\lambda}{\sigma T^4} \qquad (2.25)$$

data.

Radiation by soot represents a simpler problem in that soot emits a continuum of radiation. Provided the soot is small compared to the wavelength of light - the Rayleigh limit (Kerker 1969) - scattering by soot is negligible in relation to absorption. In this case, it has been shown both theoretically and experimentally that the absorption coefficient is proportional to soot volume fraction and inversely proportional to wavelength (Lee and Tien 1981, Dalzell and Sarofim 1967).

$$K_{a_\lambda} = C\frac{f_v}{\lambda} \qquad (2.26)$$

The constant, C, is a function of the complex refractive index of soot, where:

$$C = \frac{36\pi\eta\kappa}{(\eta^2 + \kappa^2 + 2)^2 + 4\eta^2\kappa^2)} \qquad (2.27)$$

Where η and κ are the real and imaginary components of the complex refractive index of soot. A number of studies have been undertaken to measure the complex refractive index of soot (Lee and Tien 1981, Dalzell and Sarofim 1969, Mullins and Williams 1987). Although there is a certain amount of uncertainty in the measurement techniques leading to a range in the value of C between 4 and 14, Tien and Lee 1982 show that such a discrepancy will only lead to approximately 20% error in the radiative flux calculation after integration over the wavelength range 0.5 - 10μm.

A formula of the type shown in eq.(2.26) lends itself very well to mathematical manipulation. Its use in conjunction with the optically thin limit of radiation may be used in order to yield significant simplifications.

In this limit, the absorption and scattering terms of the RTE are negligible with relation to

emission (Siegel and Howell 1981). All radiation escapes from the flame and total radiated power from a volume is given by an integral of the RTE over volume, wavelength and solid angle.

$$\dot{Q}_R = \int_0^{\infty} \int_0^{4\pi} \int_{vol} K_{a_\lambda} I_{b_\lambda} \, dV \, d\Omega \, d\lambda \qquad (2.28)$$

Substituting the soot absorption coefficient, eq.(2.26), into this equation and integrating yields a very simple expression relating emitted power to soot volume fraction and temperature (Hall 1988).

$$\dot{Q}_R = C_{RAD} f_v T^5 \qquad (W/m^3) \qquad (2.28)$$

The derivation of this expression is given in appendix (A).

2.1.4.2 COMBUSTION / RADIATION MODELS

Radiation makes its presence felt in the equations of conservation through the source term Q_R in the energy equation (2.3). Therefore, provided Q_R may be calculated using any of the above radiation models, its incorporation into a computational fluid dynamic (CFD) calculation is relatively simple.

The difficulty arises due to the necessary assumption with the conserved scalar / laminar flamelet approach that all chemistry dependent scalars have a unique, state relationship with mixture fraction, eq.(2.20). When radiation is significant, this is clearly not true.

The method used by many authors to avoid this issue is to define radiation loss perturbed flamelets (Liew 1983, Fairweather et al. 1992, Young et al. 1991). The flamelet of temperature is perturbed to embody an average level of radiationloss on the basis of laminar flame measurement or simply by an arbitrary radiation factor. The density is correspondingly modified.

When used in a calculation this will inevitaby cause underprediction of temperature lower in the flame where the radiation is small and overprediction higher where radiative loss is high.

However, providing the radiative loss is not large, the subsequent error will be tolerable.

As radiation increases the discrepancy becomes less satisfactory. Errors increase and other strategies must be adopted. It is in this area that more research is required. Studies have been made in such situations, notably Kent and Honnery 1987 and Lin 1992. The main difficulty lies with the necessity of evaluating the two dimensional PDF of mixture fraction and enthalpy that appears if an adaptation of the laminar flamelet strategy is to be adopted. Discussion of this problem is deferred until chapter 5 where a new model is proposed and implemented.

2.1.5 SOOT MODELLING

It would seem logical, in a combustion simulation using the laminar flamelet model, to treat soot parameters in exactly the same manner as other scalars. Indeed, such a strategy is employed by a number of authors (Kent and Honnery 1987, Faeth et al. 1987) who define state relationships of soot with mixture fraction.

However, in general, this approach is wholly unsuitable to soot due to the fact that its chemistry is slow with relation to mixing timescales. Soot parameters are dual functions of mixture fraction and residence time. This sub-section describes some of the models that have been developed to predict soot and the way they are incorporated into a CFD simulation.

2.1.5.1 MODELS OF SOOT FORMATION AND DESTRUCTION

Although reviews on the processes of soot formation and destruction show some degree of unity (Calcote 1981, Haynes and Wagner 1981, Glassman 1988), the exact chemical routes via which soot is formed and destroyed are not well understood due to their complexity. In general terms, however, the formation and destruction of soot may be classified by five individual mechanisms.

Nucleation - An extremely complex phenomenon which may include as many as 69 different aromatic species and radicals (Calcote 1981). Parent fuel pyrolysis followed by cyclization (if the fuel is not aromatic) produces a benzene ring structure. Further growth of the ring structure eventually results in a small nucleus of soot being formed.

Surface Growth - Generally considered to be the most important mechanism for soot mass growth (Haynes and Wagner 1981, Glassman 1988). Species are absorbed onto the soot nucleus and then undergo chemical modification to form carbonaceous material. As a result

the soot particle grows in size

Coagulation - A purely physical mechanism whereby random collisions between two or more soot particles result in one particle of larger size being formed.

Oxidation - A heterogeneous reaction which takes place in parallel with all other mechanisms. Soot is oxidised by any of a variety of radicals and molecules (eg. OH, O, O_2) to form gaseous by products.

Agglomeration - Although this mechanism is very similar to coagulation in most respects, it is usually considered separately. At long residence times (> 30ms, Calcote 1981), the soot nuclei which are roughly spheroidal in shape, join together in highly complex chain like aggregates (Megaridis and Dobbins 1989).

Primarily due to lack of knowledge, but also because the mechanisms, even if known, would be too complicated to incorporate into a practical combustion calculation, many authors develop models of soot growth by empirical means. These have recently been reviewed by Mullins et al. 1987.

Of the models of soot mass growth, the most rudimentary consider it in terms of a simple one step mechanism (eg. Khan and Greeves 1974). Typically, these models may be of Arrhenius form with a pre exponential which is a function of local composition and pressure.

The model of Tesner et al. 1974 considers soot growth as a two step mechanism. The first step being the formation of pre-cursor species, the second being the nucleation of small soot particles. They found this model to show similar behavoir to their observations.

Both the above models, however, are likely to suffer from the fact that they are not dependent upon soot surface area. Soot surface growth and oxidation may be expected to be strongly dependent upon soot surface area since this limits the material exposed to the surroundings. Both the above models contain no such information and hence, in circumstances where soot size and number are different to those that the model is based upon, the models will be inaccurate.

Gilyatzedinov 1972 considered the growth of carbon black in hydrocarbons of various aromatic content which were injected into the hot exhaust of a fuel lean premixed methane

air flame. He proposed a two step mechanism which considered the growth of soot mass and number density via the mechanisms of nucleation, surface growth and coagulation which were dependent upon temperature, surface area and parent fuel fraction.

This approach is more realistic than the ones above since surface growth is proportional to surface area and both soot number and mass are considered. The assumption that particles are spherical and monodisperse allows diameter and hence surface area to be calculated directly. This model has been developed by Moss and co workers (cf. Moss et al. 1987, Syed 1990, Stewart et al. 1991) to be used in a CFD simulation and is used in the present study. A detailed description of the model and its application is given in chapter 5.

Models of soot oxidation are also reported. The main uncertainty is exactly which species is responsible for the oxidation. Widely used, one step mechanisms of oxidation by O_2 are reported by Nagle and Strickland-Constable 1962 and Lee et al. 1962. They respectively relate the oxidation of carbon and soot in terms of oxygen concentration, pressure and temperature. However, since soot is formed in fuel rich regions in the flame, in order to reach the O_2 it must pass through zones in which the concentration of other species such as OH is significant. Fennimore and Jones 1967 cite a one step mechanism of OH oxidation from shock tube studies.

The mechanism of Nagle and Strickland-Constable 1962 is used in the present study since Kent and Wagner 1982 and Megaridis and Dobbins 1989 found that it could describe the oxidation of soot well in laminar ethylene air flames.

2.2 MEASUREMENTS IN FLAMES

As with all experimental studies which are being performed for the purposes of validation and to further the understanding of a particular problem, the more information that can be gathered the better. The present study of soot formation in turbulent kerosine / air flames is no exception and an ideal data set might contain temporally and spatially resolved measuement of all gaseous species, velocity, temperature and soot parameters throughout the region of interest. All experimental uncertainties would then be removed and the analysis could continue with great confidence.

However, such a study is, at the present time, beyond the capability of current measurement techniques and likely to remain so for some time. In view of this, a more realistic goal was aimed for.

The present study was not one in which new measurement techniques were being tested. Rather the emphasis was on the collection of a valid and reliable data set (in turbulent jet flames of kerosine at pressure) against which detailed CFD predictions could be compared. For this reason, when choosing which measurement techniques to apply, it was not necessarily those that could yield the most information that were chosen. Instead, well established and proven techniques were favoured in the interests of reliability.

Three key variables were identified which would be the minimum necessary for comparison with and validation of theoretical prediction. They were:

Soot Parameters - since it is the development of a model for the prediction of soot towards which the present is aimed.

Temperature - since this is the minimum necessary to characterise the thermochemical field of the flame.

Mixture fraction - since this will describe the mixing field within the flame.

This section provides a review of the techniques that have been used to date to measure these parameters and outlines the reasons why the techniques chosen were used in the present study. When reviewing each technique, a number of factors influence the suitability and applicability of that technique. They are expense, accuracy, applicability, disturbance to the system, response time and portability. Each technique is assessed with these criteria.

2.2.1 SOOT MEASUREMENT

Due to its physical properties and solid state, soot lends itself extremely well to measurement by a variety of techniques including sampling electron microscopy (SEM), classical and dynamic light scattering, laser induced incandescence (LII), stained filter paper techniques and gravimetric analysis.

With the exception of gravimetric analysis, methods which have been developed to measure soot in the exhaust gases of engines are not directly suited to scientific research due to their qualitative nature. Lefebvre 1983 gives a review of such techniques.

The simplest technique from an engine testing standpoint is the Ringelman chart method, the blackness of the smoke plume is measured by the observer by comparison with a blackness chart which is scaled from 1 to 10. A slightly more sophisticated technique is the stained filter paper technique, where a standard volume of sample is withdrawn through a filter paper. The change in reflectance of the filter paper gives an indication of the level of soot. Both of these techniques, although very simple, repeatable and cheap are qualitative in nature. No relationship between the 'smoke number' and mass fraction of soot is given. This renders them unsuitable for a scientific analysis.

Gravimetric analysis (Nishida and Mukohara 1982) is essentially an adaptation to the stained filter paper technique and does allow quantitative measurement of soot mass fraction. The soot from a known volume of gas is collected on a filter whose mass is weighed before and after collection. It is a very simple and cheap procedure but suffers a number of drawbacks: probe aerodynamic disturbance; only mean measurement possible; relatively long processing time; information of soot size and number is lost.

The technique which has the potential of giving the most information regarding soot is that of SEM (Megaridis and Dobbins 1989, Dalzell et al. 1970). Samples of soot from the flame are collected on quartz slides or rods and then prepared for analysis with a sampling electron microscope. Extremely detailed images of the soot particles are produced which show soot to comprise aggregated clusters of spheroidal particles of up to 50nm in diameter.

Aside from the obvious expense and expertise necessary to conduct such an experiment, SEM suffers the major uncertainty of sample disturbance. The collection and preparation procedures will undoubtedly modify the sample in some manner which is extremely difficult to quantify.

From this viewpoint, unobtrusive optical techniques are very desirable. The optical nature of soot as an absorbing and scattering medium over the whole wavelength range make such measurements very tractable. Of the optical techniques, the most widely used are those which are based upon the classical or Mie theory of elastic plane light scattering by a sphere (Kerker 1969).

Unfortunately, for the classical theory to be valid, the assumption that the soot is spherical must be made. If not, the theoretical treatment of the results becomes extremely complex. Recent attempts to generalise the theory in order to encompass fractal cluster scattering by Bonczyk and Hall 1991 have been successful but at the expense of simplicity. An important conclusion of Bonczyk and Hall, however, is that, provided that the individual monomers of a soot agglomerate are in the Rayleigh / small particle regime (Kerker 1969), then the agglomerate will have the same absorption coefficient as the individual monomers that make up the agglomerate. From electron microscopy measurements (Megaridis and Dobbins 1989), this condition is generally met for visible wavelengths.

The second limitation of classical light scattering techniques is their dependence upon the complex refractive index of soot. Various techniques have been developed to measure this parameter including transmittance, reflectance and in situ measurement. Table 3.4 shows the discrepancy between the values reported by the most commonly cited authors. The scatter in the values is large.

The simplest of the classical light scattering techniques is the Rayleigh extinction technique. If the soot is assumed to be small in comparison to the wavelength of light, the Rayleigh limit, the extinction of light by scattering is negligible in comparison to absorption and may be related to the path integral of soot volume fraction along the light beam. Such techniques are extremely easy to implement and have been used widely in a variety of combustion studies (Moss et al. 1987, Kent and Honnery 1987, Faeth et al. 1985, Flower 1988). For these reasons this technique is used in the present study. A more detailed description of the technique is given in chapter 3.

The drawbacks of Rayleigh extinction are as follows: it suffers from potentially large errors if the scattering component is large (chapter 3); no information is available regarding particle size or number; in most situations the instantaneous soot volume fraction information is lost due to the signal processing that is necessary in order to retrieve local soot volume fraction from its line integral.

More sophisticated classical scattering methods are those which take into account the scattering component of light extinction. Although the methods proposed by each author for achieving this differ quite considerably (Kunugi and Jinno 1966, Bard and Pagni 1981, Kent and Wagner 1982, Wood and Samuelson 1985), each devised experiment relies on the measurement of scattered and/or transmitted light at least two angles or wavelengths. With the further assumption that the spherical particles are distributed in a known fashion -

monodisperse, lognormal etc. - soot volume fraction, number density and diameter may be estimated.

Since the majority of such techniques require knowledge of the absolute intensity of scattered light (Kent and Wagner 1982, Kunugi and Jinno 1966, Wood and Samuelson 1985), they are often not suited to situations where light may be re-absorbed or re-scattered on leaving the probing area.

An advantage of the method first proposed by Durbin 1950 and later adapted by Bard and Pagni 1981 is that it solely relies on the measurement of local turbidity of the flame at three wavelengths. Mean turbidity may be measured directly in flames using tomographic deconvolution techniques (Ramachandran and Lachschminarayanan 1971, Shepp and Logan 1974) without being affected by re-absorption / re-scattering. This makes this technique suited to the jet flame geometry studied here and hence a further adaptation of the technique to this 2D system was attempted - see chapter 3 and 4.

A relatively new method of light scattering analysis is that of dynamic light scattering (Charalampopoulos and Felske 1987, Nazih 1989). Rather than the absolute intensity of light it is the time autocorrelation of the light that is measured using a photomultiplier detector in homodyne mode. This correlation is related to the Brownian motion of the soot particles and thus is dependent upon particle size, Cunningham slip coefficient, absolute temperature and viscosity of the bath gas.

The advantages of the technique are that the experiment is a very simple one to set up, the analysis does not require knowledge of the complex refractive index of soot, the experiment is unobtrusive in nature and, since only the correlation is required, insensitive to reabsorption and scattering of the signal beam. The main drawback of the technique is the necessity of having temperature and viscosity information at the point of interest and the cost of the autocorrelator. Also, the diameter of the particles that is measured will be the Stokes diameter or the diameter of a sphere with the same drag coefficient.

The most recent development in soot measurement has arisen as a result of the studies of soot interference on high power laser techniques such as CARS (Black and Stewart 1989). If the flame is illuminated with a sheet of high energy pulsed light, the absorption of energy will cause instantaneous heating of the soot to extremely high temperatures (4000°C, Tait and Greenhalgh 1992a). Measurement of fluorescence from the resulting vaporised material or increased incandescence from the soot particles themselves may be used in order to infer soot

volume fraction.

Although the cost of the laser source and receiving optics limit the viability of such techniques at the present, the possibility of measuring 2 dimensional, instantaneous maps of soot volume fraction make them a very interesting future proposition.

2.2.2 TEMPERATURE MEASUREMENT

Temperature is a parameter of a system at thermodynamic equilibrium which specifies the broadness of the energy distribution possessed by that system (Hirchfelder et al. 1954). When a system is not in equilibrium, however, a number of different temperatures are possible. When the energy under consideration is kinetic energy of gas molecules, the temperature is termed translational temperature. Since real gas molecules also have one or more internal degrees of freedom - vibrational, rotational, electronic - other temperatures corresponding to each of these states may also be defined.

Although in most flames of practical interest equilibrium is achieved, in some situations - such as shock waves - it is possible that equilibrium between internal and translational degrees of freedom is not attained (Fristrom and Westernberg, 1965). In such situations, the experimentalist should be aware of the possible discrepancies.

The most widely used methods of measuring temperature in flames are the thermocouple and electrical resistance thermometer. These both measure translational temperature and take the form of mechanical probes.

Resistance thermometry relies on the changing resistance of a metal wire with temperature. Regarding the choice of wire material, Platinum is often used due to its high temperature stability, almost linear resistance / temperature relationship and inert nature (TC limited). In principle, the technique does not require calibration but in practice this is often performed (Gilbert and Lobdell, 1953).

Thermocouple measurement makes use of the thermoelectric properties of metals. If two dissimilar metal are connected at two junctions which are maintained at different temperatures, a potential is developed which is a reproducible, unique function of the temperature difference. A large number of thermocouple junctions are commercially available which are suited to various applications (TC limited). The most commonly used for flames studies are Platinum Rhodium junctions due to their high temperature capability

(Pt30%Rh/Pt6%Rh, max instantaneous temperature 1750°C) and their resistance to corrosion. Thermocouples of the Tungsten Rhenium class may withstand temperatures as much as 600°C higher but are only suited to reducing environments.

Due to the similarity of probes, both techniques have very similar advantages and disadvantages. They have all the advantages associated with electronic signal processing and they may be made very small (10μm) and robust. The main disadvantages are their finite time response due to thermal inertia, the possible catalytic effect they may have (especially important in premixed systems) and, especially for thermocouples, the possibility of radiation and conduction loss.

If instantaneous information is required, time constant effects may be partially removed using the method of Ballyantyne et al. 1976. Up to a point, time constant effects may be compensated for using electronic amplification which has a frequency response inverse to that of the probe.

The catalytic effect may be overcome by coating the wire with impervious silica (Fristrom and Westernberg 1965).

Various techniques of compensating for radiation loss are available for the thermocouple from radiation correction of a bare fine wire couple (chapter 3) to the suction pyrometer which effectively removes the problem by enhancing heat transfer rates. These techniques are reviewed by Andrews 1962. Unfortunately, if any other than the radiation correction technique is utilised, the size and hence time constant of the thermocouple also increases.

An advantage of the resistance thermometry technique is that it has the potential of avoiding the radiation loss problem by utilising the 'null point' (Fristrom and Westernberg 1965). The experimental procedure is, however, more complicated than for thermocouples and it is for this reason that thermocouples are used in the present study. Their application is described more thoroughly in chapter 3.

Measurement by emission, absorption and stimulated emission of electromagnetic radiation by gas or soot also provides a useful way of measuring temperature. Such techniques have advantages over probe techniques in that they are unobtrusive in nature and are capable of instantaneous internal temperature measurement.

The more traditional techniques are described in detail by Fristrom and Westernberg 1965.

These rely on the fact that, if internal energy states are in equilibrium with themselves, they will be distributed according to the Maxwell - Boltzmann law (Hirchfelder et al. 1954). The probability of a molecule being found in a particular energy state E_i will then be proportional to $\exp(-E_i/RT)$. The intensity of emission or absorption for a given transition between internal states is also proportional to this Boltzmann factor.

The simplest techniques involve measurements of brightness temperature in a flame - measured by comparison with a calibrated light source focused at the same location. Adjustment of the lamp temperature is made until the flame and lamp images merge. More complex methods involve the measurement of emission or absorption across a whole range of spectral lines.

The drawback of traditional optical techniques has always been that only line of sight measurements are possible. In geometries in which the properties are constant along a line of sight - eg. the Wolfhard Parker burner - this causes no problems, but in most practical flames the line of sight measurement is of little use.

Recently Hall and Bonczyk 1990 have developed the technique of absorption / emission tomography on axisymmetric flames to overcome this problem, but this is only successful in optically dense regions in the flame and requires considerable optical access. Sivanathu and Faeth 1990 have devised another method of overcoming this problem. They designed a mechanical probe which only allows a small path length of the flame to be analysed. Again, this is successful, but removes one of the principal benefits of optical measurements - their unobtrusive nature.

In recent years, laser based diagnostic techniques for the measurement of temperature have become increasingly popular. Those which are, in principle, capable of the measurement of temperature are spontaneous Raman spectroscopy, coherent anti-Stokes Raman spectroscopy (CARS), laser induced fluorescence (LIF) and degenerate four wave mixing (DWFM). These are reviewed by Eckbreth et al. 1979, Ewart 1990 and Greenhalgh 1990.

At the present time, undoubtedly the most successful of these techniques has been CARS. This technique has great advantages over other spectroscopic techniques in that, by focusing the laser beams, point measurements may be made. Also the measured signal takes the form of a coherent beam rather than diffuse radiation. The possible discrimination from background noise is huge.

As a result, the CARS technique has been applied to many practical situations including gas turbine combustors, reciprocating internal combustion engines and rocket plumes (Eckbreth 1990, Greenhalgh 1990). However, the technique suffers from complexity, cost and, in the presence of soot, from interference associated with emission from the C_2 radical liberated from the evaporation of soot by the high energy pulsed laser beams used (Black and Stewart 1989). This problem also casts doubt on the assumed non-intrusive nature of the technique.

2.2.3 SPECIES FRACTION MEASUREMENT

A common and very useful measurement in flames is that of species fraction. There are essentially two methods by which this may be achieved: probe or spectroscopic techniques.

Probing techniques are the more traditional and widely used of the two techniques due to simplicity and cost. They rely on the sampling of mixture from the location of interest by means of some kind of suction probe followed by gas analysis of the sample. A necessity of all probing techniques is that the chemistry of the sample should be effectively frozen once entering the sampling probe. Obviously this is impossible for unstable species and radicals such as CH, OH, O+ etc. but it is possible for stable species such as CH_4, H_20 etc. Methods which are commonly adopted for this purpose are rapid expansion and cooling (Fristrom and Westernberg 1965).

Rapid expansion techniques typically involve withdrawing the sample through a very fine orifice (10 - 100μm Fristrom and Westernberg 1965) into larger diameter tubing. Pressure drops of approximately a factor of 10 are desirable to prevent further collision of reactive molecules and hence reaction. The alternative method of cooling may be achieved using a water cooled probe. If the water content of the sample is of interest, however, care must be taken with this technique to prevent condensation. For this reason many authors specify wet and dry species concentrations respectively to indicate whether the water is present or not.

Once the sample is obtained it may be investigated by any of a number of instruments. The simplest of such devices are the ones which measure either a single species or type of species. The most commonly used devices of this type are described in detail by Chedaille and Braud 1972 and Langelle and Verdier 1973. They include the flame ionization detector (FID) which measures hydrocarbon fraction, paramagnetic analyzer for O_2 , the infra red analyzer for CO and CO_2, and the chemiluminescent analyzer for NO and NO_x.

A more sophisticated, but as a result, more expensive and cumbersome gas analysis technique is that of gas chromatography. Individual species may be separated using a column which contains an adsorbing medium which reconstitutes each species separately. The amount of each individual species is measured by a detector. Each species has a specific residence time in the system and so may be discriminated on this basis. Alternatively, if the system is used in conjunction with a mass spectrometer, the species may be identified on the basis of its cracking pattern. Very detailed combustion studies may be undertaken using this technique (eg. Nishida and Mukohara 1982).

Of course, the mass spectrometer may be used for gas analysis without the chromatograph (eg Smyth et al. 1985). The analysis of the species can be quite difficult however due to the superimposition of species of similar mass. An example of two such species are C_2H_4 and CO, both of which have masses which are extremely close to 28 kg/kg-mole. Another difficulty arises due to molecular cracking. In the ionisation chamber of the mass spectrometer, the high electron concentration around the filament causes a proportion of molecules to be cracked into smaller fragments. The fragments may be another molecule that is under scrutiny hence causing error. To reduce these problems Smyth et al. 1985 use a high precision mass spectrometer - to allow excellent molecular discrimination - and keep the ionising current to as low a value as possible - to reduce cracking.

Probing techniques suffer from a number of disadvantages: they are unable to temporally resolve turbulent fluctuations in species concentration; they periodically require calibration with gas of a known mixture; they suffer from probe aerodynamic disturbance effects to the flowfield.

Spectroscopic techniques potentially do not suffer from two of the above disabilities and so are very desirable. They have received much recent interest due to the emergence of high power laser light sources and charge coupled device (CCD) cameras. Hanson 1986 provides a detailed review of the various techniques available.

The techniques of spontaneous Raman spectroscopy, coherent antistokes Raman spectroscopy (CARS), laser induced fluorescence (LIF) and degenerate four wave mixing are all capable of measuring species fraction on an instantaneous basis whilst being unobtrusive in nature - providing the laser itself does not affect the flame chemistry. Calibration is, however, still necessary to take into account laser structure and camera sensitivity.

At the present time, a major drawback to such techniques is complexity and expense of the

necessary equipment. Also optical interference, most notably from soot, cause practical problems (Tait and Greenhalgh 1992). The limitations of such techniques are still under investigation and, as yet, comprehensive maps of species fraction of the same detail as the ones obtained by Mithchell et al. 1980, Nishida and Mukohara 1982 or Smyth et al. 1985 by probing techniques have not been reported.

2.2.4 MIXTURE FRACTION MEASUREMENT

Mixture fraction is a very difficult property to measure directly in a flame due to its somewhat contrived nature. As opposed to soot volume fraction or species fraction which physically exist in the flame, mixture fraction is more of a conceptual property derived for the benefit of mathematical modelling.

The definition of mixture fraction is the fraction by mass of material at any location that has originated from the fuel stream. Therefore, all techniques which are used to measure mixture fraction must measure the concentration of some tracer which is known to have originated from either the fuel or air streams.

The techniques which have been developed to measure mixture fraction in flames fall into two categories:

Techniques requiring no seeding - These techniques rely on the measurement of one or more conserved scalar properties which are already present in the reactants. Examples of such properties are elemental carbon fraction from hydrocarbon fuels or elemental nitrogen fraction from the air.

Unobtrusive measurement of individual elements is difficult since they are contained in a variety of molecules which behave, chemically and physically, very differently. A method could be conceived in which use is made of radioactive isotopes of a particular element (eg. Carbon 14). This would allow good discrimination but no such technique is known at present since the combustion laboratory is usually not designed to cope with radioactive materials.

An obtrusive measurement technique has been developed and utilised by Moss and co-workers (Moss et al. 1987, Syed 1990, Stewart et al. 1991). Samples of the local mixture are withdrawn through a quartz microprobe and fully reacted in the presence of excess pure oxygen. All carbon will then be converted to its oxide and the resulting $[CO_2]/[N_2]$ level is proportional to the local fuel / air ratio. This is measured using a mass spectrometer.

Since this technique is very similar to species fraction probe sampling techniques, they suffer from the same drawbacks. This technique is employed in the present study and is described in more detail in chapter 3.

Seeding techniques - The main problem with the techniques requiring no seeding is the fact that the naturally occurring conserved scalars in flames do not lend themselves very well to direct and unobtrusive measurement. The alternative strategy is to introduce a new conserved scalar property which is much simpler to measure.

One such method is to seed the fuel or air flow with refractive particles such as TiO_4 or alumina (cf. Becker et al. 1967, Ebrahimi and Kleine 1977). The resulting flow is illuminated with a light beam or sheet and the amount of scattered light - measured at an oblique angle - is proportional to the number of particles present and hence to local mixture fraction.

Such techniques are advantageous since they are instantaneous and unobtrusive providing the particle do not affect the flow. They do, however, suffer some disadvantages.

Firstly, any soot present will also elastically scatter light causing a false reading. This limits their usefulness to relatively clean flames. Secondly, they suffer from "shot" noise (Becker et al. 1967). The seed does not exist as a continuum but as discrete particles. The scattered signal, as a result, will be subject to high frequency noise. Shot noise is reduced with higher seeding densities or with the use of low pass filters. In practice a combination of these two techniques is used but the latter will limit the frequency response. Finally, the technique relies upon the assumption that the particles follow the bulk of the flow. Although this assumption is likely to be more appropriate in fully turbulent systems with small particles, differential diffusion must expected in laminar and transitional flows.

Another seeding technique, which has recently been used in cold flow applications (Tait and Greenhalgh 1990), is the laser induced fluorescence (LIF) technique. The flow is seeded with a fluorescent marker such as acetone and is then illuminated with an ultraviolet laser sheet from a high power excimer laser source. The resulting fluorescence is a function of seed concentration and is measured with a CCD camera. Instantaneous and averaged 2D images of seed concentration are possible. In a cold flow application, the seed concentration is a conserved scalar and hence proportional to mixture fraction.

Such techniques are very desirable since the problems of differential diffusion and shot noise

found in particle seeded flows are eliminated whilst the technique remains unobtrusive. Using the seeds of acetone or acetaldehyde (Tait and Greenhalgh 1992), however, they are unsuitable for measurement of mixture fraction in combusting flows since the seed is destroyed in high temperature regions. Rather, they will indicate unburnt parent fuel. Unless an inert seed - possibly NO - is used mixture fraction may not be measured using this technique.

CHAPTER 3: EXPERIMENTAL METHOD

3.1 INTRODUCTION

This chapter describes the experimental apparatus and measurement techniques adopted to study soot formation in its present study in turbulent jet diffusion flames.

Two individual experiments were conducted: the first was on an unstabilised, free jet flame of ethylene at atmospheric pressure, the second was on a variety of stabilised, confined jet flames of kerosine vapour at atmospheric and elevated pressure.

The emphasis of the present study was towards the kerosine flame experiment. This was due to the lack of detailed experimental data available for such flames in comparison to the much more widely studied gaseous fuelled flames (Kent and Honnery 1987, Nishida and Mukohara 1982, Flower, 1988). The ethylene flame investigations were undertaken as a pilot study.

Although both experiments were designed to be laboratory based, the kerosine experiment was significantly more difficult to operate. This was due to the added complexities of fuel vaporisation, flame stabilisation and pressure vessel operation. Since the measurement techniques themselves also had to be developed to suit the present studies, this was performed in the much simpler ethylene jet flame pilot study which could be set up very easily and inexpensively.

Sections 3.2 and 3.3 of this chapter are devoted to the description of the ethylene and kerosine jet flame experimental configurations.

Five measurement techniques were used on these flames. They were: temperature by radiation compensated bare fine wire thermocouple; mixture fraction by probe sampling and mass spectrometric analysis; soot volume fraction by Rayleigh extinction; soot volume fraction, number density and diameter by multicolour extinction and differential mobility particle sizer analysis.

These techniques and the expected errors on the measured values are described in sections

3.4 - 3.7.

All detail of the experimental results and the conditions of flame operation are deferred until the next chapter.

3.2 ETHYLENE JET FLAME

The choice of ethylene fuel for the pilot study was for two reasons: firstly the fuel was gaseous which enabled a very simple and cheap experiment to be adopted, secondly because ethylene has a very similar carbon to hydrogen ratio as kerosine.

The burner geometry of Kent and Honnery 1987 was chosen for the present study for comparison purposes - jet diameter 3.1mm.

The jet was mounted on a milling machine micro positioner by means of a retort stand clamp arrangement. This allowed positioning accuracy of 0.1mm.

Above the flame, but at a height which minimised aerodynamic disturbance, was an air extraction system.

The flowrate of ethylene was monitored with a ¼ inch Fisher Porter flowmeter with a stainless steel ball float.

3.3 KEROSINE JET FLAME AND PRESSURE VESSEL

From the stand point of modelling, the most simple jet flame geometry is that of a free jet of fuel issuing into stagnant oxidant surroundings with no barriers to prevent flame development.

However, at elevated pressure, this is a very difficult condition to achieve due to the size of the pressure vessel necessary. In this case, a more practical geometry is that of a fuel jet issuing into a coflow of oxidant, all confined within a tube. There are added modelling complexities to this flow, in particular due to the presence of the tube walls , but these are minor in comparison to the added practical complexities of the larger pressure vessel. For

this reason it was the confined jet geometry that was chosen for analysis in the present study of combustion at elevated pressure.

A pressure vessel was designed and constructed under the following constraints:

1 Maximum working pressure of 17.5 bar absolute - the maximum site limit.

2 All stations of interest in the flame must be readily accessible by probe or optically without dismantling the vessel - for flexible and simple operation.

3 Radiation losses from the flame must be kept to a minimum - soot loadings and time scales in jet flames are very different from those within the gas turbine combustor causing thermal radiation to be more significant.

3.3.1 THE PRESSURE VESSEL

A general layout of the resulting design with a more detailed sketch of the central measurement section is shown in fig(3.1). The design is based on two seamless tubes made from stainless steel with flanges welded at either end, in between which is bolted a central measurement section, again made of stainless steel but machined from a single solid block of metal. The base of the vessel was sealed with a disc of stainless steel bolted to the flange of the lower tube with appropriate holes for plumbing and electrical connections. The head of the vessel was sealed with a similar disc onto which was welded a bursting disc and pressurising valve assembly.

The decision to make the central measurement section from a solid block was necessitated by the high pressure design constraint and the size of the windows necessary to make a full optical traverse of the flame. Even with the measurement section at its present size, optical windows of only 75mm diameter were possible. This would have been much less if another design route, such as welding bosses to a pipe, had been taken.

The pressure vessel assembly was mounted on a painted mild steel frame.

3.3.2 FLAME TUBE

Of primary importance in the design was the method of containing the flame. A number of options were considered but the method chosen was to that of borosilicate glass (Pyrex) tube

(inside diameter 155mm) located within the stainless steel pressure vessel tubes. This has advantages over its metal competitors due to its transparent and colourless nature (allowing the flame to be viewed) ,high temperature stability and hydraulically smooth surfaces (providing an ideal wall boundary condition).

The remaining problem regarding the pyrex tube was how to gain probe and undisturbed laser access through the glass. The solution was to cut the tube into two sections and to separate them with a thin (10mm) circular stainless steel spacer of the same diameter. The spacer had 6mm slots milled into it of appropriate length to admit the probe and laser beams but was considered sufficiently small to prevent a large disturbance to the fluid flow.

A second tube of polished aluminium was incorporated which surrounded the glass tube. The concept was that this second tube would reflect thermal radiation back to its source, thus producing near adiabatic conditions.

During initial design of the vessel, the pyrex was assumed to be entirely transparent to thermal radiation. After the experimental rig was manufactured, however, it became apparent that pyrex is virtually opaque to radiation at wavelengths above 2.5μm and hence a great deal of the thermal radiation was absorbed rather than transmitted by the glass. The effects of this are examined in more detail in the next chapter.

A more efficient design could be envisaged where the reflective aluminium shield itself was used as the flame tube instead of the pyrex. Radiation would then be reflected back to its source directly. Some scheme would have to be incorporated to allow the flame to be viewed in order to establish stable operating conditions and to check that flame blowout had not occurred but this would be tenable. Unfortunately, at the stage the problem was uncovered, it was too late to redesign and the pyrex tube was kept. Hence, in this sense, the design was inefficient.

3.3.3 EVAPORATOR / BURNER ASSEMBLY

For safety reasons the kerosine was evaporated within the pressure vessel rather than externally. This was achieved by means of a heated brass bomb. Fig(3.2). The kerosine was injected through a cooled Delavan nozzle of diameter 0.5mm into an electrically heated brass chamber typically at 400 - 500°C. The inlet side of the assembly was water cooled to prevent kerosine from evaporating before being sprayed. The nozzle itself also required cooling due to a rubber 'O' ring seal. Once entering the chamber, the kerosine spray flash evaporated and

there was no sign throughout the measurement campaign of lacquering of the inside of the chamber (a phenomenon sometimes seen within the gas turbine combustor, Lefebvre 1983). The resulting kerosine vapour was expelled from the chamber through the burner which was connected directly to the bomb. From the burner it was injected into the coflowing air stream, for subsequent combustion, through a nozzle of diameter 1.5mm. All components were heated with Philips Scientific Thermocoax heating wire and insulated with Triton Kaowool secured with metal tape.

When initially heating the evaporator before a test, there was a danger that air could get into the chamber through the burner and react with residual fuel. It was for this reason that a purge was designed into the system. During the startup sequence, a small mass flow of ethylene was introduced into the chamber. This was burned through the nozzle and prevented any oxygen from entering the bomb stopping potentially explosive mixtures from being generated. Once full operating conditions were achieved it was turned off.

3.3.4 FLAME STABILITY

One of the difficulties, when creating any jet flame is the prevention of flame liftoff. A lifted flame can not only be unstable and prone to extinguishing completely but also has a very ill defined boundary condition for modelling purposes. This is especially true for flames of kerosine vapour which, from experience, are more prone to lift off. Liftoff may be prevented by creating a small but very hot pilot premixed flame at the base of the primary flame thus producing an artificial source of ignition.

A burner was designed which had a central primary fuel nozzle (diameter 1.5mm) with an annular slot for the second flame (inside diameter 2.5mm, outside diameter 3.0mm). This very small annular flame size (width 250 microns) was essential in order to cause the minimum of disturbance to the main flame and to prevent blowback of the highly flammable mixture of ethylene and oxygen used. However, due to this very small annular gap, the tolerances required in the burner manufacture were extremely fine. In order to prevent the inside and outside diameters of the annulus from being skew a complex and high precision burner design was necessary. This was possible but the resulting burner had an overall outside diameter of 17mm.

One unfortunate consequence of this large burner diameter was the bluff backward facing step created. Fig(3.3). The resulting surround air flow separation and recirculation zone caused instabilities in the already very delicate lower regions of the flames. This problem could be relieved in one of two ways: lowering the air velocity, thus weakening the

recirculation zone, or lowering the fuel velocity, thus strengthening the lower regions of the flame. In practice a compromise between both these approaches was adopted. The exit Reynold's number for all flames studied was greater than 9000 - see next chapter.

3.3.5 VERTICAL ACTUATION

A 50mm diameter stainless steel column was attached to the centre of the base of the pressure vessel. This was free to move vertically and was pressure sealed within a brass bush by means of two 'O' rings. Contained within the column were five pipelines. Two for evaporator cooling water (in and out), one for the kerosine supply, one for a burner purge and one for premixed ethylene and oxygen for the stabilising flame. The kerosine evaporator/burner assembly was bolted on the end of the column within the pressure vessel, on the other end (outside the vessel) was bolted an S.K.F. ball screw type linear actuator with D.C. electrical motor. This allowed vertical movement of the burner/evaporator within the vessel thus partly satisfying the design constraint 2 (section 3.3). The position of the burner with relation to the probes or laser could be measured by means of a meter rule. This allowed vertical position measurements to an accuracy of 1mm.

3.3.6 AIR FLOW STRAIGHTENING

Dehumidified air was delivered to the flame by means of four 15mm pipelines which were connected to a manifold at the base of the pressure vessel. On entering the vessel the air was passed around the central column, electrical connections and evaporator assembly before reaching the burner. This caused a significant perturbation to the flow such that, on reaching the burner the unmodified air velocity profile was far from uniform. A flow straightening system was developed to correct this problem, thus giving a more homogeneous inlet velocity profile.

Given the expense of building a large pressure vessel, there were quite severe size constraints for the flow straightener. It was attached to the burner in the form of a can whose original designed length was only 40mm. After several flow straightening experiments it was concluded that it would be impossible to straighten the flow in such a small distance. A flow straightener was designed, however which could perform its task within the distance of 80mm. This was at the expense of traverse distance, allowing only 260mm of the flame to be investigated compared with the actuator throw of 300mm.

A schematic diagram of the final air flow straightener design is shown in fig(3.3). The method of straightening was based on a wind tunnel design in Cranfield (Adkins 1990). Use

was made of perforated stainless steel baffle plates which enhanced the turbulence, followed by plenum or mixing chambers in which the momentum of the air was dispersed to create a more uniform velocity profile.

Four perforated plates were used. The first was bolted near the base of the vessel 25mm above the air inlet. The holes which were directly over the four air inlet pipes were blocked thus preventing the air jets from passing straight through. The next three baffles were attached inside the can separated by two 40mm chambers. The resulting air flow distribution, measured with a Pitot static probe, was found to be reasonably uniform except for the central section where the velocity was very low. This was due to the blockage caused by the large burner.

It was also found that some form of gasket was needed in between the metal can and pyrex tube to prevent air from leaking between the two. Due to the high temperatures that the pyrex would reach during a normal run, standard rubber seal technology was unsuitable. A number of alternatives were attempted including metal wire and PTFE tubing. The best results were gained when Scotch High Temperature Glass Fibre tape was used, wrapped around a sufficient number of times to create a seal.

3.3.7 MEASUREMENT ACCESS

As was mentioned earlier in section 3.3.2, in order for windows of suitable size to be incorporated into the design a central measurement section machined from a solid piece of stainless steel was necessary. Given the mechanical strength possible from such a component, it was now viable to create access for four windows and four probes even though only two of each were required for the measurements (laser in and out, mixture fraction probe and temperature probe).

3.3.7.1 Probe Access

Each probe port consisted of a 25mm diameter hole drilled radially into the measurement section at 90° to the other probe ports. Fig(3.4). Fitting into this hole was a removable probe guide. This had a flange at one end which could be bolted to the measurement section with a gasket seal. Through the centre of the probe guide was a circular hole through which the probe passed. The hole was made to be a loose running fit with the probe, allowing free movement but also ensuring that the probe was running radially into the flame tube. Pressure sealing was achieved with a small double 'O' ring assembly screwed into the flange end of the probe guide.

The sensor end of the probe protruded from one end of the probe guide, through one of the milled slots in the stainless steel spacer and into the flame tube. The actuation end of the probe was connected to a brass probe coupling. At the other end of the coupling was connected another S.K.F. ball screw type linear actuator with D.C. motor. The electrical signal from the thermocouple or the sample from the quartz probe could be extracted at the probe coupling for analysis.

Obviously ,due to the long, thin nature of the jet flame, radial position measurement needed to be far more accurate than the vertical position measurement. A meter rule was not suitable in this case. Instead use was made of R.S. Components high precision potentiometers.

The throw of the actuator was 200mm. Unfortunately, no linear potentiometers were found of this size. However circular potentiometers were available. A circular, pulley was made, the diameter of which was known to a very high degree of accuracy. This was connected to the circular potentiometer which, in turn, was bolted to the probe actuator. Radio wire was then wrapped around the pulley a number of times and firmly fixed between two stationary posts. Hence movement of the actuator caused rotation of the pulley and allowed such flames very accurate position measurement.

Subsequent calibration against vernier callipers showed position measurement was to within ± 0.1mm.

3.3.7.2 Optical Access

The requirement for laser extinction measurements is to have two diametrically opposed horizontal slit windows of sufficient length to traverse the whole flame. Given the stability problems with the flames, however, it was very desirable to have much better optical access in order to view the flame. Hence it was decided that circular porthole windows would be a much more satisfactory alternative.

Purpose built window flanges were designed in order to house three 100mm diameter fused silica windows polished to Schlieren quality. The pressure was sealed using Silicaset rubber giving a total accessible window area for viewing of 75mm.

The window flanges were bolted to the measurement section. After passing through the first window the laser beam entered the flame tube through a slot in the spacer. It left the flame tube in a similar manner.

Regarding laser beam actuation, difficulties in aligning the sending and receiving optics made it far simpler to move the flame in relation to the laser beam rather than vice versa. For this reason the whole pressure vessel was mounted on a movable base. Actuation was by a machined screw attached to a hand wheel. Measurements were made of the vessel position by means of an independent dial gauge of accuracy 0.025mm.

3.3.8 IGNITION

Ignition was achieved using a technique similar to that used in the spark ignition engine. A simple system of a large inductance and low voltage D.C. power supply were used to generate a spark. The live electrode was connected to an insulated igniter which was passed through one of the spare probe ports. The earth was connected to the pressure vessel. Using the same sealing assembly as the probes, the igniter could be pushed into the flame tube adjacent to the burner. After successful ignition it could be withdrawn to prevent disturbance to the flow.

3.3.9 FLOW METERING

In total there were eight flows entering the pressure vessel which required monitoring. These are tabulated below with method of metering. In all cases where a quantitative value of flowrate was necessary, standard rotameter calibrations were used.

TABLE (3.1)

Flow	Method Of Metering
Evaporator Cooling Water	Water wheel - no metering required. Only a flow sensor.
Co Flow air	Fisher Porter (FP) 3/4-27-G-5/81 Tube GNSVGT 59 Float.
Ethylene (pilot)	FP 1/16-20-G-5/81 tube with sapphire float
Oxygen (pilot)	FP 1/16-20-G-5/81 tube with sapphire float
Ethylene evaporator purge	FP 1/8-12-G-5/81 tube with stainless steel float
Probe cleaner ethylene	FP 1/8-12-G-5/81 tube with sapphire float
Probe cleaner oxygen	FP 1/8-08-G-5/81 tube with sapphire float

Flow	Method Of Metering
Kerosine fuel	FP 1/8-25-G-5/81 tube with stainless steel float.

Not mentioned previously in this section is the probe cleaner flame, this is described in section (3.4).

3.4 MIXTURE FRACTION MEASUREMENT

The method used to measure mean mixture fraction was the same as the one adopted previously by Moss et al. 1988 on their laminar flame studies. The theoretical basis of the method is described below:

Consider mixing of two streams both of which contain the two conserved components X and Y.

Fraction by mass of species X in neat fuel = χ_{Xfuel}
Fraction by mass of species X in air = χ_{Xair}
Fraction by mass of species Y in neat fuel = χ_{Yfuel}
Fraction by mass of species Y in air = χ_{Yair}
At a given mixture fraction, ξ, the ratio of $[X/Y]_{mass}$ is given by equation (3.1)

$$\left[\frac{X}{Y}\right]_{mass} = \frac{\xi \chi_{Xfuel} + (1-\xi)\chi_{Xair}}{\xi \chi_{Yfuel} + (1-\xi)\chi_{Yair}} \qquad (3.1)$$

and hence:

$$\xi = \frac{\chi_{Xair} - \chi_{Yair}\left[\frac{X}{Y}\right]_{mass}}{\left[\frac{X}{Y}\right]_{mass}(\chi_{Yfuel}-\chi_{Yair}) + (\chi_{Xair}-\chi_{Xfuel})} \qquad (3.2)$$

For the case of carbon based fuel jets issuing into air surroundings obvious choices of X and Y are Carbon and Nitrogen respectively. For this case χ_{Xair} and χ_{Yfuel} equal zero simplifying the analysis greatly.

$$\xi = \frac{1}{1+\frac{\chi_{Xfuel}}{\chi_{Yair}}\left[\frac{Y}{X}\right]_{mass}} \qquad (3.3)$$

It is important to note that for the above analysis to be valid, the concentration of Carbon, [X], refers to total Carbon in the mixture, not any particular species.

For an unmodified sample, this would involve measuring the concentration of all carbon bearing species and summing the amount of carbon contained in each. This is, obviously, a very difficult and time consuming process and so in practice, once the sample of mixture was collected it was mixed with pure oxygen and reacted to completion over a heated (500°C) catalyst of platinum. The only species now containing carbon was CO_2.

From knowledge of the molecular mass of species, it may be calculated that complete combustion of one unit of mass of carbon would create 44/12 units of mass of CO_2. This may be substituted into equation (3.3) to give the mixture fraction in terms of the measured N_2/CO_2 value.

$$\overline{\xi} = \frac{1}{1+\frac{44\chi_{Cfuel}}{12\chi_{N_2air}}\left[\frac{N_2}{CO_2}\right]_{mass}} \qquad (3.4)$$

The value of χ_{N2air} is known from standard atmospheric tests as 0.75471.

For ethylene, the value of χ_{Cfuel} is 0.85714, for the kerosine used in the present study, Avtur (Jet A) the value is 0.858.

3.4.1 GAS SAMPLING AND ANALYSIS

3.4.1.1 MARK I SYSTEM

This system of was used in the atmospheric free ethylene and confined kerosine jet studies. A schematic diagram of this is shown in fig(3.5). The sample under investigation was drawn from the flame through a quartz probe, diameter 2.5mm. The sample was then passed through a series of stainless steel 16 gauge hypodermic tubes to the metering valve and catalyst. Here, it was mixed with a second stream of pure oxygen and passed over the catalyst.

The catalyst was a wire wool coated with platinum. This was contained within a narrow piece of brass tubing which was electrically heated until the brass glowed cherry red. After reacting fully in the presence of the catalyst, the sample (now only N_2, H_2O, CO_2 and excess O_2) was passed through more stainless steel hypodermic tubing into a V.G.A. Micromass Quadrupole Mass Spectrometer.

For the case of the ethylene studies it was not necessary to heat the hypodermic tubing or spectrometer since the only component of the mixture throughout which could condense was water and this was not necessary for the analysis. In practice, however, to prevent pools of condensate forming either in the tubing or the spectrometer, all components were electrically heated to approximately 50°C.

In the case of the kerosine studies where the fuel itself could potentially condense, it was vital to keep all tubing upstream of the catalyst heated above the fuel boiling point, 300°C, or false readings would result. Again, Thermocoax electrical heating wire was used, but it was extremely difficult to guarantee that all stations were kept at the high temperature.

There was evidence to suggest that small amounts of the liquid fraction of the fuel condensed and then slowly re-evaporated over a longer period of time. After some traverses, even though clean air was obviously being sampled, the CO_2 peak on the mass spectrometer would never approach zero.

Aside from these problems concerning the performance of the mark I system, due to the length of tubing between the probe tip and catalyst there was the potential for soot deposition in the lines, thus blocking the passage of the sample.

It was possible to overcome these in the ethylene studies and the kerosine studies at atmospheric pressure where the soot loadings were relatively minor. However, in the kerosine flames at the higher pressures this was not the case and, depending on the soot loadings, complete probe blockage could occur in as little as 20 seconds. It was possible to

dismantle the probe for cleaning, but, in order to break the pressure seal, this necessitated shutting down the pressure vessel and thus effectively aborting the run.

3.4.1.2 MARK II SYSTEM

A second design of probing system, the mark II system was designed to alleviate the problems found with the mark I design.

Of first concern in the system was the position of the catalyst with relation to the probe tip. All previous designs had involved a catalyst remote from the probe tip. This was undesirable due to the resulting soot blockage and kerosine condensation in the connecting pipework and so the main design criteria was to bring the catalyst as close to the probe tip as possible.

However, after doing this, it is also necessary to bring the excess oxygen required to complete the catalytic reaction to the same point and to supply sufficient heat to make the reaction successful.

A schematic diagram of the resulting design is shown in fig(3.6). A ceramic tube (diameter 2mm) was passed through the centre of the larger (diameter 6mm) quartz probe and was positioned a few millimetres away from the probe orifice. Pure oxygen was delivered through the ceramic tube and was mixed with the sample virtually as soon as the sample entered the probe orifice. Through the centre of the ceramic tube passed a length of fine (0.125mm diameter) platinum wire. At the probe end of the tube this wire was repeatedly wrapped back down the outside of the ceramic tube in coils. The wire was then attached to a metal sleeve. In total the length of the platinum wire is 2m.

The end of the platinum wire that entered the ceramic tube oxygen inlet was connected to the metal gas fitting. This was insulated by the ceramic from the rest of the system and so was used as a positive electrical terminal. The other end of the wire was connected to the metal sleeve which itself was connected to the brass probe coupling. This was used as an electrical earth. Hence the wire performed the dual purpose of acting as a catalyst and heating element.

Such a scheme offers significant advantages over the mark I system since heat is supplied directly to the catalyst which is positioned very close to the sample inlet. The sample has little opportunity to condense as does the soot to deposit on the probe walls (since it oxidises first).

3.4.2 PROBE BLOCKAGE

Although the mark II system was designed to reduce solid carbon deposition on the inside of the probe, with both mark I and mark II systems there still remained the problem of soot deposition on the outside. Not only did this build up eventually block the sampling orifice but it also increased the diameter of the probe, thus introducing more blockage to the flow and hence increasing sampling errors.

In the case of the ethylene studies this carbon could be easily removed with a hand held butane blow torch. In the case of the confined kerosine flames such a solution was not possible. Two methods were employed to clear such blockage in this case:

The first method was used to clear general soot build up along the probe length. The sooty probe was withdrawn completely out of the flame tube and into the probe guide. Since the probe guide was a loose running fit with the probe itself, the carbon was pushed off.

The second method was used to clear the probe orifice. A second flame was positioned at the opposite side of the pressure vessel to the mixture fraction probe. This flame was fuelled by an oxygen rich premixed ethylene / oxygen mixture. When the orifice became blocked, the mixture fraction probe was traversed completely through the main flame to within 5 - 10mm of the probe cleaner flame. The oxygen rich hot combustion products very effectively removed the carbon at the probe tip.

3.4.3 MASS SPECTROMETRIC GAS ANALYSIS

The quadrupole mass analyzer distinguishes between different molecules by their mass/charge ratio, m/e. Very small quantities of the gas under scrutiny enter into a vacuum chamber in which the pressure is of the order 10^{-6} torr. Inside the chamber the gas first passes through an ion source, usually an electric filament where it becomes ionised. Any molecules in the mixture will also become partially fragmented into an array of smaller molecules. These then pass into the quadrupole.

A quadrupole consists of four electrically conducting hyperbolic electrodes (rods) located in a square array. Opposite electrodes are connected together and to one pair is applied the voltage $\phi(t) = U + V\cos(2\pi ft)$ where U is a D.C. bias and V is the peak amplitude of a voltage of radio frequency, f. The same voltage, but of opposite sign is applied to the second pair of electrodes.

The path that an ion which is injected in one end of this assembly will make is described mathematically by a set of differential equations known as the Mathieu equations. Two types of motion are possible. Firstly, a stable oscillation resulting in the ion reaching the other end of the electrode rods. The second is an unstable motion which would ultimately result in the ion colliding with an electrode thus negating its charge.

The ratio of the two voltages U:V will determine the range of values of e/m which will have a stable path. A value of 1:6 will result in a stable range of only 1 atomic mass unit assuming each molecule/atom has only a single negative charge.

Once the ions have successfully passed through the quadrupole, the ion current may be measured to determine ion concentration. An electron multiplier, similar to a photomultiplier, is used to amplify this current to measurable values.

The fragmentation of the molecules is a very important feature of the mass spectrometer and must be considered. For instance, in the present case of measuring N_2/CO_2 ratios, the peak of N_2 , 28, is unsuitable since one of the possible fragmentations of CO_2 is CO which has the same atomic mass. The mass number of 14, corresponding to the fragmentation N from N_2 is used since it is not subject to the same error for the type of mixtures under study. The mass number associated with CO_2, 44, is also not affected by any fragmentation products and so is safe to use.

Although the quadrupole mass spectrometer can distinguish between atomic masses the measurement is not an absolute one. It depends upon the pressure in the vacuum chamber and the ion under study. A method of calibration is also necessary in order to measure absolute mass fractions. The method of N_2/CO_2 measurement is described in appendix B.

3.5. MEAN TEMPERATURE MEASUREMENT

3.5.1 PROBE DESIGN

Fine wire thermocouples of type R were used for temperature measurement. The junction was made between 50μm wires of Platinum and 87%Platinum / 13%Rhodium. Typical bead size was 120μm. The method adopted to mount the thermocouple junction is shown in fig(3.7).

Two thicker wires (diameter 0.5mm) made from the same materials as the fine wires were passed through a twin bore ceramic tube (outside diameter 2.5mm bore 0.7mm) and bent outward to form a V shape. The fine wires were supported between these much stronger wires. In the case of the kerosine studies, the size of the V could be no greater than the width of the slot in the spacer (20mm). This gave a typical distance between the thermocouple bead and each of the thicker wires of $\simeq$9mm (L/D=180).

The ceramic tubing was set with Araldite epoxy resin into a length of 11 gauge stainless steel hypodermic tube (outside diameter 2.946mm). The ends of the thicker wires were connected to a standard R-Type connector. From this the thermocouple voltage was monitored with a microcomputer / datalogger system.

During the ethylene flame studies the thermocouple assembly was supported with retort stands. In the case of the kerosine studies, the probe was supported and actuated in a similar manner as with the mixture fraction probe.

3.5.2. PROBE CLEANING

Again, the thermocouple had to be periodically cleaned due to soot deposition on the sensing element.

In both the ethylene and the kerosine studies it was always possible to find a location at each axial height where the temperature and local mixture was suitable to burn off carbon deposits. If the probe was extremely sooty this took tens of seconds to achieve but involved less risk to the thermocouple than using a premixed cleaning flame as with the mixture fraction probe.

This method was used to ensure the probe was soot free before entering the flame, but due to the nature of the flame it was impossible to prevent some deposition when taking an average reading. In general, this was much smaller in the ethylene studies.

3.5.3 ERROR ANALYSIS

Given the proven reliability of the thermocouple as a temperature sensing element, systematic errors associated with translating thermocouple voltage to a value of temperature are in significant. The principal sources of error are radiation loss (Fristrom and Westernberg,1965) and in the present application soot deposition.

Other factors such as aerodynamic disturbance and catalytic reactions promoted by the platinum wire are expected to be insignificant. Given the size of the thermocouple wire (50μm), aerodynamic disturbance will be minimal. The catalytic effect will also be small since non premixed combustion is essentially mixing controlled.

3.5.3.1 Radiation Loss

Fristrom and Westernberg 1965 suggest a method of radiation loss compensation. The magnitude of this loss may be estimated by equating the heat transferred to the probe from the gas with that lost due to radiation. Eq (3.5)

Per unit surface area of the thermocouple element assuming no conduction:

Radiation from the bead = Convection to the bead

$$\epsilon\sigma(T_{th}^4 - 300^4) = h(T_{gas} - T_{th}) \qquad (3.5)$$

h = heat transfer coefficient (W/m^2K)

T_{th} = Measured thermocouple temperature (K)

T_{gas} = Gas temperature (K)

ϵ = Emissivity of the thermocouple element (0.2), Hottel and Sarofim (1967)

σ = Stefan Boltzmann constant ($5.67 \times 10^{-8} W/m^2K^4$)

The heat transfer coefficient may be estimated using Nusselt number correlations such as those of Kreith and Black 1980. Nusselt numbers (hD/λ) are expressed as functions of Reynolds number. Knowledge of the thermal conductivity, λ (W/mK) and the bead diameter allow the heat transfer coefficient, h, to be estimated.

Obviously, values of the various parameters involved in the calculation will depend upon the composition and velocity of the gas at that point. Such information is not available in this study and so the values to calculate the various parameters were assumed to be constant.

TABLE (3.2)

Property	Assumed value	Source
Viscosity,μ	55.8Pa s	Value for air @1300°C
Density,ρ	0.218kg/m^3	Value for air @1300°C, 1atm
Thermal Conductivity,λ	0.088795	Value for air @1300°C
Prandtl No, Pr	0.75	Value for air @1300°C
Velocity,u	8.0m/s	Average value

Obviously there is some degree of error in these figures especially in relation to the velocity and density. These latter two values are only used when calculating the Reynolds number of the flow however which, due to the bead size (typically 100μm) is always very small. At the highest temperature measured in the present study of ethylene and kerosine flames, 1900K, the necessary radiation correction was approximately 5%.

It is a point of debate whether the thermocouple radiation loss should be compensated at all in flames which are substantially optically thick. One assumption in the above analysis is that the thermocouple is radiating to ambient surroundings at 300K and no account is taken of radiative exchange between the bead and its more immediate environment.

3.5.3.2 Probe Blockage Effects

After being removed from the most sooty regions in the high pressure kerosine flames the probe would sometimes have a coating as thick as 0.25mm of soot. This would have the effect of insulating the element from its gaseous surrounds, increasing the radiative loss of heat from the flame (due to increased size and emissivity) and increasing probe blockage effects. Although obviously important, these effects are uncertain.

It is possible to circumvent such problems when making measurements on laminar flames due to their time independent nature. Moss et al. (1988) and Honnery (1991) developed different methods of temperature measurement in laminar flames which relied on rapid insertion of the probe followed by estimation of the first order thermocouple time lag. Such techniques, however, are inappropriate in the present study due to the fluctuating nature of the flames.

A simple experiment was devised, therefore, to investigate the magnitude of the effects in the present study.

A clean probe was inserted into the flame at the location under study. The moment that the probe was in position a 7 second mean measurement of temperature was made, immediately after this a second mean measurement was made. This was repeated until the probe became completely blocked. The results of such an experiment are plotted in fig(3.8) for two different flames.

As can be seen, in both cases the drop in measured mean temperature with time, appears to be exponential in nature. Shown on the same graph are least squares fits of the data with exponential curves. Extrapolation of the curves to time zero suggests that the error between the value at time, t=0s and t=7s to be of the order 20-40°C.

Although this is a very encouraging result the extrapolation is subject to error. No consideration is given to the measured temperature drop that occurs within the first few fractions of a second since the temporal resolution of the measurements is not fine enough. Of the effects of soot blockage, the one with the shortest timescale will be the change in emissivity of the thermocouple bead which will be virtually instantaneous. The other two effects are expected to be of much longer timescale. Honnery (1991) made similar measurements on laminar diffusion flames of various fuels and found that the drop in measured temperature within the first 0.5s could be as high as 50°C. No equivalent values may be measured in the present study of turbulent combustion due to temperature fluctuations, but this error is obviously more significant.

Since no completely satisfactory method of compensating for such errors has been identified, none other than a standard radiation correction was used.

3.6 SOOT MEASUREMENT

Three different methods of soot particle size and volume fraction measurement were attempted in this study. They were:

- Rayleigh Extinction.

- Multicolour extinction.
- Differential Mobility Particle Sizer (DMPS) Analysis.

Rayleigh extinction has the advantage over the other techniques in that it is extremely simple and is less prone to systematic error provided the soot particles are small with relation to the wavelength of light used. It does, however, suffer the drawback of only providing information on the volume fraction of soot under study. The final two techniques offer the advantage of providing information on volume fraction, diameter and number density of soot but at the expense of increased systematic error and experimental simplicity. This section describes the basis and expected errors of these techniques.

3.6.1 LASER EXTINCTION MEASUREMENT

Both the methods of Rayleigh extinction and multicolour extinction depend upon the accurate measurement of turbidity at the point of interest within the flame. The extinction of an incoming light beam of intensity I_o as it passes through an aerosol of turbidity $\tau(s)$ is defined by the Beer Lambert law as:

$$\ln\left[\frac{I_o}{I}\right] = \int_0^{\infty} \tau(s)ds \qquad (3.6)$$

$\tau(s)$ = turbidity
I_o = Intensity of incoming light.
I = Intensity of transmitted light.
s = Position along the laser path. Datum corresponding to I_o.

A very simple experiment may be set up in order to measure the extinction ratio I_o/I. A schematic diagram of the method used in the present study is shown in fig(3.9). In order to make radial traverses of the flames, in both the ethylene and kerosine studies the flame was moved in relation to the optics rather than vice versa. Traversing, in both cases was achieved using a precision machined screw, positioning accuracy 0.025mm. In practice, there is a small background bias voltage of the photodiode, I_b, corresponding to no light. Hence all measured values of intensity must be appropriately corrected using eq(3.7).

$$I = I_{meas} - I_b \tag{3.7}$$

3.6.1.1 ERROR ANALYSIS

There are three possible sources of error when making such measurements: background radiation of the flame, beam steering effects and uncertainties in I_o.

Obviously, some method is required to distinguish between the unwanted background radiation issuing from the luminous flame and the signal laser beam. Two common methods adopted in such situations are lock-in amplification and narrow band pass filter techniques.

Lock-in amplification techniques distinguish between random radiation and laser radiation by modulating the incoming laser beam at a precisely known frequency and phase. After the intensity of light has been measured, the luminous and laser radiation components are electronically separated by a lock in amplifier. This method has the advantage of requiring no optics between the flame and signal detector but is quite unsuitable for a turbulent combusting analysis for the following reason: when measuring the mean turbidity it is the mean of $\ln(I_o/I)$ that is required not that of I_o/I. The lock in amplifier measures the mean value of I. Due to the non-linear nature of the logarithmic function, the resulting error can be as great as 10% depending upon the degree of fluctuation within the flame. This is studied in more detail in chapter 4.

The narrow band pass filter technique was therefore used in preference. The two components of the incoming light, in this case, are separated mechanically by means of a very narrow band pass optical filter (band width 1nm) centred on the laser wavelength. With this technique, the logarithm of the measured signal may be taken within the datalogging computer before any averaging takes place.

The disadvantage of the band pass filter technique is that it introduces an additional optical component between the flame and photodiode. Beam steering effects caused by the sharp changes of refractive index in the flame allow the possibility of inhomogeneities in the transmissivity of the filter to generate random error. A simple test of the sensitivity of the system to such noise was undertaken with a bunsen flame. Since such flames contain no soot,

when the laser beam is passed through them, the only effect on the laser beam will be that of beam steering. The experimental configuration could always be adjusted to ensure no correlation between the presence of the flame and fluctuations of the laser signal proving beam steering effects to be negligible.

The main source of error in the extinction measurements was due to uncertainties in the prescription of both I_o, the unattenuated laser intensity and I_b the background (no light) intensity. For the case of I_o these arose due to laser drift and inhomogeneities in the pressure vessel windows (only laser drift in the ethylene study), for I_b, the cause was electrical noise. The values of both these parameters were measured at the beginning and end of each radial extinction traverse. The value at each radial location was then calculated assuming the parameters to vary in a linear fashion between the two edges of the flame. The accuracy of this assumption obviously depends on the magnitude of the laser drift and, in the case of kerosine flames, window noise.

For all the traverses, the values of both I_b and I_o would vary by a small amount between the beginning and end of the traverses. The difference between the values was calculated for a sample of 20 kerosine flame traverses. The mean and maximum variations are shown in table(3.3)

TABLE (3.3)

Taken from a sample of 20 traverses	Variation in background Intensity, b (mV)	Variation in unattenuated Intensity, a (mV)
Mean	0.02509	0.89271
Maximum	0.10598	14.181

These values should be compared with typical values of I_o, 0.623V and I_b, 0.6mV and represent the degree of uncertainty to which each value is known.

Considering eq.(3.7), the value of attenuated intensity will have at least the same uncertainty as the background intensity, I_b. Therefore, if the uncertainties in I_o and I_b are named a and b respectively, the percentage error in $\ln(I/I_o)$ may be expressed as eq.(3.8).

$$Percentage\ error = \frac{\ln\left[\frac{I \pm b}{I_o \pm a}\right] - \ln\left[\frac{I}{I_o}\right]}{\ln\left[\frac{I}{I_o}\right]} \times 100 \qquad (3.8)$$

Using the maximum uncertainties in table(3.3), the worst case error bands may be estimated for the range of values of $\ln(I/I_o)$ relevant to this study. This is shown in fig(3.10). For the majority of the curve, the expected error is considerably less than 5%, however, there are two regions where the expected error rises above this. They are for very weak or very strong extinctions.

At very weak extinctions, the uncertainty in the value of the unattenuated intensity, I_o, becomes significant with relation to the level of extinction of light. Hence large errors result. As the extinction strengthens, this effect becomes less important and the error reduces.

At very strong extinctions, it is the uncertainty in I_b, which becomes important and again the expected error rises. In terms of the experimentation, there is an important consequence of this for the situation where the actual background intensity is less than the assumed background intensity. In this case, for very strong extinctions, it is instantaneously possible for the measured value of attenuated intensity, I, to be lower than the assumed background intensity, I_b. Considering eq.(3.7), this would result in the argument of the logarithm also being negative.

It is simple to avoid such a situation arising by trapping any negative arguments before the logarithmic function is applied, but this would effectively filter from the average the most important (ie. strongest) extinction signals. In practice, when such a situation arose, the extinction at that point was assumed to be $\ln(b/I_o)$, b taken to be the maximum uncertainty of I_b (table(3.3)). This took some account of the strongest signals but was obviously a source of inaccuracy. At each position the percentage of points treated in this way when making the average was also logged.

3.6.2 TOMOGRAPHIC DECONVOLUTION

With reference to eq.(3.6), the preceding section described the method by which the left hand side of the equation was measured and the expected error in doing so. This value of

extinction, however, is proportional to the line integral of turbidity, τ, along the laser path rather than the local turbidity. Some method is required to retrieve local turbidity in order to estimate the local soot concentration. A number of inversion techniques are possible. Two common ones used to study soot are onion peeling (first order Abel inversion) and Fourier inversion.

Onion peeling, used by Kent and Honnery (1987), considers the inversion from the outside of the flame inwards. The domain is considered to comprise discrete circular rings, similar to the layers of an onion. The extinction at the outermost edge of the domain is only dependent upon the turbidity in the outermost ring. If soot is considered to vary in a piecewise fashion between rings, in the outermost ring, eq.(3.6) reduces to eq(3.9). The path length, L, may be calculated by geometrical reasoning.

$$\ln\left[\frac{I_o}{I}\right] = \tau L \qquad (3.9)$$

The extinction in the next outermost ring is dependant upon the turbidity in that ring and the known turbidity in the outermost ring. Again using geometrical reasoning the unknown turbidity may be calculated. This is repeated until the centre of the domain is reached.

Although this scheme is an extremely flexible and simple one to implement it has a very important drawback. The calculated values of turbidity in the inner rings are dependent upon the turbidities of all the rings further out. Any errors in the turbidities in these rings will be truncated when calculating the unknown value. Thus errors increase towards the centre line where the error will be the greatest.

It is for this reason that the method of Fourier inversion was used in the present study. Consider fig(3.11)

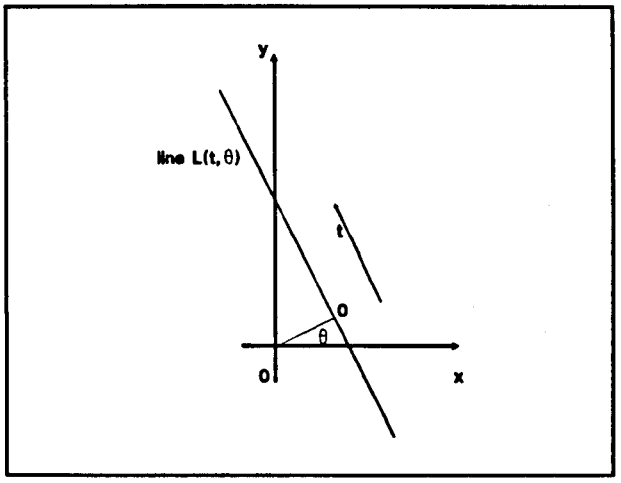

Figure (3.11)

Following the analysis of Shepp and Logan,1974. Let L(t,θ) define a line whose normal makes angle θ with the positive x axis and has length t, $-\infty < t < \infty$

ie L is the line:

$$x\cos\theta + y\sin\theta = t \quad (3.10)$$

Let P(t,θ) define the line integral of turbidity, τ(x,y), along L.

$$P(t,\theta) = \int_{L(t,\theta)} \tau ds \quad (3.11)$$

The basis of the Fourier algorithm is that the Fourier transform of P(t,θ) is equal to the Fourier transform of τ(x,y) in polar coordinates. ie

$$\hat{P}(\omega,\theta) = \int_{-\infty}^{\infty} e^{-i\omega t} P(t,\theta) dt$$

$$\hat{\tau}(\omega,\theta) = \int_{-\infty}^{\infty}\int \tau(x,y) e^{-i\omega(x\cos\theta + y\sin\theta)} dx\,dy \quad (3.12)$$

$$\hat{P}(\omega,\theta) = \hat{\tau}(\omega,\theta)$$

The Fourier inversion or convolution theorem may be applied to eq (3.12) in order to give τ explicitly in terms of P and position, (Shepp and Logan 1974). This is shown in a more

experimentally tractable discrete form in eq.(3.13)

$$\tau(x,y) = \frac{a}{2n}\sum_{j=0}^{n-1}\sum_{k} P(t_k,\theta_j)\phi(x\cos\theta_j + y\sin\theta_j - t_k) \qquad (3.13)$$

This equation is for a finite number, k, of equispaced parallel rays for n values of angle θ. $\theta_j = j\pi/n$. a is the ray spacing and $t_k = ka$, thus if m rays cover the diameter of a flame of radius r, the ray spacing, a, would be given by $a = 2r/m$.

The function $\varphi(d)$ in eq.(3.13) is the weight assigned to line $L(t_k,\theta_j)$ in reconstruction at (x,y). d is the normal distance of the line $L(t_k,\theta_j)$, from (x,y).

Ramachandran and Lachshminarayanan, 1971, suggest a weighting function as shown in eq(3.14) with φ assumed to vary in a linear fashion between rays.

$$\phi(0)=\frac{4}{\pi a^2}\ ; \quad \phi(ka)=-\frac{4}{\pi a^2(4k^2-1)} \qquad (3.14)$$

Shepp and Logan 1974 found this function to be subject to noise, producing oscillations in the reconstruction. They suggested a modified filter eq.(3.14) which behaved in a much more satisfactory manner.

$$\phi(t_l)_{shepp\ and\ logan} = 0.4\phi(t_l) + 0.3\phi(t_{l+1}) + 0.3\phi(t_{l-1}) \qquad (3.15)$$

This modified filter was used here. One point of note with the implementation of this method to the present study is that, since the flame is axisymmetric, the line integrals P are independent of angle, θ, and the complexity is reduced considerably.

The great advantage of this method over the method of onion peeling is that the reconstructed value of turbidity at a point is dependent upon all values of the measured line integral to varying degrees (according to the weighting function). Hence, in general, random noise and truncation effects are minimised. Some care has to be taken in ensuring there are enough values of line integral to resolve all features in order to prevent Fourier ringing, but, for the case of the soot profiles, the majority of which are broadly Gaussian in shape, this presents minimal problems.

3.6.2.1 Implementation of Tomographic Deconvolution

Given the sensitivity of the deconvolution technique to random noise reported by Shepp and Logan, 1974 and the requirement that the data should be equispaced about the centreline, the

following procedure was adopted to process the extinction data:

- First the extinction was measured across the complete diameter of the flame

- The data was centred to give a profile of extinction against radial distance.

- A 20th order even polynomial was then fitted to the data by means of the least squares technique. This performed well in all locations except the wings of the flame where the extinction dies to a steady value of 0. In this location a splined exponential decay was used.

- Approximately 50 equispaced radial values of extinction were then taken from the best fit curve and input into a modified version of the deconvolution program supplied by Shepp and Logan, 1974 using the weighting function, eq(3.15). The result was a table of turbidity, τ, against radial position, r.

3.6.3 RAYLEIGH EXTINCTION

The measured turbidity, τ, may be related to the local soot concentration and number density field using Mie theory (1908), a detailed derivation of which may be found in Kerker 1969. This assumes a plane wave of light, wavelength, λ, incident upon a single spherical particle of known complex refractive index, m.

$$\tau = \int_0^\infty N \pi r^2 Q_{ext}(m,\lambda,r)\, dr \qquad (3.16)$$

N Number of particles per unit volume.
r Radius of particles
Q_{ext} Extinction efficiency of the particles
m Complex refractive index of particles $m = \eta - i\kappa$

Q_{ext} is dependent upon elastic scattering and absorption of light and is a function of the wavelength of incident light, the complex refractive index of the particle and the size of the particle. The function is complex but may be defined in terms of spherical Bessel functions. (cf. Kerker 1969).

The term $\pi r^2 Q_{ext}$ is sometimes termed the extinction cross section since it may be considered as the projected area of the particle to the incident light.

If the circumference of the particles is small in comparison to the wavelength of light. ie $2\pi r/\lambda \ll 1$, then the scattering component of the extinction is negligible compared to the absorption. Particles which obey this criterion are said to be in the small particle or Rayleigh limit, in which case (Kerker, 1969):

$$Qext = 48\pi r \frac{F(m)}{\lambda} \tag{3.17}$$

Where:

$$F(m) = \frac{\eta\kappa}{(\eta^2 - \kappa^2 + 2)^2 + 4\eta^2\kappa^2} \tag{3.18}$$

Whence:

$$\tau = \frac{36\pi F(m)}{\lambda} \int_0^\infty \frac{4}{3} N\pi r^3 dr \tag{3.19}$$

Since the integral in eq.(3.19) is the volume fraction of particles, measured values of turbidity may be related directly to volume fraction. This method of soot measurement was successfully applied to the ethylene flame and all the kerosine flames reported in this study with a helium neon laser light source of wavelength 632.8nm.

3.6.3.1 Error Analysis

Even providing the measured turbidity is correct, when processing the experimental measurements with the Rayleigh limit assumption, further sources of systematic error are introduced. These are due to four factors:

1 - Uncertainty in the value of complex refractive index.

2 - Assumption that particles are small in relation to the wavelength of light.

3 - Assumption that particles are spherical.

TABLE 3.4

Source	Fuel	Complex Refractive Index	Wavelength (nm)	F(m)
Dalzell and Sarofim (1969)	Acetylene Propane	1.57 - 0.44i 1.56 - 0.52i	650	0.0342 0.0405
Lee and Tien (1981)	Polystyrene Plexiglass Iso-Octane	1.9 - 0.55i	632.8	0.0321
Sentfleben and Benedict (1917)	Propane	2.0 - 0.66i	632.8	0.0348
Mullins and Williams (1987)	Toluene Propane n-Heptane Methane	1.89 - 0.46i 1.92 - 0.45i 1.89 - 0.44i 1.93 - 0.39i	632.8	0.0273 0.0261 0.0262 0.0226
Chippet and Gray (1978)	Propane	1.9 - 0.35i	Visible	0.0209

The values of F(m) vary by as much as 100% between the extremes. To maintain continuity between this study and previous work by the same group and since it lies roughly in the middle of all reported values, the value of Mullins and Williams 1987 for propane soot at 632.8nm was used, m = 1.92-0.45i.

The assumption that particles are small in relation to λ may be analysed mathematically. As stated earlier, using eq.(3.16), the aerosol turbidity, τ, may be calculated exactly using a complex function of spherical Bessel functions (Kerker, 1969). This was done for a variety of particle radii assuming a monodisperse size distribution and compared with that from the Rayleigh limit approximation, eq.(3.19). The percentage difference between the two values is shown in fig(3.12). For small particles of radius up to approximately 30nm, the discrepancy is within 10%. This value rapidly increases to levels of the order 60% at particle radii of 100nm.

The discrepancy is due to the increasing importance of the scattering component of Q_{ext}, neglected in the Rayleigh limit. Since this component always causes greater extinctions of the incident light, the error resulting from the assumption that particles to be small is always positive (ie. measured volume fractions will always be greater than in reality).

A number of authors report measured soot size in the literature. This is most commonly done using light scattering techniques. Such techniques have been applied quite extensively in laminar flames. Bard and Pagni (1981), Garo et al (1990), Kent and Wagner (1982). Prado et al (1981) all report soot particle sizing experiments on laminar flames using various hydrocarbon fuels. Generally, the maximum mean radius measured is of the order 50nm, but this is dependent upon residence time.

Less work has been reported on turbulent flames since measurements are more problematic in these situations. Wood and Samuelson (1985), however report scattering measurements inside a swirl stabilised combustor. The flowfield is somewhat more representative of the jet flame studied here due to its turbulent nature, but the fuels used (liquid petroleum mixtures) were substantially different.

Their results show that average particle radius lies in the region of 125-150nm with some particles as large as 200nm. Although no error analysis was given with their results which are substantially higher than equivalent values in laminar flames this still raises concerns regarding Rayleigh extinction techniques.

The second source of error in the present study is the assumption that particles are spherical. Sampling electron microscopy measurements such as those reported by Dalzell and Williams 1970 or Megaridis and Dobbins 1989 suggest that soot is comprised of agglomerates of many small (typically 40nm) spheroids joined in highly complicated chain like structures. Bonczyk and Hall 1991 performed a detailed analysis of the scattering characteristics of such structures. They concluded that intra and inter-particle multiple scattering effects were unimportant to the absorption characteristics of an aerosol. As a consequence the absorption of a cluster of N monomers is equal to N times the absorption of one monomer of similar size.

Their conclusion that multiple scattering effects are negligible is also supported by Guidt et al (1990) who consider absorption by extremely dense calibrated sols suspended in a gel. They concluded that the Beer Lambert law (eq.3.6) is valid provided the following constraint is met:

$$\frac{1}{2} \geq 1.81712\left(Q_{ext}(r)\right)^{1/2} f_v^{1/3} \qquad (3.20)$$

The value of this parameter was tested for the highest value of soot volume fraction measured ($60x10^{-6}$) with a variety of particle sizes. The calculated values lay well within the limits.

3.6.4 MULTICOLOUR EXTINCTION

One of the great disadvantages of the Rayleigh limit extinction technique is the fact that it neglects the effects of particle scattering in the analysis. Figure (3.12) shows clearly the potential error associated with this if particles are large. One measurement technique that is suited to the present application which does not require such a limiting assumption is the multicolour extinction technique first proposed by Durbin (1950). This method relies on the fact that at different values of the optical size parameter , $\alpha = 2\pi r/\lambda$, particles have different extinction efficiencies, Q_{ext}. This size dependent property may be investigated in order to estimate the particle diameter.

The method adopted here to measure soot particle size, number density and volume fraction was very similar to the three colour method of Bard and Pagni 1981. To analyse the method it is necessary to consider the equations of scattering of light by a sphere (Kerker 1969).

The turbidity, τ,of a cloud of spherical particles in suspension in air is expressed in equation (3.16)

Some assumption about the size distribution of the soot particles is now necessary in order to implement the model. Assume, $N(r) = N_o \eta(r)$ where η is an arbitrary probability density function (PDF) and N_o is the total number of particles of all sizes. Then :

$$\tau = \pi N_o \int_0^\infty \eta(r) Q_{ext}(m,r,\lambda) r^2 dr \qquad (3.21)$$

Any PDF may be chosen subject to its validity and applicability. Two commonly used PDF's in light scattering analysis experiments are the monodisperse and log-normal distributions.

An important relationship emerges. At two wavelengths, λ_1 and λ_2 for example, the ratio of turbidity at those two wavelengths is a unique function of the radius of the particles (assuming the wavelength of incident radiation and the complex refractive index of the soot is known).

$$\frac{\tau_1}{\tau_2} = \frac{\int_0^\infty \eta(r)\, Q_{ext}(\lambda_1, m_1, r)\, r^2 dr}{\int_0^\infty \eta(r)\, Q_{ext}(\lambda_2, m_2, r)\, r^2 dr} \qquad (3.22)$$

The experimental ratio of τ at both wavelengths may be compared with the theoretical ratio of the distribution weighted extinction efficiency ratio (D.W.E.E) (eq.(3.22)) in order to determine particle radius. Once this is known particle number density, N, may be calculated using eq.(3.21). Volume fraction may then be calculated directly from radius and number density using eq.(3.23).

$$f_v = \frac{4\pi}{3} N_o \int_0^\infty \eta(r) r^3 dr \qquad (3.23)$$

3.6.4.1 IMPLEMENTATION OF THE TECHNIQUE

As explained, the method by which the particle size is discerned involves the comparison of the ratio of measured turbidities at two wavelengths with the theoretically determined D.W.E.E. For the purposes of demonstration, shown in fig(3.13) is a graph of the ratio of D.W.E.E., for the wavelength pairs 632.8 and 514.5nm, 632.8 and 457.9nm assuming a monodisperse PDF size distribution. These values have been calculated directly from Mie theory (Kerker (1969)) using a value of complex refractive index, m, of 1.92 - 0.45i for all wavelengths.

Although the PDF assumption in this case is the least realistic of all, similar plots using different PDF assumptions exhibit the same trends. As can be seen, in some regions the functions are double valued. This creates difficulties when relating experimental turbidity ratios from one pair of wavelengths to D.W.E.E. ratios since, in these regions,the result could be one of two radii. In these situations it is impossible to identify which is the correct value unless more information is available.

This is gained by repeating the procedure for a second pair of wavelengths. This will yield two further possible radii. Ideally only one pair of radii from both analyses will be similar. This is the correct value.

When choosing the two wavelength pairs, it is important that they should be separated from each other by a significant amount otherwise the two analyses would yield very similar sets

of possible values and it would be extremely difficult to determine the correct particle size in the presence of experimental error on the turbidity field. Bard and Pagni (1981) found that 632.8, 514.5 and 457.0nm gave good discrimination.

A computer data analysis program was written to process the three sets of experimental turbidity. It comprised four main sections:

1 - The experimental turbidity data and theoretical values of D.W.E.E. were input.

2 - Since measurements of extinction at different wavelengths were made at different days due to lack of duplicate equipment, the absorption data at different wavelengths was not known at coincident points on the flame radius. The second section of the program used a linear interpolation routine in order to calculate the turbidities for each wavelength at the same point.

3 - The experimental turbidity ratios were compared with the theoretical D.W.E.E. ratios in order to calculate diameter. For the first pair of wavelengths, all theoretical values of D.W.E.E. were compared with the experimental turbidity ratio. If only one possible value of diameter emerged then no further processing was performed and the value of volume fraction and number density were calculated. If not, the second pair of wavelengths was investigated in a similar manner. Again, if only one diameter was found, this was taken to be the correct value. If two further values were found, the four diameters established using both analyses were compared. The average value of this closest pair of diameters was then taken to be the correct value and from this the volume fraction and number density were calculated.

4 - The final section of the program was the output routine. Two files were output, the first containing the soot size, volume fraction and number density information, the second containing all the diameters calculated in section 3 with the computer's choice of the correct one.

3.6.4.2 ERROR ANALYSIS

In general, the results of all experiments based on classical light scattering are dependant on the value of the complex refractive index of soot chosen in the analysis. The multicolour extinction method is no exception to this and so a parametric study of the effect of wrong prescription of the index was undertaken.

This effect is of great concern given the degree in uncertainty of the value of the complex refractive index of soot reported in the literature - see table (3.4).

From this brief review, it is apparent that most authors tend to agree on the real component of the index but not the imaginary one. Not including the values reported by Dalzell and Sarofim (1969) which appear to lie outside the range of the other measurements, the mean value of the real component is 1.918 with few values lying outside 2% of this. The uncertainty in the value of the complex component is closer to 20%.

A mock set of experimental data was constructed of soot volume fraction, particle diameter and number density in order to investigate the affects of such uncertainties on the data analysis procedure. This is plotted in fig(3.14). If this was an experimental profile the x axis would be radial position in the flame, since it is a mock data set this axis is arbitrary.

Using values of Q_{ext} calculated with a complex refractive index of 1.92 - 0.45i (Mullins and Williams 1987), eq.(3.21) was employed in order to calculate the theoretical turbidity, τ, to these values at three wavelengths of incident light; 632.8nm, 514.5nm, 457.0nm, assuming a monodisperse distribution of particles.

Then, a new profile of Q_{ext} was generated using a slightly modified value of complex refractive index. This new profile was used with eqs.(3.21-23) to analyse the mock experimental data set generated previously.

In keeping with the uncertainties in experimentally determined refractive index, the affect that a $\pm 2\%$ change to the real and a $\pm 20\%$ change to the imaginary component had on the data processing technique was investigated.

The results of this exercise are shown in fig.(3.15). The effect of perturbing both real and imaginary components of the index on the key variables; soot particle diameter and volume fraction is shown. The discrepancy in the results is of two types:

Erroneous values - the reconstructed data differs from the original data.

Unphysical values - the value of the D.W.E.E. ratio, for all size distribution PDF assumptions has a minimum value, the magnitude of which is dependent upon the complex refractive index. In some cases, perturbing the complex refractive index has the effect of increasing this minimum value. When analysing the mock turbidity data

generated using the original complex refractive index, there are some regions where the value of turbidity ratio is below the minimum value possible for the perturbed D.W.E.E ratio profile used. Since no further data processing is possible at that point it will appear as a blank space in the plots. This is a phenomenon quite often seen when analysing the experimental information.

When physical values occur, the effect of perturbing either component is more pronounced in the calculation of soot volume fraction than particle diameter. In all cases the effect of perturbing the imaginary component is more severe. It is clear that if the wrong index of refraction (or indeed size distribution) is used to analyse a particular data set, the resulting error could be great.

Shown in fig(3.16) are a number of plots of the theoretically derived D.W.E.E. ratios assuming monodisperse and lognormal size distributions and with values of complex refractive index from Mullins and Williams 1987 (values close to the mean), and Dalzell and Sarofim 1969 (values which differ considerably from the mean).

All profiles have a very distinctive shape and the maximum and minimum values of the ratio do not appear to vary very much between cases. It is in the ordinates of the graphs in which the main differences lie. The minimum value of D.W.E.E. ratio occurs at a much smaller value of mean diameter when log - normal size distributions are considered. This is due to the non linear effects of the larger particles being felt at a much smaller mean diameter. Due to the uncertainties, each of these profiles was used individually to analyse the experimental data in the hope that one was most appropriate to kerosine soot. The application of the technique to real applications is deferred until the next chapter.

3.7 DIFFERENTIAL MOBILITY PARTICLE SIZER ANALYSIS

Early in the measurement campaign, a T.S.I. inc. model 3071 Differential Mobility Particle Sizer (DMPS) was made available by Rolls Royce plc. for studies on the ethylene jet flame. Although such an application lies outside the instrument's customary role of sampling much less heavily laden aerosols, it was, in principle, capable of measuring soot size, number density and volume fraction for soot particles sizes ranging between 0.017μm and 0.886μm.

3.7.1 THE DMPS INSTRUMENT

The DMPS measures the number and size distribution of sub-micron particles in a sample

aerosol. A schematic diagram of the instrument is shown in fig(3.17). There are three major components:

1 Impactor: After entering the DMPS the sample passes through the impactor. The purpose of this device is to remove particles of diameter greater than the maximum size range of the instrument. This is achieved by accelerating the flow through a nozzle and the deflecting it around a 90° corner. Particles of 1μm and above are unable to follow the flow; they impact and adhere to the opposing face of the corner.

2 Neutraliser/Electrostatic Classifier: Particles are then exposed to a high concentration of positive and negative ions generated by a Krypton-85 source in the neutraliser where they acquire a standard Boltzmann charge distribution.

They then enter the electrostatic classifier. This consists of a vertical column in which there is a constant laminar flow of air from the top to the bottom. The polydisperse sample aerosol is injected into the air stream from a narrow orifice. In the centre of the column is an electrode to which the charge particles subsequently are attracted.

The DMPS distinguishes between particles by virtue of their electrical mobility in the air stream. Due to their very small size and hence very large specific drag coefficients, they reach terminal velocity in the column extremely quickly. This velocity is dependant upon a balance between electrical attraction and aerodynamic drag forces and hence for a known charge is dependant upon size of the particles.

The vector combination of this horizontal drag velocity with that of the vertical sheath air flow will determine the trajectory of the particles. At the base of the column, there is a very narrow slit through which only particles within a very narrow range of trajectories may enter. Thus particles are classified.

The exact expression which is used by TSI inc. to define electrical mobility is based upon the assumption that particles are spherical.

$$Z_p = \frac{neC\times 10^7}{3\pi\mu D_p} \qquad (3.24)$$

where n = no of electronic charges
e = charge per electron (C)

μ = gas viscosity (poise)
D_p = particle diameter (cm)
C = Cunningham drag coefficient

3 Condensation Nucleus Counter (CNC): A supersaturated butanol vapour condenses on the monodisperse aerosol of particles entering the CNC. The droplets formed grow to diameters of approximately 12μm.

The number of droplets per unit volume of flow is then counted using an optical light scattering technique. This information is passed to a microprocessor which adjusts the measurement to take into account the Boltzmann charge distribution and outputs the results to the user.

It is important to note that the DMPS is only capable of measuring the electrical mobility of particles and not size directly. Given the dependence of this term to the drag coefficients of the particles and given the highly complex geometry of soot, the conversion to some characteristic size is extremely difficult. In order to circumvent this ambiguity, the makers of the instrument assume spherical particles for which drag is well specified. The result being that the measured quantity is Stokes-drag diameter. The relationship between this and the actual size of the particles is, however, unknown.

3.7.2 SAMPLING OF AEROSOLS

The probe sampling arrangement adopted in the turbulent ethylene jet flame studies is shown in fig(3.18). The aerosol sample (0.3l/min) was drawn through a quartz probe of orifice diameter 1mm and through approximately 1m of 6mm PTFE tubing. It was then diluted with room air before finally entering the impactor. The dilution was necessary since the DMPS was designed to examine aerosols of lower number density than those in the present study. Problems with impactor blockages were encountered and in regions of high soot volume fraction ($> 10^{-6}$) these became severe. Measurement of the dilution flow proved difficult in the limited time that the apparatus was available and hence all information on particle number density was lost. Only information on size distribution is therefore accessible.

One source of concern in the arrangement described was the sampling method. Although the DMPS itself had been calibrated by its manufacturers there was good reason to believe that the aerosol sample was affected by the probe system. This can arise due to a number of reasons:

(1) Anisokinetic sampling and other similar factors could cause an unrepresentative sample to be drawn from the flow.

(2) Brownian diffusion and settling causing certain fractions of the sample to condense on the pipe walls.

(3) Particle oxidisation in the uncooled quartz probe which was partially immersed in the flame.

(4) Coagulation of the particles in the pipework.

In view of these uncertainties a parametric study of the DMPS was undertaken to ascertain the effects of these four mechanisms.

The parametric study undertaken was incomplete given the time constraints. Certain parameters of the sampling system which were considered to have potentially important effects on the sample were varied systematically whilst soot from a single location in the flame was being sampled. Changes in measured profiles could then, in principle, be attributed to particular parameters.

Orifice Size

Since larger particles have a higher inertia, they are affected by changes in flow direction to a lesser extent. Therefore, if the probe is anisokinetic, an unrepresentative sample will be drawn (cf. fig(3.19a)). The effect of this has been quantified and is shown in fig(3.19b) (cited from Fissan). As can be seen however, this effect is not significant for particles smaller than 1μm.

The main sampling error for such a probe system is likely to arise because of the large sample volume flow. The required flowrate of 0.3litres/min will locally distort the flowfield in regions of high property gradients and the precise origin of the sample will be uncertain.

In order to check the dependence of the sample drawn on probe orifice size this was varied from 0.4mm to 1.9mm. The region from which the sample was drawn had high property gradients but, for each orifice size, the size distributions were indistinguishable within experimental error.

Sedimentation

As mentioned earlier, this occurs due to two main mechanisms - Brownian diffusion and gravitational settling.

Gravitational settling is described by Wiley, 1987. He reports that it is dependent upon an aerodynamic parameter T_s, the settling time. With knowledge of this and the residence time in the pipeline, the effective settling rate may be estimated. It appears that the effects of gravitational settling will be small in the present application.

Fissan defines a dimensionless parameter, f, the ratio of particle transport/diffusion times. He states that Brownian diffusion becomes 'important' for values of f exceeding 0.01. Shown in fig(3.20) is a plot of f against particle diameter for the sampling geometry used. Unfortunately, it appears that diffusion becomes important for particle diameters less than approximately 0.1μm. This diameter is within the range of the DMPS. For the smallest particles measurable (0.019μm) diffusion becomes 'important' for line lengths of 6cm and above.

In the parametric study both line length and diameter were varied - length from 33cm → 3m, diameter from 1.5mm → 5mm. There was visible sedimentation in the lines but the measured profiles again showed no dependence upon these parameters.

Oxidation

At its widest point, the ethylene jet flame was approximately 150mm in diameter. The quartz probe was not cooled, thus any unfinished chemical reaction in the sample, including the oxidation of soot, could in principle continue.

An experiment was devised whereby the probe was inserted into oxygen rich and fuel rich regions of the flame whilst being heated externally from the flame by bunsen burners.

The profiles measured showed now dependence to probe heating.

Dilution System

As stated earlier in this section, in regions of high soot volume fraction, the impactor of the DMPS would block readily. The dilution system used to alleviate this problem was also investigated.

As part of the parametric study, the amount of dilution was varied between 0 and 80%. Again, although the number count obviously changed due to the increased dilution, the

relative amounts did not and hence the profiles remained the same.

The result of the experimental parametric study was therefore that the sampling system appeared not to influence the sample in any way. Although an encouraging result this was also unexpected and in contradiction to other work. The parametric study performed here was not exhaustive due to lack of time. The effects of the probe sampling system need to be studied in far greater detail before it can be confirmed to have no affect on the sample.

Fig(3.1)[a]:SCHEMATIC DIAGRAM OF THE KEROSINE JET FLAME PRESSURE VESSEL INCLUDING A MORE DETAILED ASSEMBLY OF THE CENTRAL MEASUREMENT SECTION.

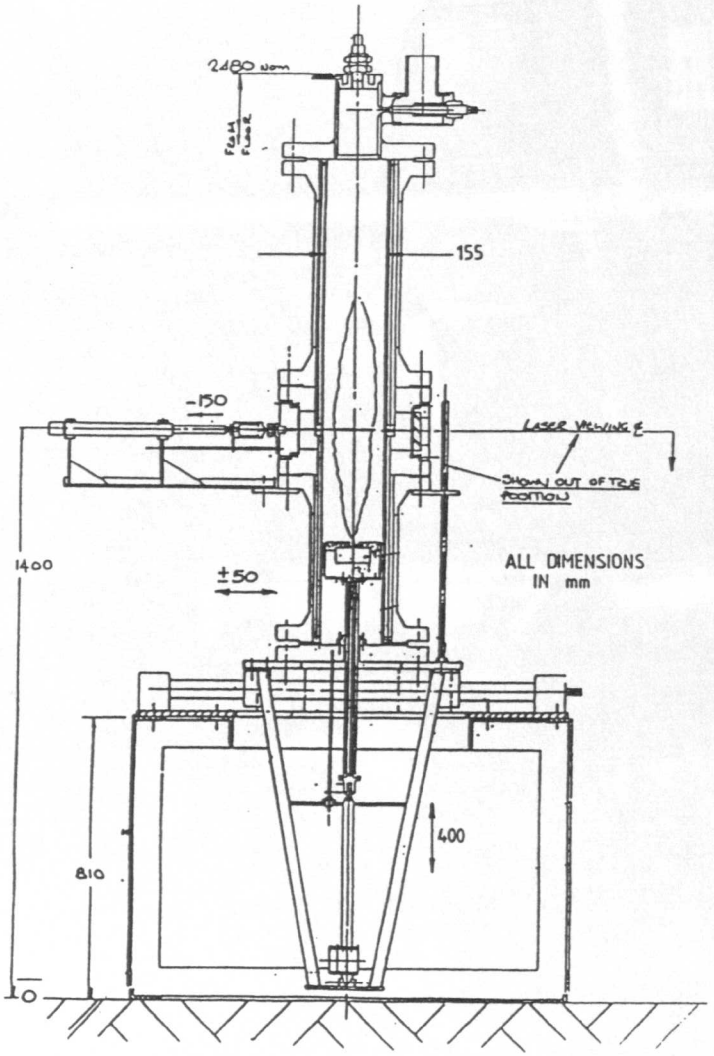

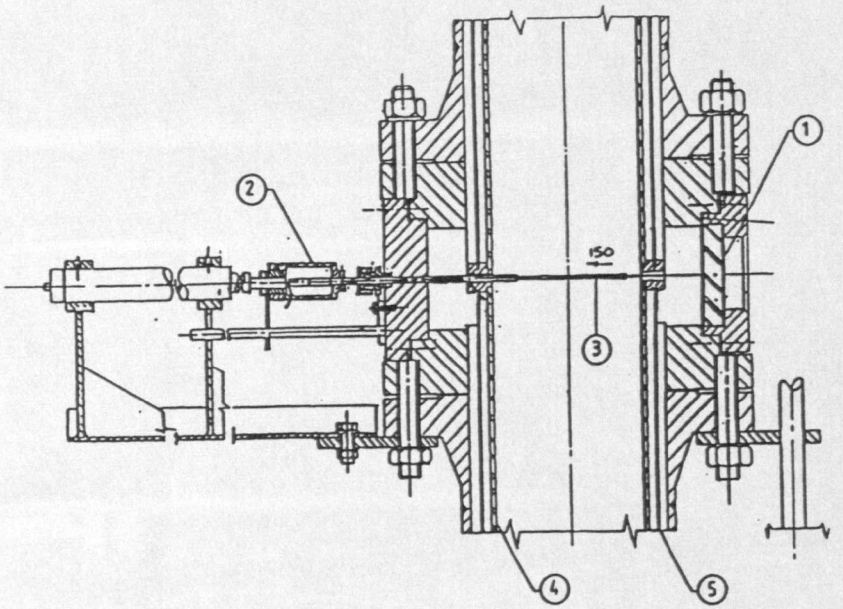

1 - Optical window
2 - Probe actuator assembly
3 - Probe
4 - Borosilicate glass tube
5 - Polished Aluminium tube

FiG (3.1b) PHOTOGRAPH OF THE KEROSINE JET FLAME RIG.

Fig(3.2) THE KEROSINE EVAPORATOR / BURNER ASSEMBLY

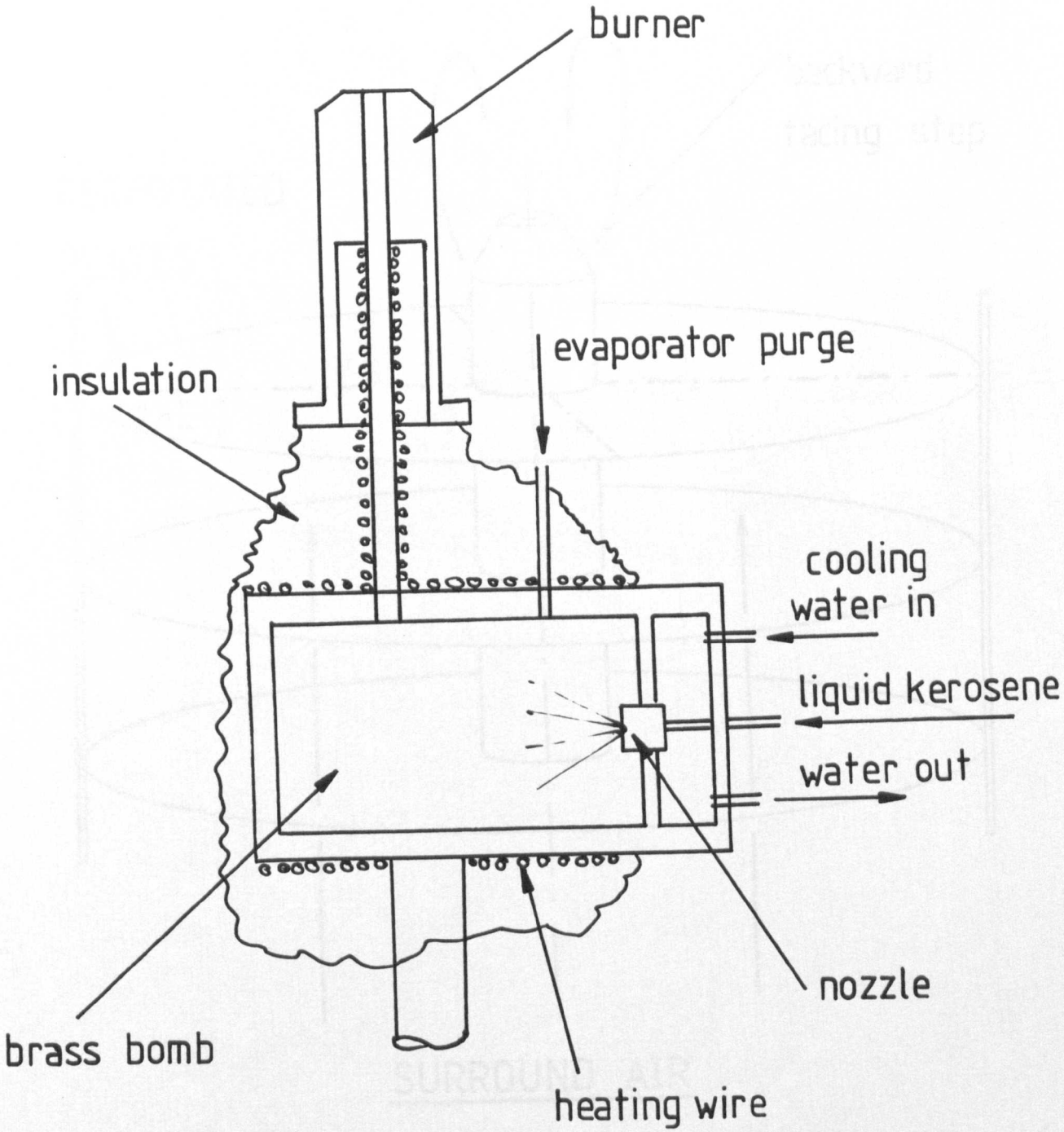

Fig(3.3) THE AIR FLOW STRAIGHTENING SYSTEM IN THE KEROSINE FLAME PRESSURE VESSEL SHOWING THE EFFECT OF THE BURNER BACKWARD FACING STEP

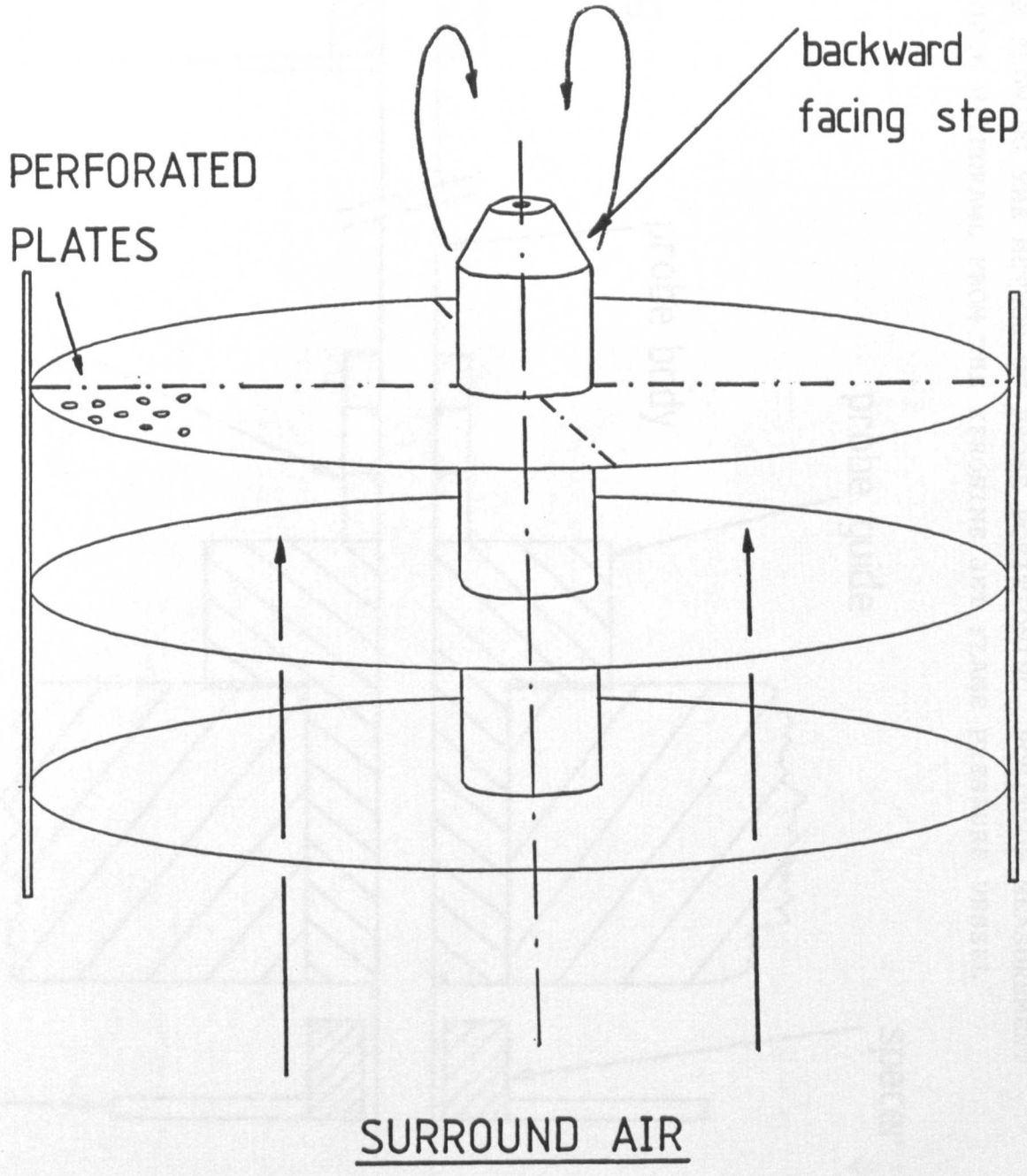

Fig(3.4) DIAGRAM SHOWING THE METHOD OF PROBE POSITIONING, POSITION MEASUREMENT AND SAMPLE WITHDRAWL FROM THE KEROSINE JET FLAME PRESSURE VESSEL

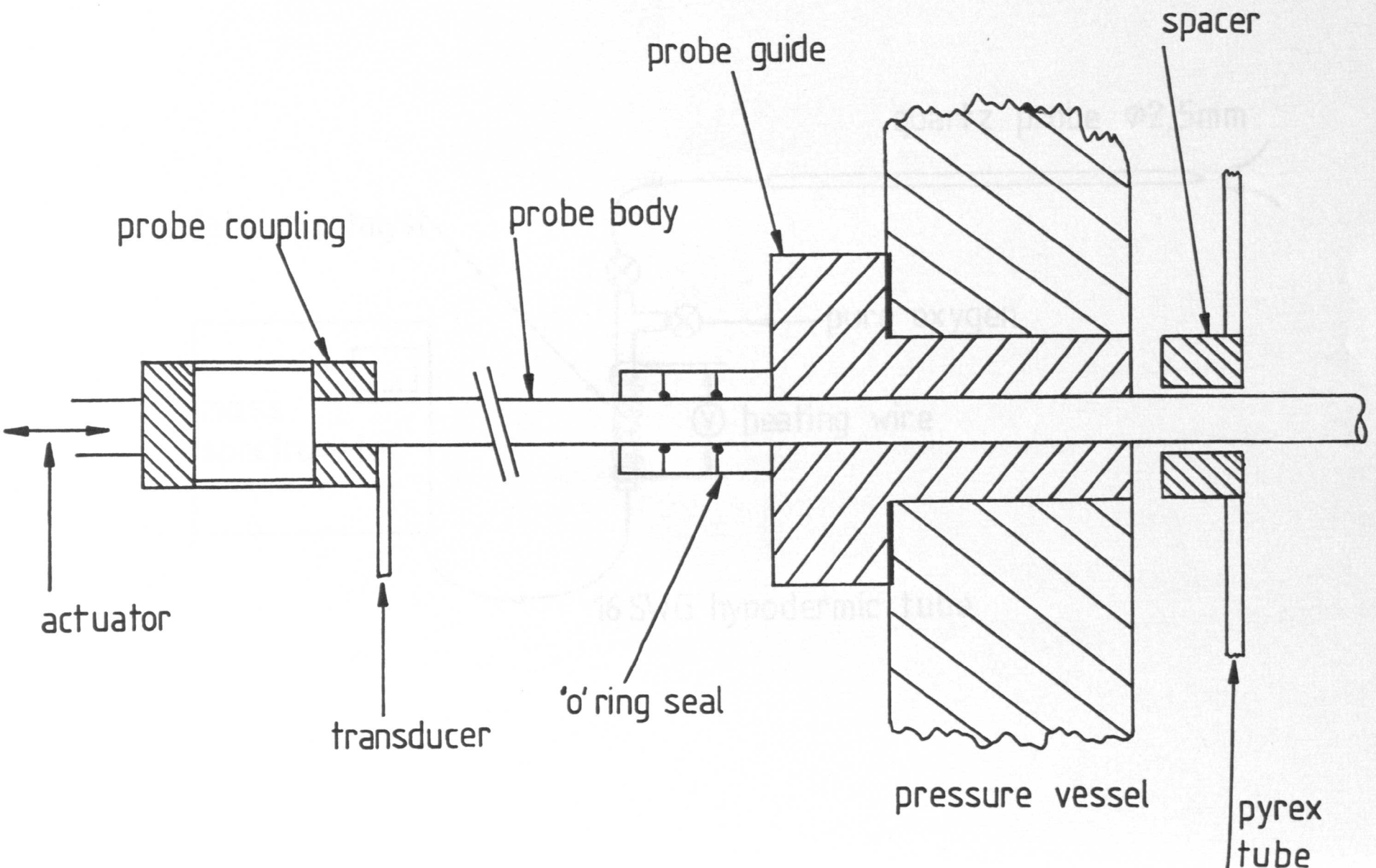

Fig(3.5) SCHEMATIC DIAGRAM OF THE MARK I MIXTURE FRACTION SAMPLING TECHNIQUE.

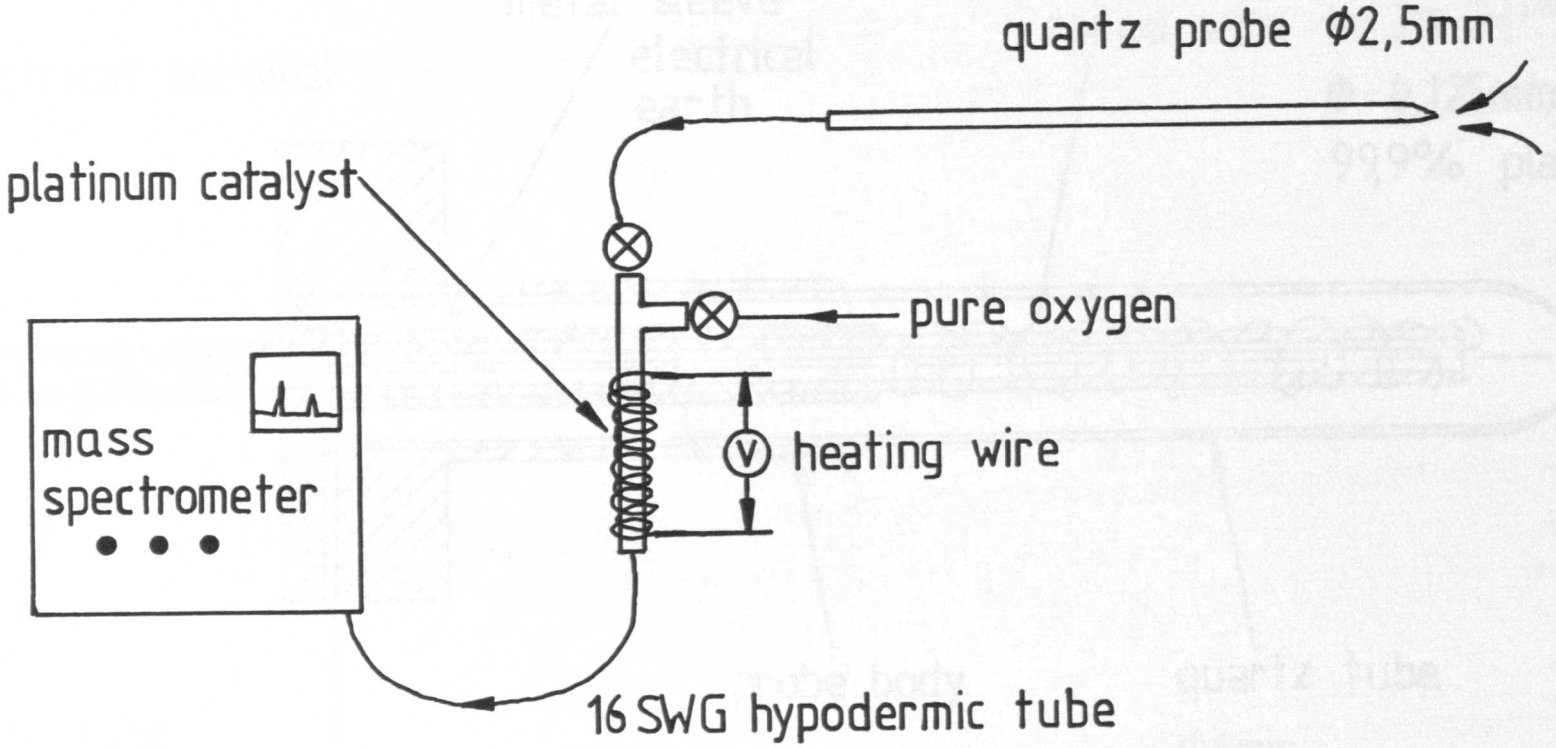

Fig(3.6) SCHEMATIC DIAGRAM OF THE MARK II MIXTURE FRACTION PROBE (gas sampling system as mark I system).

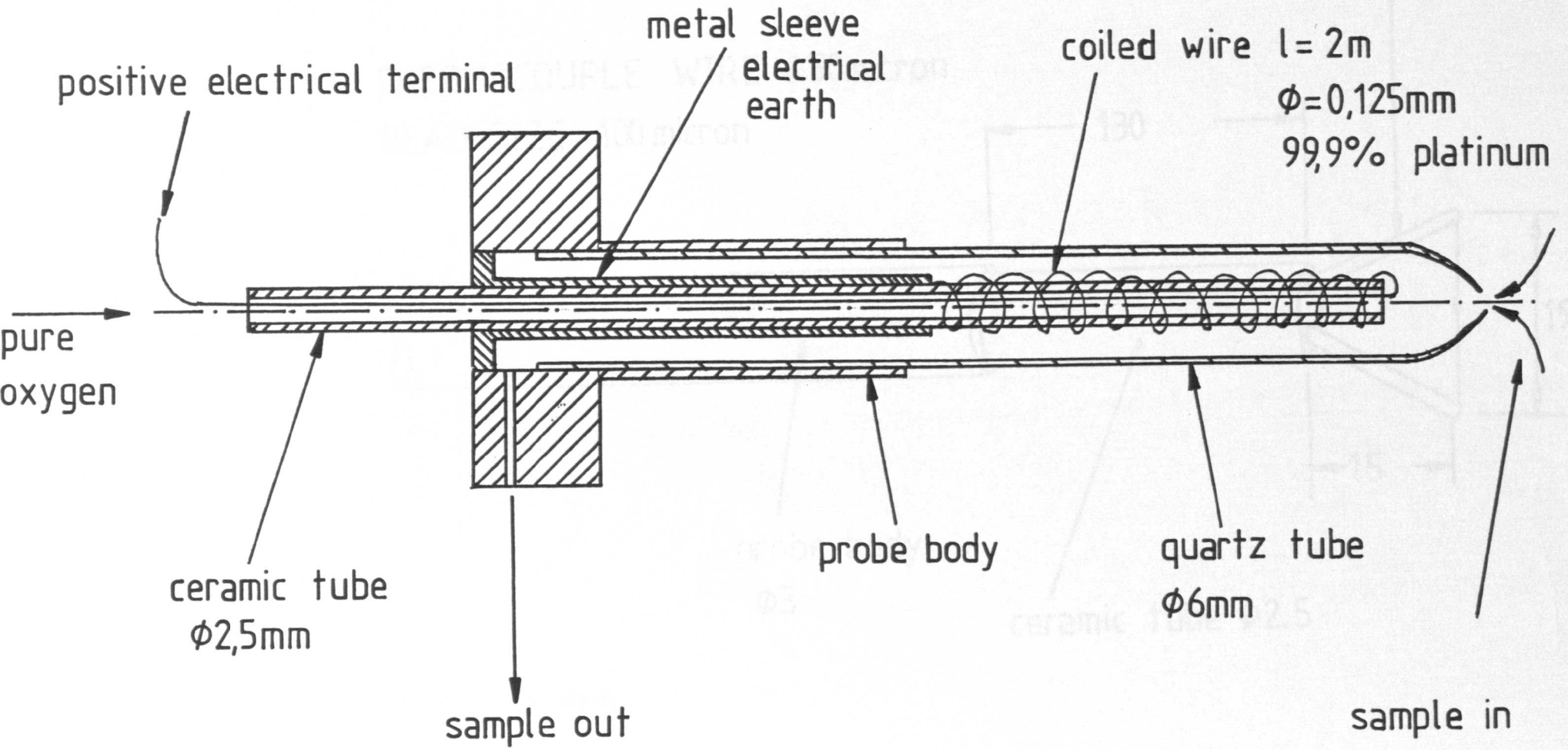

Fig(3.7) SCHEMATIC DIAGRAM OF THE BARE FINE WIRE THERMOCOUPLE MOUNTING ARRANGEMENT.

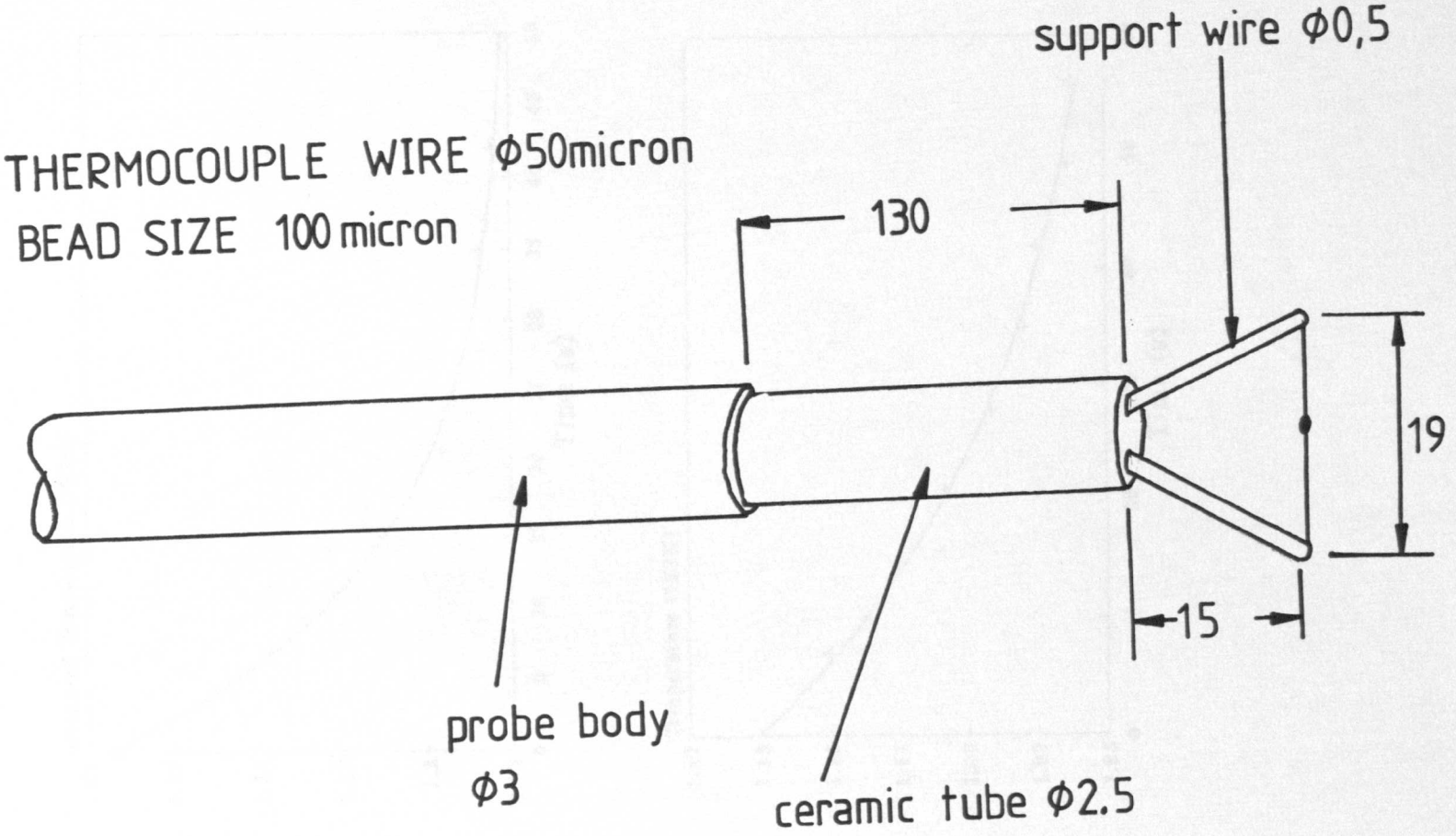

dimensions in mm

Fig(3.8) MEASUREMENTS OF TEMPERATURE AS A FUNCTION OF TIME IN HEAVILY SOOTING REGIONS OF A KEROSINE JET FLAME.

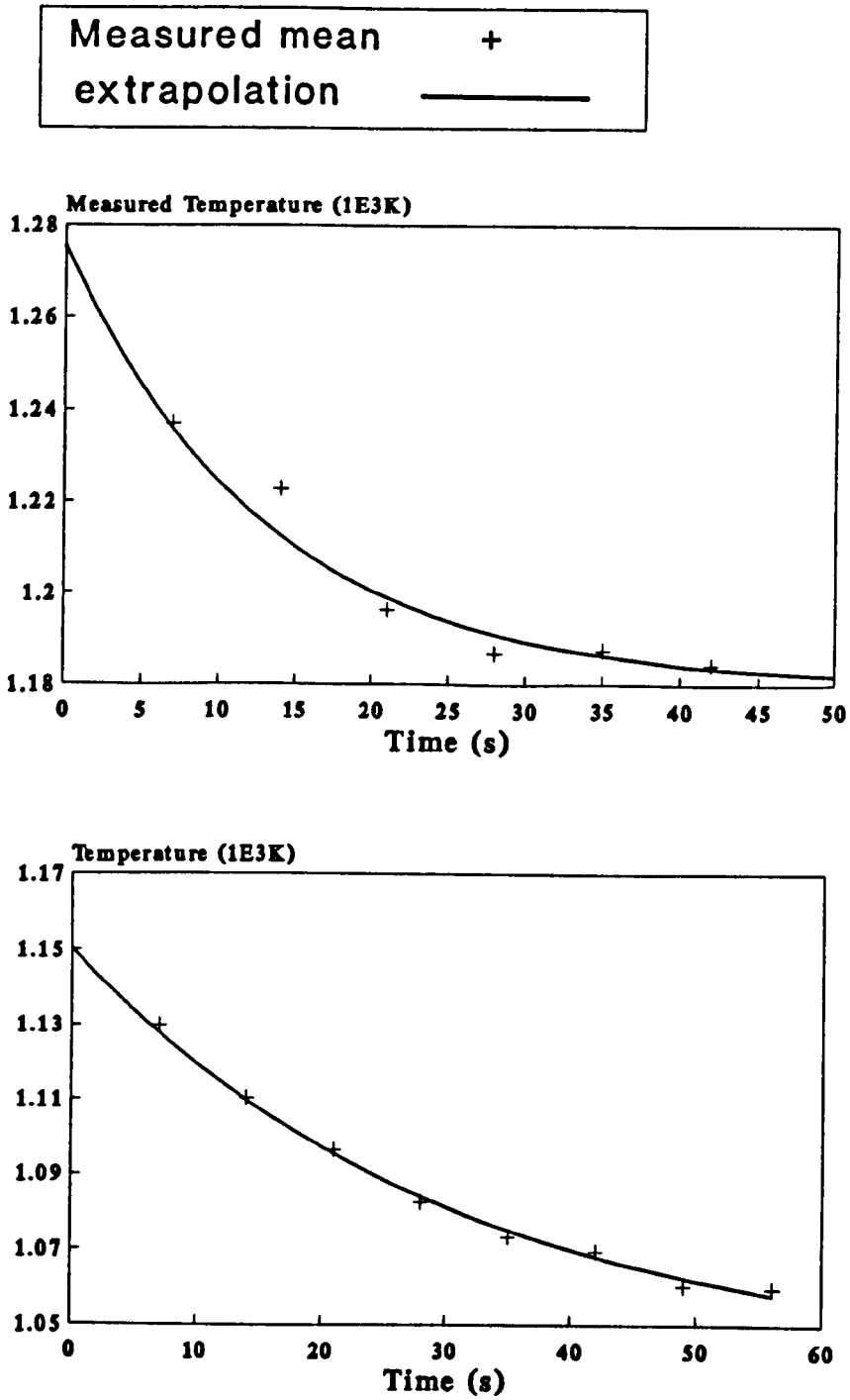

Fig(3.9) SCHEMATIC DIAGRAM OF THE LASER EXTINCTION EXPERIMENTAL CONFIGURATION.

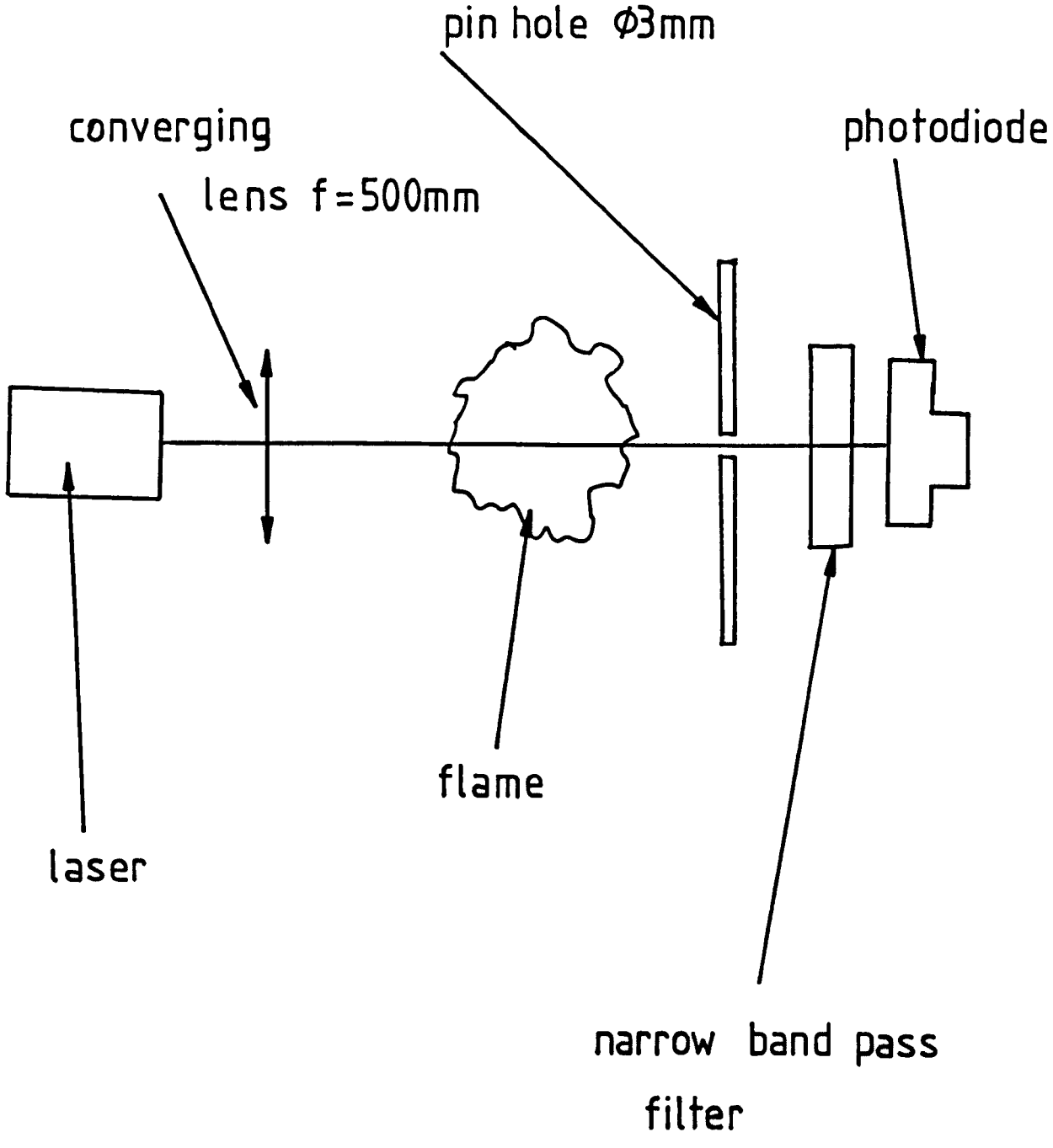

Fig(3.10) EXPECTED ERROR IN EXTINCTION MEASUREMENT RESULTING FROM UNCERTAINTIES IN THE VALUES OF UNATTENUATED AND BACKGROUND LIGHT INTENSITY BASED UPON WORST CASE ESTIMATES.

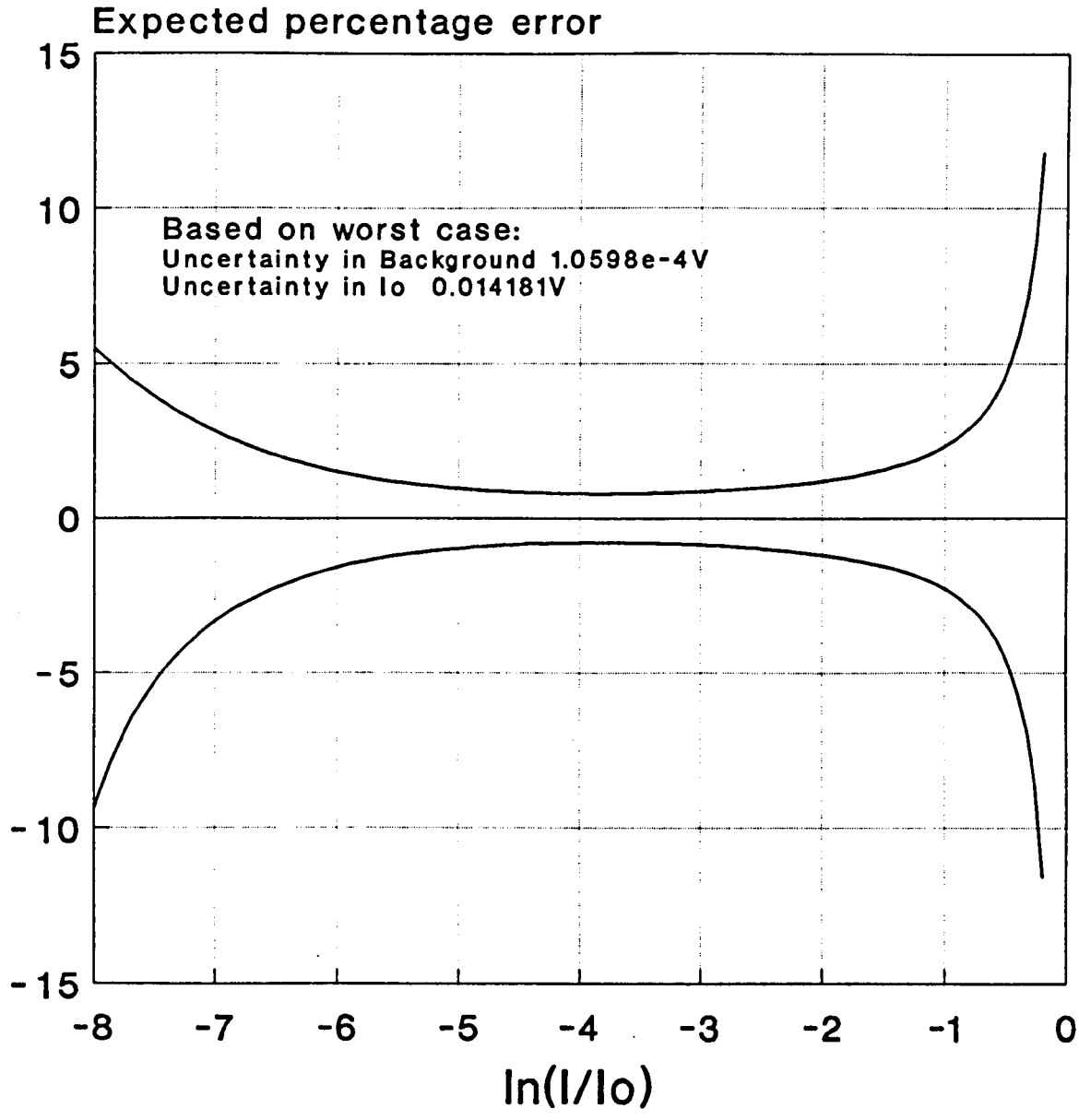

Fig(3.12) PERCENTAGE ERROR ASSOCIATED WITH MAKING THE ASSUMPTION THAT PARTICLES ARE SMALL WITH RELATION TO THE WAVELENGTH OF LIGHT

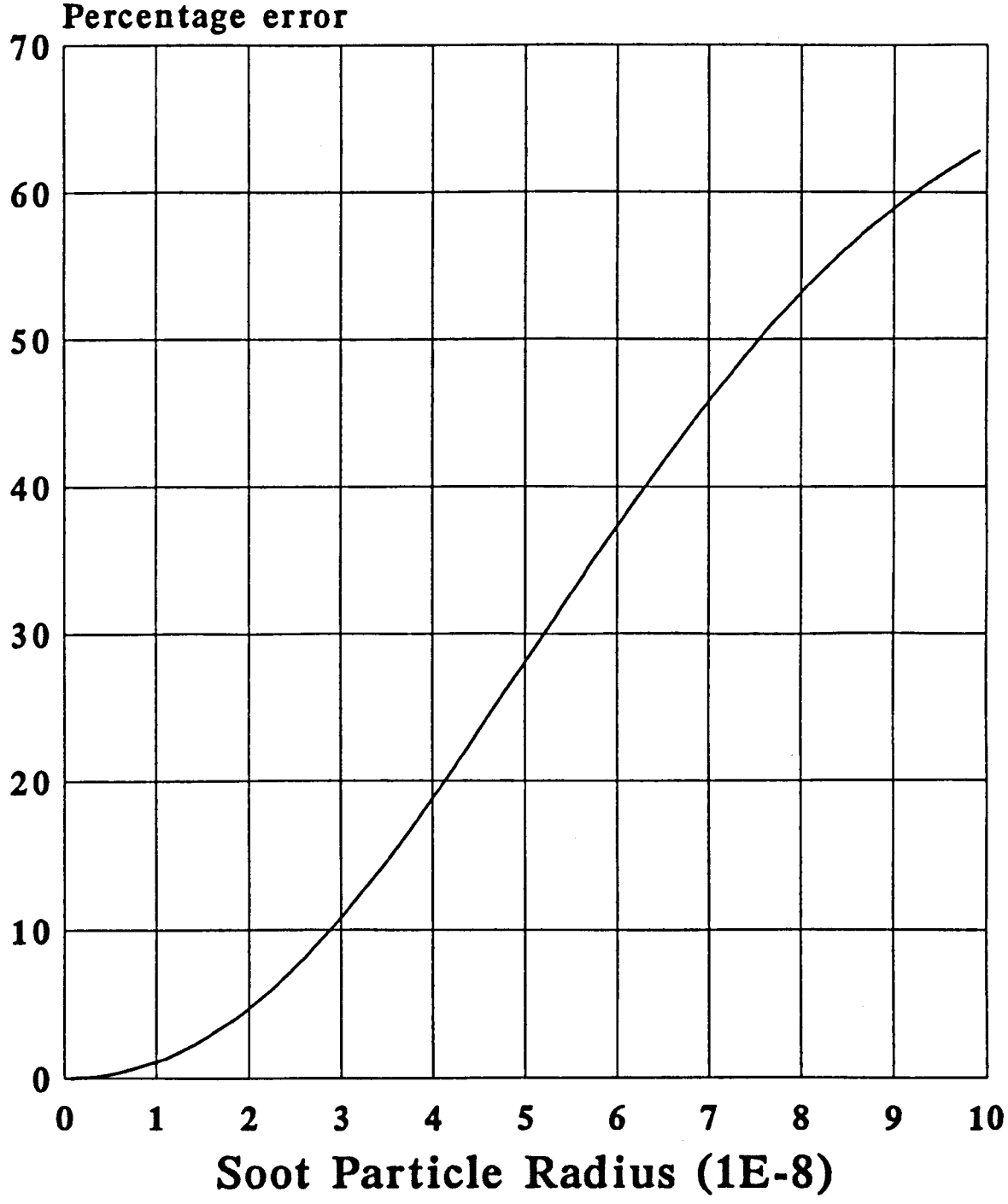

Fig(3.13) GRAPH OF THEORETICALLY DERIVED D.W.E.E. RATIO VS. PARTICLE DIAMETER FOR THE WAVELENGTH PAIRS 632.8 / 457.9nm AND 632.8 / 514.5nm ASSUMING A MONODISPERSE PARTICLE SIZE DISTRIBUTION

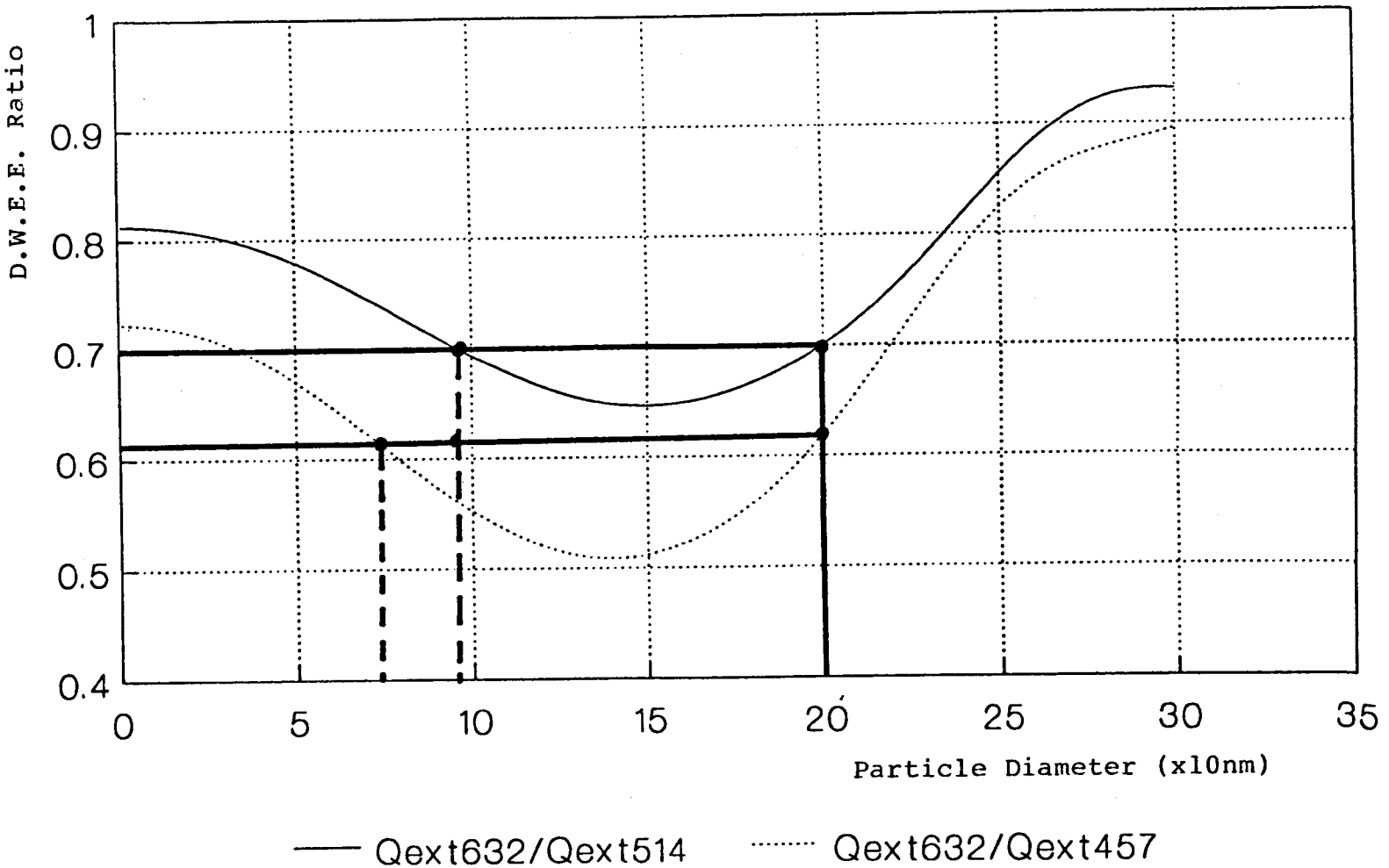

Complex Refractive Index = 1.92 - 0.45i
(Mullins and Williams 1986)

Fig(3.14) SAMPLE DATA SET USED IN THE MULTICOLOUR EXTINCTION SENSITIVITY ANALYSIS

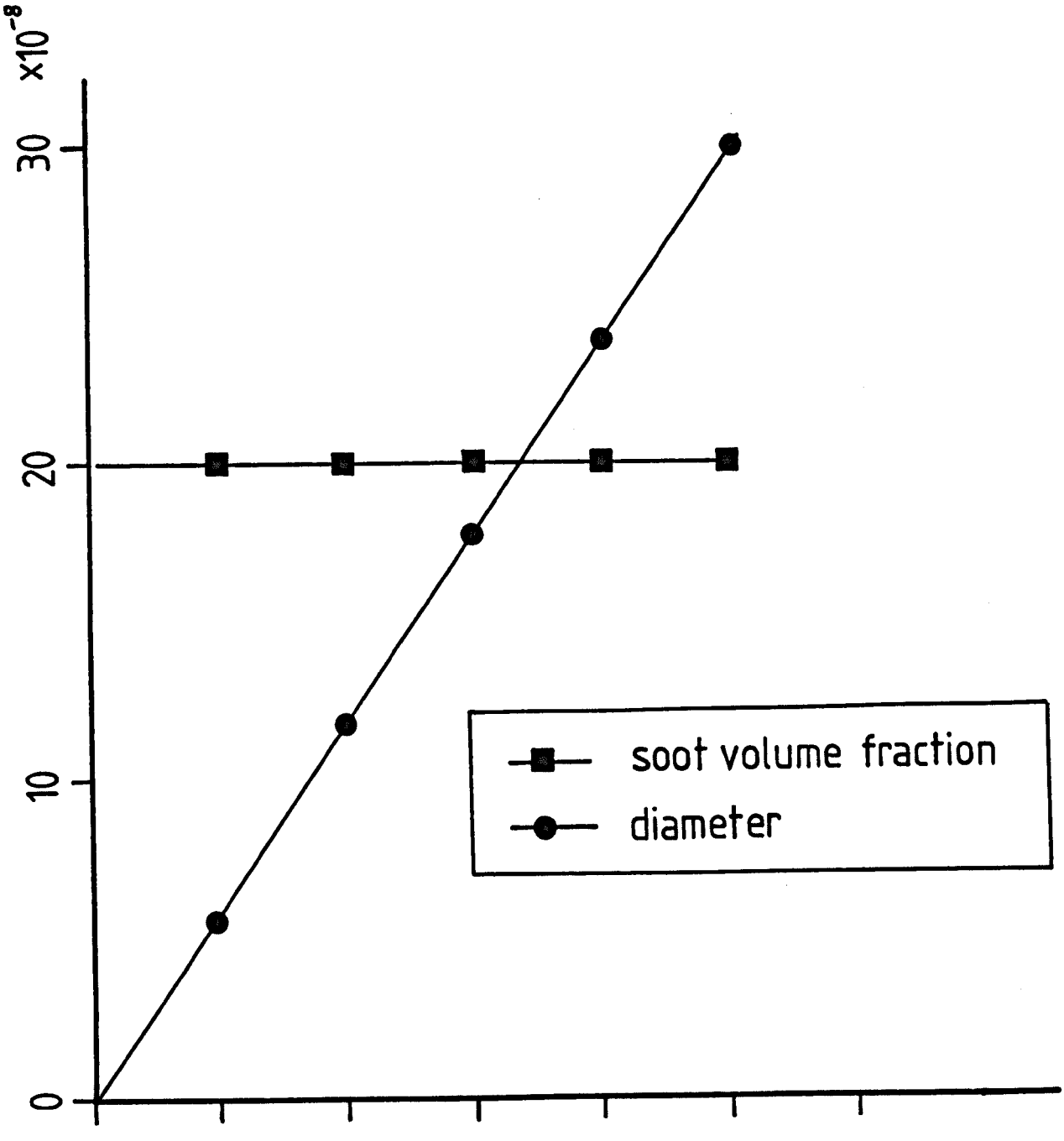

Fig(3.15) RESULTS OF THE SENSITIVITY ANALYSIS OF THE MULTICOLOUR EXTINCTION PARTICLE SIZING TECHNIQUE SHOWING THE EFFECTS OF WRONG PRESCRIPTION OF THE COMPLEX REFRACTIVE INDEX OF SOOT.

REAL COMPONENT PERTURBED BY +2%

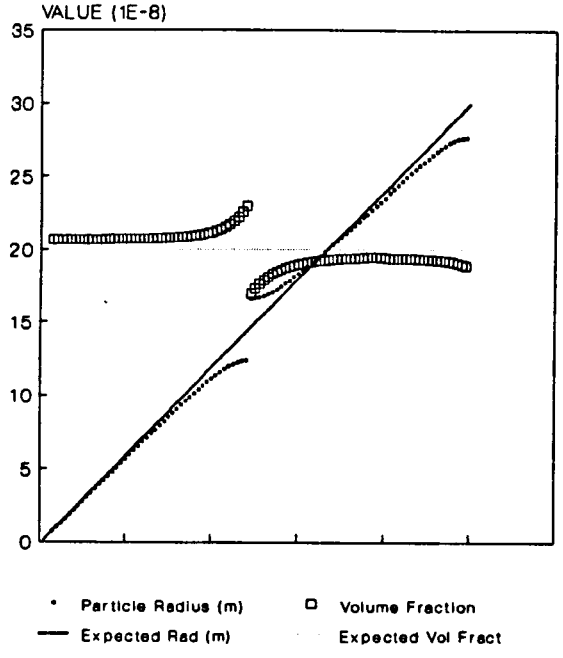

REAL COMPONENT PERTURBED BY -2%

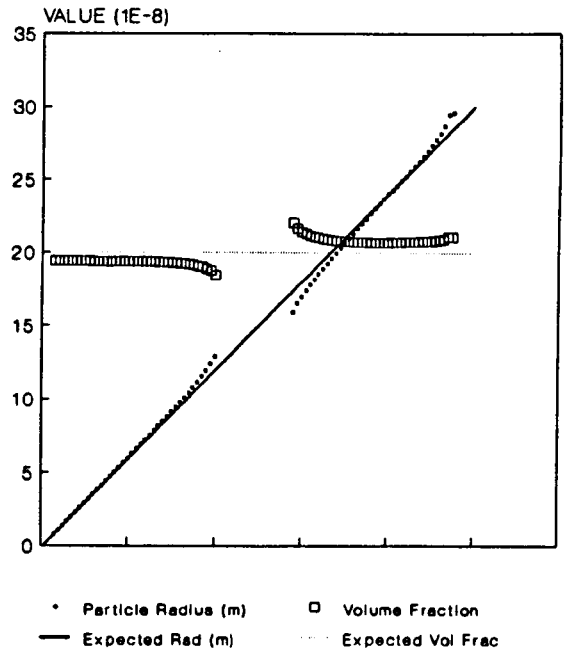

IMAGINARY COMPONENT PERTURBED BY +20

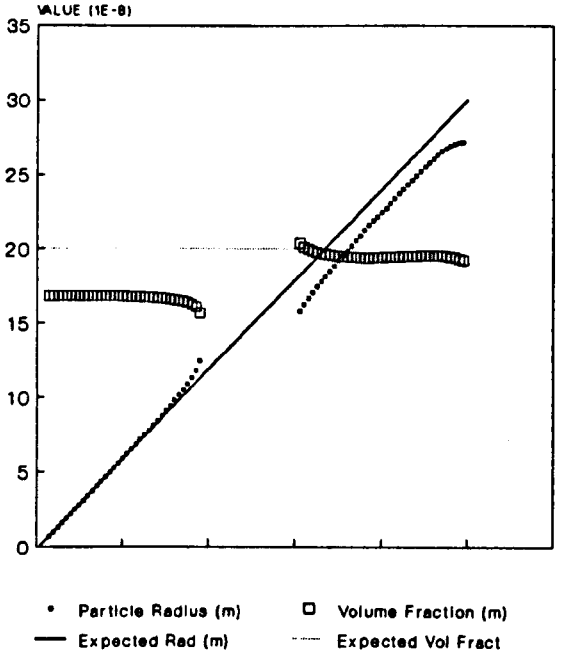

IMAGINARY COMPONENT PERTURBED BY -20%

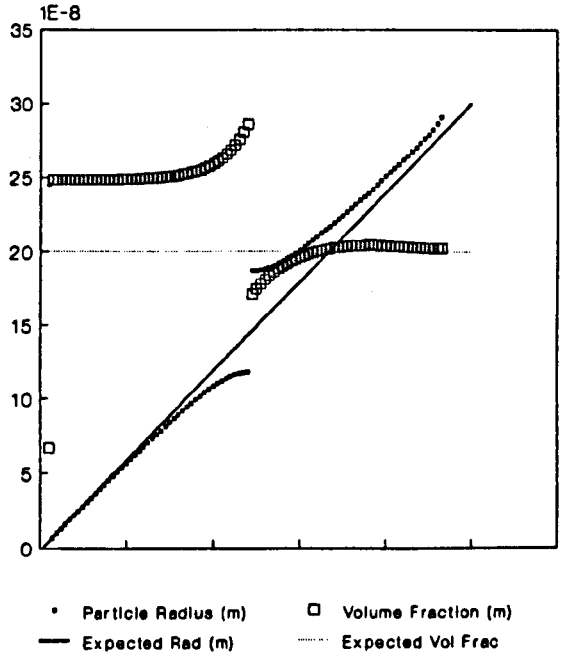

Fig(3.16) PROFILES OF D.W.E.E ASSUMING A VARIETY OF PARTICLE SIZE DISTRIBUTION ASSUMPTIONS AND VALUES OF COMPLEX REFRACTIVE INDEX

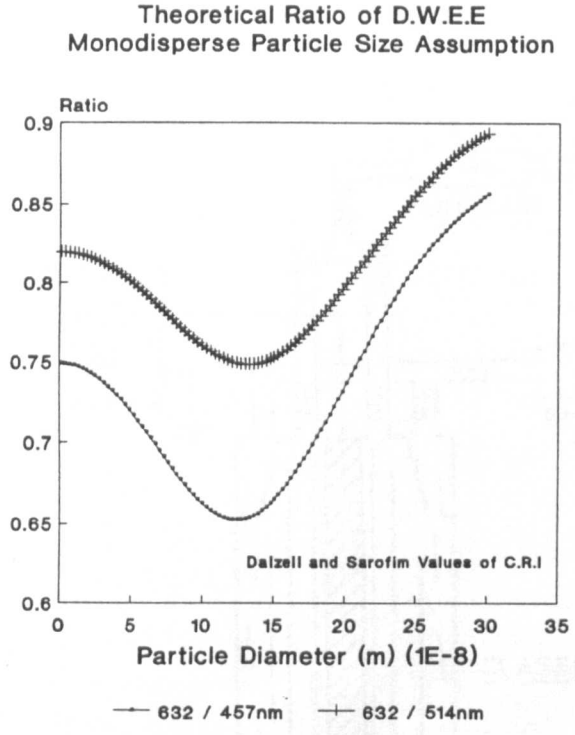

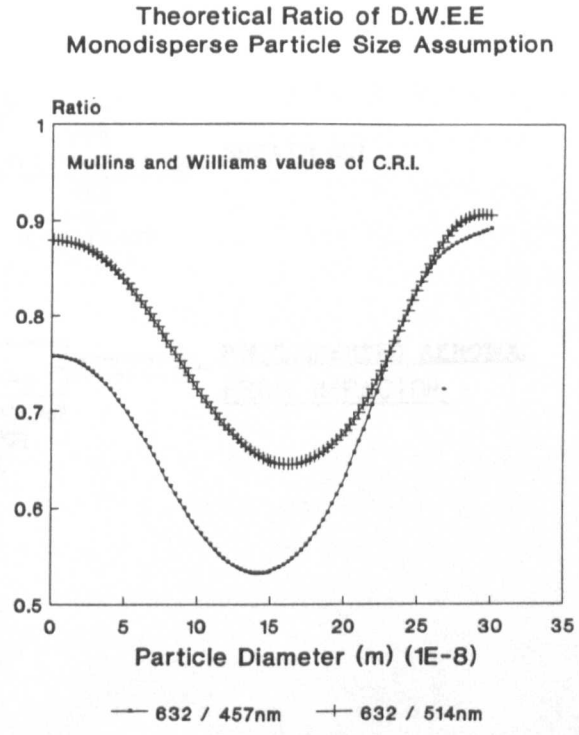

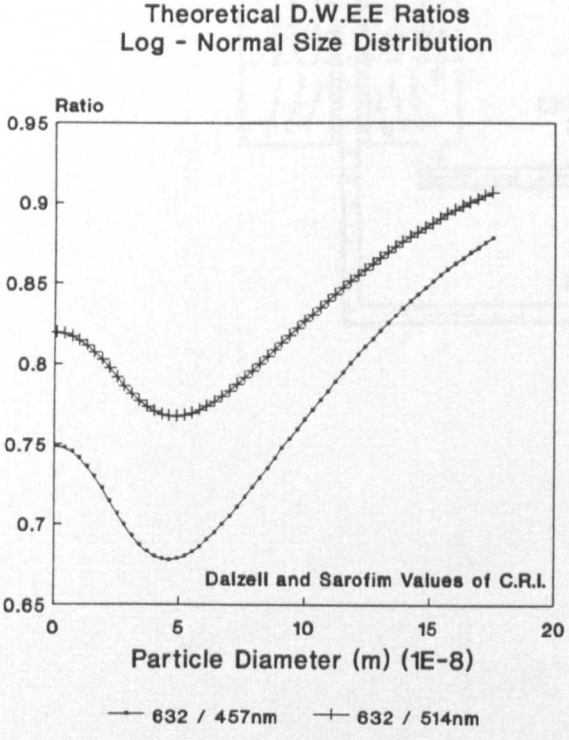

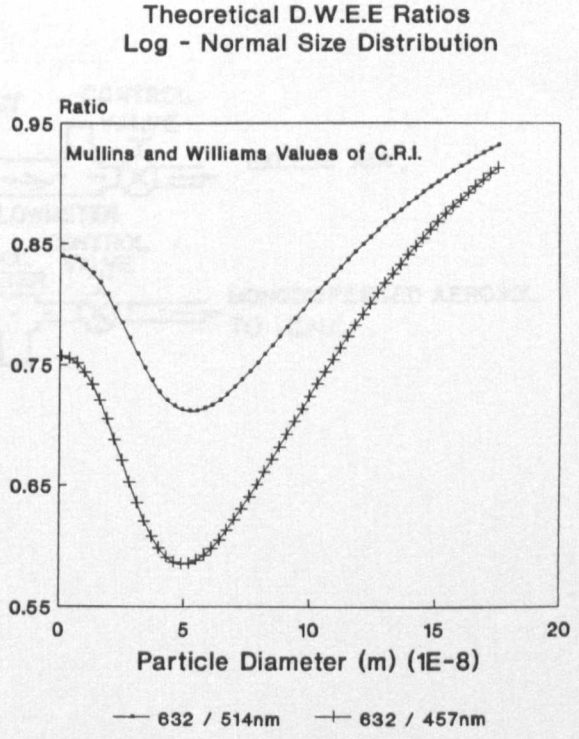

Fig(3.17) SCHEMATIC DIAGRAM OF THE MAIN COMPONENTS IN THE T.S.I. inc. DIFFERENTIAL MOBILITY PARTICLE SIZER. (cited from the operations manual)

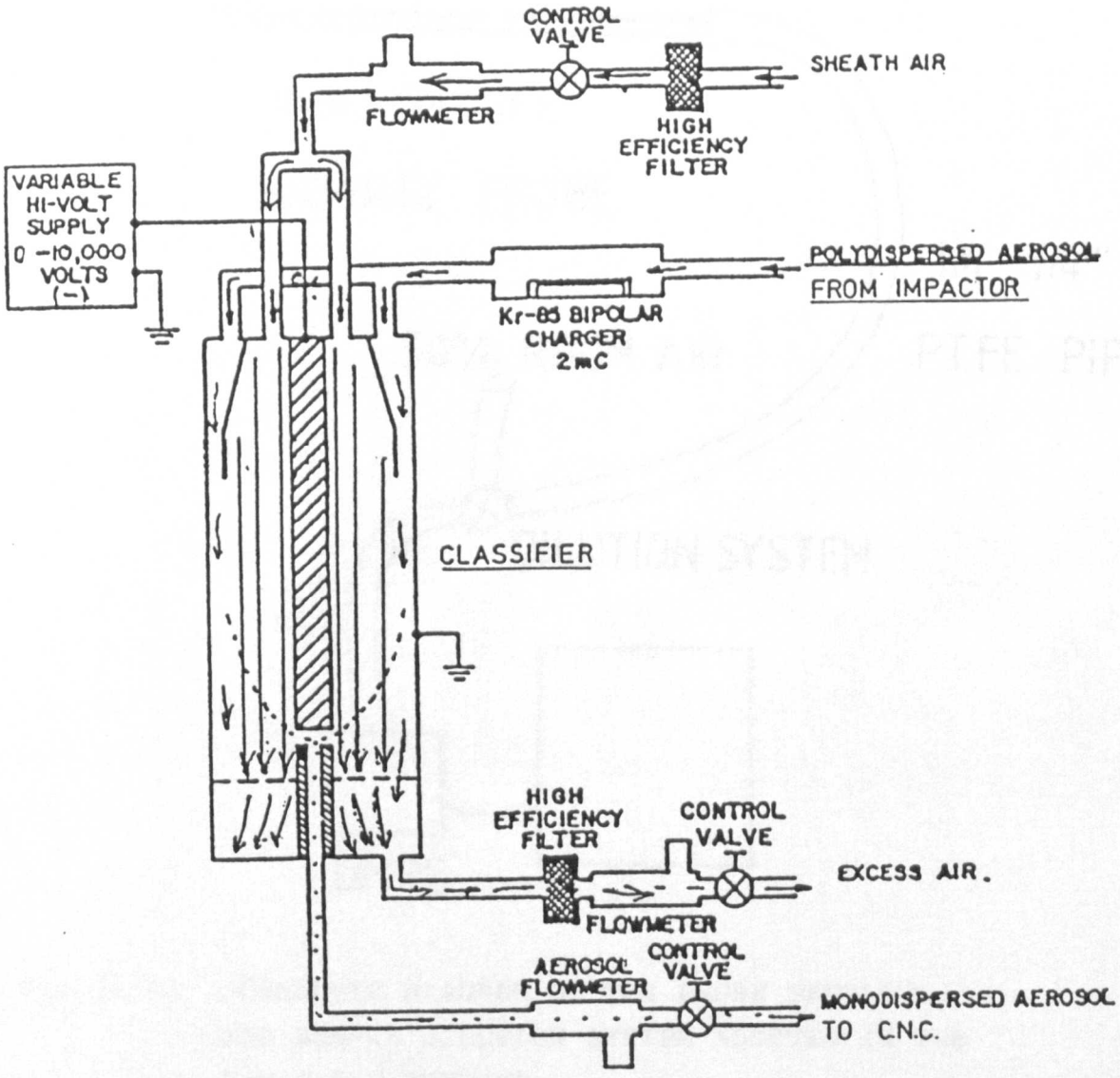

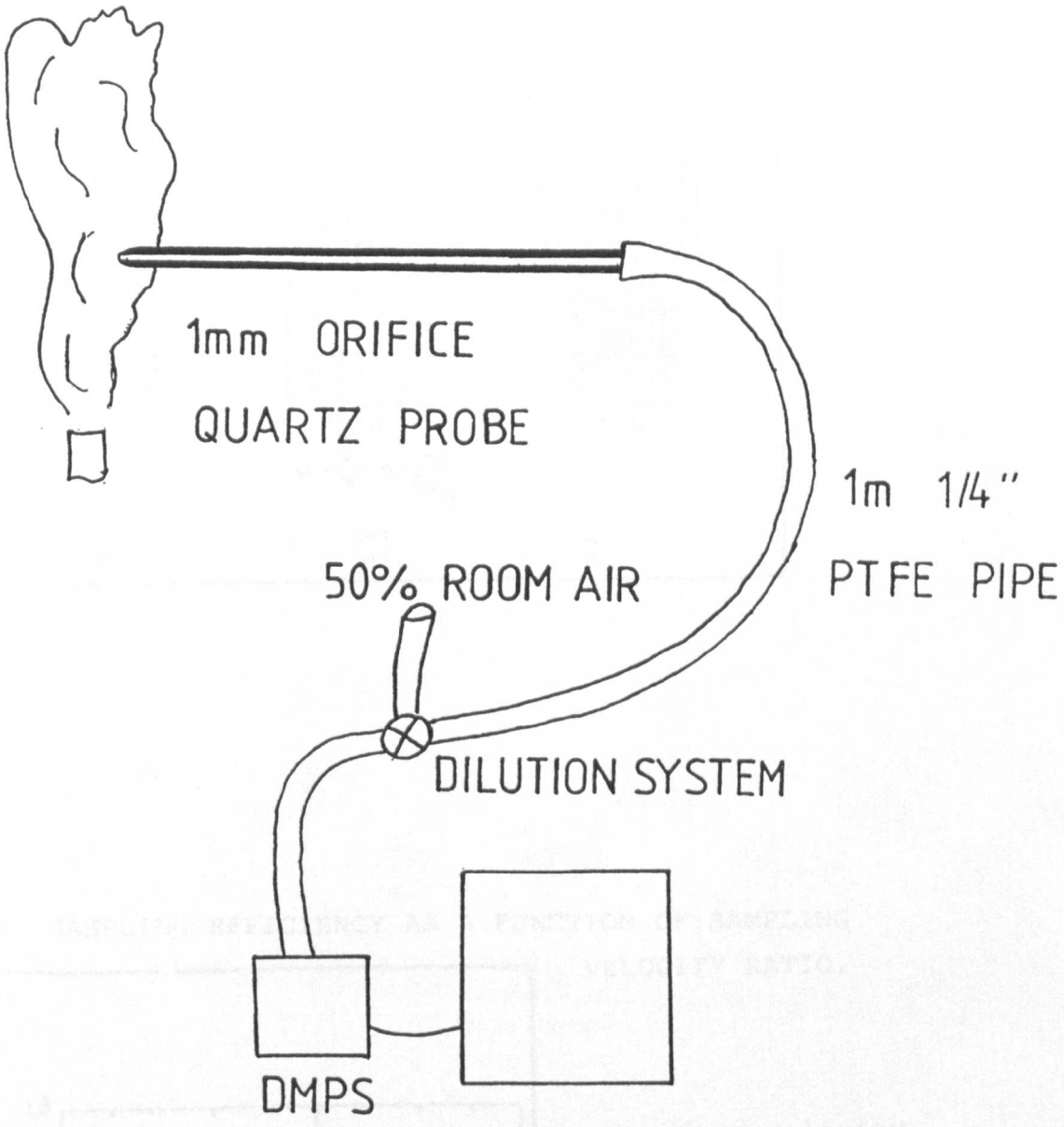

Fig(3.18) SCHEMATIC DIAGRAM OF THE PROBE SAMPLING AND SAMPLE DILUTION SYSTEM ADOPTED IN THE D.M.P.S. STUDIES.

Fig(3.19) THE EFFECTS OF ANISOKINETIC SAMPLING ON THE AEROSOL SAMPLE GAINED (cited from Fissan)

(a) ANISOKINETIC SAMPLING OF AEROSOLS.

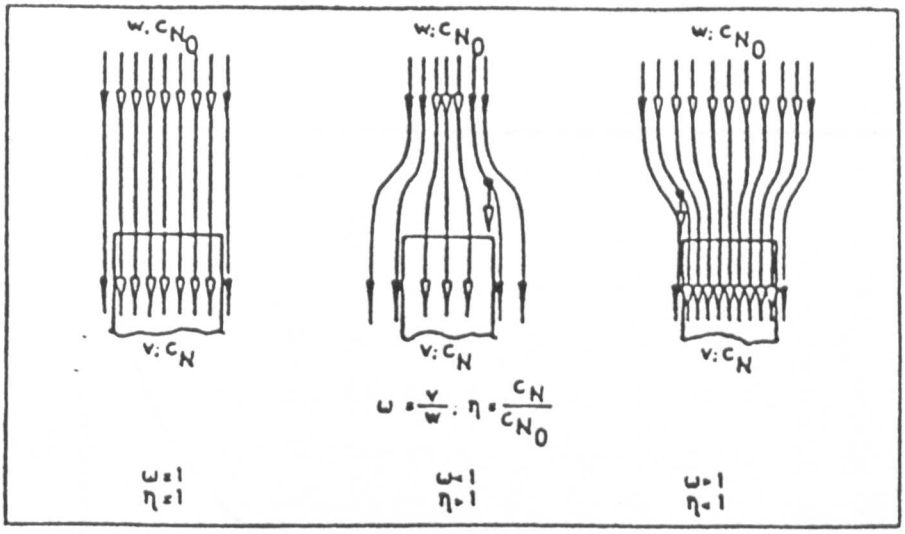

(b) SAMPLING EFFICIENCY AS A FUNCTION OF SAMPLING VELOCITY RATIO.

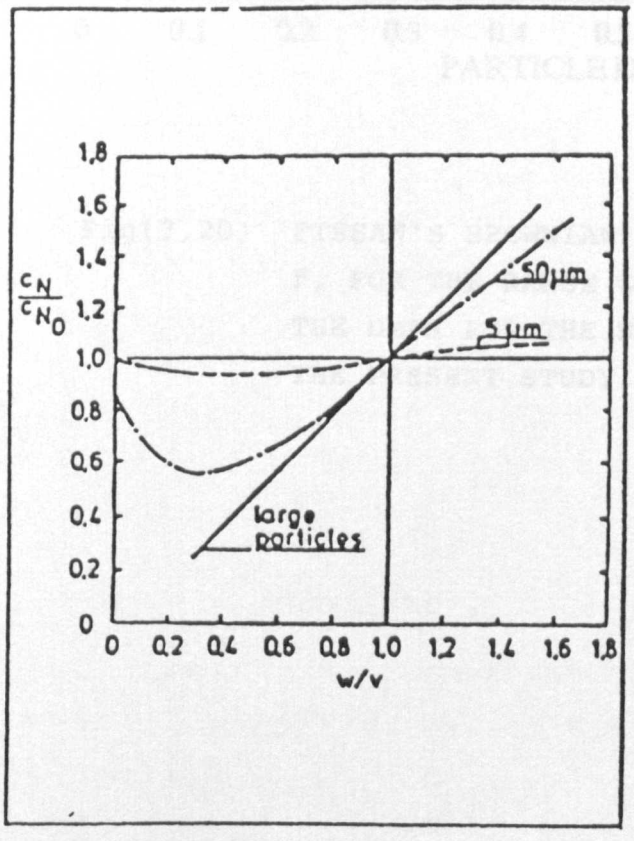

W = face velocity

V = suction velocity.

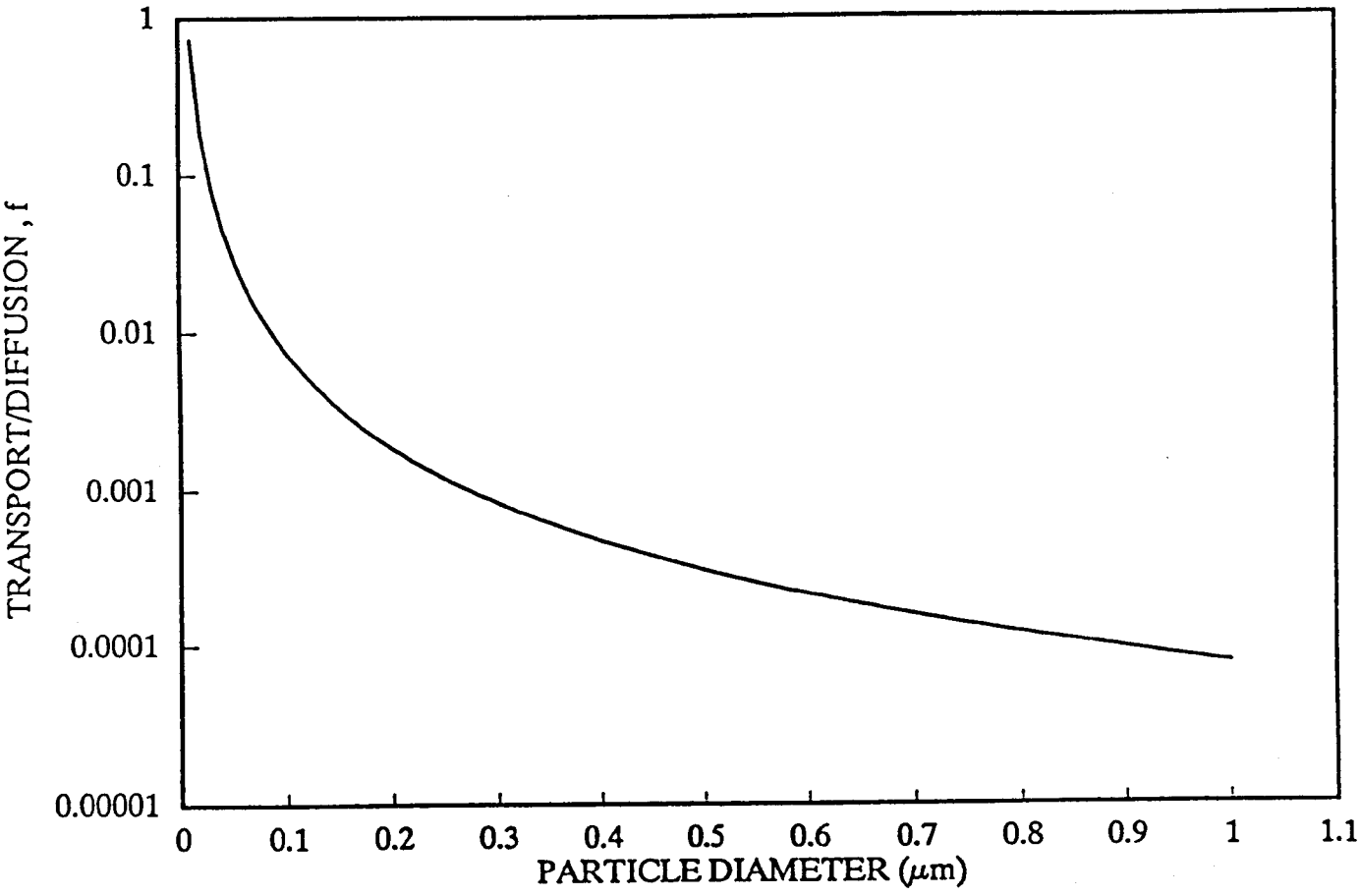

Fig(3.20) FISSAN'S BROWNIAN DIFFUSION SETTLING PARAMETER, f, FOR THE RANGE OF DIAMETERS MEASURABLE BY THE DMPS FOR THE SAMPLING GEOMETRY USED IN THE PRESENT STUDY.

CHAPTER 4: EXPERIMENTAL RESULTS

This chapter describes the application of the experimental techniques described in chapter 3 to the free ethylene and confined vaporised kerosine jet flames studied here.

4.1 ETHYLENE JET FLAME

All the experimental results reported in this section were taken from a vertical jet flame of ethylene issuing into stagnant atmospheric air surroundings. The burner diameter was 3.1mm with a fuel flowrate of 14g/min. Assuming a top hat velocity profile, this corresponded to an exit velocity of 24.5m/s and Reynolds number $\simeq$ 8600 (viscosity, μ, of ethylene @1atm,20°C = 10.08kg/ms Weast 1973) . The flame had a visible height of approximately 0.65m with the first visible soot occurring at the 50mm height.

The choice of burner flowrate was based entirely upon stability. The maximum possible flowrate allowable before the flame became unstable and lifted off was chosen. It was found that stability was improved if the burner was surrounded with a cylindrical piece of fine gauze. This had the effect of shielding the very fragile first few centimetres of the flame from small air movements in the laboratory. A much more efficient method of improving stability was the co-annular stabilising flame technique used in the later kerosine studies. The gauze was utilised in this pilot study, however, due to the resulting simplicity of burner design.

The flame was ensured to be vertical by means of two plumb lines suspended near the flame at 90° to each other. The burner was adjusted such that, when viewed, its axis was coincident with the axis of both plumb lines.

4.1.1 SOOT MEASUREMENT

Of the three methods of soot measurement attempted on the various flames in the present study two were utilised on the turbulent ethylene flames. They were the Rayleigh extinction and DMPS techniques.

4.1.1.1 RAYLEIGH EXTINCTION

The experimental configuration has been described in the previous chapter and incorporated a helium neon laser light source (λ = 632.8nm). Before any measurements of average extinction were made, the size of the sample necessary to give a stable mean value was investigated. A simple program was written to be used in conjunction with the datalogging system to monitor the laser intensity and calculate its running average. The time that was necessary to give an average that was independent of increased sampling time was thus found. In all locations in the flame, a 7 second average proved sufficient with a large factor of confidence. Using an assembly language datalogging program (rather than the slower BASIC) with a BBC master computer and an Oasis MADC12 analogue to digital converter, this corresponded to approximately 40,000 measurements.

At the time of making the extinction measurements in the ethylene flames, the significant discrepancy between the value of $[\ln(I/I_o)]_{mean}$ and $\ln(I_{mean}/I_o)$ was not appreciated. Unfortunately, in the ethylene study, it was the latter of these two parameters that was measured, the former being the required value. The discrepancy is dependent entirely on the degree of fluctuation in the sample. This was investigated more thoroughly on the atmospheric kerosine flame (See section (4.2.2)), but could be as great as 7%.

RESULTS

Shown in fig(4.1) is the result of the centralising and curve fitting procedure for two representative axial locations in the flame, X = 100 and 300mm. These two cases represent the locations at which the measured extinction is respectively at a minimum and a maximum. At the 100mm height the peak value of I/I_o is of the order 98.5%, whereas for the 300mm height this value is 67%. Referring to the analysis of the extinction procedure (section 3.6.1), the expected error is therefore much greater for the 100mm case.

As can be seen, the profile at the 100mm height does have increased scatter especially in the edges of the flame, where extinction tends to the zero level. This results in some uncertainty in the position at which the extinction dies to the zero level and the fitted line passes through the centre of the measured data. Of note is the fact that at the edges of the 300mm height profiles, the value of $\ln(I_o/I)$ attains values of similar magnitude to those in the 100mm height profile. The degree of uncertainty as a result, however, is less significant due to the increased peak extinction.

The deconvoluted turbidities were processed assuming a complex refractive index of 1.92-0.45i. This value was reported by Mullins and Williams 1987 - see chapter 3.

Radial traverses were made at eight axial locations, 100mm (x/D=32.2), 130mm (41.9), 160mm (51.6), 200mm (64.5), 250mm (80.6), 300mm (96.8), 350mm (112.9), 450mm (145.2). Data at four of these locations is shown in fig(4.4). The data plotted against axial position is shown in fig(4.5). The peak mean soot volume fraction is displaced from the centreline at the low heights. The centreline values increase very rapidly with height until at 300mm the peak has reached the flame axis. The overall peak measured value of 2.1×10^{-6} also occurs at this location. This value is approximately 23% of that reported by Moss et al. (1987) in laminar flames of the same fuel and oxidant.

4.1.1.2 DIFFERENTIAL MOBILITY PARTICLE SIZER ANALYSIS

The description of the DMPS technique is described in chapter 3. The DMPS was in principle capable of measuring soot size distribution in an aerosol for the size range between 0.017 and 0.886μm. Two types of information are accessible to the DMPS, the number of particles of a given diameter per unit volume of aerosol and the size distribution of the particles. However, due to lack of calibration of the dilution system, absolute number concentration information was lost. The probe used was made of quartz with an outside diameter of 4mm and an orifice size of 1mm.

RESULTS

Shown in fig(4.2) is a typical soot particle size profile obtained using the DMPS. The abscissa has a logarithmic scale of particle diameter which varies between the minimum and maximum range of the instrument, the ordinate is number density of particles. The scale 'Particle diameter' is not strictly correct given the irregular shape of soot particles. Rather, the scale should read 'Stokes-drag mean diameter' as explained in the previous chapter.

Fig. (4.2) is an ensemble of all the profiles measured successfully in the turbulent ethylene jet flame. As can be seen the centreline of the flame was explored extensively in the lowest regions where soot formation is predominant, although in this region probe aerodynamic disturbance will be the greatest. There are fewer measurement points between the 200 and 400mm axial heights since the soot volume fraction in this region is high (order(10^{-6})) and problems with probe blockage were encountered. Also shown are measurements at various radial positions at the 130mm and 450mm heights.

This diagram qualitatively shows the development of the particle profiles with height and radius very clearly. The first measurable particles on the centreline occur at the 25mm height. These are 0.017μm in diameter (the lower range of the instrument).In this region of the flame, the characteristic yellow emission from the soot is negligible compared with the

blue emanating from the CH and OH radicals. The first visible soot emission occurs at the 50mm height, by which time the measured particle size has increased dramatically and the small particles have disappeared. The profiles between the 200mm and 400mm height show some unusual features such as double peaks. These profiles were subject to some error due to probe blockage, as described earlier, and hence little confidence can be placed on them.

In fig(4.3), mean soot size is compared with 'Rayleigh extinction' soot volume fraction along the flame axis. This figure shows the mean soot diameter increase until a maximum of 0.4μm is reached at the 350mm height. The trends shown by the diameter mirror those of soot volume fraction reasonably well as might be expected since the two variables are intimately linked. However, the size of the particles seem to be a great deal larger than most that are quoted in the literature - see the general conclusions of this chapter.

4.1.2 MEAN TEMPERATURE

As with the laser extinction technique, the size of sample necessary when making mean temperature measurements with thermocouples was tested first. Using the same technique it was found that a 5 second average (corresponding to 30,000 measurements) was sufficient to give a stationary mean value. The smaller sample necessary was assumed to be due to the thermal inertia of the small thermocouple bead (d $\simeq$ 100μm).

The same datalogging arrangement was used, but due to the non-linear calibration of the thermocouple voltage with temperature, more sophisticated software was necessary. The thermocouple calibration was digitised and stored in a tabular form in the computer's memory. Each value of measured thermocouple voltage was then referenced to this calibration in order to derive the temperature.

The mean temperature profiles were also centred about the flame axis. This effectively doubled the resolution of measurements when plotted against radius and acted as a check that the profiles were axisymmetric.

Thermocouple blockage was minimal in comparison to the kerosine flames, but, in regions of peak soot volume fraction it was necessary to clean the probe of a small deposit between readings. At all axial heights in the flame, this could be achieved by moving the probe to a hot, oxygen rich location.

RESULTS

Radial Traverses of mean temperature were made at the same eight locations as the laser extinction. Repeatability was again very good.

The radiation corrected mean temperature - see chapter 3 -, plotted against radial position, for four representative axial heights are shown in fig(4.4). The results plotted against axial height are shown in fig(4.5). Radial profiles of mean temperature at the lower heights (< 200mm) reveal sharp peaks, corresponding to the flame zone away from the centreline. The peak mean temperature declines from a value of 1982K at the lowest height investigated (100mm) and gradually migrates towards the centreline. At the 350mm height, the value has reached the centreline but has broadened and declined to 1639K.

4.1.3 MEAN MIXTURE FRACTION

The experimental configuration used throughout the ethylene studies to make mean mixture fraction measurements was the mark I probe system (described in the previous chapter). The probe used had an outside diameter of 4mm with an orifice of 200μm. The small orifice size, compared with that used with the DMPS, was made possible due to the small volume flow rates required by the mass spectrometer.

Problems with probe blockage (mainly by deposition of soot in the inside passages of the quartz) were encountered in the regions of high soot concentration. This was identified by a sharp drop in the measured values of the [14] and [44] peaks on the spectrometer. In this case, the flowrate of the ethylene was reduced to allow a hand held butane blow torch to be played onto the probe, burning off the soot. Once the probe was clean again, the test was resumed.

RESULTS

A traverse was made of the flame centreline and radial traverses were made at eight radial locations (50, 100, 160, 200, 250, 350 and 450mm). The aerodynamic disturbance due to the probe was most severe at the lower heights, but was reduced by inserting the probe at an angle of approximately 45° to the flame axis.

The degree of scatter in both the raw and centred profiles was noticeably higher for mixture fraction than either temperature or soot volume fraction. This is especially true in regions of higher soot volume fraction and was largely due to probe blockage. At all locations in the flame, every effort was made to ensure that the reading was stable before being logged. This

could take up to 20 seconds. In the regions of high soot volume fraction, however, blockage could occur on a similar timescale and so some compromise had to be made.

Four representative radial profiles of mixture fraction are shown in fig(4.4) with the axial profile in fig(4.5). All profiles have a broadly Gaussian shape, the peak always being on the axis. The peak measured value of 0.889 was made at the 50mm height, this had dropped to 0.1 by the 200mm height.

4.1.4 SUMMARY OF ETHYLENE JET FLAME EXPERIMENTAL STUDY

Measurements of mean soot volume fraction and size, temperature and mixture fraction were made on the ethylene jet flame. Of all the measurement techniques used, those requiring probe sampling, ie DMPS and mixture fraction, proved to be the most problematic.

The normalised plots of mean Rayleigh soot volume fraction, temperature and mixture fraction in fig (4.4) and (4.5) are useful in cross checking the measurements. As might be expected, at all locations, when the peak soot volume fraction occurs away from the flame axis, it is always closer to the centreline than the peak mean temperature. Also, the spread of all profiles is in extremely good agreement.

The growth of mean DMPS particle diameter and Rayleigh soot volume fraction on the axis of the flame, fig(4.3) again correlate very well, but the particle sizes are considerably larger than any reported elsewhere measured mechanically or optically. Discussion of the possible causes of this are deferred until the conclusion of this chapter.

Another piece of information that can be gleaned from the dataset is an estimate of the fraction of total available carbon at any point which is bound in the solid phase. Local ratios of solid/total carbon can be estimated from the following relationship.

$$F_c = \frac{\rho_{soot}\overline{f_v}}{0.86\,\overline{\rho\xi}} \qquad (4.1)$$

Where $\varrho_{soot}f_v$ is the mass concentration of particulate soot, $\varrho\xi$ is the mass concentration of local mixture originating in the fuel stream and 0.86 denotes the approximate carbon fraction for the parent fuel. The mean mixture density, ϱ, was not measured directly but has been

inferred from the mean mixture fraction using a flamelet relationship. ($\varrho = \varrho(\xi)$). A plot of this fraction along the axis of the ethylene flame is shown in fig.(4.6). The peak measured value of F_e on the flame centreline is 0.25. The implications of such values are described in the conclusion of this chapter.

4.2 KEROSINE JET FLAME EXPERIMENTAL STUDY

4.2.1 OPERATION OF THE JET FLAME PRESSURE RIG

Although the rig was quite a complex one to operate, with eight flowrates, two electrical supplies, two pressure readings and three temperatures to monitor, once stable conditions were established, they remained very stable. Also, providing the pressurising valve was not moved between runs the operating condition could be replicated from day to day with a minimum of effort.

Regarding the performance of the rig, it fulfilled all but one of its design parameters - chapter 3 - ,that one being the minimisation of radiative loss from the flames. It became clear at an early stage that radiative loss was significant and not merely redistributed within the chamber. This is discussed in more detail later in section(4.2.1.3).

4.2.1.1 OPERATING SCHEDULES

The experiment was designed to be laboratory based. It was, however, a potentially dangerous one due to the elevated pressure and the potential for unburnt mixtures of fuel and air to accumulate in an enclosed environment. For this reason, operating schedules were devised to ensure safe running. They are laid out in appendix C.

4.2.1.2 PREMIXED FLAME FLASHBACK

During the whole start up procedure, the most critical point was the establishment of the premixed flames. They were especially susceptible to flashing back during power up if too much oxygen was allowed into the mixture. This would quite often cause the main flame to extinguish. Therefore, the igniter was always kept very close to the main flame until stable conditions were reached for instant relight. If either of the premixed flames did flash back, the flow of oxygen would be stopped until the line was purged with ethylene and then re-introduced.

At higher pressures, the probe cleaner flame became extremely susceptible to flash back. So

much so that at the highest pressure at which mixture fraction measurements was possible, 3.72At., a stable flame was virtually impossible to establish. The problem was that a stable gas supply to the cleaner flame could not be achieved. Although the flowmeter and rig pressure gauge readings were steady, the flame visibly fluctuated with time. The fluctuation appeared to be caused by the presence of the main flame since, if this was turned off, the probe cleaner flame became stable. This behaviour was not replicated by the pilot flame which, once stable flowrates had been achieved, remained very steady. The root cause of this phenomenon is uncertain.

4.2.1.3 RADIATIVE LOSS

After a length of time which was dependent upon the pressure at which the rig was operating, the metal pressure casing would become too hot to touch. This obviously represented a significant heat sink considering the bulk of metal involved. After one run, close inspection of the aluminium radiation reflector revealed evidence that the metal had annealed. This would require temperatures in excess of 700°C and obviously questioned the usefulness of the shield.

As an alternative, the pyrex was wrapped with highly reflective aluminium cooking foil and radial temperature profiles at similar locations in two flames were repeated to see if there was any improvement. The two flames tested in this way were kerosine flame B @2.03bar and D @3.72bar (see "operating conditions" later in this chapter). The centred profiles are shown in fig(4.7).

Three sets of points are shown for two axial heights in each flame. Two sets are for the aluminium tube on its own to show expected repeatability and one is for the tube with the addition of the cooking foil. No clear increase in measured temperatures is seen as a result of including the foil.

Further investigation revealed that pyrex is virtually opaque at infra red wavelengths much above 2.5μm. Using Wien's displacement law (Siegel and Howell 1981), at 1200K, 50% of the energy emitted from a black body would be at longer wavelengths than this. Clearly, this contributes significantly to the radiative loss. Unfortunately, at this late stage a redesign with a different material was not feasible and so testing was continued regardless.

4.2.1.4 SOOT DEPOSITION AND BUILD UP

Given the nature of the experiment, some soot build up and deposition was inevitable. The main area of soot build up was high in the pressure vessel, well above the measurement

station at the point where the jet impinged on the pyrex walls. A layer of soot would build up here which would have to be cleaned periodically to prevent excessive growth. This would require a strip down of the rig.

A much more troublesome location where soot could grow was in the small region (0.5mm) between the main kerosine jet and pilot flame. Presumably a recirculation was generated in this region which entrained kerosine fuel and hot products from the pilot flame. In some of the high pressure runs soot would grow as a thin wafer which would ultimately block the flow or cause the jet to lean to one side. It was found that reducing the oxygen flowrate in the pilot flame, and hence the pilot temperature, would prevent this growth but obviously at the expense of the efficacy of the pilot flame.

Other locations in which soot deposition was a hindrance was on probes and pressure vessel windows. The way in which soot build up on the probes was dealt with is described in chapter 3. Deposition on the windows was slight, since they were not exposed directly to the flame, but still of concern since it could give false extinction information. Therefore, they were thoroughly cleaned of any deposit at each strip down of the rig.

4.2.1.5 OPERATING CONDITIONS

At each pressure, the operating conditions chosen were based entirely on the maximum flowrate at which a stable, attached flame was possible. The only parameter which was kept roughly constant between flames at different pressures was the fuel exit temperature ($\simeq$ 340°C) but this was not important since the data has been compiled for the purposes of model development and detailed computer prediction, not dimensional analysis. A list of the operating inlet conditions for the six kerosine flames studied is shown below:

TABLE 4.1

	FLAME A	FLAME B	FLAME C	FLAME D	FLAME E	FLAME F
Pressure (Bar Abs.)	1.0	2.03	2.70	3.72	4.81	6.44
Fuel flowrate (g/min)	8.0	9.5	12.5	12.5	18.5	28.0
Fuel exit velocity (m/s)	22.28	13.80	12.991	9.699	11.169	13.172
Fuel exit temp. (K)	598	633	623	626	630	658

	FLAME A	FLAME B	FLAME C	FLAME D	FLAME E	FLAME F
Air flowrate (kg/min)	0.324	0.956	0.925	1.193	1.295	1.247
Air exit velocity (m/s)	0.234	0.357	0.2528	0.2384	0.2027	0.1442
Air exit temp. (K)	288	293	291	292	296	293
Pilot flame flowrate (g/min)	0.198	0.371	0.4468	0.569	0.722	1.114
Pilot equivalence ratio	5.08	4.221	3.938	4.02	4.134	4.338
Probe cleaner flame flowrate (g/min)	0.236	0.699	0.6779	N.A.	N.A.	N.A.
Probe cleaner equivalence ratio	3.878	10.49	10.08	N.A.	N.A.	N.A.

The air flowrate of flame F was the maximum flowrate possible using the compressed air supply to the laboratory where the present tests were undertaken. In future tests, where higher pressure flames will be studied, the experiment must be moved to the test area of Cranfield where the continuous compressed air supply is more substantial.

Such characteristics as visible flame length or maximum width were impossible to measure due to the flames being encased in a pressure vessel with limited optical access. The axial height of first visible soot was noted, however, and in all cases was 0mm (burner exit), emphasising the increased sooting propensity of this fuel compared to ethylene.

The luminous flame surface implied that the turbulence levels increased with increasing pressure. This trend was evidenced by the values of burner exit Reynolds number shown below (viscosity of kerosine vapour @656K, 1.183×10^{-5} kg/ms):

TABLE 4.2

Flame	Exit Reynolds Number
A	9500
B	11300
C	14400
D	14800
E	21900
F	32800

The increase is largely due to increasing density of the pre vaporised fuel with increasing pressure.

4.2.2 MEASUREMENTS IN THE KEROSINE JET FLAMES

The table below gives a summary of all radial and axial profile measurements made on vaporised kerosine flames at all pressures studied. The following codes are used:

T Mean temperature.
R Mean soot volume fraction measured by Rayleigh extinction.
M1 Mean mixture fraction measured using mark I probe system.
M2 Mean mixture fraction measured using mark II probe system.
3C Mean soot size, number density and volume fraction using the multicolour extinction method.

TABLE 4.3. RADIAL MEASUREMENTS

Axial Position (mm)	Flame A	Flame B	Flame C	Flame D	Flame E	Flame F
29	T R					
50		T R	T R	T R	T R	T R
70	T R M1					T
80	R					R
90		R	R	R	R	R
100	T R M1	T R	T R	T R	T R	T R
109	R					

Axial Position (mm)	Flame A	Flame B	Flame C	Flame D	Flame E	Flame F
120		T R	T R	T R	T R	T
140		R	R	R	R	
150	T R M1 M2 3C	T R M1 M2	T R M2	T R	T R	T R
160	R					
170					T R	T
180		T R	R	R		
185	R					
200	3C	T R	T R	T R	T R	
210	T R M1					
220		R		R	T R	
236	R					
250	T M2 3C	T R M1 M2	T R M2	T R	T R	
260	T R M1					
300	T R M1 3C					
350	T R M1 3C					
406	T R M1					

TABLE 4.4. AXIAL MEASUREMENTS

Flame A	Flame B	Flame C	Flame D	Flame E	Flame F
T M1 M2	T M2	T	T	T	T

N.B. Single point axial measurements requiring the extinction / deconvolution method are impossible due to the nature of the technique.

The measurements made in the atmospheric flame span heights to 400mm whilst in the elevated pressure flames measurements stop at 250mm. Referring to fig(3.1), the pressure vessel is made of three sections: the lower tube, the measurement section and the upper tube. The upper and lower tubes are completely interchangeable and have different lengths. If the longer length tube is put below the measurement section, then heights of 100mm - 400mm are accessible through the measurement section. If the smaller tube is used, however, the accessible heights are 0mm - 250mm.

Due to manufacturing delays, more time was available for measurements in flame A. Hence the two tubes were interchanged to allow a more complete data set to be compiled. For the other flames, this was not possible due to time constraints.

Obviously, the vast amount of data gathered is too great to allow plots of all profiles to be displayed in this chapter. For this reason, only a selection of profiles have been chosen for presentation and discussion. For reference, the full set of the collected data is tabulated and

reported by Young 1992.

4.2.2.1 SOOT MEASUREMENT

Of the three methods that were used throughout this study to measure soot parameters the Rayleigh and multicolour extinction techniques were used on the kerosine jet flames.

4.2.2.1.1 RAYLEIGH EXTINCTION

Although the principle of measurement of extinction in the confined kerosine jet flames was identical to that in the free ethylene jet, some new difficulties arose. The first of these was caused by the presence of the pressure vessel windows. They had been polished to schlieren quality by their manufacturers but inhomegeneities in transmissivity were still present. A traverse of the pressure vessel windows alone was performed to examine the severity of this problem. It was found that the value varied by no greater than $\pm 0.4\%$ with the windows compared to a similar value in the ethylene study of $\pm 0.1\%$ in which no windows were necessary.

The consequence of this and also the increased turbulence and soot levels in the kerosine flames was that the data collected from them was subject to more noise. This can be clearly seen in the repeatability study. Fig(4.8) shows the results of this study for a selection of kerosine flames at different pressures and locations. The centred data has significantly more scatter than equivalent plots for the ethylene flame. However, the peak value and spread of profiles collected on different days do tally.

A second problem associated with the pressure vessel windows was the geometrical limitation (useful diameter, 75mm). If the radial extent of the soot zone was greater than this limit, extinction measurement in the edges of the flame was impossible. Since the deconvolution technique requires data across the full width of the flame, the data that could be attained was of little value. In an attempt to make some use of this data extrapolations of the splined exponential curve were used. Fig(4.9) shows an example of such an extrapolation for flame A at the highest height investigated, 406mm. Such an extrapolation was necessary for the following situations:

Flame A @ 406mm
Flame C @ 250mm
Flame D @ 220,250mm
Flame E @ 200,220,250mm

Although the extrapolation appears to be acceptable, soot volume fraction profiles at these heights must be treated with some scepticism.

Another difficulty experienced when making the kerosine flame measurements that was not seen in the ethylene studies was total absorption of the laser light. As described in the previous chapter, in situations of extreme absorption, there is the possibility of measuring a value of extinction below the assumed background (no-light) intensity, I_b, since this is only measured at the beginning and end of the traverse. In this situation the argument of the logarithm will be negative. Obviously, such points must be rejected to prevent a computer error, section (3.6.1).

Shown in fig(4.10) is a plot of the maximum percentage of rejected points at each axial height studied in the kerosine flames (N.B. the atmospheric flame, flame A, has not been included in this plot since, in all cases the rejection was zero). The maximum rejection rates are modest (< 5%) for flame B (2.03bar) and C (2.70bar), but rise quite considerably to values of order 20% in flame D (3.72bar). In the two highest pressure flames, flame E and F, the maximum rejection rises to values of order 60% at the most soot laden locations. Clearly, the extinction measurements thus made will be subject to significant error.

RESULTS

Radial profiles of soot volume fraction are shown for a variety of axial heights in the kerosine flames in fig(4.16a-f). The axial profiles are shown in fig(4.17a-e). Again these have been derived assuming the value of soot complex refractive index to be 1.92-0.45i (Mullins and Williams, 1987).

The profiles grow and develop in a very similar manner to those measured in the ethylene jet flame. There is a striking difference, however: the magnitude of the values in the kerosine flame are very much larger. Even in the atmospheric kerosine flame, A, the measured soot volume fractions are five times larger than equivalent ethylene values. In flame, F (6.4bar), they are 10 times greater still.

4.2.2.1.2 MULTICOLOUR EXTINCTION

The present application of the multicolour extinction soot particle sizing technique was limited to kerosine flame A. The three wavelengths chosen for the analysis were the same as those used with success by Bard and Pagni 1981. They were: 632.8nm (Helium Neon laser), 514.5 and 457.0nm (Argon Ion laser).

Lack of duplicate equipment prevented the three turbidities from being measured simultaneously and so care was taken not to move the burner position between traverses at particular wavelengths. Signal noise, however, was unavoidable. Depending upon location in the flame, the repeatability study of Rayleigh extinction showed that random variations for a given profile could be as high as 5-6%.

Examination of the repeatability of the measurements focused attention on the measured parameter $\ln(I_o/I)$. Previously, $\ln(I_o/I_{mean})$ had been measured, the required value, however, was $[\ln(I_o/I)]_{mean}$. An investigation was undertaken into the discrepancy between these two parameters.

Two radial extinction traverses were repeated for the 632.8nm wavelength measuring both representations of the average. The results of these are shown in fig(4.11). At the lower of the two heights investigated, X = 150mm, the discrepancy is significant. The two data sets are visibly distinct from each other. At the higher height, X = 300mm, there is a much closer correlation and the two data sets are indistinguishable. The discrepancy is obviously dependent upon the degree and nature of fluctuation in the intensity, I, and this study shows that it can be significant in certain areas of the flame.

Unfortunately, at this stage, it was too late to revisit the ethylene jet flame and repeat those measurements. Little may be inferred of the associated error since no measurement was made of the degree of fluctuation in the ethylene flames, but presumably they will be of similar order as those the kerosine flames. However, the correct form of the average was measured for all subsequent studies.

RESULTS

Mean extinction was measured for the three probe wavelengths in kerosine flame A at 6 heights ranging from 150mm to 400mm, see table 4.2. It was noted that the beam intensity of the Helium Neon laser was far more stable than that of the Argon ion laser. This was especially true for the blue (457nm) line which was particularly unstable.

A probable explanation for this lay in the Argon ion laser power control system. This relied upon a feedback system whereby the intensity of laser light output was measured and fed back to a power control circuit. At the modest output powers required for the present analysis, 300mW (cf. max output 2W), the light measuring device was probably not operating at optimum conditions. The laser fluctuation did not degrade extinction measurements to an unacceptable level however.

Shown in fig(4.12) are plots of the raw turbidity data for two representative heights, X = 150, 350mm. The spread and shape of profiles at all wavelengths is in broad agreement. From the plots of D.W.E.E. ratio, fig(3.16), it can be seen that, for a given value of particle diameter, the turbidity at lower wavelengths should always be the highest, ie. $\tau_{red} < \tau_{green} < \tau_{blue}$. This is because elastic scattering is more efficient at lower wavelengths. As can be seen from the results, in general this condition is met, however, at certain locations, the value of blue turbidity drops below that of the green, implying some error in the measurement at that wavelength.

Before applying the multicolour analysis, the raw turbidity data was processed using the Rayleigh extinction assumption, eq(3.19). The results of this analysis are shown for the same two heights in fig(4.12). If the soot particle size is in the Rayleigh limit then the soot volume fractions computed should be independent of probe wavelength. For both locations, the soot volume fraction using the green light collapses reasonably well to that from the red, although the value from the green is always slightly higher. The soot volume fraction from the blue turbidity measurement is, however, substantially higher than the other two.

Referring to the multicolour extinction technique, a typical example of how the particle diameter is derived from the experimental data is shown in fig(4.13). For the experimental turbidities, all four possible diameters are found at each point (section 3.6.4). Ideally, two of these diameters should be identical, the other two being significantly different. In this case, however, no two diameters are exactly the same but it would appear that, in most cases, the pair of values which have larger size are closer than the pair which have smaller size. The computer has therefore chosen the mean of these two values as the correct value. In one region along the radius, however, the pair of possible diameters of smaller size converge. This causes the computer to choose this small value in this region. The result being a discontinuity in the results. This type of ambiguity is seen quite often in the analysis.

The results from analysis of the experimental data were not very promising. The values of experimental turbidity data were analysed using all the four combinations of D.W.E.E. ratio shown in fig(3.16). In a large proportion of the cases, the data produced was very scattered and showed no trend at all with a substantial number of unphysical values.

Of all the complex refractive indices and size distributions used to analyse the data, the most successful combination in terms of continuity of profiles and number of unphysical values, was that of Mullins and Williams 1987 with a monodisperse size distribution. A selection of the results from this analysis are shown in fig(4.14). Although some of the individual profiles

show trends which seem realistic, the continuity between profiles at different heights is small. Using this particular theoretical D.W.E.E. ratio, the soot diameters are generally of the order 200nm. These values are high compared to those obtained using other D.W.E.E. ratios. A diameter of $\simeq$ 150nm was most commonly inferred.

4.2.2.2 MEAN TEMPERATURE

The measurement of mean temperature was the least problematic of all measurement techniques attempted in the kerosine jet flames. The technique used was identical to that adopted in the ethylene jet flame studies and no further modification was necessary.

As discussed in section (3.5), of most concern to the accuracy of the measurements was soot build up on the thermocouple bead. A rapid insertion / withdrawal technique was adopted, the thermocouple being cleaned between measurements. Some soot build up was, however, inevitable and unavoidable in the highly soot laden regions in the flames. This build up was greatest in rich regions where the temperature was between 1000 - 1200°C. Above these limits the soot would not grow on the bead and any soot already existing would burn off - a phenomenon used with success to clean the bead - below these limits soot growth was greatly reduced, presumably because pyrolysis rates were lower.

Although some apprehension was felt concerning the applicability of thermocouple radiation compensation - see chapter 3 - in the enclosed, optically thick kerosine flame environment it was used. The correction was, however, never more than 70°C.

As shown already in fig(4.7), the repeatability of temperature measurements was, again, very good.

RESULTS

The radial profiles of mean temperature for a selection of four axial heights in each of the kerosine flames studied are shown in figs(4.16a-f). The axial profiles are shown in fig(4.17a-f).

In general, the profiles are very similar in both magnitude and shape to those of the ethylene jet flame. The profiles lower in the flame have distinct, sharp peaks away from the flame axis which gradually migrate towards the centreline and reduce in magnitude.

The degree of scatter in the profiles tends to be slightly higher in the kerosine flames and in

some cases, eg. flame C @ 150mm, flame D @ 100mm, flame E @50mm, it is evident that the initial profile, before centring, was not very symmetric. This was caused by probe aerodynamic blockage.

Another point of note is the temperature of the surround air. Lower down in the flames its temperature is close to ambient, $\simeq$ 15°C, but this value gradually increased with height to values as high as 140°C. This increase is, obviously, due to convective heating from the pyrex tube.

4.2.2.3 MEAN MIXTURE FRACTION

Both the mark I and mark II mixture fraction probing systems were used in the kerosine flame studies with varying degrees of success.

4.2.2.3.1 MARK I PROBE

The mark I system was only successful in kerosine flame A. Even in this case probe blockage and fuel condensation problems were severe.

On average, it would take $\simeq$20s to achieve a steady reading on the mass spectrometer used (VGA micromass). Quite often, probe blockage would occur on a similar, or shorter, timescale making the measurement process somewhat haphazard in nature.

This difficulty was just possible to overcome in kerosine flame A, but was too severe in all other flames to make measurements practical. Probe blockage, by soot, would not only occur on the outside the probe, where it could be easily burned off with the cleaner flame, but also inside. Then, the only successful method of unblocking the flame would be to strip down, clean, and rebuild the probe. Other techniques, such as back purge with nitrogen, were attempted to no avail.

The second, more fundamental reason why this type of probe was unsuitable for kerosine flame applications was fuel condensation. Due to a glued joint between the quartz probe and its metal sleeve it was impossible to keep the quartz section at sufficiently high temperature to prevent fuel condensation. The boiling point of kerosine, $\simeq$300°C was higher than the softening point of the epoxy resin glue used, $\simeq$100°C.

When rich mixtures were sampled, fuel condensation was visible in the tip of the quartz

probe. This would, not only, cause artificially low values of mixture fraction to be measured in this region but also artificially high values in subsequent reading as the fuel gradually re-evaporated. The effect of this could be clearly seen if pure air was sampled after sampling a rich mixture. The level of CO_2, indicating the presence of fuel, would not drop to its initial, low value.

4.2.2.3.2 MARK II PROBE

As described in section 3.4.1.2, this probing system was designed to tackle both the problems found with the mark I system. The internal heating of the probe and the fact that the oxygen and sample were mixed at the point of sample entry proved very successful. Mixture fraction measurement with this technique was possible in flames A - C.

Probe blockage was greatly reduced outside the probe due to probe heating and completely eliminated inside the probe due to soot oxidation. Fuel condensation was also eliminated for the same reasons.

Other than its increased size (diameter 6mm cf. mark I probe, 3.0mm) the probe had two problems, both of which occurred when rich mixtures were sampled. The first was caused by the chemical heat release of the sample when reacting with the pure oxygen. A blue flame could clearly be seen inside the probe at some locations resulting in the platinum catalyst / heating wire melting and hence breaking the electrical circuit. The wire would always melt at the tip of the ceramic inner tube, fig(3.6), in the first few coils of the wire. Reducing the voltage to the heating wire would lower the chances of this happening but not stop it. If the wire did melt, a complete probe strip down was required.

The second problem was balancing the O_2 / sample mixture ratio. This ratio was set at the beginning of each traverse. In rich regions, where large O_2 flowrates were necessary to oxidise the sample, it proved impossible to find a good balance. Either too little or too much oxygen was set. The finest possible adjustment of the 1/16" fine metering valves used was too coarse.

These factors limited the use of this system to leaner mixtures in which it performed very well.

RESULTS

Of primary concern, given the two probing systems utilised in the present study, was the comparison between measurements made at the same location by each system. Shown in

fig(4.15) are two such comparisons from radial traverses of kerosine flame A at heights X = 150, 250mm. In fig (4.17a) is a similar comparison along the flame axis.

Considering, first, the radial profiles at X = 250mm, the repeatability of the mark II system is very good in both radial spread and peak value. Unfortunately, no similar study had been undertaken with the mark I system.

The spread of the radial profiles using both systems is very similar. However, a significant difference in the peak values is evident. At the 150mm height, this difference is of order 20%, at the 250mm height, it is of order 40%. Scatter of the axial measurements using the mark I probe system, especially in the highly soot laden regions, can be of the same order, however, and so little significance can be given to this discrepancy .

Radial profiles of mean mixture fraction for a selection of axial heights in flames A, B and C are shown in fig(4.16a-c). Axial profiles are shown for flames A and B in fig(4.17a,b). Since a larger set of measurements were made on flame A using the mark I system, it is this data set that is plotted in fig(4.17a). The mean mixture fraction in the other figures is measured using the mark II system.

The scatter in the profiles of flame A (mark I probing system) is significantly greater than for profiles using the mark II probing system or using the same probing system in the ethylene jet flame. This was attributed to the combined probe blockage and fuel condensation problems experienced with the mark I system.

In general, however, all radial profiles of mean mixture fraction have the expected gaussian shape with peak values occurring on the centreline and falling away sharply with axial height in an exponential fashion.

4.2.3 SUMMARY OF KEROSINE FLAME MEASUREMENTS

The experimental rig, designed for the present study of vaporised kerosine combustion at elevated pressure, fulfilled all but one of its design criteria. That one being the minimisation of thermal radiation from the flames. The flames studied proved to be stable with time and repeatable from day to day. The rig could be operated easily by two novices or by one experienced person in a laboratory environment.

Thermocouple mean temperature and Rayleigh extinction soot volume fraction were measured

With few exceptions, the radial spread of the different properties is in close agreement and peak soot volume fraction, when occurring away from the flame axis, always occurs to the rich side of peak temperature.

The measured values of soot volume fraction may be used to estimate the dependence of soot growth on pressure. However, before this can be done, a suitable abscissa must be chosen in order to compare jets with different velocities on the same scale.

The most obvious choice for such an abscissa would be that of residence time. However, in the absence of detailed velocity information in the present experimental database, the characteristic time of flow, T_c, is used. The only accessible velocity information that is available is the average burner exit velocity, v_b, which is based upon the measured volumetric flow rate of kerosine. Characteristic time is simply the axial position in the jet, X, divided by burner exit velocity, v_b.

$$T_c = X / v_b \tag{4.2}$$

Centreline soot volume fraction is plotted against characteristic time for all the kerosine flames studied in fig.(4.18). The first observation is that soot volume fraction increases with increasing pressure. This is not surprising given the incompressible nature of soot. For a constant mass fraction of soot as pressure increases the volume fraction of soot will also increase as the gas compresses. Assuming ideal gas behaviour, this volume fraction increase will be linear with pressure. Therefore, the effect of pressure on the mechanisms of soot growth is that over and above (or under) this baseline linear growth rate.

In mathematical terms, if pressure has no effect on soot growth rate, the value of the exponent, n, in equation (4.3) will be unity. Any deviation from this value will be due to a change in the soot growth mechanism.

$$\frac{df_v}{dt} \propto p^n \tag{4.3}$$

The value of n may be calculated from the present data provided a representative growth rate for each pressure is available.

With reference to the plots of centreline soot volume fraction (fig(4.17a-e)), it can be seen that there are three distinct regions of soot growth in each case.

Initially, close to the burner exit, the centreline soot volume fraction grows very slowly since residence times are short and centreline temperature modest in this region. This is followed by a region of rapid growth as temperatures rise whilst the mixture remains rich. The final region occurs as the stoichiometric contour is approached and the soot is exposed to hot, oxygen rich mixtures resulting in oxidation and a decline in soot volume fraction.

In all cases, in the second region (of rapid growth), the rate of growth of centreline soot volume fraction with characteristic time remains constant over a significant period of time and may be well approximated by a linear relationship.

The gradient of linear growth in this region was calculated for each flame and compared in order to evaluate the effect of pressure. The results are tabulated below.

TABLE 4.5 PRESSURE DEPENDENCE OF SOOT GROWTH

16Flame	Pressure (atm)	Exit Reynolds number	Range of T_c (ms)	Max. no. of reject points	df_v/dT_c (ms^{-1})
Ethylene	1.0	8600	6.5 - 12	0	0.31
Flame A	1.0	9500	3 - 14	0	0.93
Flame B	2.03	11300	3.5 - 16	0.5	1.84
Flame C	2.70	14400	4 - 16	6	2.54
Flame D	3.72	14800	5 - 16	25	3.23
Flame E	4.81	21900	4 - 14	60	4.63
Flame F	6.44	32800	5 - 9	62	12.89

The table shows the rate of centreline soot volume fraction growth with characteristic time.

Also shown are other relevant parameters which could influence soot growth: jet exit Reynolds number, the range in characteristic time over which the linear growth regime occurs and the maximum percentage of total laser extinction points in the sample at that pressure.

The growth rates are also plotted against pressure on a log - log scale in fig (4.18b). Referring to eq.(4.3), if this type of relationship is valid, the gradient of this plot will yield the exponent, n. The plot shows that, up to 4.81bar abs, there is indeed a linear relationship, the gradient of which is unity. The point at pressure 6.4bar abs, however, clearly does not follow the same trend as the others and shows that the pressure exponent for the lower pressures is no longer valid. Unfortunately, since only one point has been measured in this region, the value of the exponent which governs there cannot be calculated.

The implication of this is that, for pressures up to 4.8bar abs, there is no effect of pressure on the absolute mass growth rate of soot. It is merely compressed into a smaller volume resulting in linear growth of soot volume fraction with pressure. However, at greater pressures, the exponent of the pressure dependence, n, is undoubtedly higher but of unknown magnitude. The absolute mass growth rate of soot is observed to increase due to increasing pressure.

Such an affect could be caused by a more effective chemical mechanism becoming dominant at the higher pressures. Alternatively, it could be caused by some physical mechanism which is related to the proximity of the soot particles. However, there are a number of ambiguities and uncertainties in the measurements which could also be used to explain the observations.

Firstly, there could be some affect of the increased turbulence levels in the jets. The exit Reynolds number of the jets does increase with increasing pressure (table 4.5) and indeed jet Reynolds number has been observed in studies of atmospheric jets to influence soot growth rates (Lege et al 1993). However, this explanation cannot soley account for the sudden jump in soot growth rate seen in fig (4.19). Firstly, observations show increasing Reynolds number to decrease soot mass fraction rather than increase it, and secondly, the exit Reynolds number in the present analysis increases gradually from the lower to the higher pressure flames. No sudden jump exists as is observed in fig (4.19).

An alternative explanation is that the linear soot growth regions from which the gradients are taken differ in flame F. There is some evidence to support this in that the range of characteristic times in which this regime occurs (table 4.5) is smaller for flame F than for

the other flames. However, again this cannot satisfactorily explain the anomalies since there are no regions at any time in the other flames in which the growth rate is significantly higher than in the linear growth region.

Another explanation lies with the validity in the measurements themselves at the highest pressures. The problem of total extinction of light was severe for flames E and F necessitating dubious assumptions in the analysis - see chapter 3. Regardless, the accuracy of the instrumentation for the highest extinctions in flame F was restricted due to the very small photodiode signals measured. At the point of greatest light extinction in flame F, the mean value of measured photodiode voltage was 1.1mV. The smallest increment detectable by the analogue to digital converter as it was set up was 0.2mV. The effect may be purely due to inreased measurement errors in flame F.

Finally, the growth rate of soot will undoubtedly depend upon the temperature, time history of the soot particles as they are transported. The above analysis assumes this to be the same at different pressures. Considering the plots of centreline temperature in the flames, they do indeed exhibit very similar trends. However, the peak centreline temperature measured at 6.4bara is approximately 100°C higher than at other pressures. The reason for the increase is unclear although the increased turbulence levels in these flames is thought to play a large part by increasing mixing rates and combustion efficiency. Such an increase in temperature would cause a corresponding increase in soot growth rate and could therefore explain the anomaly.

Further investigation is clearly required into kerosine flames which produce less soot - and hence are more amenable to measurement and prediction - before this result may be confirmed.

Finally, again in regions where mixture fraction information is available, the fraction of total available carbon that is bound in the solid phase may be estimated using eq(4.1). The centreline value of this fraction is plotted in fig.(4.6) against axial position for the two flames, A and B (the only ones in which axial measurements were possible). Although these values will be subject to error due to the uncertainty in mixture density, their magnitude is large. In flame B, it rises to $\simeq 60\%$. Again discussion is deferred until chapter 5.

4.3 GENERAL CONCLUSIONS

The aim of the present measurement campaign on jet flames fuelled by both ethylene and kerosine was to generate a dataset which could be used for soot model validation and

development. This aim was fulfilled and detailed property maps of mean temperature, soot volume fraction and mixture fraction were compiled in atmospheric ethylene flames and kerosine flames up to pressures of 6.4bar abs.

Measurements in atmospheric ethylene and vaporised kerosine jets posed relatively few problems from a practical standpoint. Those in the kerosine flames at elevated pressure conditions however became more difficult due to the very large amounts of solid carbon liberated. Estimates of the percentage conversion of fuel carbon to soot suggest that as much as 60% conversion is possible in kerosine flames at pressures of 2.72bar abs. Even in the relatively soot free atmospheric ethylene flame studied, this value was of order 25%. In some cases, these levels of soot caused severe probe blockage problems of sampling and thermocouple probes and caused total extinction of probe laser light.

A more important consequence of these large values, however, was the implied perturbation to the gas phase chemistry due to soot in the flames. A necessary assumption, when using the conventional laminar flamelet model of non-premixed combustion is that the soot causes merely a small perturbation to the underlying thermochemistry. This assumption is quite inappropriate with the present soot levels and creates more modelling uncertainties and difficulties in the definition of mixture fraction for example. This will be addressed in chapter 5.

The cause of such high conversion of carbon to the solid phase in these flames, compared to most practical devices, is a combination of the relatively poor mixing and/or larger timescales. If soot loadings are to be reduced whilst still maintaining the other benefits of this flame geometry - namely very good optical and probe access and cylindrical flowfield symmetry - strategies must be incorporated to either inhibit soot growth or improve soot oxidation. These will be discussed in the recommendations of further research.

The other main difficulties that were encountered in the measurement campaign were related to soot particle sizing. Two techniques were attempted: the D.M.P.S and the multicolour extinction particle sizing techniques.

Soot blockage created major problems for the D.M.P.S. which was designed for less heavily laden aerosols. This could be overcome in part by sample dilution, however the remaining problem of sample coagulation remained. The system design allowed excessive opportunity for soot agglomeration in the sampling lines and inside the D.M.P.S. resulting in significant measurement uncertainties.

A further concern with the instrument, as with other particle sizing techniques, was the embodied assumption that particles are spherical. Particles are discriminated by their terminal velocity in a coflowing air stream. This would presumably be very different for an agglomerated soot particle than for a sphere.

The results gained from the instrument, on the ethylene flame, showed behaviour which was consistent with other measurements on the same flame, but with soot sizes far greater than any measured in the literature. At the positions of greatest soot loading, particle sizes of 0.886μm were sampled. The largest value found in the literature was 0.4μm, Wood and Samuelson 1985. Most studies suggested values closer to 100μm to be more appropriate (eg. Bard and Pagni 1981, Garo et al. 1990, Kent and Wagner 1982).

Although the implementation of the multicolour extinction particle sizing technique was simpler than that of the D.M.P.S., its application was less successful. Rather than simply generating uncertain results, as with the D.M.P.S., the technique clearly failed. The extinction measurements, when processed with a variety of different refractive indices and size distribution assumptions, showed no consistent trends and a number of unphysical values of turbidity were inferred. The failure of the technique was attributed to a variety of factors.

Firstly, the measurements of laser extinction at the three wavelengths were not simultaneous. From the repeatability study of extinction, the magnitude of scatter could be as great as 5%, fig(4.7). Considering the theoretical curves of D.W.E.E., fig(3.16), to which the measured turbidity ratio must be compared, this discrepancy is significant.

Secondly, the wavelengths chosen were not ideal. Although Bard and Pagni, 1981, used them with success in idealised laminar flames with a variety of fuels, Indices et al, 1990, suggest that a larger spread of wavelengths would give better discrimination. In their study of the characterisation of optically thick sols suspended in gel, they use an infra red wavelength together with two visible wavelengths.

More fundamental reasons for failure could lie with the necessary assumptions for the theoretical analysis. Soot particles are assumed: to have a known complex refractive index, to have a known size distribution and to be spherical in geometry. The sensitivity of the technique to complex refractive index was demonstrated in section (3.6.4), electron microscopy analysis of soot, eg. Megaridis and Dobbins 1989, show it to be substantially non spherical and no evidence has been found to suggest that soot has a standard size distribution, be it monodisperse or log-normal.

Another explanation can be inferred by processing the turbidities gained from the multicolour extinction analysis using the simpler Rayleigh extinction analysis, fig(4.12b). The soot volume fraction from the green and red wavelengths are very close to each other implying that the scattering component of the extinction efficiency, Q_{ext}, is small. The collapse of the blue line is not as good however. Values of 'blue' soot volume fraction are, in some locations, 40% higher than either red or green, implying a much greater scattering efficiency.

For large particle sizes (200μm), Mie theory does indeed predict circumstances in which the scattering at 457nm would be greater than that at 632.8nm by this magnitude. In these situations, however, the scattering at the 514.5nm would also be large. The collapse of the green and red lines suggests this not to be the case.

It is possible that some other species, such as a poly-aromatic hydrocarbon, is absorbing at the relatively short blue wavelength but not at the others. Friedel and Orchin, 1951, show absorption by aromatic compounds with four benzene rings, such as benzanthracene, to be significant at 457nm but not at 514.5nm. This absorption increases with increased number of rings. The smallest poly-aromatic which absorbs significantly at 514.5nm is coranene, which has seven benzene rings in a line. It seems quite plausible to suppose that poly-aromatics with four membered rings exist in the kerosine flames in sufficient quantities to perturb the blue absorption whereas species such as coranene are far more scarce.

Bard and Pagni 1981, found no such problems in their extinction measurements at similar wavelengths, but they did not use an aromatic fuel.

Although it would appear that, due to fundamental design constraints, the D.M.P.S. is an inappropriate device for measurement of soot in the quantities found in jet flames, a modified version of the multicolour extinction technique may still be of use. If the optical lines used had more widely varying wavelengths, chosen so as not to correspond to any vibrational or rotational level of the gas molecules, and if extinction of each line was measured instantaneously, then more reliable data may be gained. However, irrespective of the reasons of particle sizing failure in the present application, the unfortunate conclusion is that soot particle size still remains uncertain in these flames.

Fig(4.1) Demonstration of the expected repeatabilty of laser light extinction measurements at

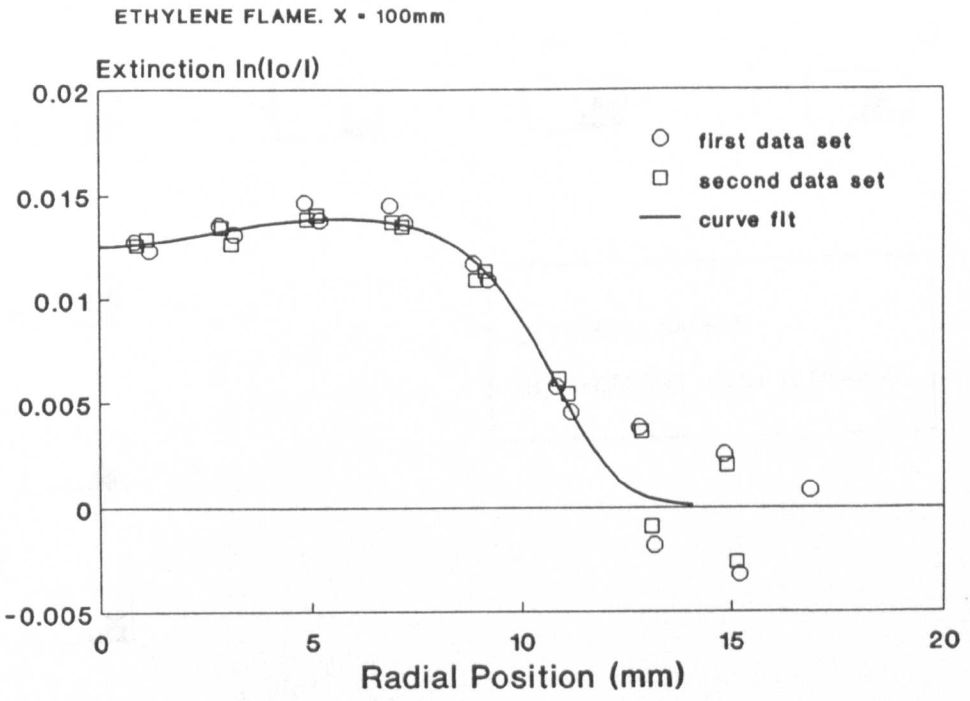

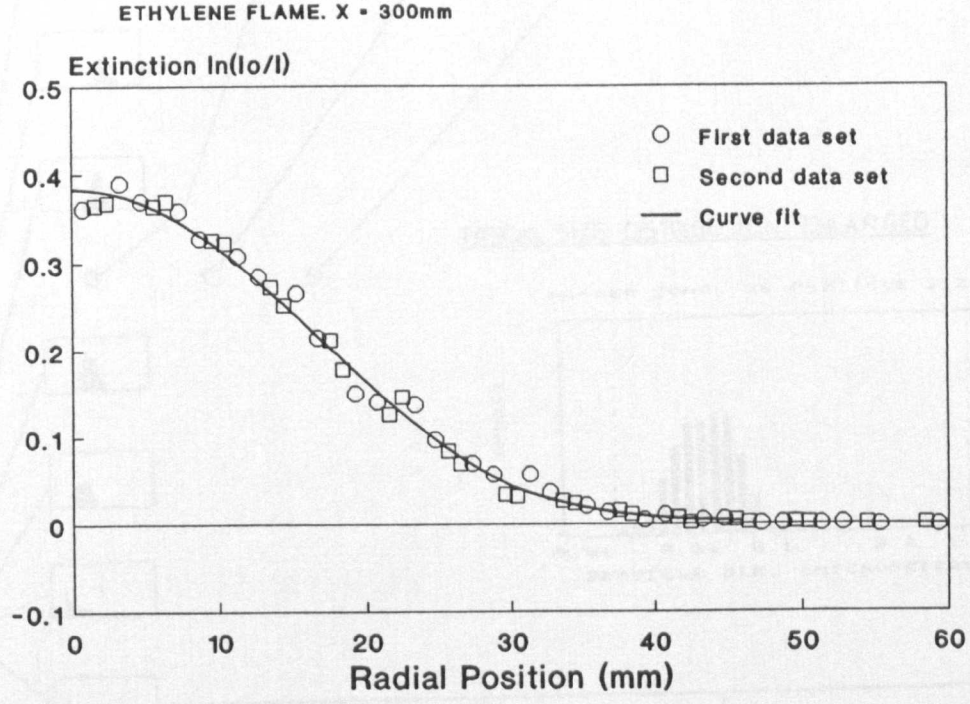

Fig(4.2)

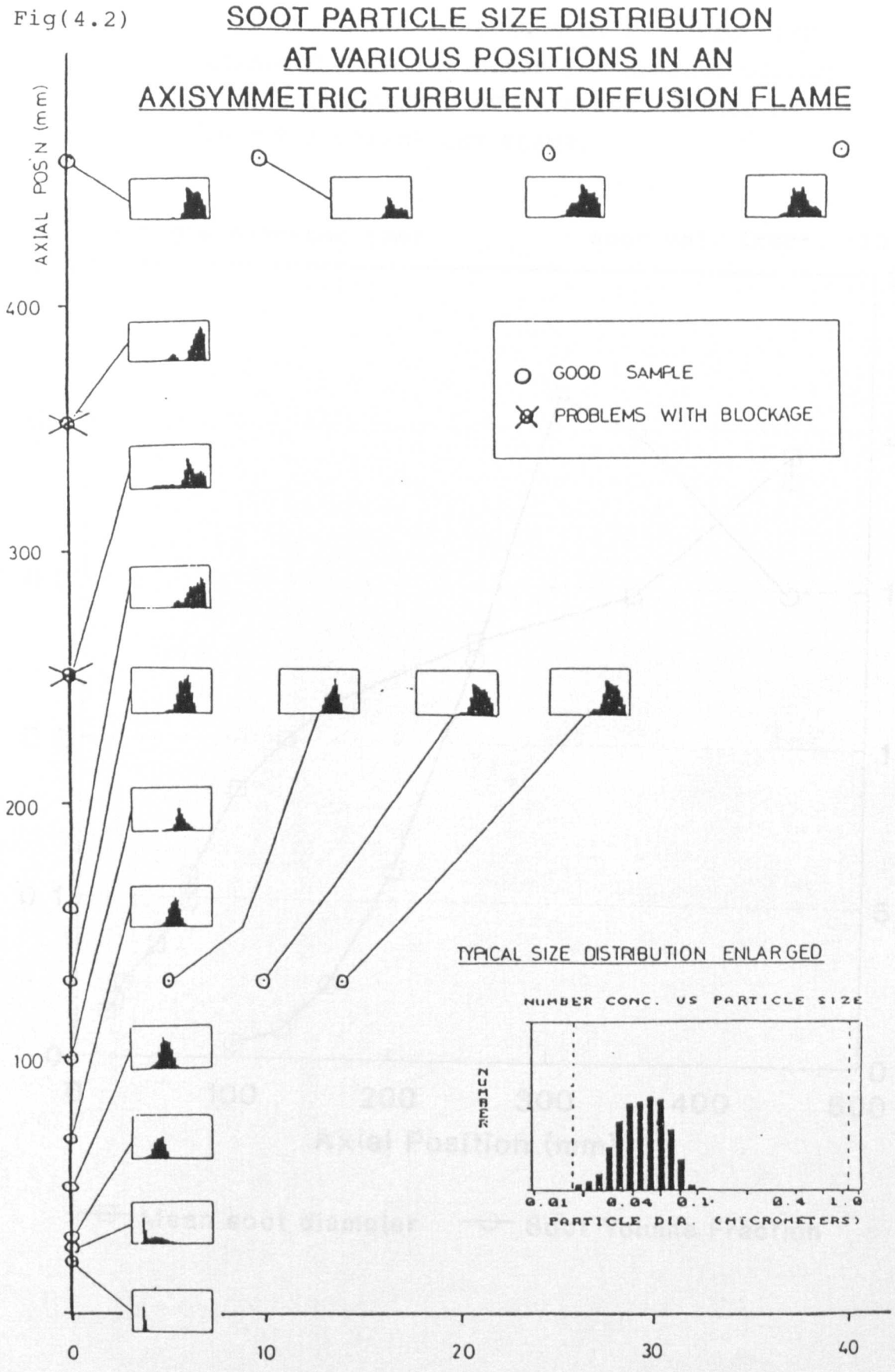
SOOT PARTICLE SIZE DISTRIBUTION
AT VARIOUS POSITIONS IN AN
AXISYMMETRIC TURBULENT DIFFUSION FLAME
AXIAL POS'N (mm)
400
300
200
100
0
10
20
30
40
GOOD SAMPLE
PROBLEMS WITH BLOCKAGE
TYPICAL SIZE DISTRIBUTION ENLARGED
NUMBER CONC. VS PARTICLE SIZE
NUMBER
0.01
0.04
0.1
0.4
1.0
PARTICLE DIA. (MICROMETERS)

Fig(4.3) COMPARISON BETWEN MEAN SOOT PARTICLE SIZE MEASURED WITH THE D.M.P.S. AND SOOT VOLUME FRACTION MEASURED BY RAYLEIGH EXTINCTION IN THE ETHYLENE JET FLAME.

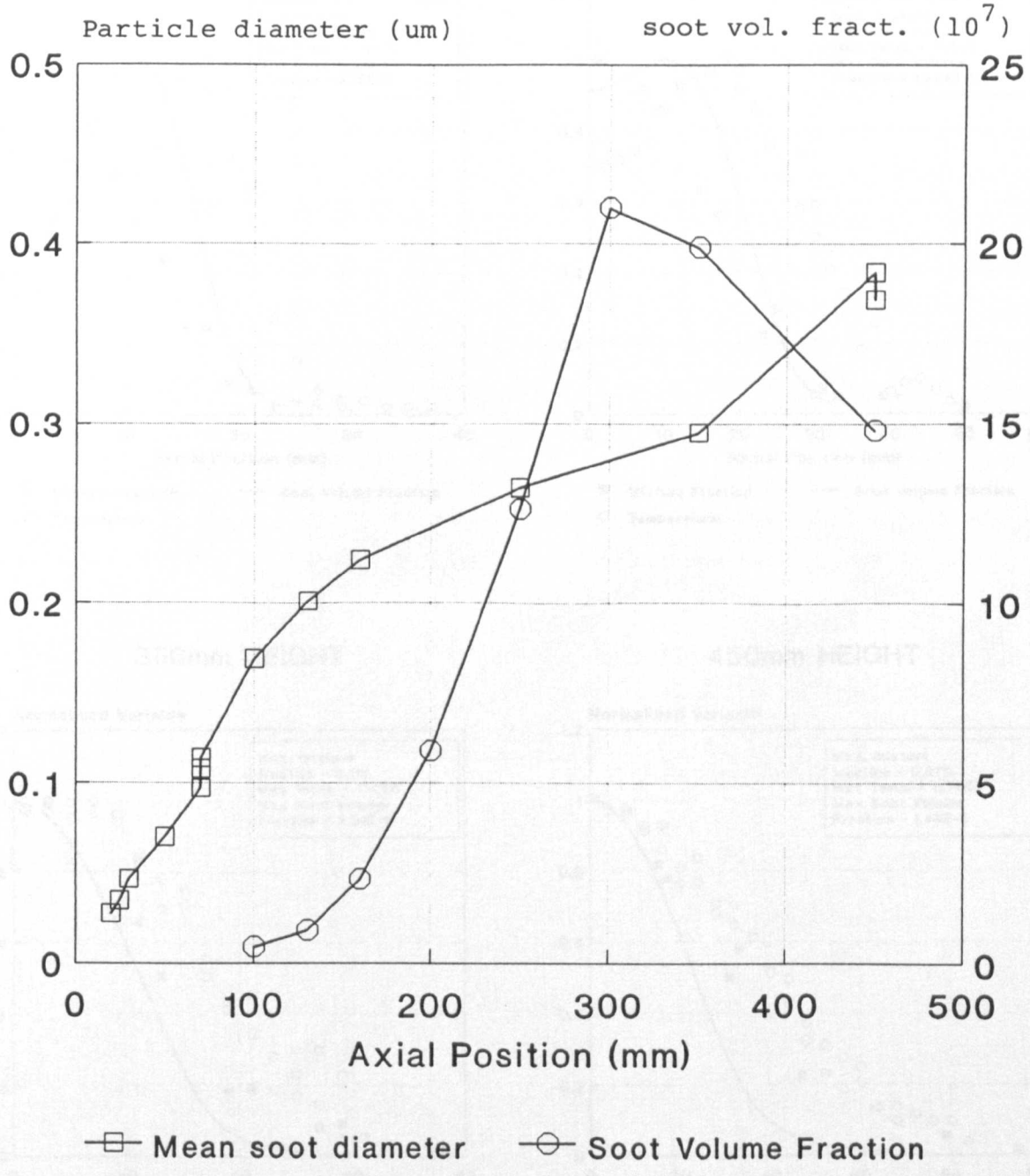

Fig(4.4) A SELECTION OF FOUR RADIAL PROFILES OF NORMALISED MEASURED PROPERTIES IN THE ETHYLENE JET FLAME.

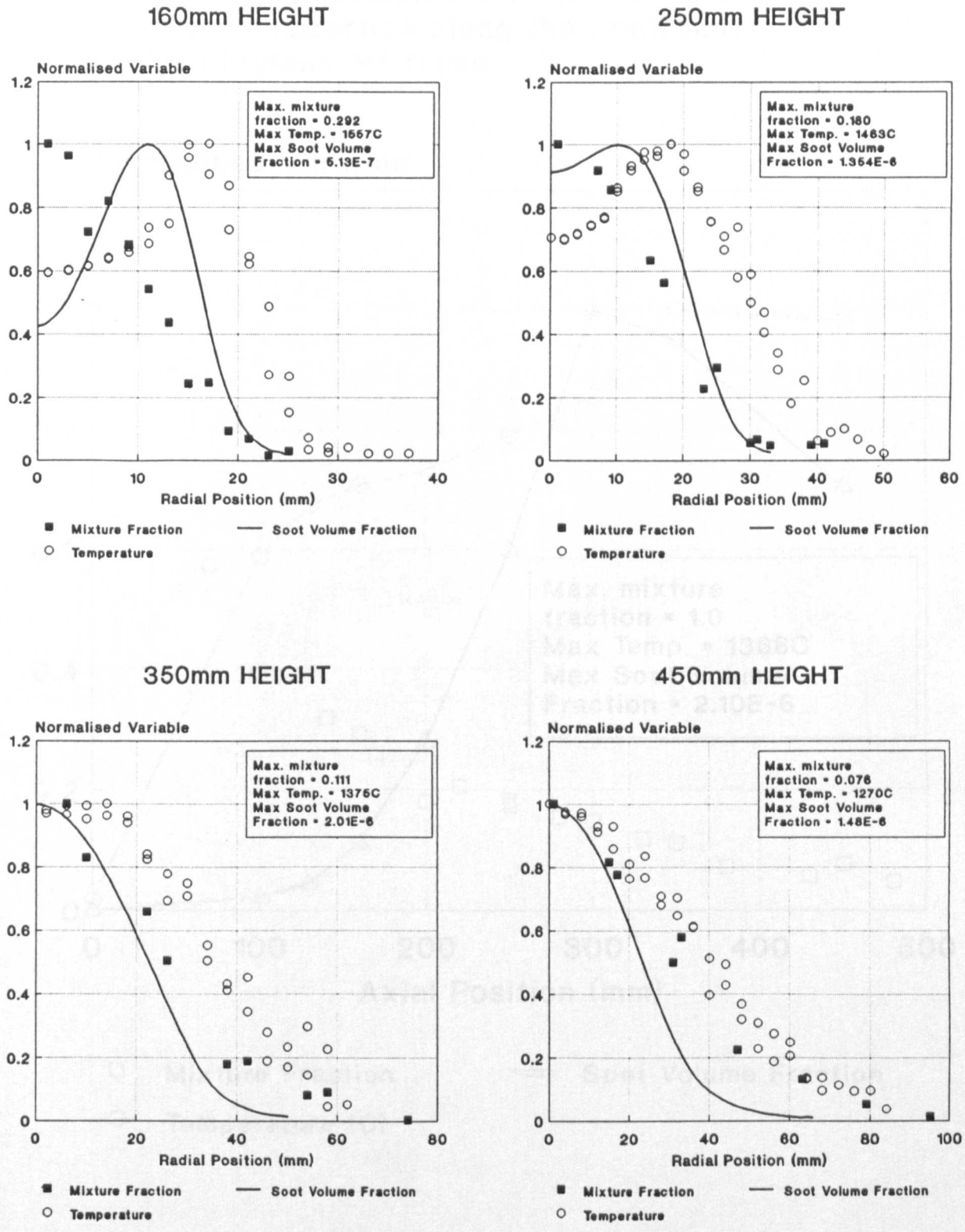

NB: mixture fraction measured with the mark I probe system.

Fig(4.5) The development of normalised, measured properties along the centreline of the ethylene jet flame

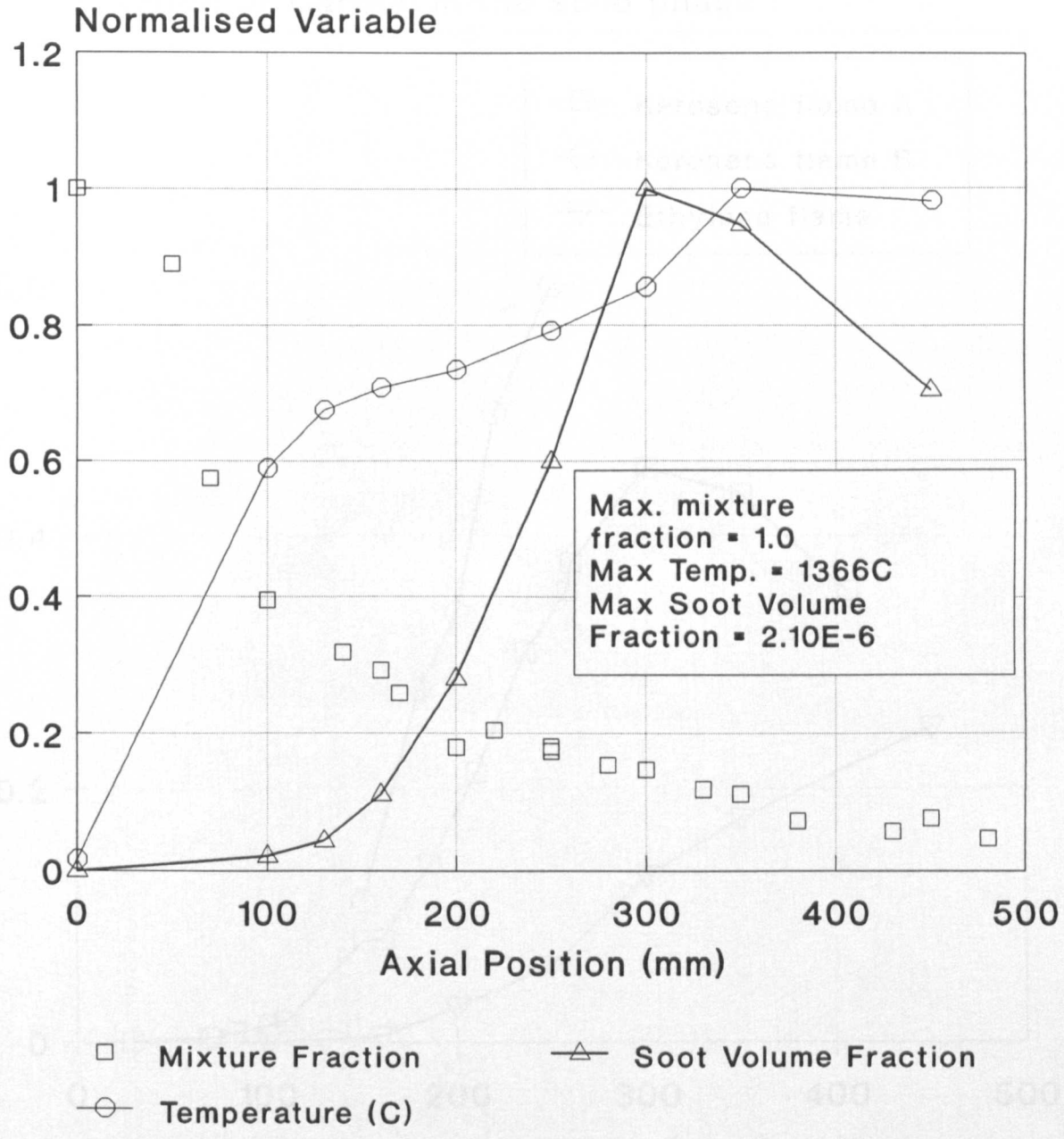

Fig(4.6) ESTIMATE OF THE FRACTION OF TOTAL AVAILABLE CARBON LOCKED IN THE SOLID PHASE IN ETHYLENE AND KEROSINE FLAMES BASED UPON MEASURED MIXTURE AND SOOT VOLUME FRACTION.

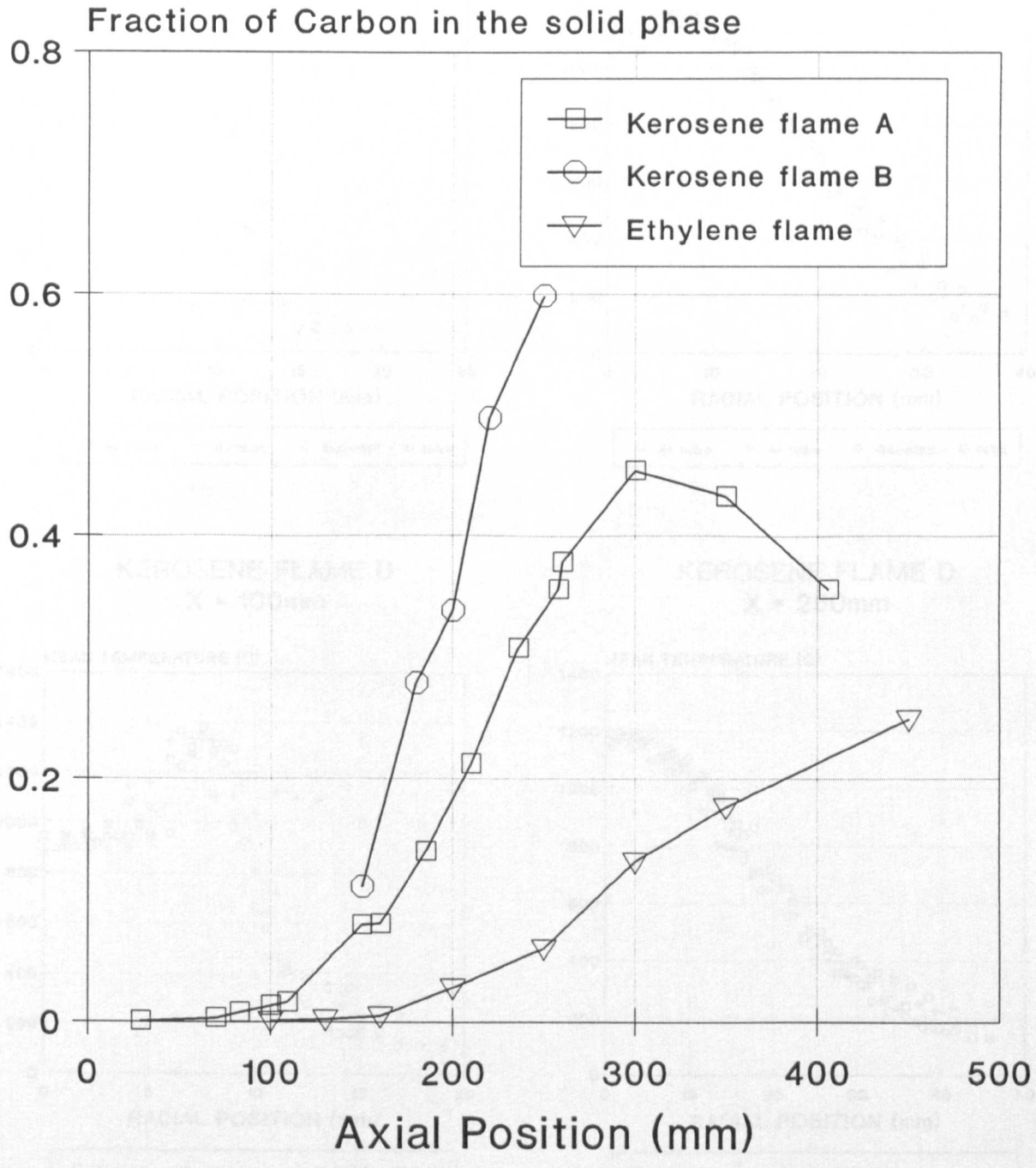

Fig(4,7) DEMONSTRATION OF THE AFFECT OF IMPROVING THE RADIATION SHIELDING OF THE KEROSINE JET FLAMES

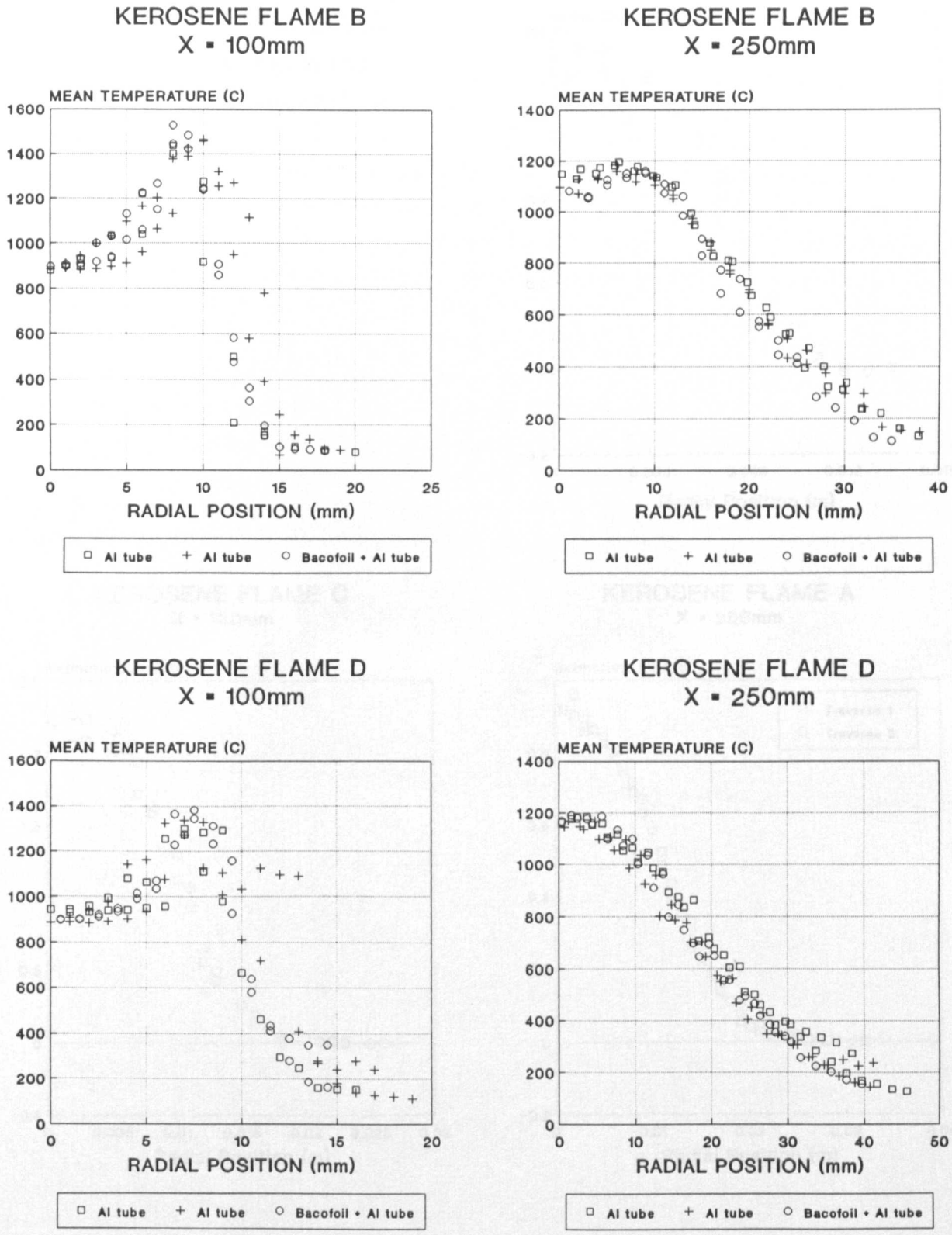

Fig(4.8) Demonstration of the expected repeatability of light extinction measurements in the kerosine jet flames at a variety of conditions.

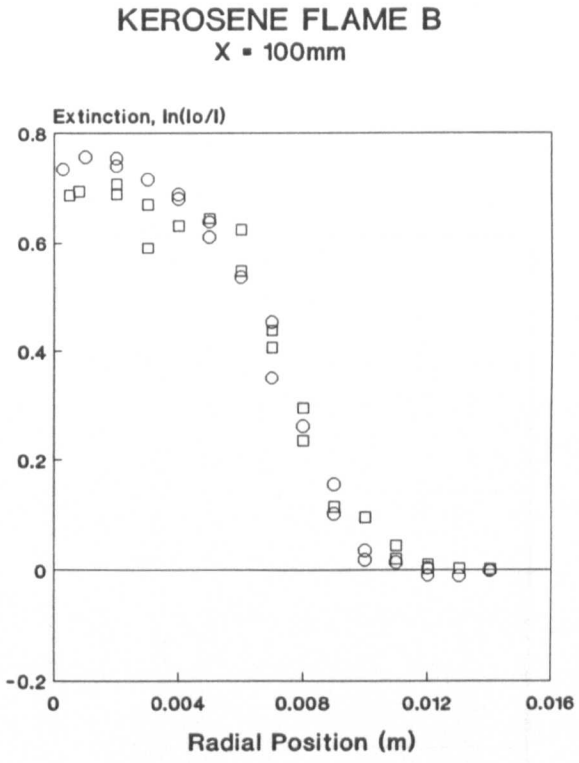

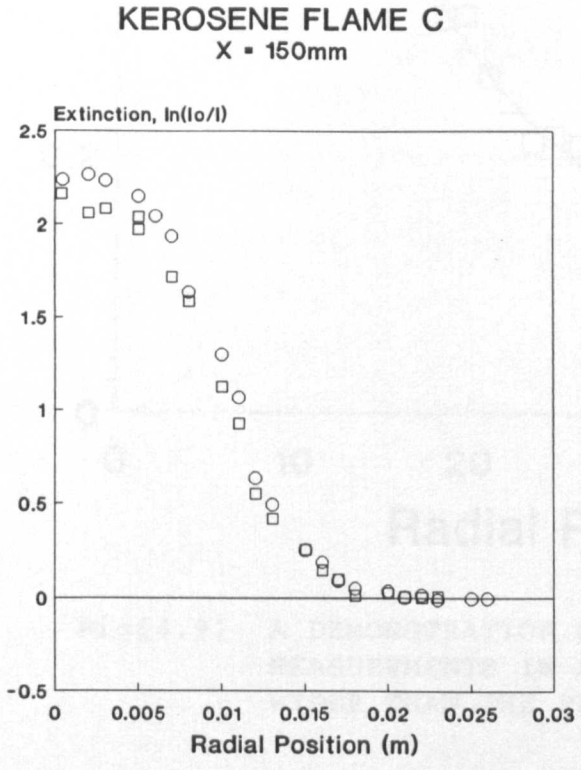

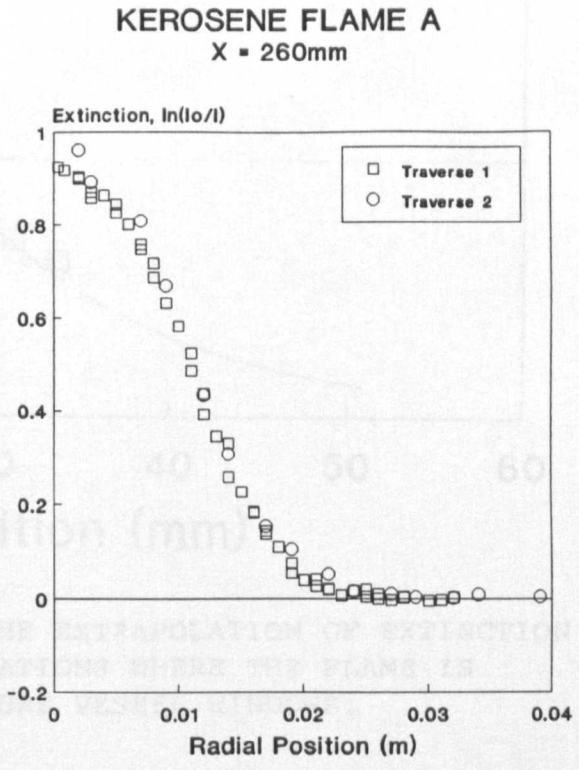

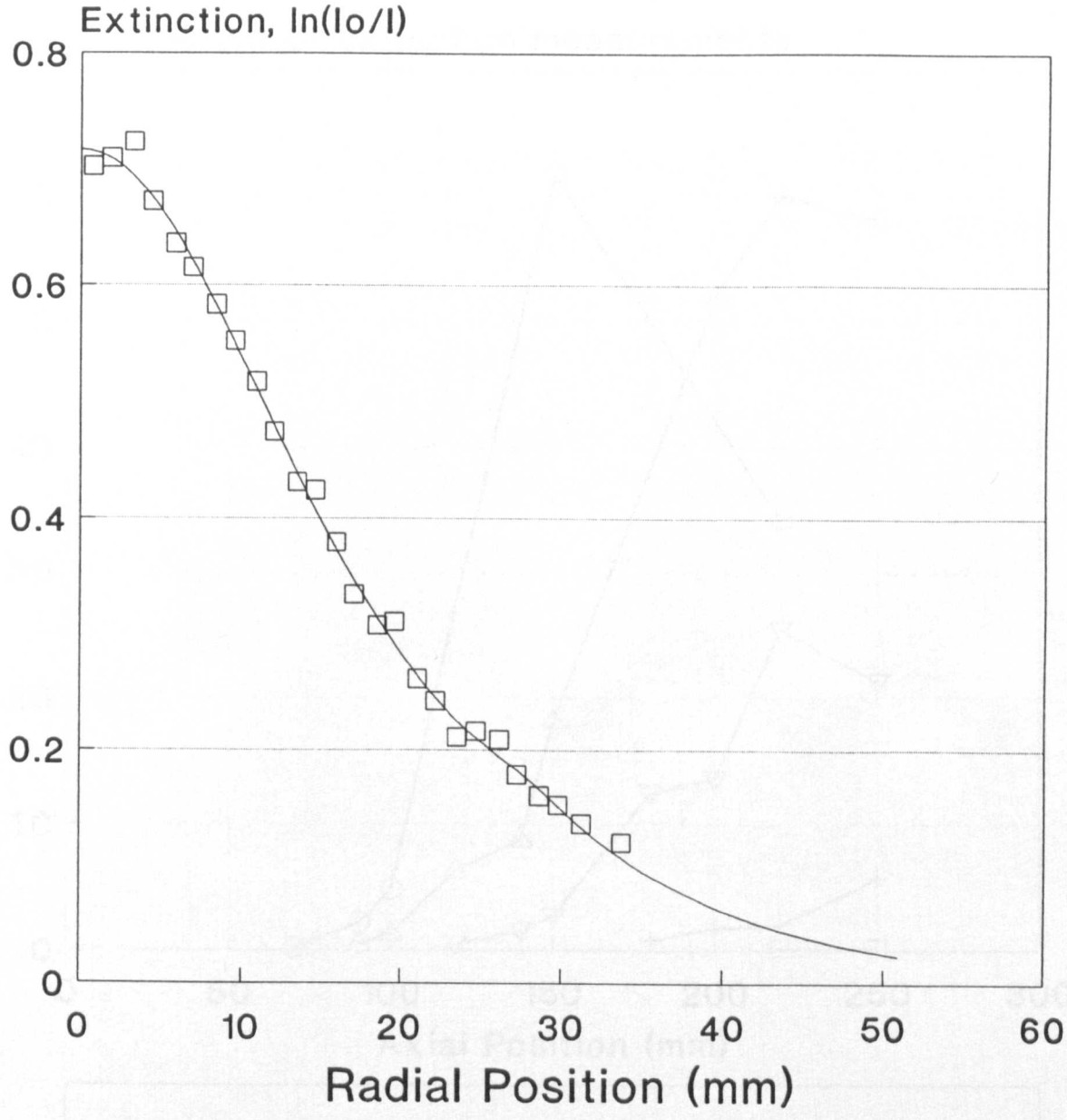

Fig(4.9) A DEMONSTRATION OF THE EXTRAPOLATION OF EXTINCTION MEASUREMENTS IN SITUATIONS WHERE THE FLAME IS WIDER THAN THE PRESSURE VESSEL WINDOWS.

Fig(4.10) THE PERCENTAGE OF REJECTED LIGHT EXTINCTION MEASUREMENTS AT VARIOUS HEIGHTS IN THE KEROSINE JET FLAMES B - F. (flame A not included since rejection was zero throughout)

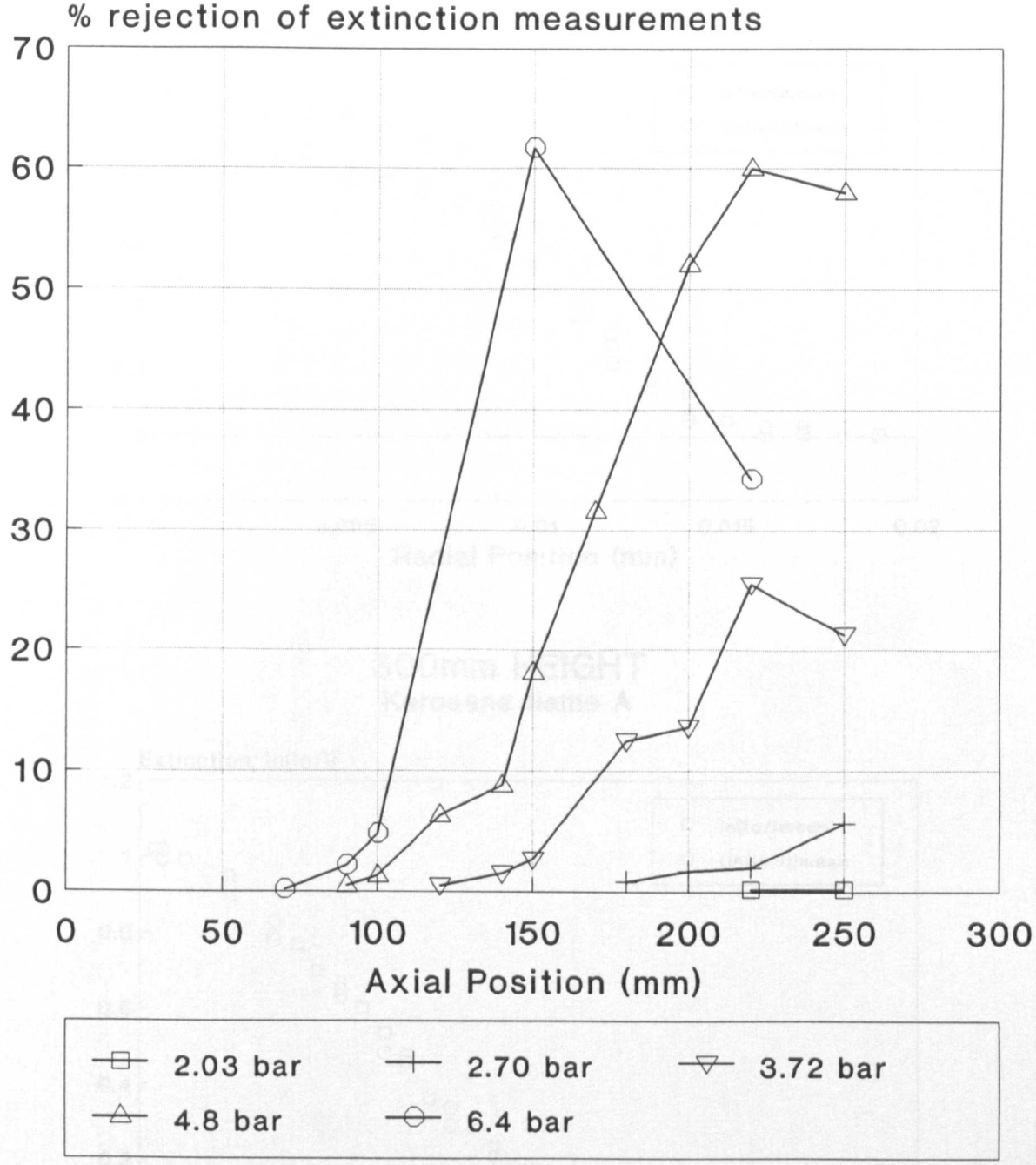

Fig(4.11) THE DIFFERENCE BETWEEN THE MEASURED VALUES OF ln(Io/Imean) AND [ln(Iǿ/I)]mean IN KEROSINE FLAME A AT TWO AXIAL LOCATIONS.

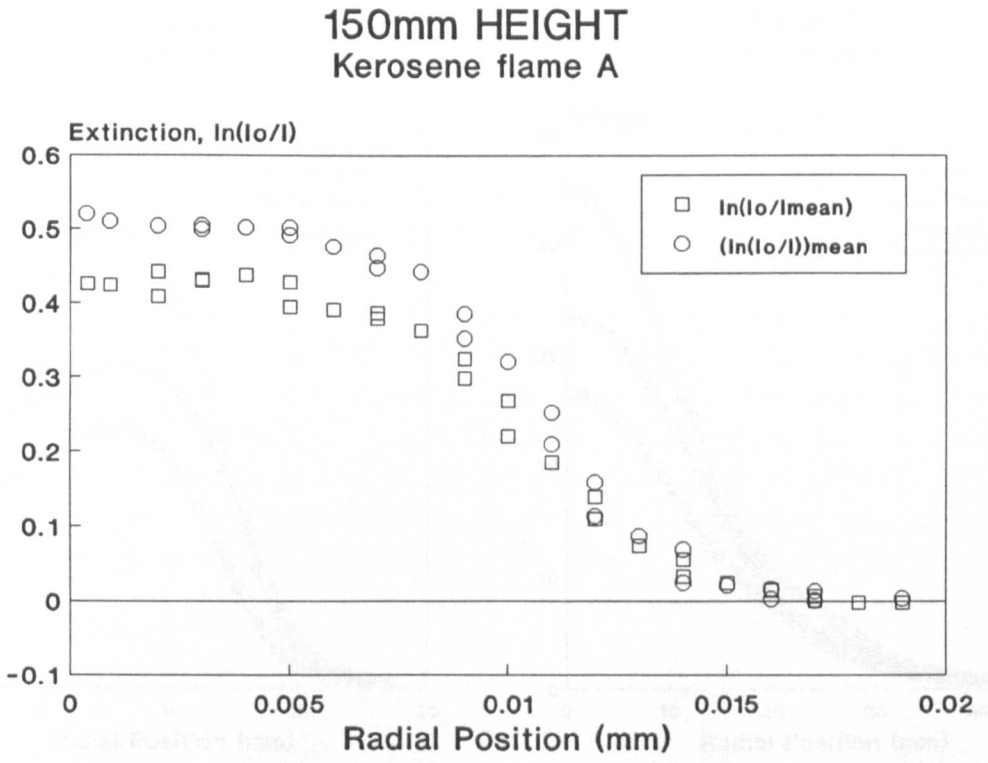

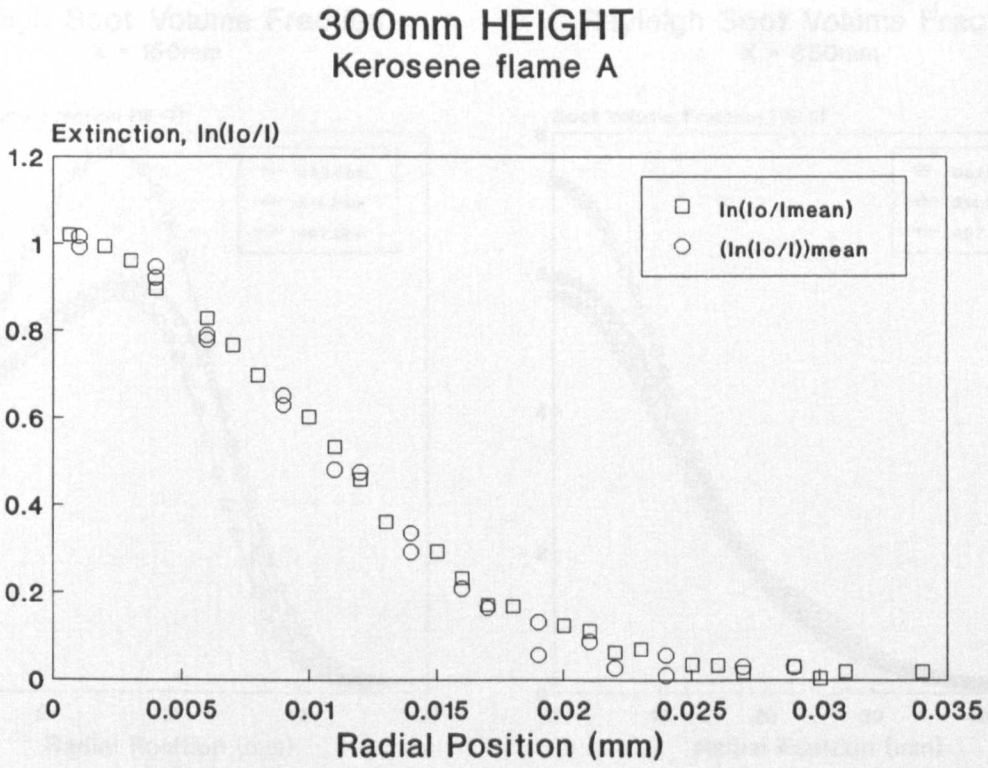

Fig(4.12) MEASUREMENTS OF TURBIDITY AT THREE WAVELENGTHS IN KEROSINE FLAME A AT TWO REPRESENTATIVE HEIGHTS PLUS THEIR ANALYSIS BASED UPON THE RAYLEIGH LIMIT.

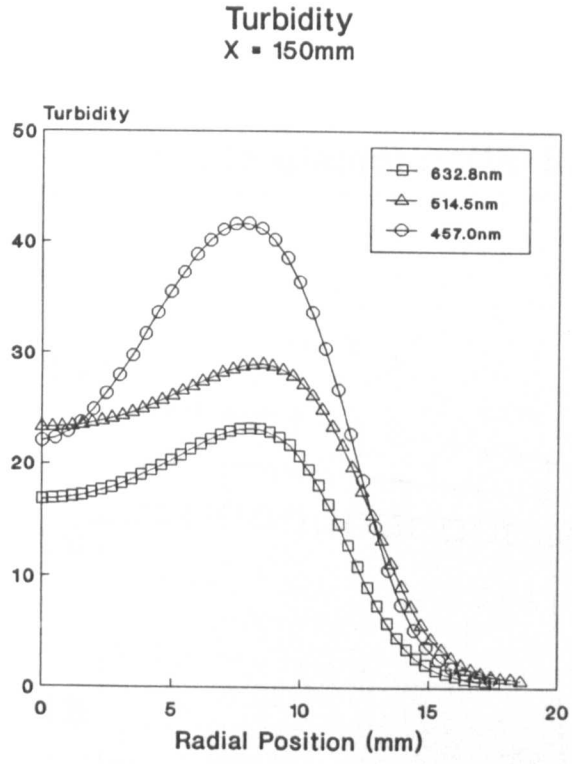

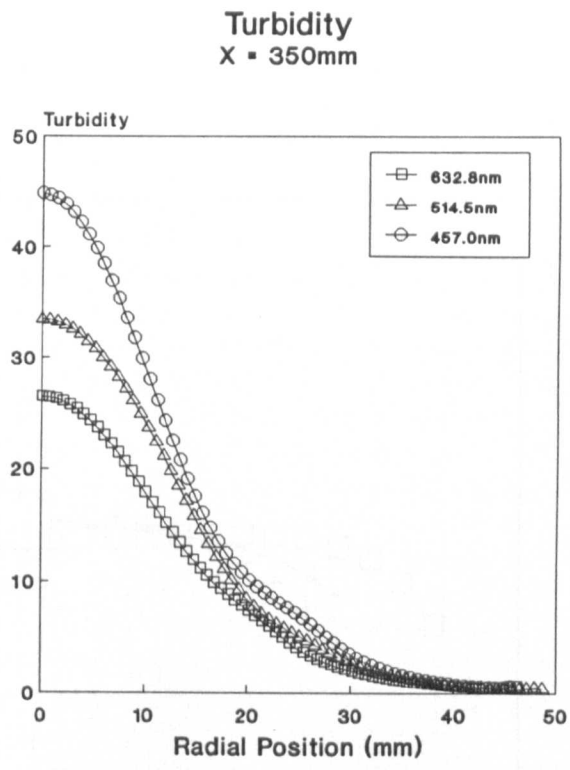

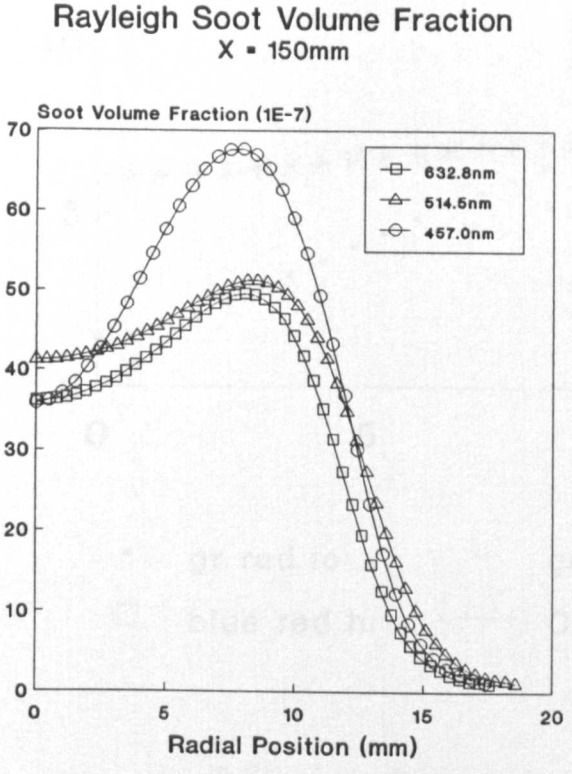

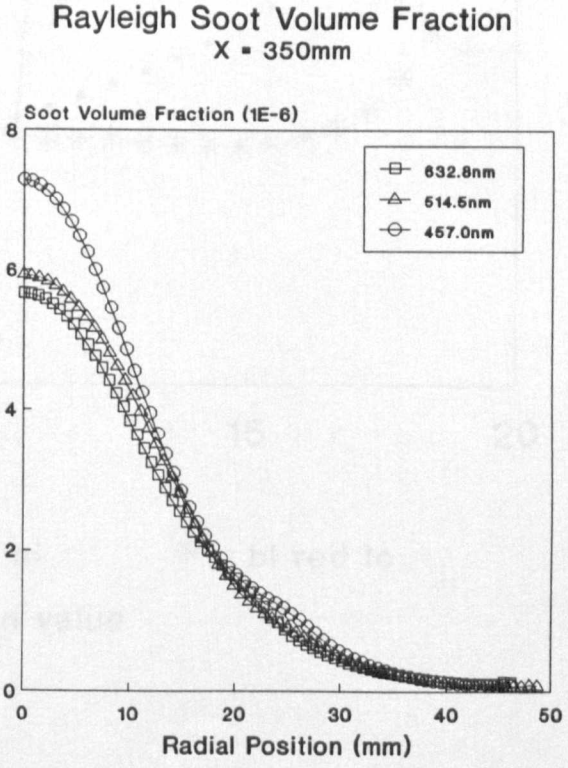

Fig(4.13) EXAMPLE OF A TYPICAL MULTICOLOUR EXTINCTION ANALYSIS OF AN EXPERIMENTAL TURBIDITY DATA SET

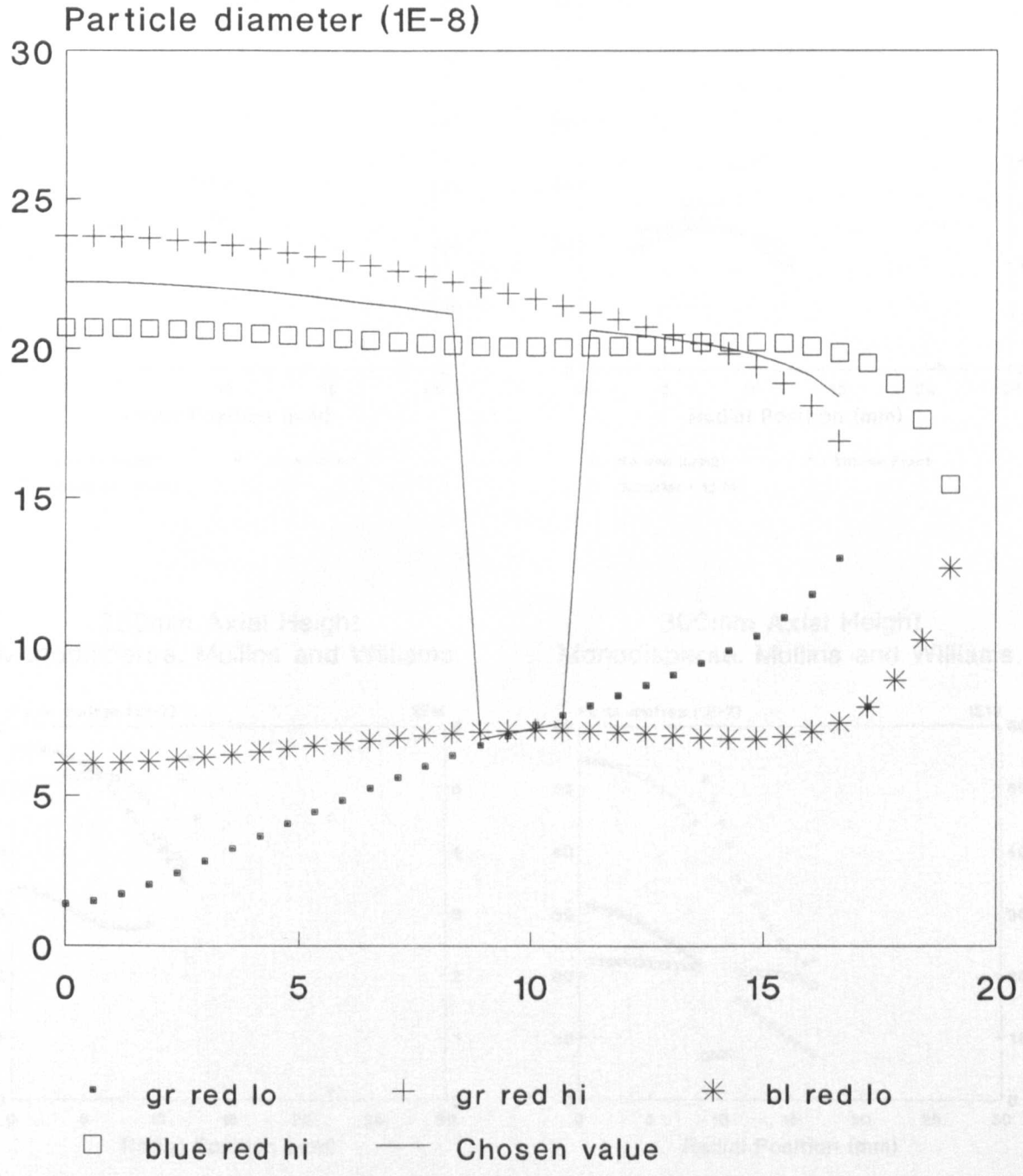

Fig(4.14) THE RESULTS OF PROCESSING THE EXPERIMENTAL TURBIDITY DATA MEASURED IN FLAME A

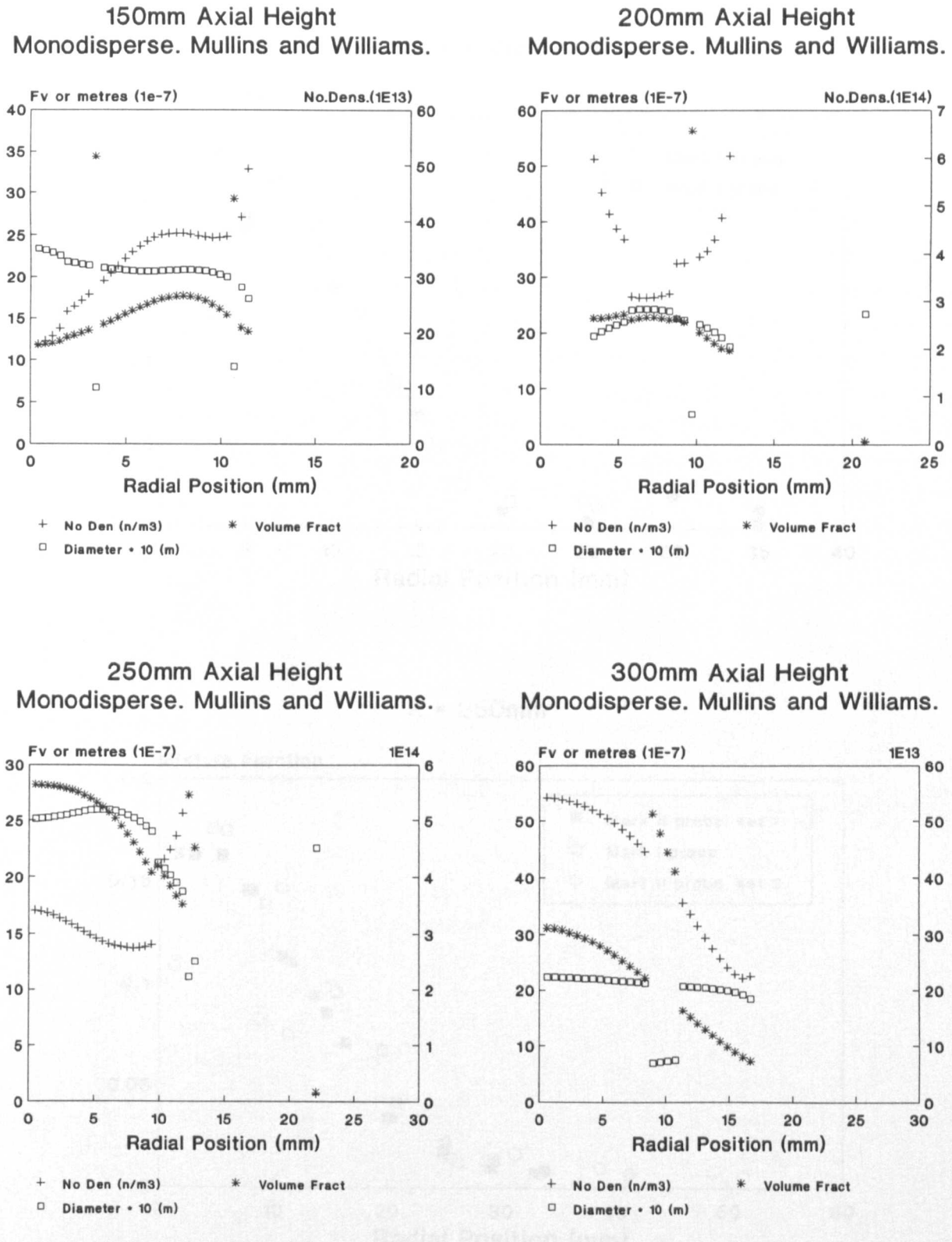

PARTICLE SIZE DISTRIBUTION - MONODISPERSE
COMPLEX REFRACTIVE INDEX - 1.92 - 0.45i
(Mullins and Williams 1986).

Fig(4.15) COMPARISON BETWEEN MIXTURE FRACTION MEASURED WITH BOTH MARK I AND MARK II SAMPLING SYSTEMS AT TWO LOCATIONS IN KEROSINE FLAME A.

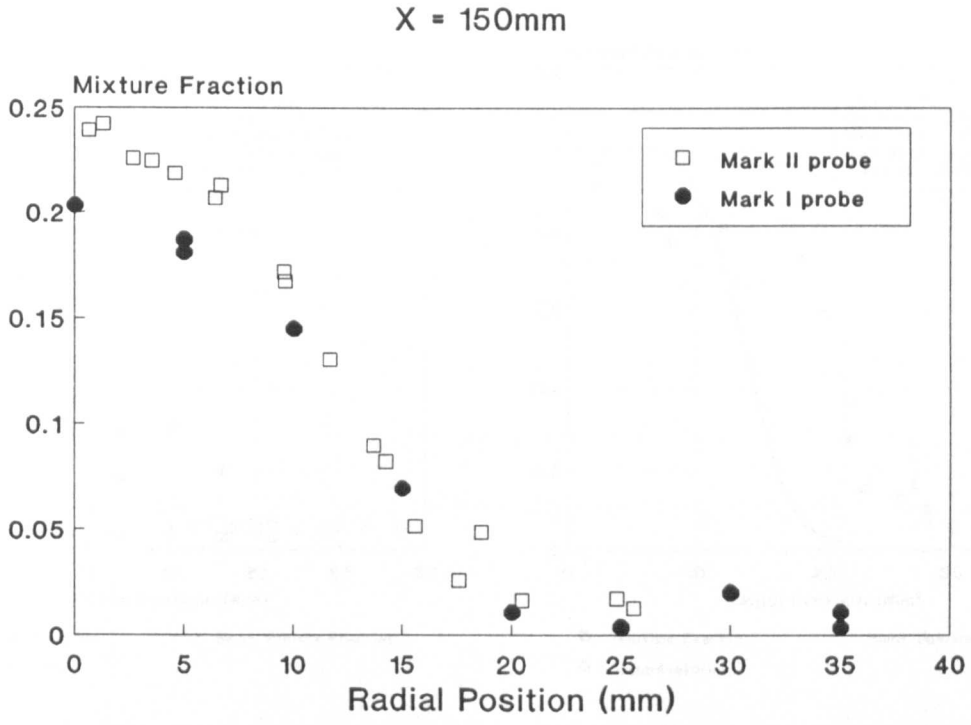

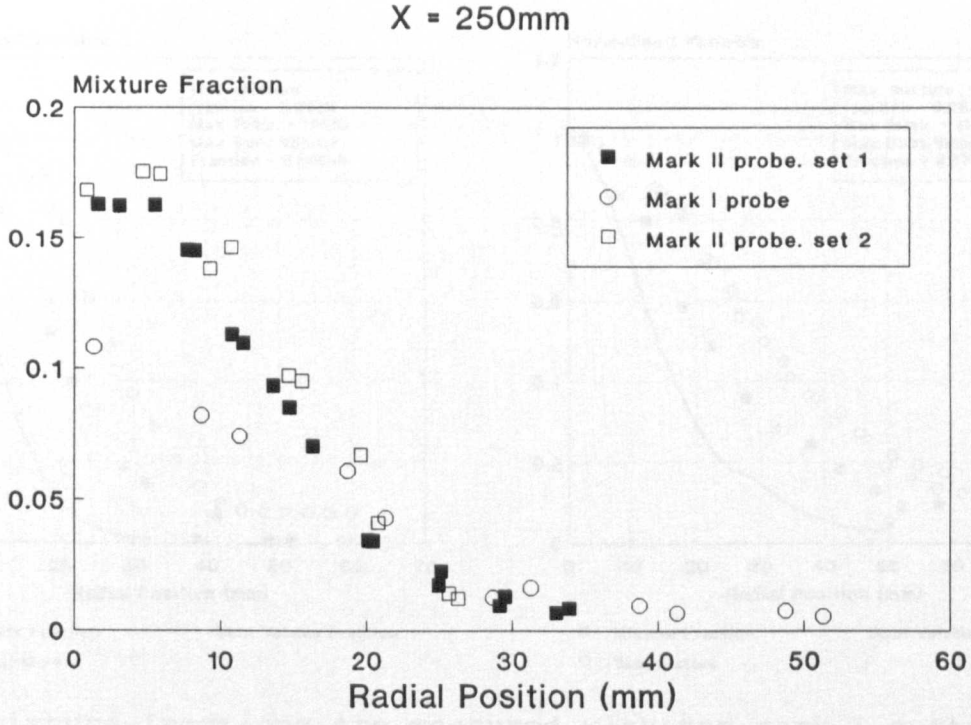

Fig(4.16a) A SELECTION OF FOUR RADIAL PROFILES OF NORMALISED , MEASURED PROPERTIESIN KEROSINE FLAME A (1.0atm)

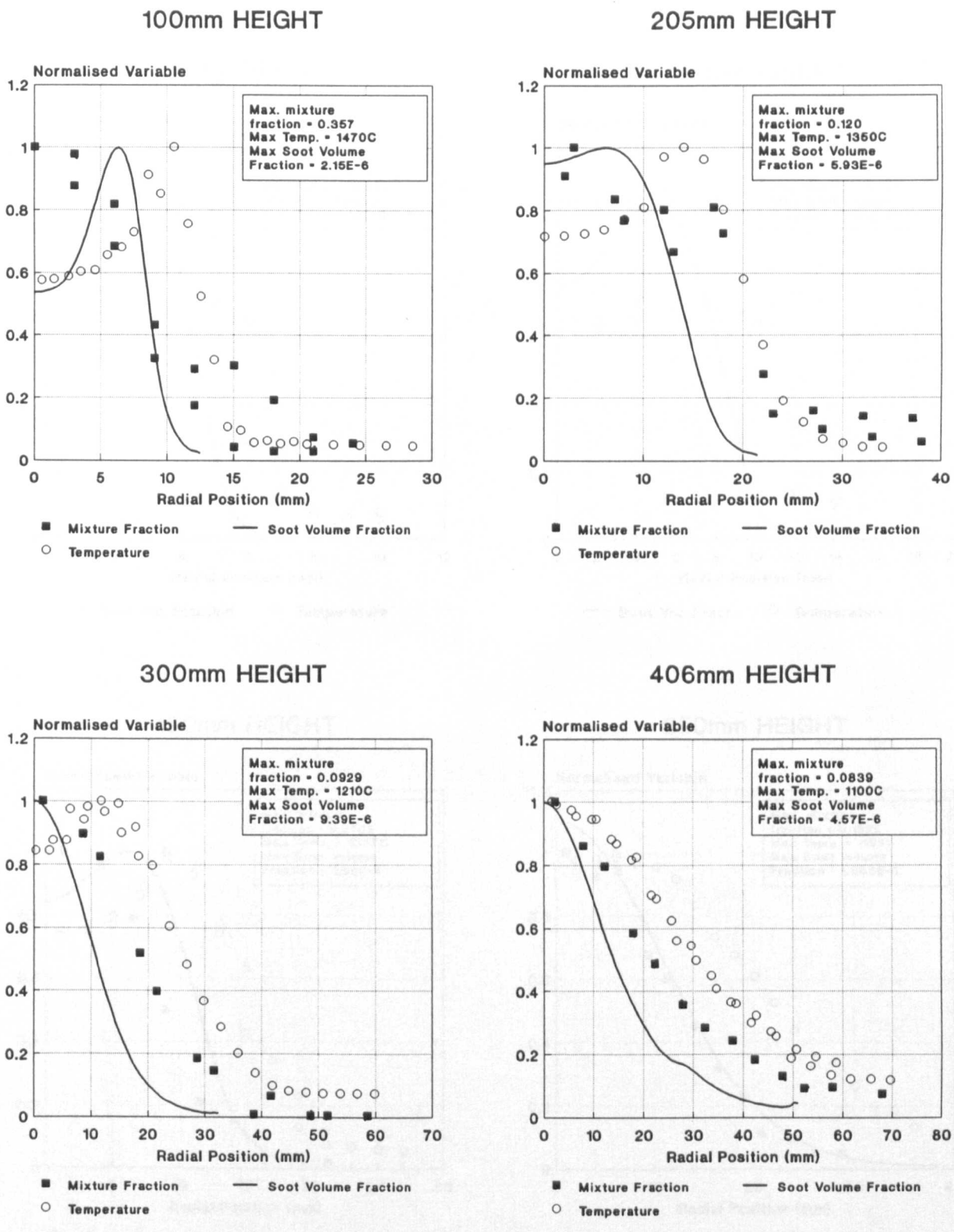

NB: mixture fractions are measured with the mark I system.

Fig(4.16b) A SELECTION OF FOUR RADIAL PROFILES OF NORMALISED MEASURED PROPERTIES IN KEROSINE FLAME B (2.03atm)

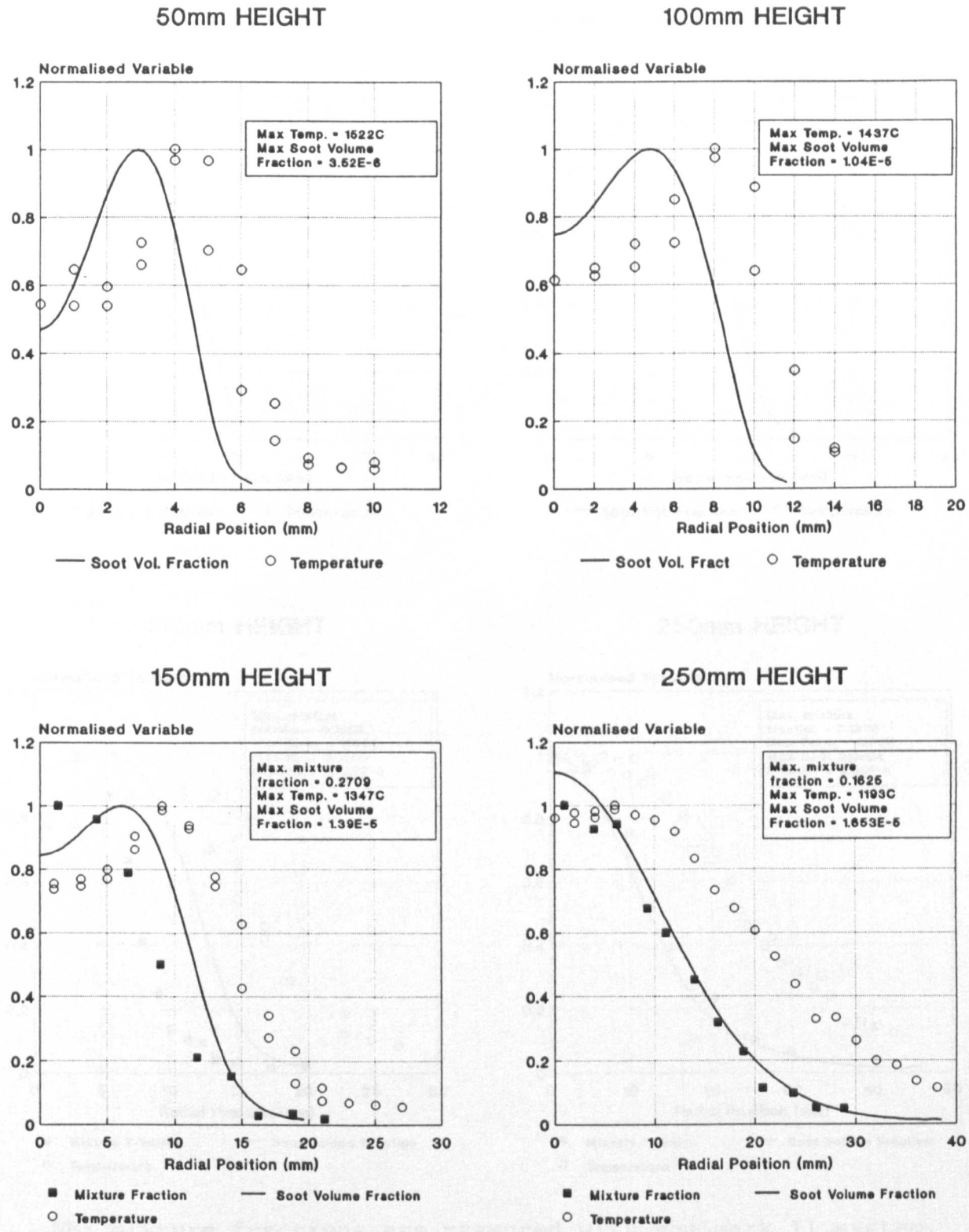

NB: mixture fractions are measured with the mark II system

Fig(4.16c) A SELECTION OF FOUR RADIAL PROFILES OF NORMALISED MEASURED PROPERTIES IN KEROSINE FLAME C (2.7atm)

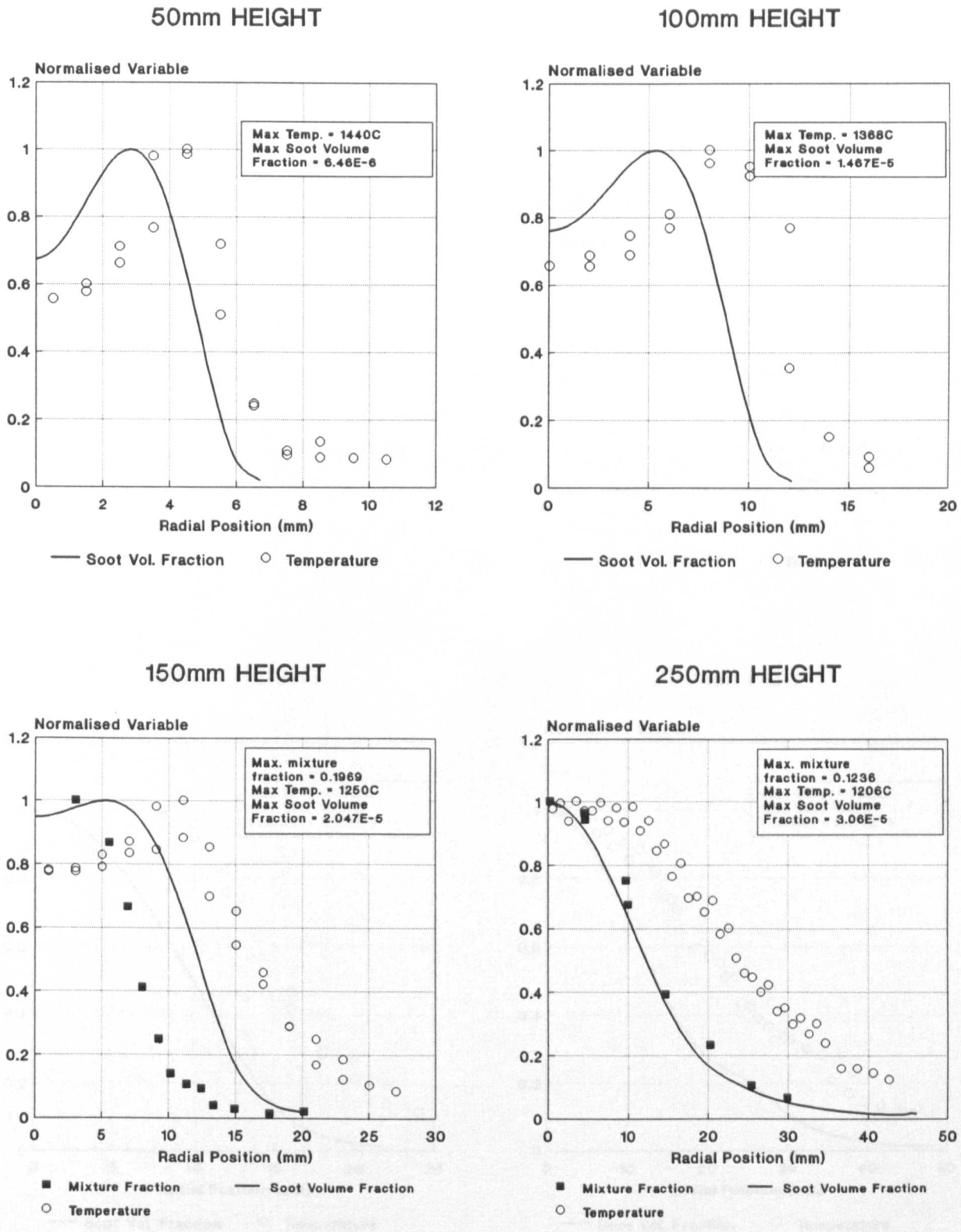

NB: mixture fractions are measured with the mark II system.

Fig(4.16d) A SELECTION OF FOUR RADIAL PROFILES OF NORMALISED MEASURED PROPERTIES IN KEROSINE FLAME D (3.72atm)

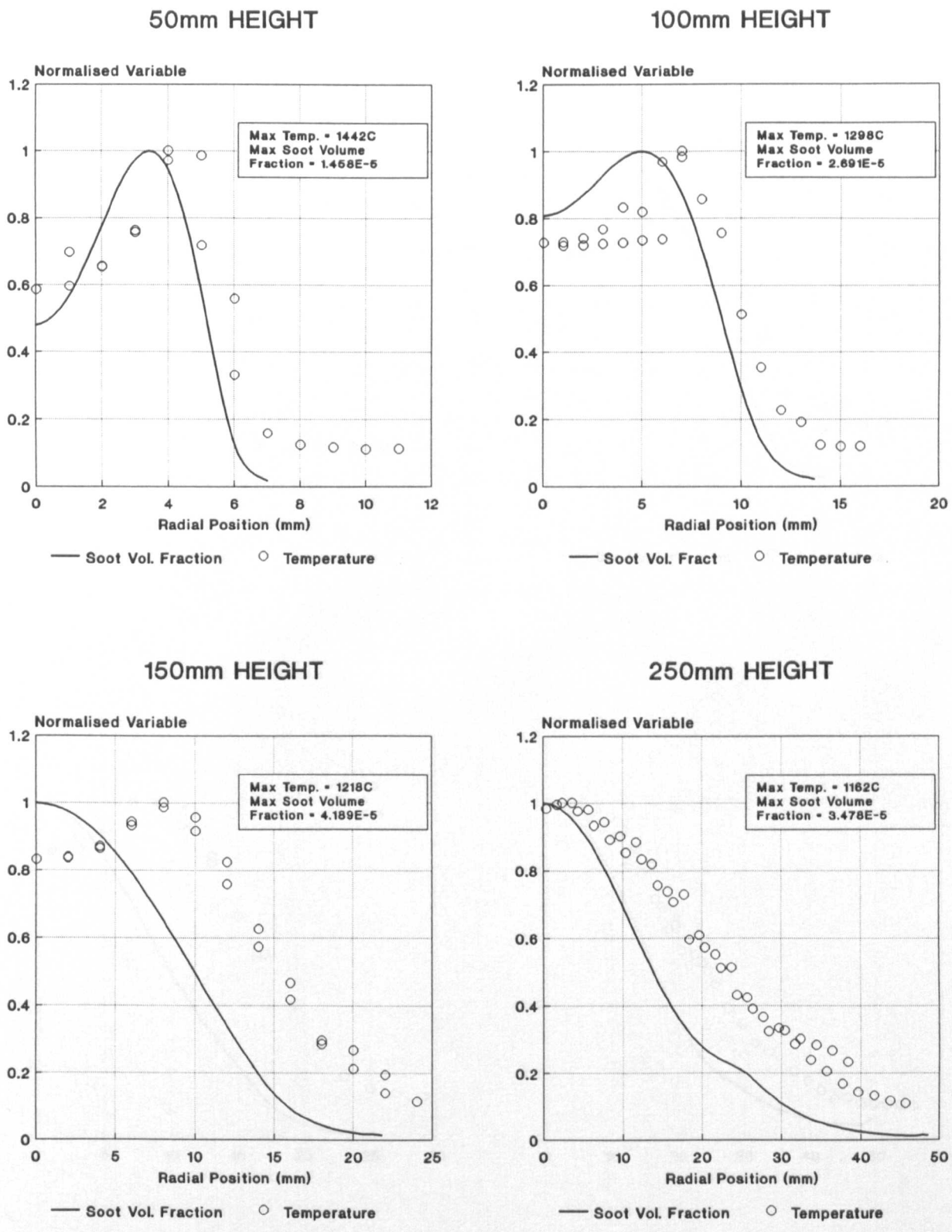

NB: measurement of mixture fraction was impossible with either technique.

Fig(4.16e) A SELECTION OF FOUR RADIAL PROFILES OF NORMALISED MEASURED PROPERTIES IN KEROSINE FLAME E (4.8latm).

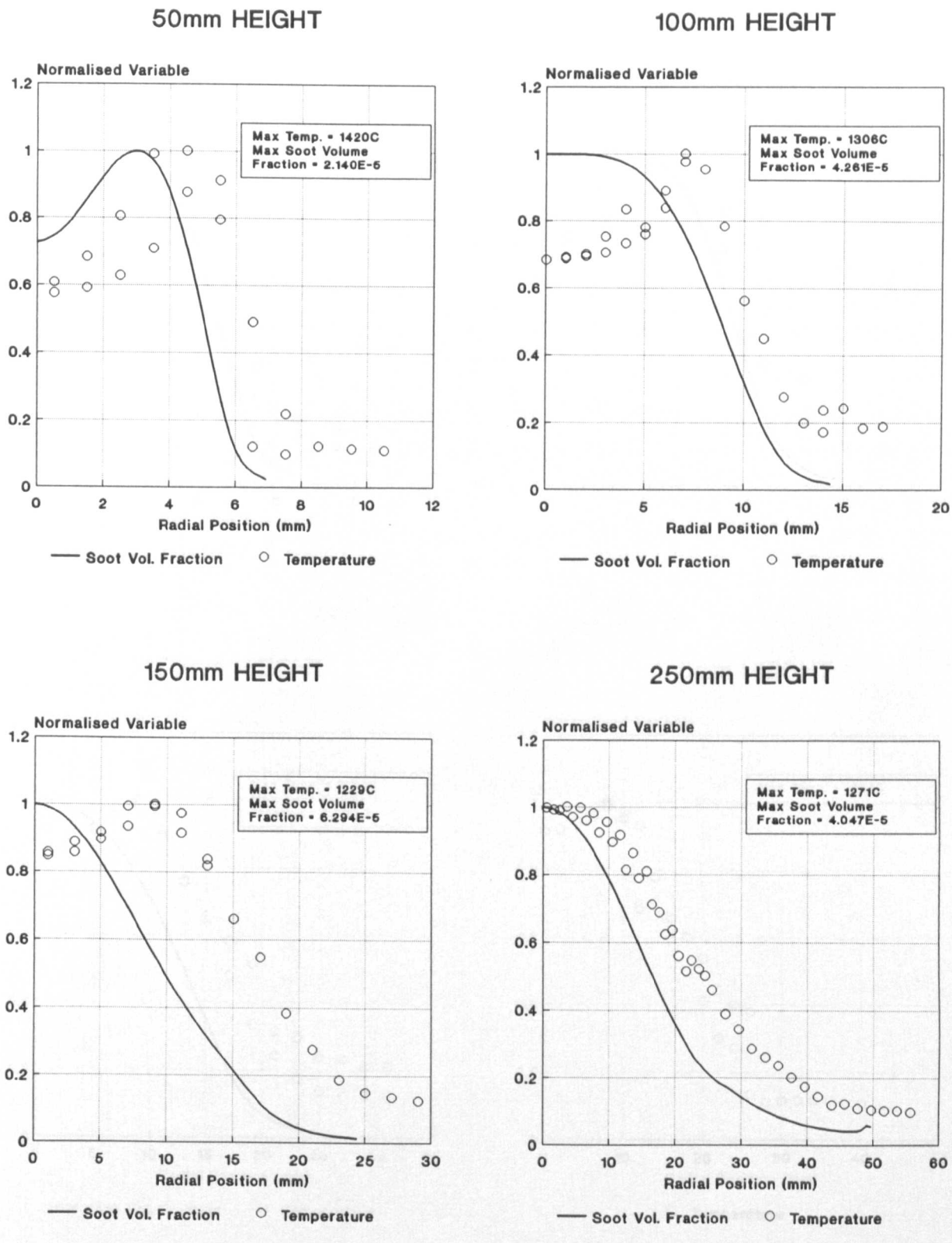

NB: measurement of mixture fraction was impossible with either technique.

Fig(4.16f) A SELECTION OF FOUR RADIAL PROFILES OF NORMALISED MEASURED PROPERTIES IN KEROSINE FLAME F (6.44atm).

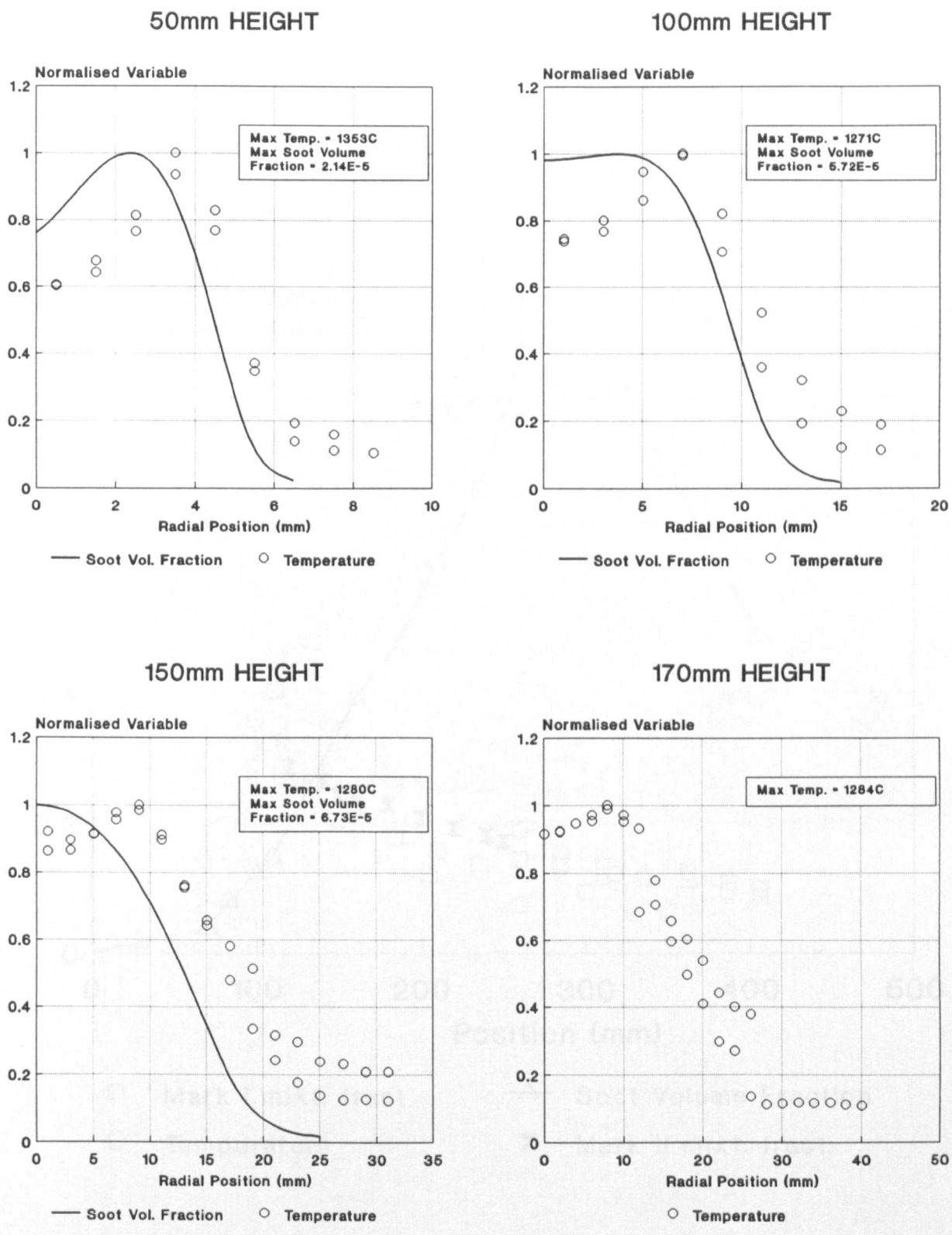

NB: measurement of mixture fraction was impossible with either technique.

Fig(4.17a) THE DEVELOPMENT OF NORMALISED, MEASURED PROPERTIES ALONG THE CENTRELINE OF KEROSINE FLAME A (1.0atm).

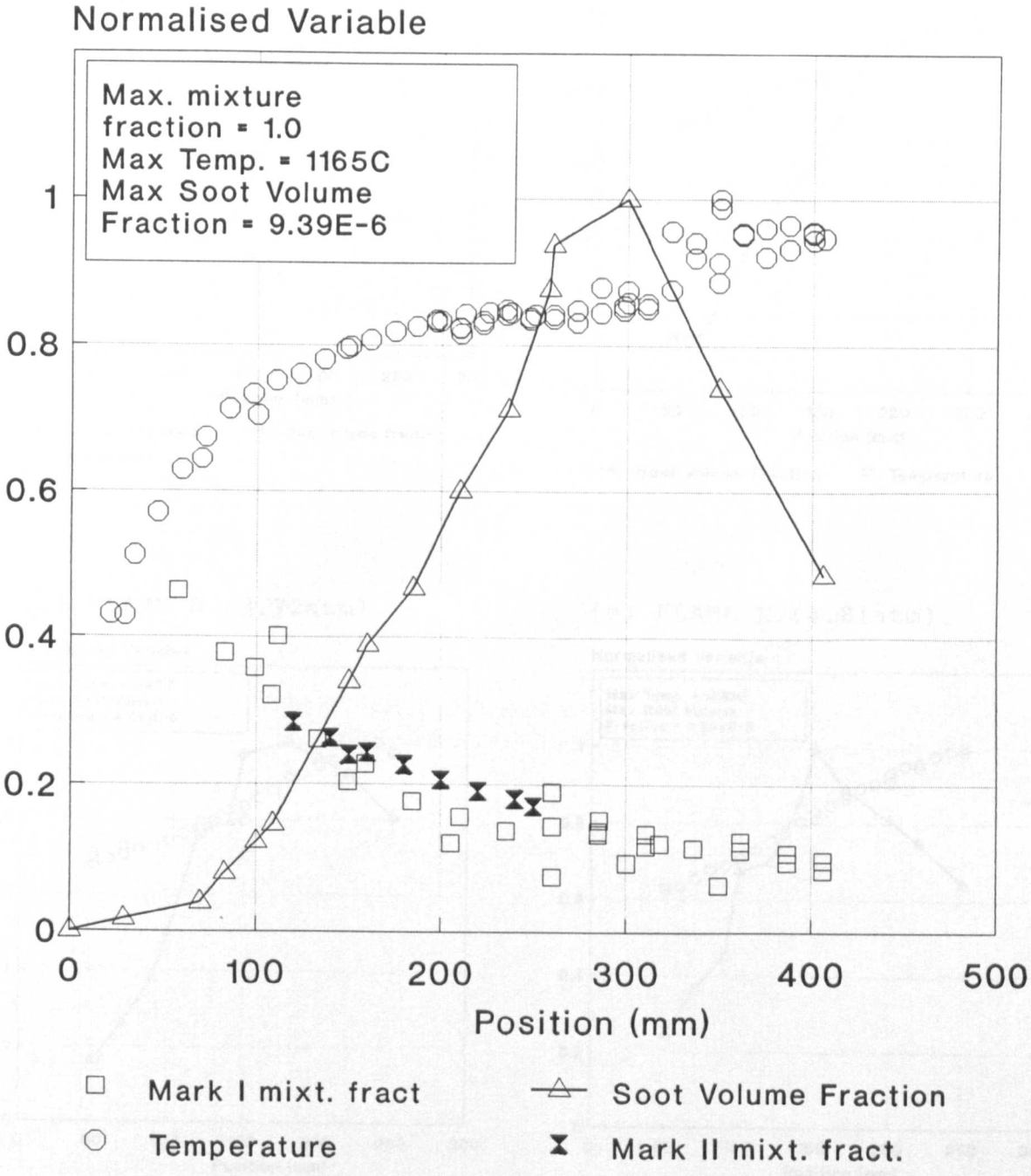

Figs(4.17b-e) THE DEVELOPMENT OF NORMALISED, MEASURED PROPERTIES ALONG THE CENTRELINES OF KEROSINE FLAMES B - E.

(b) FLAME B (2.03atm).

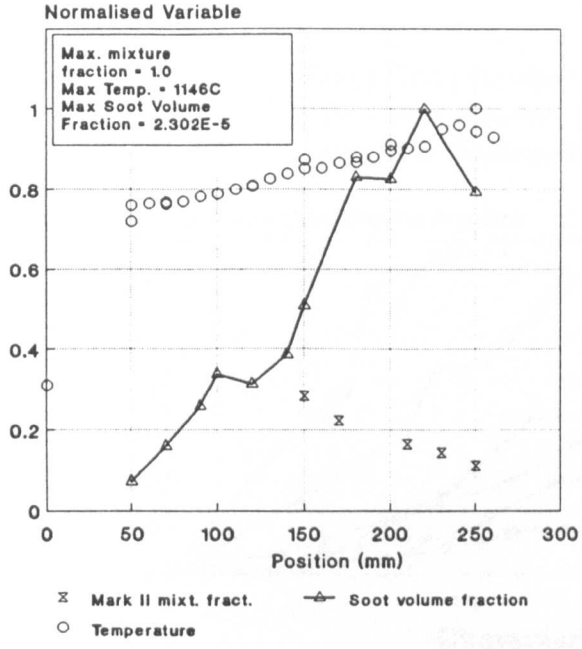

(c) FLAME C (2.72atm).

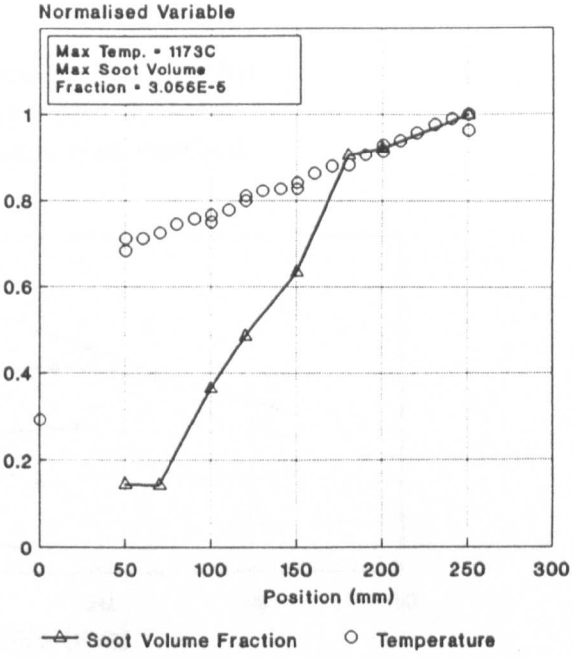

(d) FLAME D (3.72atm).

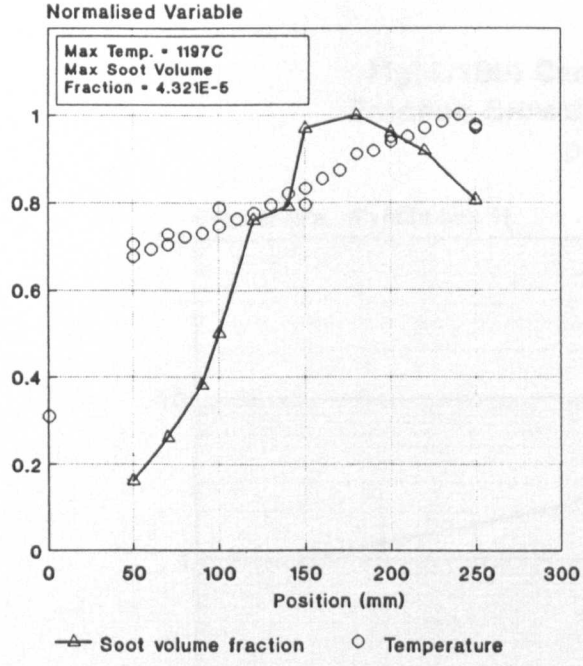

(e) FLAME E (4.81atm).

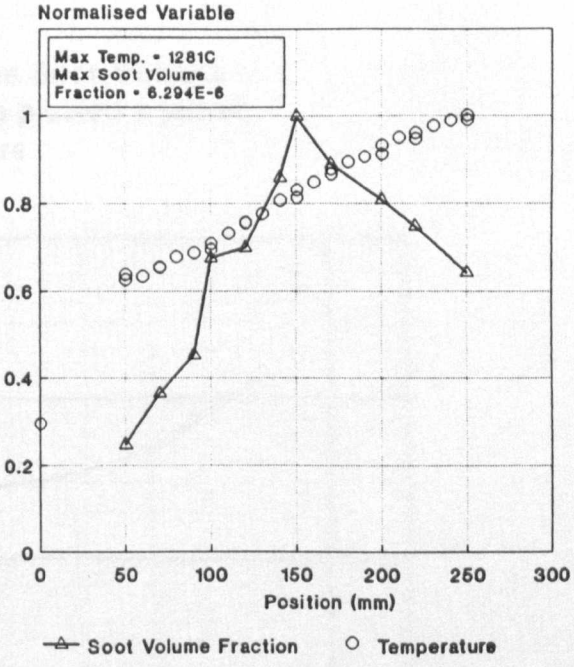

Fig(4.18a) Measured Centreline Soot Vol Fraction against characteristic time for kerosine flames at all pressures studied

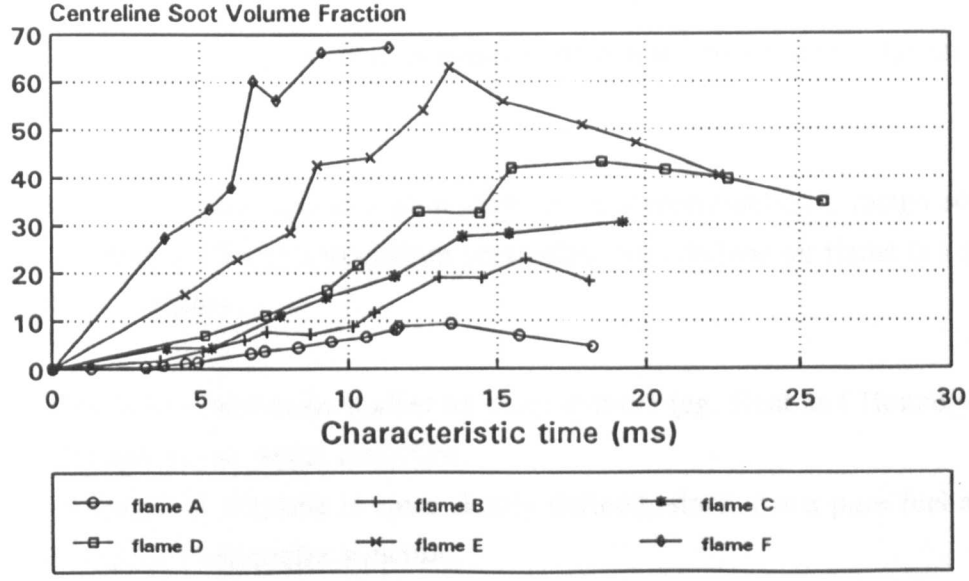

Fig(4.18b) Centreline Soot Volume Fraction Growth Rate plotted against pressure

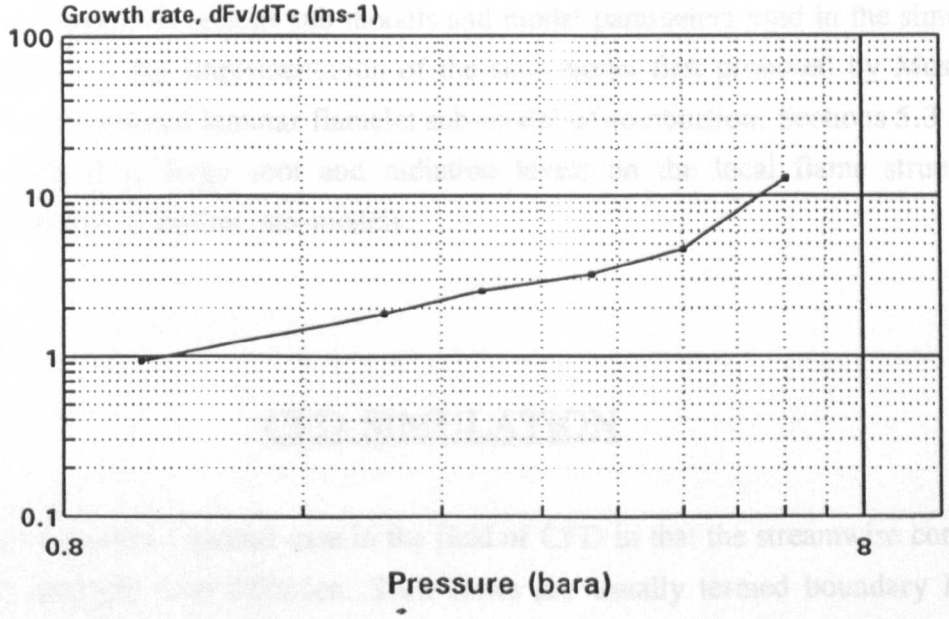

CHAPTER 5: COMPUTATIONAL STUDY

This chapter describes the computational simulation of two of the experimental jet flames described in chapter 4.

Just as the ethylene flame was used as a pilot study in the experimental campaign so it was in the computer simulation. From a modelling standpoint, the ethylene jet flame is a simpler case for a number of reasons.

1) Ethylene flames have been studied by other authors (eg. Kent and Honnery 1987, Syed 1990) and so are better classified.
2) The chemistry of ethylene is more clearly defined, since it is a pure fuel and has a relatively simple molecular structure.
3) The boundary conditions of the kerosine flame are more complex owing to the presence of the wall.
4) The modelling difficulties associated with radiation loss and high soot loadings are less severe in the case of the ethylene flame.

Sections 5.1 describes the various sub models and model parameters used in the simulation. Section 5.2 describes the implementation of the soot model first proposed by Moss et al. 1988 with the conventional laminar flamelet sub-model of combustion. Sections 5.3 and 5.4 describe the affects of large soot and radiation levels on the local flame structure by analysing the effects of further sub-models.

5.1 CFD SIMULATION

The jet flame represents a special case in the field of CFD in that the streamwise convection is very much stronger than diffusion. Such flows are usually termed boundary layer or parabolic flows and great simplification to the solution of the governing equations is possible

by neglecting their streamwise diffusion term. In this case, the flowfield downstream of a particular location will have no influence on that upstream and hence the solution may be performed using a marching procedure in the streamwise direction with only one pass necessary at each location. Using the eddy viscosity hypothesis to model the Reynolds stresses or turbulent scalar fluxes, the resulting Favre averaged governing equation for a general variable ϕ may be written:

$$\overline{\rho}\,\tilde{u}\frac{\partial\tilde{\phi}}{\partial x} + \overline{\rho}\,\tilde{v}\frac{\partial\tilde{\phi}}{\partial r} = \frac{1}{r}\frac{\partial}{\partial r}\left[\frac{\mu_T}{\sigma_\phi}\frac{\partial\tilde{\phi}}{\partial r}\right] + \overline{S_\phi} \qquad (5.1)$$

Where x and r are axial and radial position, u and v are their respective velocity components, ρ is the fluid density, μ_T is the turbulent viscosity, σ_ϕ is the turbulent Prandtl/Schmidt number and S_ϕ is the volumetric source term.

In order to solve the set of governing equations of momentum, mixture fraction, turbulence parameters etc., a modified version of the computer code GENMIX was used throughout (Spalding 1977). Spalding 1977 provides a very detailed description of GENMIX and so only a brief summary is given here.

The general 2D boundary layer equation (5.1) is cast into the Patankar-Spalding coordinate system. This is based upon the Von-Mises system in which the cross stream distance is replaced with the stream function, ψ.

$$\partial\psi = r\rho u\,\partial r \qquad (5.2)$$

With the Von-Mises transformation, the grid follows streamlines. Since, by definition, no mass may cross a streamline there is no cross stream convection term in the resulting equations.

Although obviously advantageous to the solution, the Von-Mises system is uneconomical since the grid is not necessarily bounded by the width of the jet. It is for this reason that the Patankar-Spalding system was developed. The equations are recast with a new cross stream coordinate, the normalised stream function, ω.

$$\omega = \frac{\psi - \psi_I}{\psi_E - \psi_I} \tag{5.3}$$

Where E and I refer to the external and internal flow boundaries of the domain. This new coordinate is, by definition, bound by the flow domain and grows with it. No wastage of grid nodes and hence computational storage and effort results.

The generalised differential equation cast into this coordinate system then takes the following form (Spalding 1977):

$$\frac{\partial \phi}{\partial x} + (a + b\omega)\frac{\partial \phi}{\partial x} = \frac{\partial}{\partial \omega}\left[c\frac{\partial \phi}{\partial \omega}\right] + \frac{1}{\rho u}S_\phi \tag{5.4}$$

The cross stream convection term reappears since the grid no longer follows streamlines and is multiplied by the factor of (a + bω). This factor may be shown (Spalding 1977) to be equal to the mass flow rate across the line of constant ω divided by (ψ_E - ψ_I). In situations where the entrainment rate is zero, the lines of constant ω will follow streamlines.

In order to solve the exact set of analytical equations (5.4), they are discretised using the finite volume technique. The equations are integrated over a number of small control volumes or cells in order to yield a finite number of simultaneous equations. In order to calculate the value of the variables at the cell boundaries from the values at the centre, a hybrid differencing scheme is used.

The resulting set of algebraic equations are then solved using a tri-diagonal-matrix-algorithm (TDMA) and the solution proceeds in a marching manner with the equations solved simultaneously at each forward step.

The variable, ϕ, in equations 5.1 and 5.4 may be any vector or scalar quantity which obeys the laws of conservation. For each variable, the turbulent Prandtl/Schmidt number σ_ϕ and volumetric source term, S_ϕ, must be specified.

A maximum of eight Favre averaged, simultaneous equations have been solved in the present

study. They are:

- mean streamwise velocity, $\tilde{u}$
- turbulence parameters, k and ϵ
- mean and variance of mixture fraction, $\widetilde{\xi}$ and $\widetilde{\xi''^2}$
- mean soot mass fraction and normalised number per unit mass, $\widetilde{\phi}_m$ and $\widetilde{\phi}_n$
- mean mixture enthalpy, $\widetilde{h}$

The Prandtl/Schmidt numbers and source terms used for each of these equations is given in table 5.1.

5.1.1 VELOCITY

The source term of mean streamwise velocity contains two terms: gravitational and pressure gradient body forces.

The gravitational component of this term is simple to calculate since it merely consists of the known gravitational acceleration, g ($=9.81 ms^{-2}$), multiplied by the mixture density, ρ, which is taken from the upstream station.

The pressure gradient term is somewhat more difficult to calculate since it depends upon conditions downstream. Since, in the parabolic GENMIX calculation, the marching solution procedure permits no re-iteration to any previous upstream location, the value of dP/dx must be estimated before the step is made.

This estimation is made on the basis of changes in flow area, density and wall shear stress. Once the step is made, mass continuity is checked to confirm an appropriate guess was made. If this is within 0.1% of the actual value, the solution continues, otherwise the velocity field is corrected by a small factor to re-establish continuity.

In practice, this correction procedure is called very infrequently. However, instabilities in the beginning of the calculation sometimes necessitated its use in the first few forward steps. Although the very small corrections necessary had negligible effect on the overall calculation, they could cause problems with the turbulence model - see section (5.1.3).

5.1.2 WALL FUNCTIONS

For the case of the kerosine jet flame studies in which the flames were enclosed in a pyrex flame tube (chapter 3), the presence of the tube wall as the external flow boundary created particular modelling problems. Near walls property gradients, especially of velocity and turbulence parameters, can be very high. If these gradients are to be resolved using conventional CFD procedures a large number of computational nodes would be required.

In a practical calculation in which computer storage and time are at a premium such 'low Reynold's number' methods are very expensive. The alternative solution of using pre-defined wall functions - the high Reynolds number method - is therefore often adopted. The wall functions describe the properties at the node adjacent to the wall based on the shear stress which prevails at that location.

Launder and Spalding 1974 have defined wall functions for velocity and turbulence parameters which have proved to be very successful. Avva et al. 1990 show that, for a variety of flow geometries the high Reynolds number approach gives at least as good agreement with experiment as low Reynolds number methods but with substantial computing savings. The high Reynolds number technique is also adopted within GENMIX. For a detailed description of its implementation to the algorithm, the reader is referred to Spalding 1977.

5.1.3 TURBULENCE MODEL

The two equation turbulence model of Jones and Launder 1972 has been adopted in the present study due to its simplicity and known accuracy for the jet flame geometry.

The constants $C_{\epsilon 1}$ and $C_{\epsilon 2}$ in the modelled source term of dissipation rate, ϵ, (table 5.1) and the constant C_{μ} in the definition of turbulent viscosity (eq.2.16) have been empirically determined in plane, cold jets to be 1.44, 1.92 and 0.09 respectively (Jones and Launder 1972). However, there are no grounds for using these constants or indeed the model itself in reacting jets. For example Libby and Bray 1980 suggest that making the gradient diffusion assumption precludes phenomena such as counter gradient diffusion resulting from the differential affect of pressure on fluid elements of different density. However, the unmodified two equation model has been shown by a variety of authors (Liew 1983, Kent and Honnery 1987, Syed 1990) to give accurate results in the prediction of the circular, jet flame and so

is adopted here.

A number of works have been concerned with the so called round jet / plane jet anomaly. It has been widely demonstrated that the spreading rate of round jets is overpredicted by a factor of $\simeq$ 40% when using the uncorrected k - ϵ model of Jones and Launder 1972 which was originally developed on planar jets. An explanation to this anomaly has been proposed by Pope 1978. He suggests that positive strain on vortex tubes in a flow will cause that vortex to reduce in size and increase in frequency in order to maintain angular momentum. Therefore, in regions of the flow where this occurs there will be a greater scale reduction leading to an increased dissipation and reduced turbulent viscosity.

In planar 2D flows, no vortex stretching occurs since the mean vorticity is aligned with the plane of the flow. In axisymmetric jets, however, as the jet spreads rings of vorticity may be stretched and hence the effective viscosity reduced.

This concept led Pope 1978 to propose a more generalised version of the eddy dissipation equation which takes these factors into account. Other authors (eg. Morse 1977, McGuirk and Rodi 1977, Launder et al. 1972), however, have proposed simpler empirical modifications to the existing equations which, although restricting the generality of the model, have proven useful and accurate.

Liew 1983 and Syed 1990 found the correction proposed by Morse 1977 to be accurate in the case of free, round jets. This takes the form of a modification to the constant $C_{\epsilon 1}$:

$$C_{\epsilon_1} = 1.4 - 3.4\left[\frac{k}{\epsilon}\frac{d\tilde{u}}{dx}\right]^2_{cl} \qquad (5.5)$$

The subscript cl refers to centreline values and the effect of the expression is to increase the value of $C_{\epsilon 1}$ and hence dissipation rate in regions of rapidly decaying centreline velocity. This expression was used in all calculations of the unconfined ethylene jet reported in this study where it proved to be the best. For all calculations of the confined kerosine jets, however, the correction by Rodi 1972 was used in preference, eq (5.6):

$$C_{\varepsilon_2} = 1.92 - 0.0667\left\{\frac{\delta}{\tilde{u}}\frac{d\tilde{u}}{dx}\right\}_{cl}^{0.2}$$

$$C_{\mu} = 0.09 - 0.04\left\{\frac{\delta}{\tilde{u}}\frac{d\tilde{u}}{dx}\right\}_{cl}^{0.2} \qquad (5.6)$$

Where δ is the half width of the jet - the radius at which the velocity has dropped to half its centreline value.

The reason for this was due to initial instabilities in the confined jet calculation resulting from larger pressure corrections with this geometry - section (5.1.1) - due to the presence of the wall boundary. Although the corrections were small, so also was the initial step size. The resulting velocity gradient taken to the third power in Morse's expression (5.5) were sometimes large enough perturb the calculation significantly. The modification proposed by Rodi 1972 was less sensitive to this initial instability since the exponent of the velocity gradient was only 0.2.

5.1.4 COMBUSTION MODEL

As explained in chapter 2, the benefits - in terms of computer time and effort - which are possible by making the fast chemistry, equal diffusivity assumptions are very desirable and hence are exploited here. Under these assumptions, the chemistry becomes independent of the flowfield and all chemistry dependent scalars may be expressed as unique functions of the conserved scalar mixture fraction, ξ, which has no volumetric source term, S_ϕ.

In a turbulent calculation, in which the governing equations are averaged and instantaneous information is lost, knowledge of the PDF of mixture fraction is still required in order to perform the integration to retrieve averaged scalar information - chapter 2.

The presumed PDF technique was employed whereby the PDF of mixture fraction was prescribed on the basis of its first and second moments, ξ and ξ''^2. Two popular forms of the assumed PDF are the normalised beta function (cf. Liew 1983) and the clipped gaussian (cf. Lockwood and Naguib 1975). The beta function is more attractive since it is naturally bounded between 0 and 1 and is simply defined by its mean and variance. Since Bilger 1980 found that both forms of the PDF gave good agreement with experimental data the

normalised beta function was used here.

The beta function is defined

$$B = \xi^{(\alpha - 1)}(1 - \xi)^{(\beta - 1)} \tag{5.7}$$

(Abramowitz and Stegun 1964), where the exponents α and β are:

$$\begin{aligned} \alpha &= \tilde{\xi}\left[\frac{\tilde{\xi}(1 - \tilde{\xi})}{\widetilde{\xi''^2}} - 1\right] \\ \beta &= \frac{\alpha(1 - \tilde{\xi})}{\tilde{\xi}} \end{aligned} \tag{5.8}$$

The total area under the beta function is not unity and so the function must be normalised by this integral in order to yield the PDF:

$$P(\xi) = \frac{B(\xi)}{\int_0^1 B(\xi')\, d\xi'} \tag{5.9}$$

In the CFD simulation, the mean and variance of mixture fraction are obtained by the solution of their respective conservation equations.

The equation of mean mixture fraction is simple since it has no source and requires no further assumptions than the gradient diffusion approximation (chapter 2). The equation of variance of mixture fraction, ξ''^2, is derived by multiplying the instantaneous equation for ξ with ξ'' and averaging. The resulting equation contains a source due to turbulent generation and dissipation, the modelled form of which is written in table (5.1) (Spalding 1971).

The modelled terms contain two new constants C_{g1} and C_{g2}. Although most authors agree on the value of $C_{g2} = 2.8$ (Faeth et al. 1985, Syed 1990, Spalding 1971). There is more ambiguity in the magnitude of C_{g1}. Reported values vary between 1.25 and 2.0 (Spalding

1971). The value chosen here is that used by Faeth et al. 1985 and Syed 1990, $C_{\varepsilon 1} = 1.89$.

The value of the turbulent Prandtl / Schmidt numbers, σ_ϕ, for the mean and variance of mixture fraction are also subject to some ambiguity. Although the most commonly used value for jet flame predictions is 0.7 (Godoy 1982, Liew 1983, Kent and Honnery 1987) values as high as 0.9 have been reported (eg. Jones and McGuirk 1979). Often, in the absence of experimental mixture fraction data in combusting flow, this value is chosen on the basis of cold flow measurements.

Given the experimental data of mean mixture fraction available from the present study, it was possible to test a variety of values of σ_ϕ for agreement of mean mixture fraction with measurement. It was found that a value of 1.0 gave the closest agreement with experiment and so this was used for both mean and variance.

5.1.5 SOOT MODELLING

As described in chapter 2, soot presents difficulties from a modelling standpoint since its chemistry is slow with relation to the mixing timescales associated with a diffusion flame. As a result, if single state relationships of soot parameters are prescribed (eg Kent and Honnery 1987, Faeth et al. 1987), they will only be valid in a very narrow regime. In reality, soot concentration also depends upon residence time.

In tackling a similar problem but for the trace species nitrous oxide, NO, Bilger(1976) postulated that, although, the species fraction itself could not be described by a unique state relationship of mixture fraction, its volumetric source term may.

Adopting this strategy, Moss et al. 1987 proposed a model of soot formation, based upon the work of Gilyatzedinov 1972, which could be coupled with the conventional conserved scalar / laminar flamelet model.

The two step model characterises soot formation by its volume fraction, f_v and volumetric number density n. Under the assumption that the particles in the soot aerosol are spherical and monodisperse these two parameters may be linked with particle diameter.

$$f_v = \frac{1}{6} n \pi D^3 \tag{5.10}$$

Due to the typical magnitude of soot number density in flames (cf. Kent and Wagner 1984, order $\{10^{17}\}$), it is normalised by Avogadro's number, N_o, for convenience to give the new parameter N (= n/N_o).

Conservation equations for Favre averaged soot mass fraction, ϕ_m ($=\rho_s f_v/\rho$) and normalised number per unit mass, ϕ_n ($=N/\rho$) are written where ρ_s is the density of soot (= 1800kg/m^3). Reynolds averaged properties may be inferred from these directly since they include the reciprocal of density:

$$\widetilde{\left(\frac{\Phi}{\rho}\right)} = \frac{\overline{\Phi}}{\overline{\rho}} \tag{5.11}$$

and hence:

$$\begin{aligned} \overline{\rho_s f_v} &= \tilde{\phi}_m \overline{\rho} = \overline{m} \\ \overline{\frac{n}{N_o}} &= \tilde{\phi}_n \overline{\rho} = \overline{N} \end{aligned} \tag{5.12}$$

The volumetric source terms of these two parameters may be described by the processes of nucleation, coagulation, surface growth and oxidation (Kent and Wagner 1984). In a turbulent situation, since surface growth, coagulation and oxidation rates will themselves depend upon the soot parameters, the exact source terms of these two parameters may be expressed as follows.

$$\overline{S_{\phi_s}} = \int_0^\infty \int_0^1 S(\phi_s, \xi)\, P(\phi_s, \xi)\, d\xi\, d\phi_s \tag{5.13}$$

The evaluation of such an integral, even if the joint statistics of mixture fraction and soot were known, would be extremely time consuming in a practical combustion calculation.

Therefore, when applying the model of soot formation first proposed by Moss et al. 1987, Syed et al. 1990 assume the resulting cross correlation terms - between mixture fraction, soot volume fraction and number density - to be negligible in order to simplify the calculation greatly:

Source of number

$$\overline{S_{\phi_n}} = \overline{\frac{dN}{dt}} = \underbrace{\overline{\alpha}}_{nucleation} - \underbrace{\overline{\beta}\,\overline{N}^2}_{coagulation} \qquad (5.14)$$

Source of mass

$$\overline{S_{\phi_m}} = \overline{\frac{d}{dt}(\rho_s f_v)} = \left.\begin{matrix} \overline{\gamma}\,\overline{n} \\ \overline{\gamma}\,\overline{n}^{1/3}\,\overline{m}^{2/3} \end{matrix}\right\}_{surface\ growth} + \underbrace{\overline{\delta}}_{nucleation} \qquad (5.15)$$

where:

$$\begin{aligned} \alpha &= C_\alpha \rho^2 T^{1/2} X_f^{M_\alpha} \exp(-T_\alpha/T) \\ \beta &= C_\beta T^{1/2} \\ \gamma &= C_\gamma \rho T^{1/2} X_f^{M_\gamma} \exp(-T_\gamma/T) \\ \delta &= C_\delta \alpha \end{aligned} \qquad (5.16)$$

$C_{\alpha-\delta}$, $T_{\alpha,\gamma}$ and $M_{\alpha,\gamma}$ are empirical constants derived from laminar flame experiment coupled with detailed flowfield prediction, χ_f is the parent fuel mole fraction based on the flamesheet assumption.

Attention is drawn to the two possible forms of the surface growth term in the source of soot mass, eq(5.15). One is proportional to number whilst the second is proportional to surface area. Although, physically, the latter of these two seems the most plausible, Moss et al. 1988 found the growth of soot mass in laminar ethylene / air flames to be virtually linear with residence time which, under the assumption of plug flow (appendix D), suggests the former to be most appropriate.

Stewart et al. 1991 give another explanation to this phenomenon which they also observed

in conjunction with a pronounced migration of peak soot volume fraction to richer mixtures and lower temperatures in laminar Wolfhard Parker flames of kerosine / air at a variety of pressures and dilutions. In previous work Moss and coworkers (cf. Moss et al. 1987, 1988, Syed 1990) had always assumed a linear dependence of the surface growth and nucleation source terms with flamesheet parent fuel fraction, χ_f (ie. $M_{\alpha,\gamma} = 1$), when in reality dependence on some other intermediate species seems more likely. They, therefore, proposed a higher order fuel fraction dependence of the source terms in order to address this issue without compromising model simplicity.

Recent work by Leung et al. 1991 on sooting propane flames has taken this concept to the next order of complexity. With a soot model that is very similar in form to that of Moss and coworkers they propose the surface growth and nucleation terms to be proportional to the concentration of acetylene, C_2H_2, a species strongly linked with soot formation (cf. Glassman 1988). Such a strategy requires knowledge of the acetylene concentration which is gained via detailed or reduced scheme chemical kinetic simulation.

Neither model implicitly includes the mechanism of soot oxidation since this occurs in different regimes than formation. In turbulent flames, however, this is not the case. Due to stronger mixing and turbulent fluctuations, the distribution of mean oxidant concentration is more widespread and soot oxidation must be considered in all locations.

For reasons outlined in section (2.1.5), the mechanism of Nagle and Strickland-Constable 1962 is used here. The mechanism describes oxidation of heated carbon rods of various quality by a jet of oxygen at various partial pressures. The results are empirically fitted to a mechanism under the assumption that carbon surface is covered by two types of reactive site which react with oxygen at different rates and whose relative abundance depends upon surface temperature. The specific oxidation rate is then specified with the following expression:

$$\begin{aligned} K_A &= 20\exp(-15100/T) \\ K_B &= 4.46\times10^{-3}\exp(-7650/T) \\ K_T &= 1.51\times10^{5}\exp(-48800/T) \\ K_Z &= 21.3\exp(+2063/T) \end{aligned} \qquad (5.17)$$

$$X = \frac{1}{1+\frac{K_T}{K_B p_{O_2}}} \tag{5.18}$$

$$\dot{\omega}_{OX} = 120\left[\left(\frac{K_A p_{O_2}}{1 + K_Z p_{O_2}}\right)X + K_B p_{O_2}(1 - X)\right] \ (kg\, m^{-2} s^{-1}) \tag{5.19}$$

Where p_{O2} is the partial pressure of oxygen molecule in atmospheres.

The surface area per unit volume of the soot may be specified from its volume fraction and number density in order to give the contribution of oxidation to the volumetric source terms (cf. appendix E).

$$\left|\frac{d\phi_m}{dt}\right|_{ox} = - N_o^{1/3} e\, \dot{\omega}_{ox} m^{2/3} N^{1/3}$$

$$\left|\frac{d\phi_n}{dt}\right|_{ox} = - N_o^{1/3} e\, \dot{\omega}_{ox} m^{-1/3} N^{4/3} \tag{5.20}$$

Where $\epsilon = (36\pi/\rho^2)^{1/3}$.

Following the predictions of Syed 1990 who used the same model in similar calculations of jet flames and buoyant fires, the Prandtl / Schmidt numbers of both number density and soot volume fraction were assigned the value of 1.

5.1.6 RADIATION LOSS

It has been found by many workers (eg. Liew 1983, Fairweather et al. 1992) that, for a variety of fuels, the solution of the energy equation in a sooting combustion simulation is not necessary since the prescription of a single, radiation perturbed temperature flamelet, incorporating a fixed amount of radiation loss suffices to give good agreement of predictions with measurements.

The vaporised kerosine jet flames studied here, however, represent a far more extreme case in that soot loadings and hence radiation losses are far greater than most laboratory scale flames of this type. Although the single radiation perturbed flamelet strategy was attempted, its validity and accuracy were greatly compromised. For this reason, although the resulting calculation procedure becomes a great deal more complex and time consuming, fully coupled radiation loss calculations were performed in an attempt to improve the predictions. The procedure used is outlined in section 5.4. This requires the solution of a further equation of Favre averaged mixture enthalpy, $\tilde{h}$.

In view of the complexities of performing such a fully coupled calculation, the source term of this equation was kept to its simplest. Rather than solving a further equation - the radiative transfer equation, chapter 2 - in order to estimate local radiation intensity, I_λ, the radiation was assumed to be predominantly from soot and the flame in the optically thin regime. Although, from extinction measurements, in the visible regime the latter of these assumptions is somewhat dubious, it sufficed as a good starting point.

The assumptions allow a simple, analytical expression of the volumetric source term of mixture enthalpy to be derived. The one used here is similar to that derived by Hall 1988 - see table 5.1 - its detailed derivation is given in appendix A.

Since mixture enthalpy is another conserved scalar in adiabatic, unity Lewis number systems, it was assigned the same value of Prandtl / Schmidt number, σ_ϕ, as mixture fraction - 1.0.

5.2 SINGLE FLAMELET MODELLING

5.2.1 ETHYLENE FLAME

Syed 1990 found that one of the main difficulties in testing the validity of a soot model developed from laminar flames was the lack of suitable experimental data for comparison. In his study of jet flames, he found the most suitable data set for this purpose to be that of Kent and Honnery 1987. Although mean temperature and soot volume fraction are reported, the absence of any data on the local mixture state or composition created uncertainties. The addition of mean mixture fraction in the data set of the ethylene jet pilot study here is, thus, very useful. The fluctuating component or shape of the PDF, however, remain uncertain.

Before the soot simulation, the calculation of the mixing and thermochemical fields was made in order to check the suitability of the boundary conditions and finite difference grid used.

Since the flame was axisymmetric, only half the flame was modelled with an axis of symmetry (zero gradient, zero flux) boundary defined at the centreline. 40 grid nodes proved sufficient to make the solution grid independent.

The inlet boundary conditions where possible were taken from experimental information. However, no information on the turbulence parameters was available and so intuition was used. Following Liew 1983 and Syed 1990, the turbulent intensity was assumed to be dependent upon mean velocity and hence:

$$k = A\,\tilde{u}^2 \tag{5.21}$$

Liew 1983 chose a value of A of 0.0004 whilst Syed 1990 chose a value of 0.003. The value of 0.003 was used here. By relating the integral scale of turbulence to the burner radius the dissipation rate was then estimated:

$$\epsilon = \frac{k^{3/2}}{r} \tag{5.22}$$

The sensitivity of the calculation to these somewhat arbitrary values was investigated by Syed 1990 who found order of magnitude changes in both parameters to affect the calculation only in the near burner region.

Although the mass flow rate of fuel was known (12.0g/min), the profile of velocity at the burner exit was also uncertain,. Tests again showed the calculation to be insensitive to the profile and so the simplest was used - a top hat profile.

The initial mean mixture fraction was set to unity in the fuel stream, zero in the air stream. The variance was set to zero throughout.

Regarding the flamelets of temperature and density, two sources were considered: diffusion flamelet predictions and experimental measurements. The computer program of Warnatz (cf. Warnatz 1981) which models the stagnation streamline of a counterflow burner was available. This was used to make adiabatic laminar flamelet predictions. The strain rate was set to the value of $100s^{-1}$, a low value in keeping with the lower degrees of stretch possible in a co

flowing situation.

Experimental data is reported by Moss et al. 1988 for an ethylene / air laminar Wolfhard-Parker type flame. Since radiative loss is a gradual process in the flame, the reported best fit flamelet of experimental temperature at different flame heights will incorporate an average radiative loss. Density was estimated with knowledge of the species composition from flamelet calculations.

Shown in fig.(5.1) are the flamelets of temperature and density thus derived. The effect of radiative loss in the experimental flamelets is evident. Considering temperature, the two flamelets agree well on the lean side but differ by up to 200K on the rich side largely due to the increased radiating propensity of soot which is formed in this region. Since the experimental flamelet has been used to give accurate predictions of temperature of both laminar and turbulent laboratory flames (Moss et al. 1988, Syed 1990), it was also used here.

Shown in fig.(5.2) are the resulting predicted mean and variance of mixture fraction and mean temperature on the centreline of the flame. The agreement of mean mixture fraction is excellent throughout the region of measurement. Although there is no data to compare the variance, the shape and magnitude of the profile is comparable to the measurements of Becker, Hottel and Williams 1967 in hydrogen jet diffusion flames. Axial measurements of temperature are, unfortunately, sparse. The expected initial underprediction of temperature followed by overprediction - due to the gradual radial heat loss in the flamelet - is observed to some extent, although it is surprising that the predicted temperature is only 50K lower than the measured values at height X=160mm by which time the flame has not had sufficient time to radiate significantly (X/D = 52, t_{res} = 11.5ms, $f_v = 2\times10^{-7}$ {cf. Max value 2.1×10^{-6} @x = 300mm}). This observation is not unique to these predictions but may also be seen in many jet flame simulations (Liew 1983, Syed 1990, Fairweather et al. 1992). Discussion is deferred until section 5.4.

Plotted in fig.(5.3) are radial plots of mean mixture fraction and temperature at two representative heights X = 160, 350mm. Agreement of predicted mixture fraction is again excellent both in terms of peak values and radial spread. The agreement of temperature is also good, although the high gradients of temperature seen in the measurements at the lower stations are not predicted to be so large.

The general agreement with the mixing and thermochemical fields with experiment was considered satisfactory to apply the soot model. Although measurements suggest that it could be significant (see chapter 4), the effect of soot as a sink to gaseous mixture fraction was not considered in the initial calculation.

The soot model of Moss et al. 1988, which describes the growth of soot in laminar ethylene / air flames, was used here. The surface growth term was proportional to number density alone (eq(5.15) and the fuel fraction dependence of the nucleation and surface growth terms (α and γ) was linear (ie. $M_{\alpha,\gamma} = 1$).

The values of the constants cited in the original paper are as follows:
$C_\alpha = 1.7\text{x}10^8$ ($m^3kg^{-2}K^{-½}s^{-1}$), $C_\beta = 1.0\text{x}10^9$ ($m^3K^{½}s^{-1}$), $C_\gamma = 4.2\text{x}10^{-17}$ ($m^3K^{-½}s^{-1}$),
$C_\delta = 144$ (kg), $T_\alpha = 46100$ (K), $T_\gamma = 12600$ (K)

Flamelets of soot parameters derived using these were found to be unrealistic. From the plug flow analysis of the soot source terms (appendix D) it was found that the saturated number density was of the order $10^{20}m^{-3}$. With the peak measured volume fraction ($2.1\text{x}10^{-6}$), this would imply a peak soot particle diameter of $\simeq$5nm, a value far smaller than those reported by most particle sizing techniques (cf.Bard and Pagni 1981, Charampopoulos and Felske 1987, Kent and Wagner 1982).

Syed 1990 used this model in his prediction of a similar jet flame and found it necessary to reduce the oxidation rate reported by Nagle and Strickland-Constable 1962, eq.(5.20), by a factor of 70 in order to get more realistic values. The surface area of a soot aerosol is proportional to $n^{1/3}$ (eq.(5.10)). This - and hence oxidation rate - would also be reduced by a factor of 70 if number densities were reduced to values of order 10^{14}. This would imply a peak soot particle diameter of $\simeq$ 200nm - a value in much closer agreement with measured values including the DMPS measurements in the present study.

In order to reduce the predicted numbers to these values either the coagulation rate must be increased or the nucleation rate decreased. Since reducing the nucleation rate would also affect the mass equation, the former strategy was adopted. Since from plug flow analysis (appendix D), the saturated number density is proportional to $\beta^{-½}$, C_β was increased to a value of $9\text{x}10^{19}m^3K^{½}s^{-1}$. C_γ was accordingly decreased to a value of $1.26\text{x}10^{-11}m^3K^{-½}s^{-1}$ in order to bring the surface growth term back to its original value.

At first glance, such a significant deviation of the coagulation term from its original value seems unreasonable. However, the modelled form of the nucleation term - assuming soot to be a monodisperse aerosol when undoubtedly it is a polydispersion in which a highly complex cascade process of size changing exists - should be expected to require a large degree of empirical modification and so this is not suprising.

The flamelet of parent fuel fraction, χ_f, in the source term equations (5.14,15) was taken from its Burke Schuman flame sheet approximation as with the original paper (Moss et al. 1988), the partial pressure of oxygen, p_{o2} in the oxidation mechanism, eq.(5.20), was taken from the laminar flamelet simulation.

The resulting flamelets of the soot parameters using the modified constants are plotted in fig.(5.4). Of particular note are the curves of α and ω_{ox}. They are both extremely restricted in mixture fraction space due to their high activation energies. Such functions represent a much sterner test to the presumed PDF laminar flamelet technique than other more continuous flamelet profiles such as temperature.

Shown in fig.(5.5) is a plot of predicted soot volume fraction, f_v, along the axis of the flame and three radial plots at axial heights, X = 100, 250, 350mm. Considering, first, the formation of soot with no oxidation, it can be seen that the growth rate is in error. The predicted point of inception of soot on the centreline - X = 40mm - occurs before that measured - X = 100mm - and results in an early overprediction of soot. The subsequent rapid growth of measured soot is not matched by the predictions resulting in underprediction for X > 200mm.

The incorporation of the oxidation mechanism reduces the predicted soot levels quite substantially and, although the peak value is predicted incorrectly, the shape of the predicted axial profile is in good agreement with measured values. However, some features are poorly reproduced. The predictions imply that oxidation is significant across the complete flame width at all heights, for example, and does not simply reduce levels of soot volume fraction in the flame wings as might be expected.

It is difficult to unambiguously evaluate the oxidation process due to the different factors involved. Firstly, as discussed earlier, the rate is very dependent upon the size and geometry of soot. Secondly the oxidation mechanism is itself uncertain, a number of authors quote

different mechanisms of oxidation by many species (Lee et al. 1962, Fennimore and Jones 1967). Finally, especially, in the earlier parts of the flame, soot is essentially restricted to locally fuel rich mixtures from which oxidising species are absent. The unsatisfactory accommodation of such unmixedness effects - whether or not the PDF of mixture fraction is used to partly close the oxidation source term - can lead to substantial overestimation of the effect of oxidation.

In the absence of reliable soot size information and instantaneous measurements of sot volume fraction, oxidant concentration (or mixture fraction) and / or temperature these uncertainties are impossible to resolve. However, given the complexity of the processes involved, the predictions are very encouraging.

5.2.2 KEROSINE FLAME

The main difference between the kerosine and ethylene jet flames studied here was the presence of the wall boundary condition in the case of the kerosine flame. Not only did this require further modelling assumptions (see previous section), it also prevented the possibility of restricting the finite difference grid to the jet alone. The whole domain from the jet to the wall had now to be considered. This meant substantial increase in the number of nodes and hence computer time required.

When defining the grid, again use was made of the axisymmetric nature of the system - only half of the flowfield was modelled. Even with this, however, an equispaced grid was impossible due to the relative dimensions of the jet / flame tube (1.5/155mm). The grid had to be sufficiently refined to model the initial jet structure whilst being limited in size by computer resources. Extensive investigations into cold jets of Argon in air accompanied by coarse measurements of velocity by pitot static tube and mixture fraction by mass spectrometer proved that a grid of 100 nodes was sufficient to model the flow accurately - 20 nodes equispaced in the fuel jet, 80 equispaced in the air stream.

Due to the difficulties encountered relating to both the radiative heat loss and level of carbon conversion to soot in the kerosine flames, studies were limited to kerosine flame A which was at atmospheric pressure.

The boundary conditions of the turbulence parameters were prescribed in the same manner

as those in the ethylene jet predictions, the integral scale of turbulence of the air stream was given the value 5mm, the diameter of the holes in the perforated plate immediately upstream of the burner. Fuel and air velocities were again given top hat profiles with mass flows matched to experiment. Mean mixture fraction was set to unity in the fuel flow, zero in air and variance was set to zero throughout.

The flamelets of temperature and density were more uncertain. Detailed kinetic schemes of kerosine are not yet defined owing to the complexity and variable nature of this blended fuel. In his study of laminar flamelet modelling of combustion chemistry for practical fuels, Askari-Sardhai 1987 utilised a simple 1 step mechanism to describe the breakdown of kerosine to CO and H_2. Using the SNECKS (Liew 1983) algorithm, he generated flamelets of temperature and species concentration for the kerosine / air system at 1 atmosphere pressure. Although the original computer program is lost, the flamelets were tabulated.

Stewart and Moss 1989 attempted to generate experimental flamelets of temperature for laminar kerosine / air flames at a variety of pressures and fuel dilutions in Wolfhard Parker type flat flames. The conditions of their flame A are most equivalent to flame A in the present study.

The flamelet of Askari-Sardhai 1987 and the experimental measurements of Stewart and Moss 1989 are shown in fig.(5.6). As with the ethylene / air system (fig(5.1)), the agreement to the lean side of stoichiometric is very good. The discrepancy for all measurement stations to the rich side is, however, extremely large. Even at the lowest measurement stations in the laminar flame at which measurements were made (X = 5.0, 8.0mm), the difference between adiabatic flamelet and measurements is of order 700K. Radiant heat loss alone cannot explain such large departures. Other factors such as local quenching of the flame close to the burner exit and air entrainment in this region must add to the discrepancy. Also, the simple 1 step fuel breakdown mechanism used by Askari-Sardhai 1987, in the calculation of the adiabatic flamelet is unrealistic. This precludes the affects of complex chemical intermediates - which have larger heats of formation - resulting from fuel pyrolysis in the rich zone.

Initially, the best fit experimental flamelet was used in the turbulent jet flame simulation. The resulting predictions, however, were extremely poor. The amount of heat loss in the flamelet to the rich side of stoichiometric was too large resulting in initial underprediction of centreline temperature by as much as 300K. This was followed by an overprediction of

similar magnitude as leaner mixtures were reached and the effects of the essentially adiabatic lean side of the flamelet were seen.

Since the agreement between turbulent experiment and predictions was not sufficiently accurate to incorporate a soot prediction, a modified flamelet which was a compromise between the adiabatic and experimental ones was derived. By trial and error it was found that depressing the adiabatic temperature given by Askari-Sardhai 1987 by 45% with relation to the unreacted mixture temperature gave the best agreement with experiment. The flamelet temperature to the lean side of stoichiometric was unchanged in order that peak temperatures away from the centreline lower in the flame would still be modelled accurately. This modified flamelet is plotted in fig(5.6).

The resulting predictions of centreline mean and variance of mixture fraction and mean temperature are plotted in fig.(5.7). Radial plots of mean mixture fraction and temperature at two axial heights, X = 100, 300mm are shown in fig.(5.8). The agreement of mean mixture fraction is excellent both in terms of radial spread and peak values. The general agreement of mean temperature, however, is poor. Although the radial spread and trends of measured temperature are predicted accurately, the single radiation loss flamelet technique in such a heavily radiating and sooting system is obviously unsatisfactory resulting in initial underprediction followed by overprediction of temperature. However, below the 250mm height, errors in mean centreline temperature are limited to 100K. Mindful of this, the soot model proposed by Stewart et. al. 1991 for dilute kerosine flames was applied.

Since the model was originally developed for a heavily Nitrogen dilute kerosine (N_2 = $75\%_{mass}$)/ air flame at elevated pressure (2.28atm.), a significant amount of extrapolation - in pressure, temperature and fuel fraction - was necessary in order to use it in the present application. Shown in fig.(5.9) are the flamelets of α, β, γ and ω_{ox} calculated using the modified flamelets of temperature described above. Of particular note are the flamelets of α and γ. The very mixture fraction specific nature of soot formation observed in laminar and turbulent experiment is not replicated. Indeed, the flamelet of γ has significant values in the mixture fraction range $0.2 < \xi < 1.0$.

The unphysical shape of these flamelets is mainly due to the increased fuel fraction dependence of the source terms. In order to more closely model the linear growth rate of soot with residence time and the migration of soot towards richer mixtures at higher axial

heights in their laminar Wolfhard-Parker flames, Stewart et al. 1991 assumed fuel fraction dependence of nucleation and surface growth terms, $M_{\alpha,\gamma}$, to be 2 and 5 respectively. The activation temperatures of the terms, $T_{\alpha,\gamma}$ were also lowered with relation to the values for ethylene to 21000K and 12100K respectively.

The result of the extrapolation from initial fuel concentrations of 25% to 100% on the surface growth term thus formulated is an increase of three orders of magnitude, on the nucleation term one order. Such an extrapolation in addition to those in temperature and pressure is very questionable. When applying this model to the present calculation the level of soot mass was, not surprisingly, overpredicted by a similar order.

In order that a new model could be generated to more accurately describe the growth of soot in the case of 100% kerosine fuel, the original laminar experiments of Stewart and Moss 1989 were revisited. The data set included measurements on a flame of neat fuel at 1 atmosphere pressure - Stewart and Moss' 1989 kerosine flame A. Although the initial conditions of this flame were very close to flame A in the present study an important drawback was discovered. In the laminar flame, the percentage of carbon in the solid phase (eq.(4.1)) was calculated to have values of the order 100% by the 16mm height. This helps to explain the difficulties in measurement that were experienced in this flame and also the migration of peak soot to richer mixtures higher in the flames - the migration could be due to the lack of any more available carbon for conversion to soot at the leaner mixtures.

Since no other model was available to describe soot formation in kerosine combustion and since the effects of soot on the mixture fraction field and radiation loss could not be investigated without one, the ethylene soot growth model (Moss et al. 1988), which had been shown to predict the trends of soot growth accurately in turbulent jet flames, was empirically modified to match the experimental data reported herein. However, due to uncertainties in the modelling of turbulent combustion and the poor agreement between measured and predicted temperatures, the new soot model constants thus derived were not proposed to be universal but are merely used as a vehicle to examine other soot related phenomena. Therefore there was little reason to optimise the new constants to give the best fit with experimental data and so this was only done to a minimal degree.

In order to predict the extremely rapid growth of soot observed in the kerosine jet flame experiments, the more physically realistic surface area dependent surface growth formulation,

eq.(5.15), was used. The fuel fraction dependence of both nucleation and surface growth terms was assumed to be unity. The values of the constants $C_{\alpha,\beta,\gamma}$ were modified in an essentially ad hoc basis although once C_γ had been modified from the ethylene value to take into account the different source term formulation, its value was increased in sympathy with the nucleation term to prevent any imbalance in the soot mass source term.

The new model constants were:
$C_\alpha = 2.12\text{x}10^{14}$, $C_\beta = 2.38\text{x}10^{19}$, $C_\gamma = 2.57\text{x}10^{3}$, $C_\delta = 144$, $T_\alpha = 46100\text{K}$, $M_{\gamma,\alpha} = 1$, $T_\gamma = 12600\text{K}$

The resulting flamelet properties are shown in fig(5.9) and predictions of soot volume fraction along the flame axis and for three radial sections is shown in fig.(5.10). Although there is a consistent underprediction of the level of soot throughout, the general trends shown by the model mimic the experimental data very well.

The agreement is largely attributable to the empirical nature of the model which was modified to fit this set of data. Uncertainties in turbulence / chemistry interaction, radiant heat loss, affect of solid carbon on the gas phase chemistry all render the basis of the model extremely fraught. In the present situation, however, it suffices to test other sub - models.

5.3 CARBON FEEDBACK MODELLING

Concern was felt regarding the experimental discovery that significant quantities of the total available carbon for combustion in the jet flames was being converted locally to the relatively unreactive solid phase of soot. This was a result of the relatively poor mixing and/or long residence time of the jets with relation to most practical combustors. The unfortunate consequence of such levels of soot is that the mixture fraction of gaseous species has a sink and, hence, may no longer be considered as a conserved scalar. In the case of a laminar flame simulation this renders the whole conserved scalar / laminar flamelet approach to combustion modelling inappropriate since soot diffuses in a very different way to gaseous species. In a turbulent situation, however, where molecular diffusion is small with relation to turbulent transport, a modified form of the laminar flamelet model may still be envisaged providing the turbulent transport of soot and gaseous species is assumed equal. Such a

strategy was attempted in the present study and is described in this section.

The model was based upon that proposed by Jones and McGuirk 1979 to model droplet combustion in gas turbine chambers. The presence of fuel in the form of soot or droplets effectively reduces the amount of material available for combustion. To mimic this real effect, the computed mixture fraction is apportioned between the gaseous and solid phase. The scalar field is then calculated from the gaseous mixture fraction alone assuming the effect of the solid phase on the local gas phase to be negligible.

Key features of the model may be summarised as follows: total mean mixture fraction - which remains a conserved scalar - comprises contributions from both solid and gaseous phases.

$$\widetilde{\xi_{tot}} = \widetilde{\xi_{gas}} + \widetilde{\xi_s} \tag{5.23}$$

Where ξ_s is related to soot volume fraction as follows:

$$\widetilde{\xi_s} = \frac{\overline{\rho_s f_v}}{\overline{\rho}} = \tilde{\phi}_m \tag{5.24}$$

ξ_{tot} and ϕ_m are calculated from their conservation equations and hence the magnitude of each component of mean mixture fraction may be calculated.

The variance of total mixture fraction is computed in the conventional way from its balance equation but that of the gaseous component is less accessible.In the absence of supporting information on fluctuating soot concentration, the ratio of gaseous mixture to the total is assumed to be linearly related to the ratio of their first moments. In particular:

$$\widetilde{\xi_{gas}''^2} = \widetilde{\xi_{tot}''^2} \left[\frac{\tilde{\xi}_{gas}}{\tilde{\xi}_{tot}} \right]^2 \tag{5.25}$$

In parallel with these calculations, soot weighted density may also be calculated.

$$\overline{\rho} = \overline{\rho_s f_v} + \overline{\rho_{flamelet}[1 - f_v]} \qquad (5.26)$$

Since soot volume fraction must attain values in excess of $1x10^{-4}$ before mixture density is affected significantly, this perturbation was ignored.

As described in eq.(5.23), the values of ξ_{gas} and ξ_s are interdependent. Thus, in order to calculate these two properties within each forward step of the calculation, internal iteration is necessary. Referring to fig.(5.11), in the first step of the iteration, ξ_{gas} is given the value of ξ_{tot} - ϕ_m using ϕ_m from the previous step. Scalar calculations, based on the gas phase mixture fraction calculations, are then undertaken in the conventional manner. Using this information, the conservation equations are updated. If the new value of gaseous mixture fraction differs from that used in the scalar calculations by more than 0.1%, the procedure is repeated.

It is possible that this iterative cycle is responsible for the oscillations that Bond 1990 observed in his application of a similar procedure to an elliptic calculation. Small changes in mixture fraction do produce significant variations in temperature - and hence the soot source terms - in certain mixture fraction regimes. The marching solution procedure and small forward steps possible with the parabolic formulation does not appear to generate such troublesome oscillatory behaviour.

5.3.1 ETHYLENE JET FLAME

The carbon feedback model was applied to the ethylene jet flame simulation using identical inlet boundary conditions and flamelets as with the calculation described in the previous section (5.2.1) in which the carbon was assumed to be a small perturbation to the gaseous mixture fraction field.

A comparison of the two predictions is shown in fig(5.12). As expected, the effect of the carbon feedback is to locally lean out the mixture fraction available for combustion. In this case, the predicted maximum conversion of available carbon to soot is 10%. Such levels appear to affect the temperature and soot fields to a modest degree and the comparison with experimental data is essentially unchanged

5.3.2 KEROSINE JET FLAME

Again the feedback model was applied to a calculation with identical boundary conditions and

using the same flamelets as the calculation above (section 5.2.2). For the case of the kerosine flame, however, the carbon conversion was considerably greater and presented a much sterner test to the feedback mechanism.

The axial predictions, fig(5.13), show the predicted conversion of total carbon to soot to have peak values of order 40%. The resulting effect on the predicted temperature is large. Although the agreement of predicted temperatures using the perturbation assumption with measured values is poor - due to the unsatisfactory accommodation of widely varying radiant loss with a single flamelet - that resulting from the carbon feedback mechanism is significantly worse. The local leaning out of the gaseous mixture fraction by up to 40% in previously rich regions moves conditions closer to stoichiometric. Hence, carbon feedback temperatures are predicted to be higher than those based on the assumption that soot is a small perturbation to the gaseous field by up to 250K.

The opposite of this situation occurs when the total mean mixture fraction is leaner than stoichiometric since the gaseous mixture fraction will be leaner still. This effect is seen in the axial profiles at the highest heights and more clearly in radial plots - see fig.(5.14).

The consequential effect on the soot field is also large. The predicted levels of soot volume fraction are reduced by 50% - again, since leaner, oxygen rich gas mixtures are predicted to occur much earlier in the flame.

5.3.3 CONCLUSIONS

Although the application of the carbon mass loss scheme to the present application was successful in that the oscillatory behaviour of the solution procedure witnessed by Bond 1990 was not encountered, the trends shown by the predictions were not those expected by intuition. Although, the soot will undoubtedly affect the nature of the flame substantially, the increase in predicted temperatures by as much as 250K as a result of considering the carbon bound in the unreactive solid phase was surprising.

Although all the assumptions necessary in order to use this model have little basis theoretically or experimentally, the assumption that the solid carbon has negligible effect on the local gas phase chemistry is thought to be the least valid for high soot loadings. The effect of soot as thermal ballast to the local mixture is not accommodated to any degree in the calculation. In reality this can be far from the truth. The deficiency may easily be

demonstrated by considering the droplet burning case where total mixture fraction is equal to 1.0 whilst that of the liquid phase is equal to 0.94. The mean mixture fraction used in the flamelet calculations would therefore be close to the stoichiometric value resulting in very high predicted temperatures. In reality the enthalpy released by reaction of the very small gaseous component of the mixture must be shared by all material resulting in a much reduced temperature.

In order to quantify this effect, the simple model of flamesheet chemistry was investigated allowing the conversion of fuel carbon to solid carbon to be varied. The reaction scheme was as follows:

$$\begin{aligned} C_{12}H_{24} + x(0.21O_2 + 0.79N_2) \rightarrow y\,C_s \\ + a\,CO_2 + b\,C_{12}H_{24} + c\,O_2 + d\,H_2O + 0.79x\,N_2 \end{aligned} \qquad (5.27)$$

The number of moles of solid carbon, y, created from 1 mole of kerosine was varied and the temperature of the products for a range of mixture fractions then calculated by equating the enthalpy of reactants and products - ie. adiabatic. The detailed analysis is given in appendix F.

The resulting temperature for three cases (0%, 20% and 40% carbon mass conversion to soot) assuming a reactant temperature of 650K are shown in fig(5.15). The ordinate of the graph is mixture fraction based upon the original reactant mixture and so is total mixture fraction, ξ_{tot}. The effect of the solid carbon is to move the stoichiometric point to richer mixtures since less carbon is available for combustion. Also temperatures to the lean side of the original stoichiometric point are depressed, those to the rich side increased. The depression to the lean side is larger than the increase to the rich side. For example, for the 40% conversion case, the maximum depression compared to the 0% loss case to the lean side is 400K whilst the maximum increase to the rich side is of order 100K.

Using this data, it is also possible to calculate the temperature that is implied from the carbon feedback model. Carbon feedback temperature is related to the 0% loss flamelet above using the gaseous mixture fraction, $T(\xi_{tot}) = T_{0\%}(\xi_{gas})$. For the 40% loss case, $\xi_{gas} = 0.6 \times \xi_{tot}$. This curve is also plotted in fig.(5.15).

Although, the trends shown by this curve are similar to those resulting from the more exact analysis, the magnitudes of the discrepancies are very different. Compared to the 0% loss case the maximum depression in temperatures to the lean side of stoichiometric is 700K whilst the maximum increase to the rich side is 350K.

This clearly demonstrates that, for this simple system, the assumption that solid carbon has no effect on the gaseous phase is inadequate for large carbon loadings and may lead to errors in the predicted temperature by as much as 300K for the 40% conversion case.

Although this explicitly reveals flaws in the carbon mass loss scheme, in its present formulation, the error for a real system is less certain. Some trends shown by the flamesheet model are not observed even in the most soot laden flames. Most notably, the shift of the stoichiometric point to richer mixtures is not seen even in the kerosine flame A of Stewart and Moss 1989 (see fig(5.5)) where carbon conversion rates are extremely large. It is very difficult to resolve this discrepancy without further, more complex analysis, but a number of factors could be responsible:

- It is uncertain whether the measured mixture fraction is the total value or its gaseous phase component.
- The above model assumes the conversion rate to be the same for each mixture when it is known that, in the real situation, carbon formation is very mixture fraction specific.
- Experimentally, it is impossible to separate the effects of heat loss and carbon mass loss on the measured temperature profiles.
- The above model does not consider the effects of differential diffusion or finite rate chemistry.

The incorporation of a fully coupled soot and radiation model with detailed chemistry into a laminar flame simulation of such a flame as that reported by Stewart and Moss 1989 would aid the understanding of this very complicated system greatly. From this simulation, it may be possible to generate a library of flamelets of varying carbon conversion of the type in fig.(5.15). The most appropriate flamelet at a given location could then be chosen from within the computer program.

The viability of such a scheme must be assessed carefully since radiation loss will also be

important in highly sooting environments. The necessity of a three dimensional flamelet (in mixture fraction, radiant loss and carbon conversion) is apparent.This would be extremely expensive in computer storage and time. The validity of the laminar flamelet approach in such circumstances must also be considered before continuing. The whole concept of the existence of the conserved scalar, mixture fraction in such cases becomes dubious. Other combustion models in which a single flamelet description of local flame chemistry is not necessary are more desirable from this standpoint. For example, PDF transport techniques - recently reviewed by Pope 1990.

5.4 RADIATION LOSS MODELLING

The single flamelet modelling strategy described in the previous section and in chapter 2 was shown, for the kerosine jet flames studied here, to be inappropriate. The widely varying degrees of heat loss in the flame, even at atmospheric pressure where the measured soot volume fractions were less, could not be accommodated satisfactorily using one flamelet. A technique was required, therefore, which allowed the benefits of the mixture fraction / laminar flamelet technique to be utilised whilst enabling widely varying degrees of heat loss to be taken into account. This chapter describes the development and implementation of one such technique to the present application.

Kent and Honnery 1987, in their study of ethylene jet flames, use a method which is based upon the solution of a Favre averaged enthalpy conservation equation including heat loss. Using the mean enthalpy thus gained and species fractions calculated using the laminar flamelet strategy, they calculate the mean temperature via an averaged form of the calorific equation of state, eq.(2.5). Species fraction is assumed independent of heat loss.

To relate enthalpy and temperature together, the curve fitted data of Gordon and McBride 1971 is used. The data is expressed as a power series up to T^5. In their analysis, however, since only mean enthalpy is available, the turbulent correlations between enthalpy, species fractions and temperature to the various powers is assumed negligible and neglected.

$$\tilde{h} = \widetilde{\sum Y_i h_i} = \overbrace{\sum Y_i(a_i + b_i T + c_i T^2 + \cdots + f_i T^5)}^{} \approx \sum \tilde{Y}_i(a_i + b_i \tilde{T} + c_i \tilde{T}^2 + \cdots + f_i \tilde{T}^5) \quad (5.28)$$

The source term of the enthalpy equation was that proposed by DeRis 1978. Assuming the flame to be optically thin and that soot alone was the radiating species in the flame, an alternative expression to that of Hall 1988 used here (section 5.1) is derived. Integration of the simplified form of the radiative transfer equation possible under these assumptions along a path length, x, yields an equivalent emissivity of the soot along that path. The emissivity is related to soot volume fraction, temperature and path length via the complex pentagamma function. This is then used in the source term of enthalpy assuming each cell in the solution to emit only from its area.

Kent and Honnery 1987 also required the local value of soot volume fraction in order to calculate the source of enthalpy, but at the time of writing, no model was available. They derived an assumed relationship between soot volume fraction and instantaneous mixture fraction based on their measurements using this with the conventional laminar flamelet strategy. Although no comparison between measurements and resulting predictions of soot volume fraction are reported, the agreement is expected to be extremely poor with large initial overprediction of soot volume fraction due its observed, highly residence time dependent nature.

Lin 1992 used a similar technique to that of Kent and Honnery 1987 but with a more sophisticated enthalpy source term and a more realistic description of soot. In his study of wall fire combustion, he solved a two flux form of the radiative transfer equation, Viskanta and Menguc 1987. In addition to that by soot he also considered the radiative emission of heat by the species H_2O and CO_2. Although he calculated temperature using the same technique as Kent and Honnery 1987, he used the model proposed by Moss et al.1988 to model the growth of soot. Since the soot source terms are also highly temperature dependent, a library of soot source term flamelets were derived incorporating varying degrees of heat loss. The deviation of enthalpy with respect to its adiabatic value was then used to decide which set of flamelets was locally most appropriate.

Although both the above techniques showed promising results and are of sufficient simplicity

to be incorporated into more complex elliptic calculations, the assumptions necessary to calculate mean temperature are not valid in a highly turbulent system. It is easy to demonstrate in a jet flame calculation that the difference between $\widetilde{T}^5$ and $\widetilde{T^5}$ may be as great as 30% in some locations. With the addition of further cross correlations with species fraction, such discrepancies could result in a large errors in predicted temperature. For this reason a new model of radiation / chemistry interaction was proposed which avoided this issue.

The new model relies on the calculation of enthalpy using its conservation equation and its laminar flamelet description, both with heat loss. In an adiabatic, unity Lewis number system, enthalpy has no source and therefore is another conserved scalar. The effect of heat loss to the system is to create a sink to enthalpy and to cause deviation from this behaviour. When turbulence is also present, the calculation of enthalpy using the laminar flamelet strategy must be performed using a double integral of flamelet enthalpy in mixture fraction and radiant heat loss. If the symbol, Λ, represents the percentage heat loss then:

$$\overline{h(x)} = \int_0^{100\%} \int_0^1 h(\xi, \Lambda; x)\, d\xi\, d\Lambda \qquad (5.29)$$

Such an integral would be very time consuming to evaluate in a practical combustion simulation and so a simplifying assumption is made. At any given location in the flame, the enthalpy, even though subject to varying degrees of heat loss, is assumed to remain a unique function of mixture fraction. Under this assumption, the double integration is not necessary and mean flamelet enthalpy may be calculated in the conventional manner. However, the form of functions of enthalpy for varying heat loss is uncertain.

Since no instantaneous measurement of enthalpy and mixture fraction exist, arbitrarily, enthalpy for a given radiant loss level is assumed to be that corresponding to a reduction in temperature across the whole mixture fraction range by a fixed fraction with relation to ambient conditions - taken to be 300K. In particular.

$$h_{loss} = h(T_{ad}(\xi) \times (1 - \Lambda/100)) \qquad (5.30)$$

In order to relate temperature and enthalpy in this way the calorific equation is used, eq(2.5). However, since this is now applied directly to the laminar flamelet values of enthalpy rather than averaged turbulent values, the errors implied in the scheme of Kent and Honnery 1987 are avoided. However, the assumption that species mole fractions at a given mixture fraction are unaffected by radiant heat loss is still necessary. Flamelets of all other scalar properties of interest may be generated for each heat loss fraction as before.

In a combustion system, at any point, depending on the amount of heat loss, one such set of flamelets - from an infinite number of similar sets of flamelets with differing heat loss - will be most appropriate. Using this set, the mean values of all scalars at that point may be calculated conventionally. However, the question remains, which set of flamelets is most appropriate? The answer is addressed by considering the enthalpy calculated by solution of its conservation equation with a heat loss source. If the heat loss in the set of flamelets is the same as that implied from the conservation equation, then the mean enthalpy calculated using both techniques will be identical.

A scheme could be conceived whereby the set of flamelets is chosen by iteration. Such a procedure would be extremely expensive in computer time and so an alternative was developed.

- A finite number of sets of flamelets (in practice 9) of varying heat loss were derived using the procedure described above.
- At each point in the domain, all mean scalar values of interest - including enthalpy were calculated from the two sets of flamelets whose level of heat loss bounded that of the conservation equation enthalpy. In this case conservation equation enthalpy, $\tilde{h}_{CE}$ will lie between the two flamelet values, $\tilde{h}_{FL1,2}$. In particular $\tilde{h}_{FL2} < \tilde{h}_{CE} < \tilde{h}_{FL1}$ (NB: $\tilde{h}_{FL2}$ is the flamelet enthalpy incorporating the greatest amount of heat loss).
- The interpolation fraction that the conservation equation lies between the two flamelet values is then calculated:

$$F_h = \frac{\tilde{h}_{CE} - \tilde{h}_{FL1}}{\tilde{h}_{FL2} - \tilde{h}_{FL2}} \qquad (5.31)$$

- All other flamelet scalar variables may then be estimated using this fraction to interpolate between the two values at different heat losses. That is:

$$\tilde{\phi} = \tilde{\phi}_{FL1} + F_h(\tilde{\phi}_{FL2} - \tilde{\phi}_{FL1}) \qquad (5.32)$$

Since the laminar flamelet approach is used to infer the mean temperature from conservation equation enthalpy, turbulent correlations between species fraction and temperature to the various powers are completely accommodated and the associated errors with the techniques of Kent and Honnery 1987 and Lin 1992 are avoided. The remaining sources of error now lie with the assumption that enthalpy remains a unique function of mixture fraction even when heat loss is important and with the interpolation routine.

5.4.1 ETHYLENE FLAME

The above radiation modelling strategy was applied to a simulation of the ethylene jet flame with identical boundary conditions to those in the previous two sections (5.2,3). Flamelets of varying degrees of heat loss were derived using results from the laminar diffusion flamelet calculation with the program of Warnatz 1981 - see section 5.2.

The radiation loss modelling strategy, as with all laminar flamelet based models, is founded upon the assumption that all species have equal diffusivities. This allows the definition of the conserved scalar property and also allows simplification to the energy conservation equation by removing the Soret terms from its diffusion term (Libby and Williams 1980).

The program of Warnatz 1981, which solves the full set of governing equations in the simulation of the stagnation streamline of a counterflow burner does not require this assumption and therefore, since it is more physically realistic, takes into account the differing diffusion rates of species. Therefore, mixture fractions based upon any of the atoms in the system differ by small amounts since they and enthalpy are no longer conserved scalars.

This effect can be clearly seen in fig(5.16) in which adiabatic mixture enthalpy is plotted against mixture fraction based upon the carbon atom. Although, the relationship mimics closely that of a conserved scalar (ie. linear), there is significant deviation from this behaviour - especially around the stoichiometric point 0.068 - resulting from differential diffusion.

Using the single flamelet approach, such small discrepancies cause little problem to the solution since the mixture fraction - whether based upon any element - is only used to

reference the particular scalar property of interest at that point. The small discrepancies between the various mixture fractions will therefore cause similar changes to the solution but the solution is still possible.

For the case of the multiple flamelet strategy proposed here, however, since flamelet and conservation enthalpies are compared with each other to determine the local level of heat loss, it is critical that they are derived on the same basis. For this reason, a linear relationship of adiabatic enthalpy / mixture fraction was imposed - using the calorific equation of state (eq.(2.5)) - upon the diffusion flamelet species fractions in order to calculate a corresponding modified flamelet of adiabatic temperature. Both unmodified and modified adiabatic enthalpy and temperature are plotted in fig.(5.16) against mixture fraction based upon carbon.

A more satisfactory solution to this problem would be to perform a second laminar diffusion flamelet calculation in which the unity Lewis number constraint had been enforced. However, since the maximum modification to temperature in order to achieve linear enthalpy / mixture fraction behaviour was only 40K, this was considered unnecessary.

A library of flamelets of all scalars of interest was constructed using this modified flamelet. The level of heat loss between each set of flamelets was 6%. The resulting set are plotted in figs(5.17,18). The values of mixture enthalpy have been biased throughout by a constant value of 2×10^6 to prevent negative values occurring. The bias has no effect on the radiation model but prevents instabilities in the GENMIX (Spalding 1977) solution procedure.

Of particular note are the flamelets of the soot parameters α, γ and ω_{ox}. Relatively small changes in the flamelet of temperature produce large effects on these properties due to their highly temperature dependent nature. Since the soot formation parameters were initially derived by Moss et al. 1988 assuming a single flamelet with an average level of heat loss, extrapolation from these initial model conditions is required. The validity of such an extrapolation is questionable when such high activation temperatures are involved.

Two radiative loss calculations were performed. The first was a fully coupled calculation. Conservation equations of momentum, turbulence parameters, mean and variance of mixture fraction, enthalpy and soot mass and number density were solved simultaneously. The calculated soot volume fraction was used in the source term of enthalpy and vice versa with

internal iteration as required. The second calculation was partially coupled. Soot mass and number density were not calculated. Instead, the measured soot volume fraction was used in the enthalpy source term. For simplicity, the measured centreline soot volume fraction was assumed to prevail across the entire flame width.

In both cases the flamelet of T^5 was also calculated since it was demonstrated that the difference between this and T^5 could be as great as 30% in some locations due to the effects of turbulence on this highly non-linear function.

Shown in fig(5.18) are plots of axial mixture fraction, percentage heat loss, temperature and soot volume fraction for both partially and fully coupled calculations compared with those from the single flamelet technique - section (5.2). The effect of radiative loss on the mixture fraction field is not surprisingly small since this is only affected via the mixture density.

The effect on the calculated soot volume fraction in the case of the fully coupled calculation is much more striking. Due to the greatly increased values of the soot source terms α and γ at the lower heights when the flame is essentially adiabatic, the initial growth rate of soot volume is very much higher than that using the single flamelet technique. This offset is amplified since the simplified soot mass source term formulation was used in which mass growth is assumed proportional to number alone as apposed to surface area - section 5.1. The predicted initial mass growth follows directly that of nucleation. If the more realistic surface growth dependent formulation was used, the initial growth would also be dependent upon mass itself and so would be more gradual.

Although the rate of growth and the peak value of axial soot volume fraction are predicted more accurately using the fully coupled radiation model, its position in physical space is inaccurate by 150mm.

The effect of the radiation model on the axial temperature predictions is also apparent. The prediction with both partially and fully coupled calculations is very much better than that using the single flamelet in the initial 150mm of the calculation where the flame is essentially adiabatic. The temperature prediction by the fully coupled calculation remains very good up to the height X = 250mm, however beyond this point there is a substantial underprediction. The temperature predictions from the partially coupled calculation, however, deviate from the measurements beyond X = 150mm resulting in an overprediction of order 200K at X

= 200mm followed by an underprediction beyond X = 300mm.

This behaviour is not consistent with the predicted soot volume fraction curves. The gross overprediction of initial soot mass growth in the case of the fully coupled solution must be accompanied by a corresponding overprediction of the radiative loss term and therefore would be expected to result in a significant underprediction of temperature throughout. Whereas, although the assumption that measured centreline soot volume fraction prevails across the whole flame width in the partially coupled calculation is also erroneous, it is clearly less inaccurate than the predicted soot volume fraction from the fully coupled calculation. This would be expected to result in a more accurate enthalpy source term and hence better temperature prediction.

Such an irregularity is also seen in the predictions of Kent and Honnery 1987 who use a similar technique to model the effects of radiation.

Since no model of soot was available at the time of writing, they assumed a single flamelet relationship to describe soot which was based upon their measurements. Due to the highly residence time dependent nature of soot, such a strategy will also cause initial overprediction of soot volume fraction by a large amount. Yet, again, no underprediction of temperature results.

There are a number of possible explanations to this irregularity:

1 - The radiation model assumptions are erroneous. The assumptions that unique flamelet relationships of chemistry dependent scalars exist at each point even though radiation loss is important and that species fractions are independent of heat loss are clearly in error. The degree to which these affect the predictions is, however, unclear.

2 - The source term used in the calculations are inappropriate. There are a number of simplifying assumptions to the source term, the most tenuous of which, in this application being the assumption that the system is optically thin and the neglect of radiation from the gaseous species. The neglect of turbulent correlations between soot volume fraction and temperature is also a source of error given the mixture fraction specific nature of both these parameters.

3 - The laminar diffusion flamelets used in the calculation are inaccurate. Although the chemistry incorporated in the laminar flamelet calculation is to present knowledge accurate, other factors such as local strain in the flamelets is not considered. Such factors are especially important in the lower regions of the flame where strain is greatest.

4 - The Beta function approximation to the PDF of mixture fraction is inappropriate. The soot source terms and T^5 are highly mixture fraction specific and hence pose a sterner test of the validity of the assumed PDF technique.

Explanation (1) is extremely difficult to confirm or deny without significantly more detailed instantaneous measurements of enthalpy and mixture fraction in turbulent flames of the type presently unavailable. However, more insight could be gained regarding explanation (2) if radiation from the flame was monitored. The heat fluxes measured with a radiometer could be compared with the integrated fluxes of the radiation source term to assess the accuracy of the radiation loss description.

There is some evidence in the present study to allow insight into explanations (3) and (4). Considering the measurements in the ethylene flame, the first measurable soot volume fraction occurred at X = 100mm which, by the 160mm height, had reached 5.3×10^{-7} (20% of its peak value). The predicted residence time of the axial streamline at the 160mm height is 11.5ms. The predicted percentage heat loss at this point with the partially coupled calculation was only 0.5%, fig(5.19). From a physical viewpoint this seems reasonable since there was neither time nor sufficient soot to radiate significantly, yet the resulting temperature predictions are very poor.

Considering the temperature predictions using the single flamelet technique on the same flame. Even though the radiation perturbed flamelet is depressed with relation to the adiabatic flamelet by 200K to the rich side of stoichiometric, the underprediction of axial temperature at the same point - X = 160mm - is only 50K. Similar comments can be made of the kerosine predictions in the present study, the methane jet flame predictions of Liew 1983, the ethylene predictions of Syed 1990 and the propane predictions of Fairweather et al.1992.

This provides evidence to suggest that either the pdf or laminar flamelet description of the local flame structure is inadequate. However, other considerations such as the assumption

that unique flamelets exist at all in strongly radiating systems must also create error. A more detailed study of a laminar flame in which the affects of radiation are important will provide more insight into the problem by removing the uncertainty of property fluctuations.

5.4.2 KEROSINE FLAME

The radiation loss method could not be attempted even for the 1 atmospheric kerosine flame, A, in the present study due to lack of suitable flamelet information. As described in section 5.2, the only suitable laminar diffusion flamelet calculation that was available was that of Askari Sardhai 1987. However, the effects of differential diffusion resulting from the widely varying molecular masses of the species in this system made the associated problems too great to use in the present application.

Shown in fig(5.20) is a plot of adiabatic enthalpy and temperature plotted against mixture fraction. As can be seen the divergence of enthalpy from linear (conserved scalar) behaviour is extremely large and cannot be rectified in a similar manner to the flamelet of ethylene - section 5.3.1 - since the necessary modifications to the adiabatic temperature are of order 400K.

The author is aware of some unpublished recent work by Lindstedt and Leung (Imperial College, London) on the generation of reduced mechanisms for kerosine combustion which may be used with the constraint of unity Lewis number in order to generate more useful laminar diffusion flamelets for the present study, but until such a flamelet is available, the radiation loss model described here may not be applied to the kerosine flames.

5.5 CONCLUSIONS

In this chapter the conventional laminar flamelet / assumed PDF model of combustion chemistry coupled with the eddy diffusivity based k-ϵ model of turbulence has been applied to the free, ethylene and confined, vaporised kerosine jet (A) flames described in chapter 4.

A modification of the conventional laminar flamelet model was used to describe soot parameters which cannot be approximated as having unique relationships with the conserved

scalar mixture fraction owing to their slow chemistry. Following the hypothesis of Moss et al. 1988 - that the rate of soot growth may be assumed to be a unique function of mixture fraction - two further balance equations for soot mass and number density of soot were solved whose volumetric source terms were partially closed by the laminar flamelet technique. This avoided the problems associated with chemical source term closure in turbulent environments in which temperature fluctuations are high but necessitated the assumption that correlations between the fluctuating components of soot parameters and chemical source terms were negligible.

The original purpose of the experimental study (chapters 3 and 4) was to create a detailed database that would be useful for the purposes of soot model validation in turbulent environments. This was especially true for kerosine fuelled flames for which little other data is available. It soon became clear from the experimental study that the effects of both high soot and thermal radiation levels on the local flame chemistry could not be ignored in the computations. Due to these added complexities, the computational study was limited to the ethylene flame and kerosine flame A which were at atmospheric pressure.

In section 5.2 the simplest approximation which could give reasonable agreement between measured and predicted temperature was used as a starting point to apply the model of soot formation. Radiation was accommodated using the single flamelet strategy in which chemistry dependent scalars (excluding soot) were described by single functions of mixture fraction which incorporated a fixed, average level of radiative loss throughout the domain. The affects of the soot on the gaseous phase chemistry was also assumed negligible.

The model proposed by Moss et al. 1988 on laminar ethylene/air flames was used to predict soot growth in the turbulent ethylene flame. With no modification to the mass equation, the predicted soot volume fraction was very encouraging. However the oxidation term in the equations was less certain. This term is dependent upon the chemistry of soot oxidation, the available area and the joint presence at any time of soot and the oxidising species. Instantaneous information of oxidising species and soot in turbulent flames is necessary to fully understand the process.

The model of Stewart et al. 1991 which describes soot growth in laminar dilute kerosine / air flames at pressure was applied to the prediction of the kerosine jet flame A to less success. Due to the severe effects of soot and thermal radiation on the flame structure the

single flamelet technique was stretched to the limits of its validity resulting in significant errors in the prediction of temperature throughout the domain. Soot predictions using the model were also in error by over three orders of magnitude. The poor agreement was mainly due to the required extrapolation of the model in temperature, pressure and fuel fractions far beyond those in which the model was defined.

In order that other sub - models could be investigated further, a new model of soot growth was developed based upon the ethylene model (Moss et al. 1988) since this had already been shown to give good agreement with experiment. A satisfactory model was found by changing the model constants in a controlled manner. This however is not expected to be general due to the poor temperature fit and the uncertain affects of turbulence on the model.

Section 5.3 describes the application of a carbon feedback model in which the effects of soot on the gaseous phase were accommodated in a tractable form for calculations. For simplicity, the single flamelet description of temperature with gaseous mixture fraction was kept. The model was based upon that of Jones and McGuirk 1979 in which the total (conserved) mixture fraction was apportioned between the two phases of solid and gas. The gaseous phase was the only one allowed to take part in reaction.

With the assumption that the ratio between solid and gaseous components of mixture fraction was constant a closed model was defined. When applied to the prediction of the ethylene flame in which predicted fraction of carbon in the solid phase, F_c, was never more than 10%, the affect of this model on the calculation was minor. For more substantial levels such as those in kerosine flame A (40%), the affect was more dramatic. The local leaning out of the gaseous mixture had the effect of compressing the predicted flame in physical space and resulted in a significantly worse prediction of reality.

More detailed analysis of the effects of removal of solid carbon from a simple flamesheet model of combustion chemistry showed the carbon feedback scheme to be inadequate since no account is taken in this model of the thermal ballast that soot represents. However the flamesheet chemistry model itself is an inaccurate description of reality and hence more work is suggested in which the affects of soot on a detailed chemistry laminar flamelet calculation are studied.

Section 4.4 describes the development and application of a new method of incorporating

radiative heat loss into practical C.F.D. simulations in which the single flamelet approach is deficient.

By creating a library of flamelets which incorporate varying degrees of heat loss and comparing flamelet enthalpy with conservation equation enthalpy, the method allows the selection of the most appropriate flamelet at any location to be chosen in a systematic manner. Due to the complex nature of the procedure, a simple radiative loss term was used in the energy equation in which radiation is assumed to be purely from soot and in the optically thin regime.

Due to uncertainties in the flamelet of kerosine only the ethylene flame was studied. Two calculations were made, one which was entirely coupled with the soot model, the second being coupled to measured values of soot volume fraction.

The magnitude and growth rate of predicted soot volume fraction with the fully coupled calculation was very accurate but its location in physical space was in error. The large changes in predicted values over those with the single flamelet technique was attributed to the extremely temperature sensitive Arhennius type soot source terms.

Although at the lower heights in the flame both the above calculations showed better agreement of predicted temperature with measured values, the fit deteriorated at higher heights. A number of explanations to this behaviour are postulated but little may be confirmed in the absence of much more detailed experimental information.

Again more insight could be gained if the added uncertainty of the turbulence was removed and a more detailed investigation of the effects of radiation on the local flame structure undertaken.

TABLE 5.1

Variable	Prandtl Schmidt number, σ	Volumetric source term, S_ϕ
u	1.0	$\frac{\partial \bar{p}}{\partial x} + \bar{\rho} g$
k	1.0	$\mu_T \left[\frac{\partial \tilde{u}}{\partial r}\right]^2 - \bar{\rho}\,\epsilon$
ϵ	1.3	$C_{e_1} \frac{\epsilon}{k} \left[\frac{\partial \tilde{u}}{\partial r}\right]^2 - C_{e_2} \frac{1}{k} \bar{\rho}\,\epsilon$
ξ	1.0	0
ξ''^2	1.0	$c_{g1}\,\mu_T \left[\frac{\partial \tilde{\xi}}{\partial r}\right]^2 - C_{g2}\,\bar{\rho} \left[\frac{\epsilon}{k}\right] \xi''^2$
ϕ_m	1.0	$\left.\begin{array}{c} \bar{\gamma}\,\bar{\rho}\,\tilde{\phi}_n \\ (\bar{\gamma}\,\bar{\rho} N_o^{1/3}/\rho_s^{2/3})\,\tilde{\phi}_m^{2/3}\,\tilde{\phi}_n^{1/3} \end{array}\right\} + \bar{\delta} - N_o^{1/3}\left[36\,\pi/\rho_s^2\right]^{1/3} \bar{\rho}\,\overline{\omega_{ox}}\,\tilde{\phi}_n^{1/3}\,\tilde{\phi}_m^{2/3}$
ϕ_n	1.0	$\bar{\alpha} - \bar{\beta}^2\,\bar{\rho}\,\tilde{\phi}_N^2 - N_o^{1/3}\,(36\pi/\rho_s^2)^{1/3}\,\overline{\omega_{ox}}\,\bar{\rho}\,\tilde{\phi}_n^{4/3}\,\tilde{\phi}_m^{-1/3}$
h	1.0	$- C_{RAD} f_v T(T^4 - T_a^4)$

Fig(5.1) EXPERIMENTALLY AND THEORETICALLY DERIVED FLAMELETS OF TEMPERATURE AND DENSITY FOR THE ETHYLENE AIR SYSTEM AT ATMOSPHERIC PRESSURE.

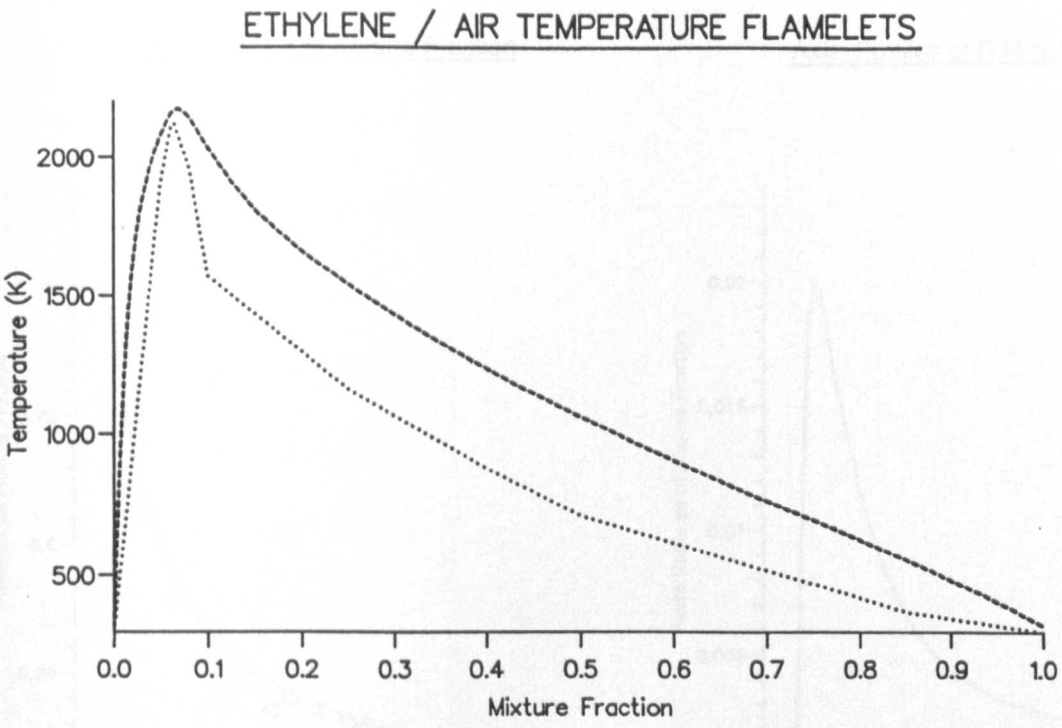

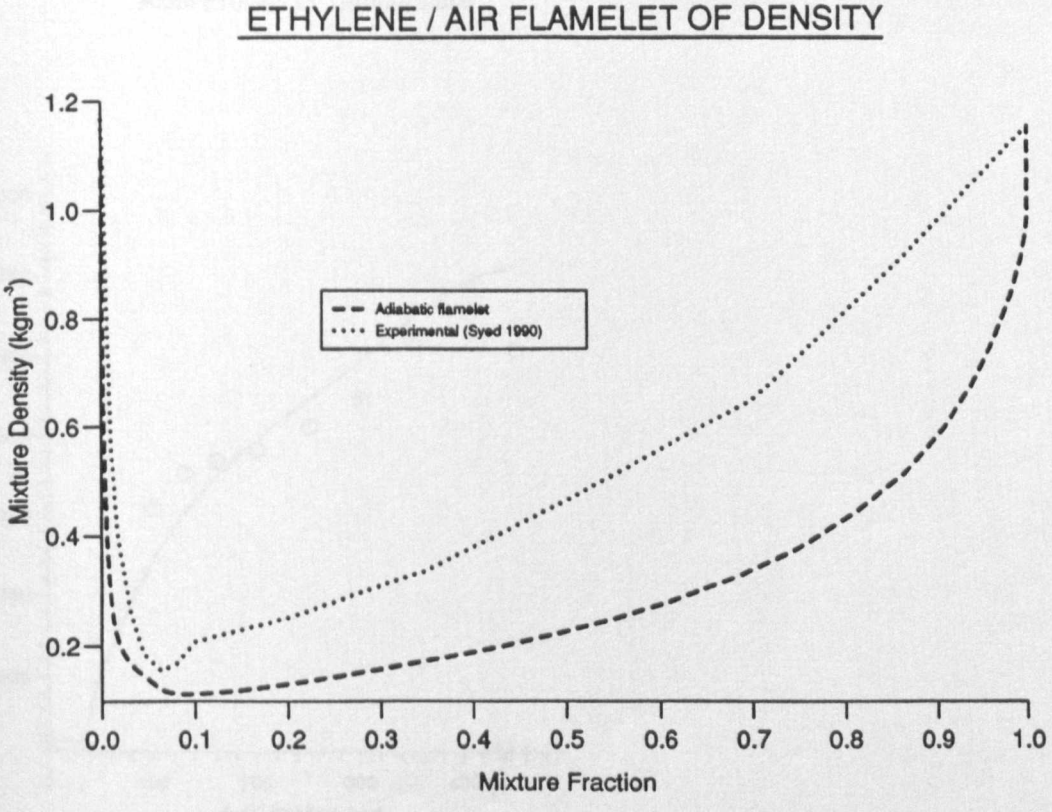

Fig(5.2) RESULTS OF THE SINGLE RADIATION LOSS FLAMELET GENMIX SIMULATION OF ETHYLENE FLAME ALONG THE FLAME CENTRELINE.

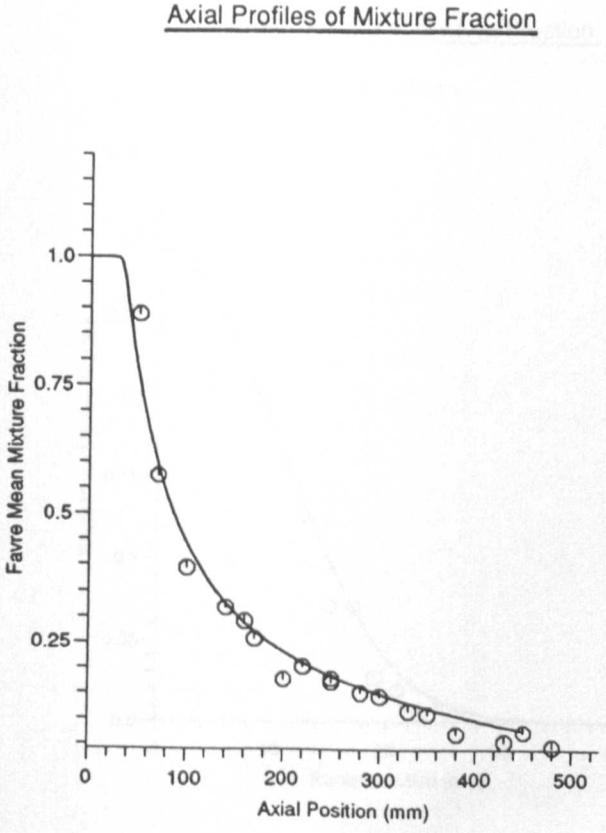

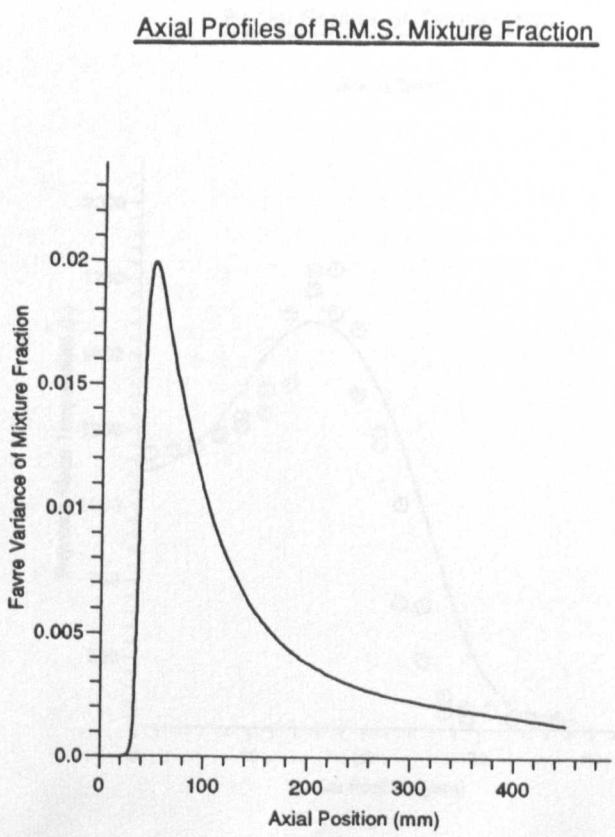

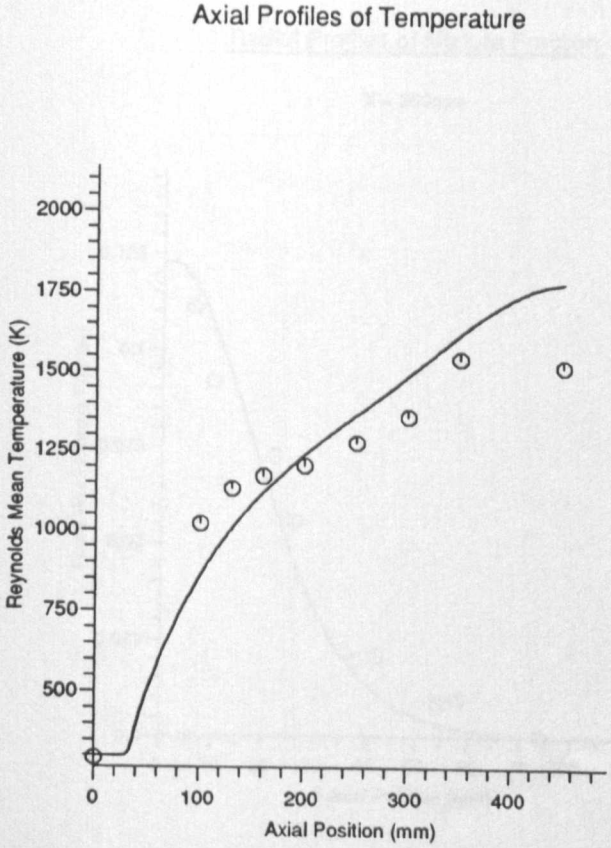

Fig(5.3) A SAMPLE OF TWO RADIAL PROFILES OF EXPERIMENTAL MEAN TEMPERATURE AND MIXTURE FRACTION IN THE ETHYLENE FLAME WITH THE GENMIX PREDICTIONS.

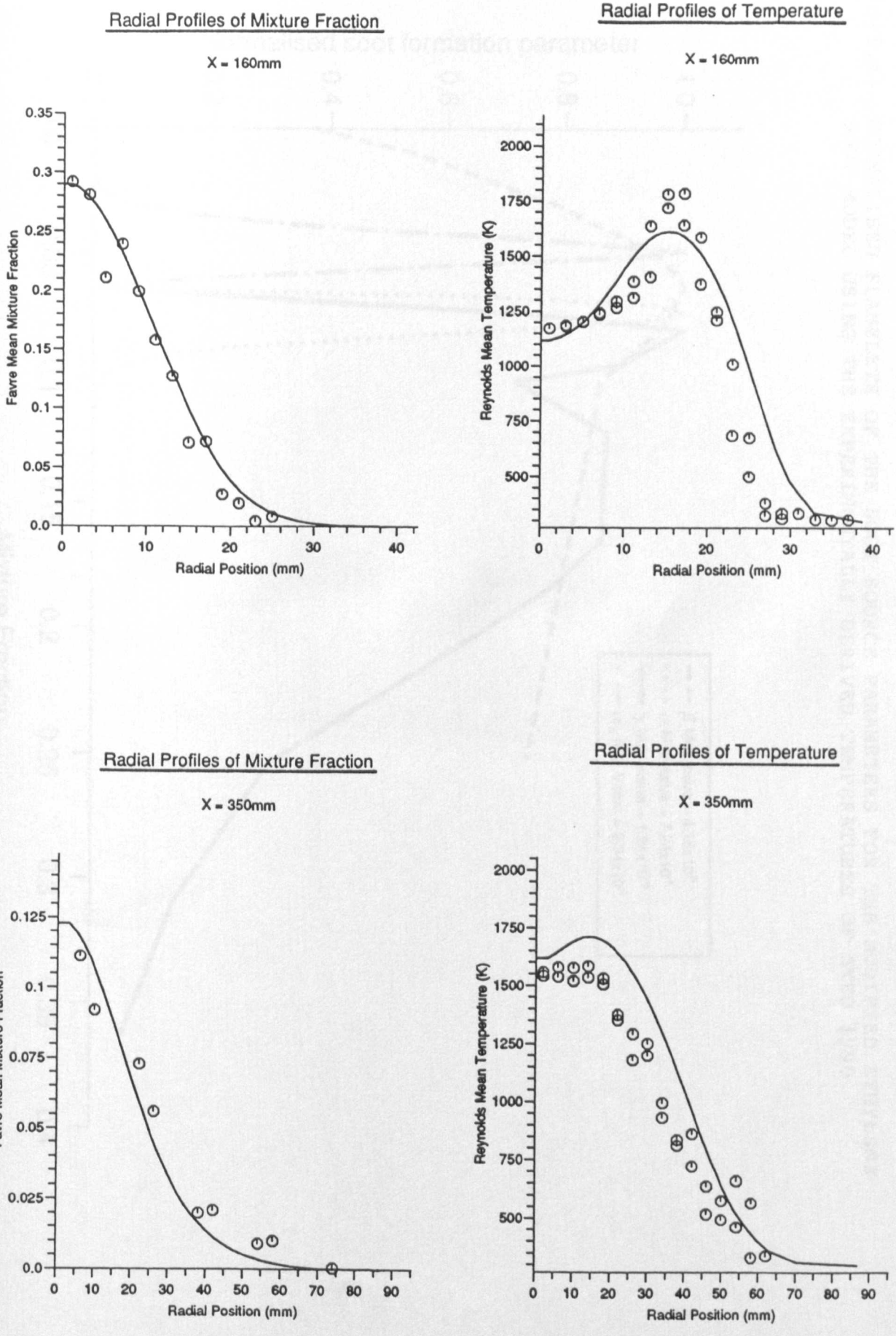

Fig(5.4) NORMALISED FLAMELETS OF THE SOOT SOURCE PARAMETERS FOR THE MODIFIED ETHYLENE SOOT MODEL USING THE EXPERIMENTALLY DERIVED TEMPERATURES OF SYED 1990

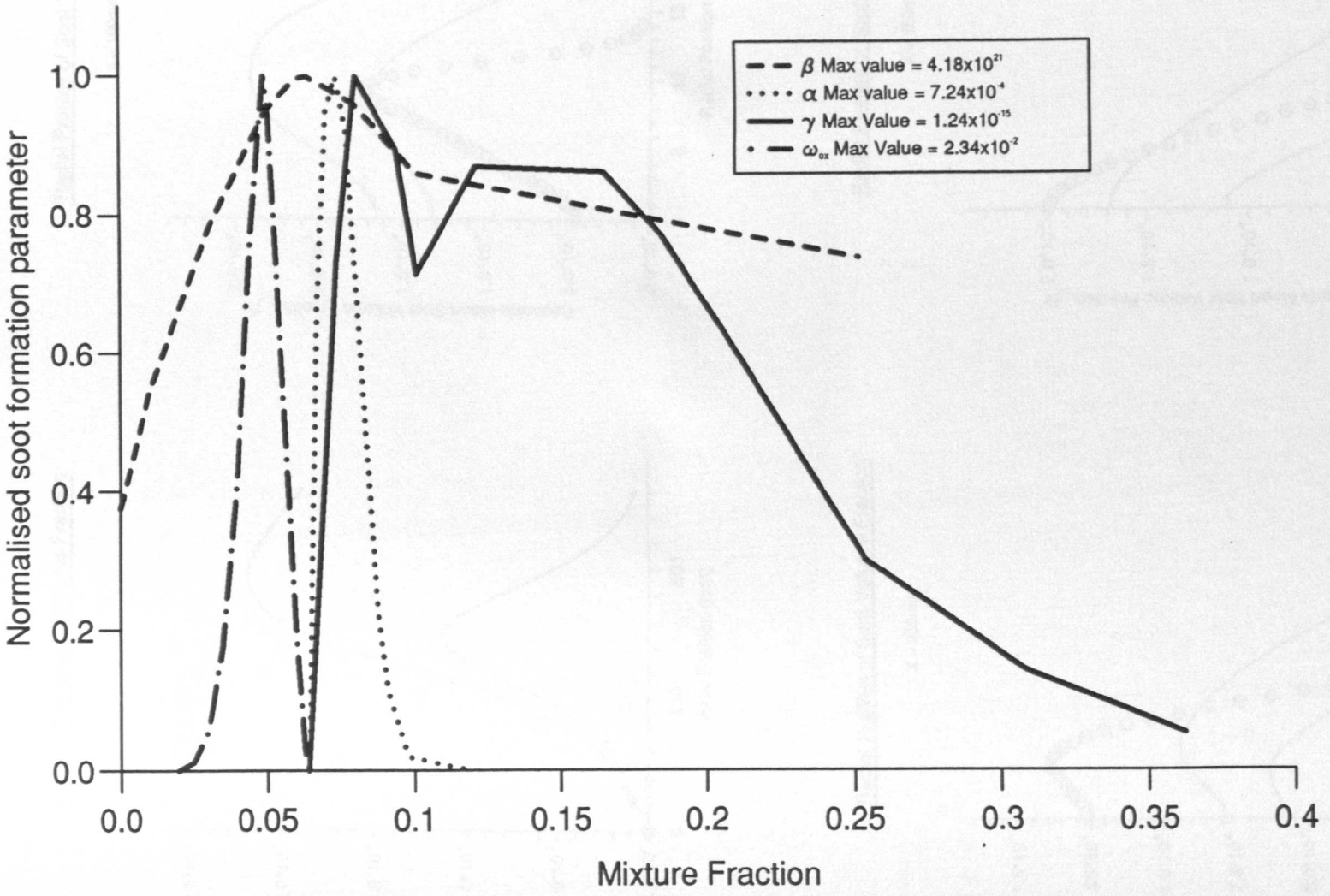

Fig(5.5) APPLICATION OF THE MODIFIED ETHYLENE SOOT MODEL TO THE PREDICTION OF SOOT IN THE ETHYLENE FLAME WITH AND WITHOUT THE OXIDATION MECHANISM ASSUMING SOOT TO BE A PERTURBATION TO THE GAS PHASE.

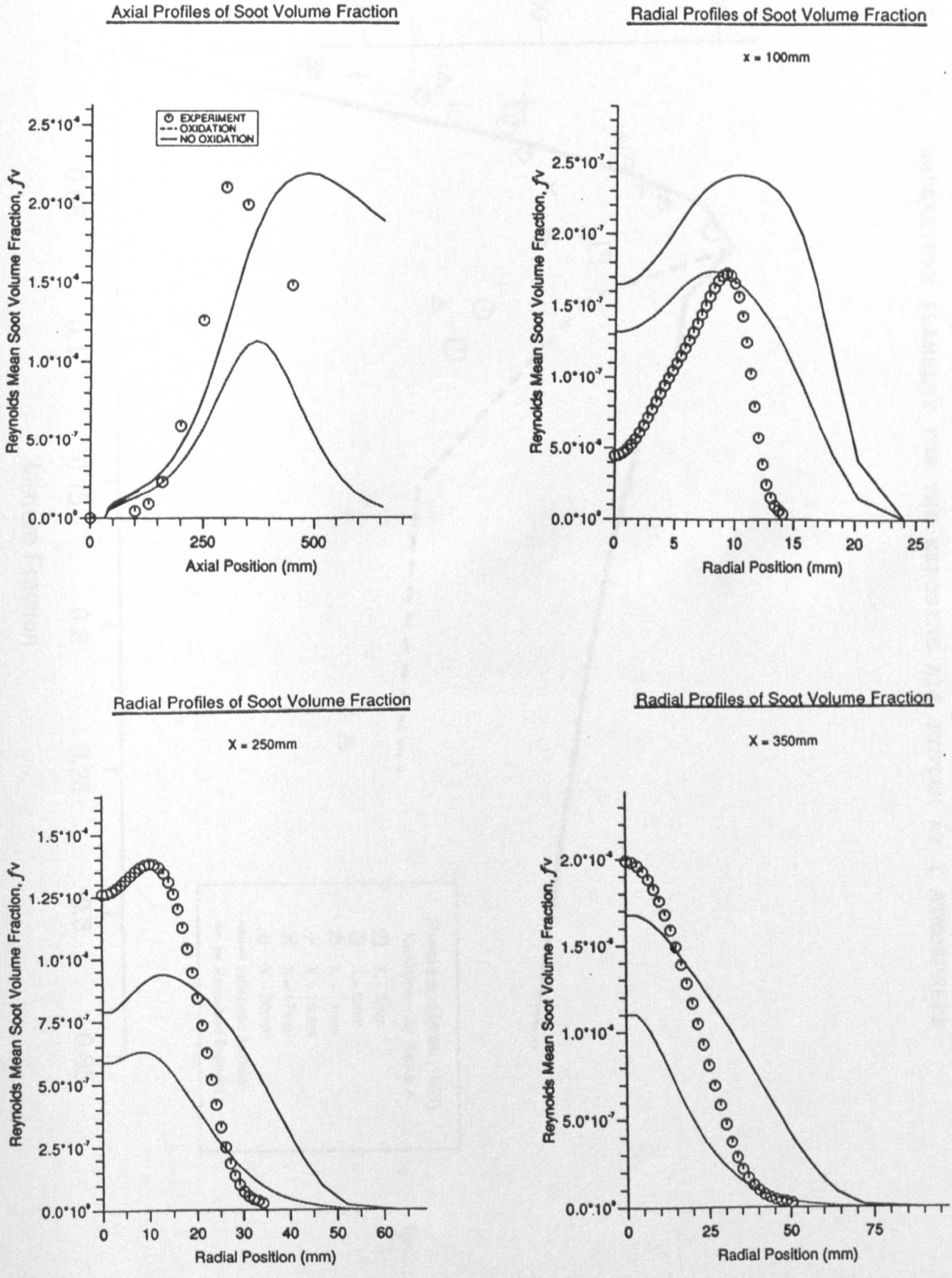

Fig(5.6) TEMPERATURE FLAMELET FOR THE KEROSINE AIR SYSTEM AT 1 ATMOSPHERE PRESSURE.

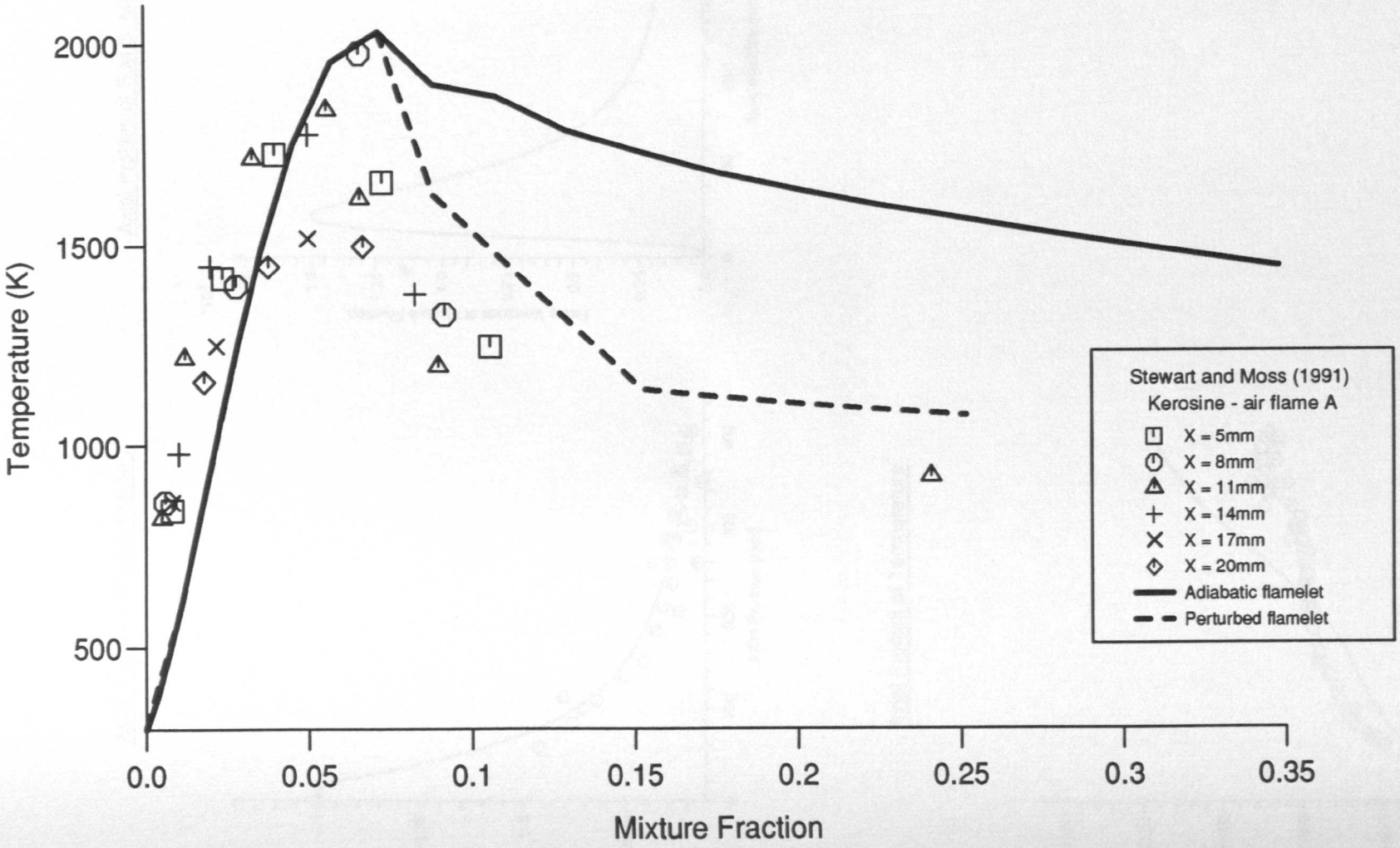

Fig(5.7) RESULTS OF THE GENMIX SIMULATION OF KEROSINE FLAME A ALONG THE FLAME AXIS.

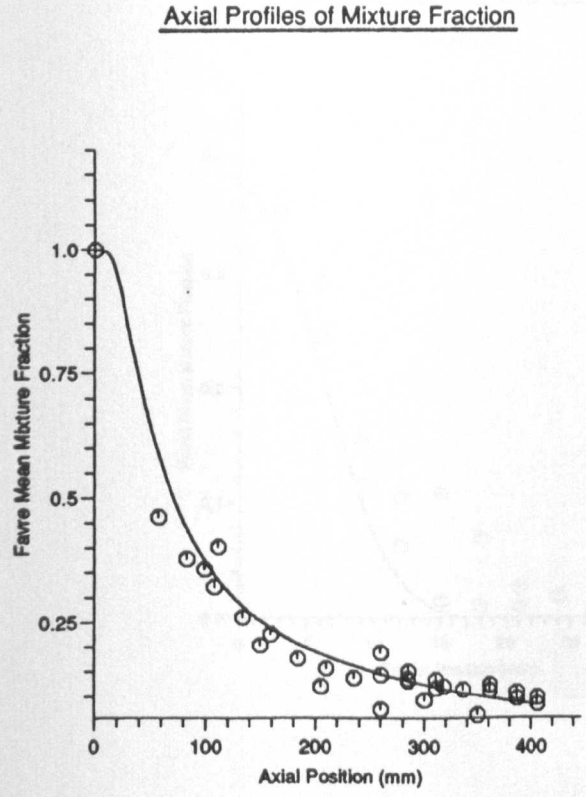

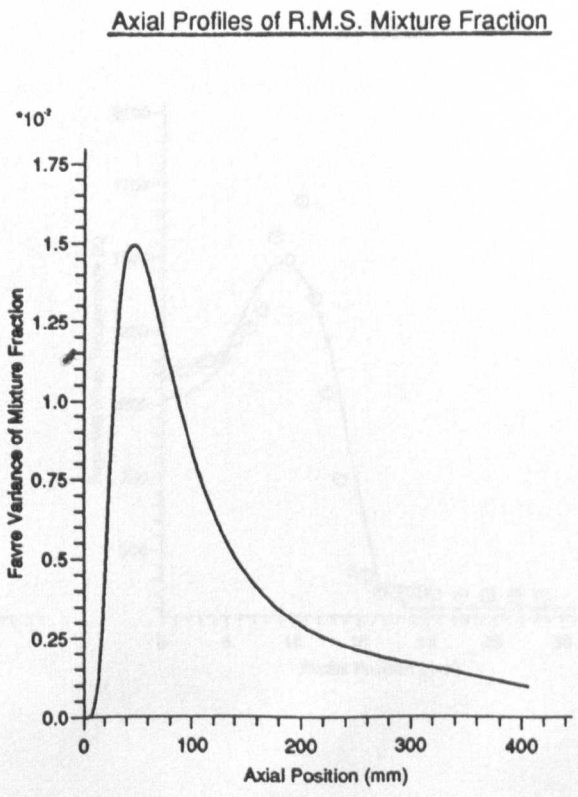

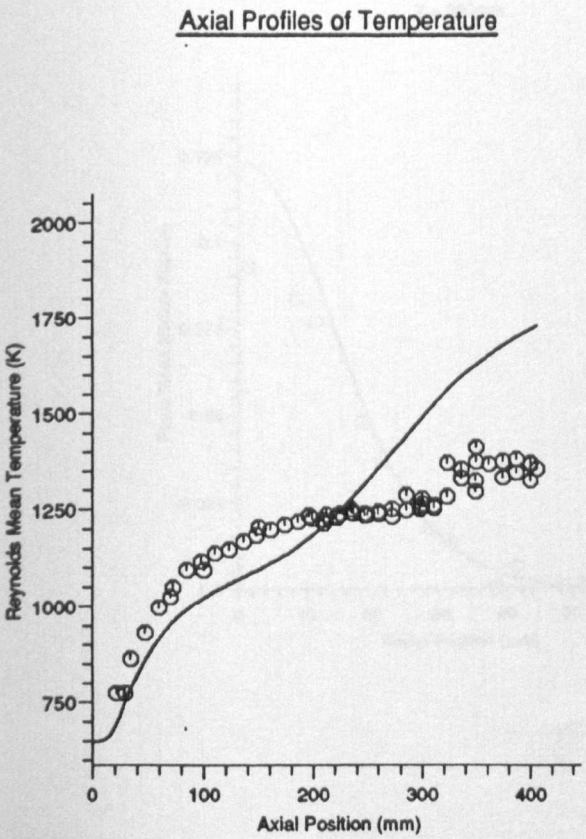

Fig(5.8) A SAMPLE OF TWO RADIAL PROFILES OF EXPERIMENTAL MEAN MIXTURE FRACTION AND TEMPERATURE IN KEROSINE FLAME A WITH THE GENMIX PREDICTIONS.

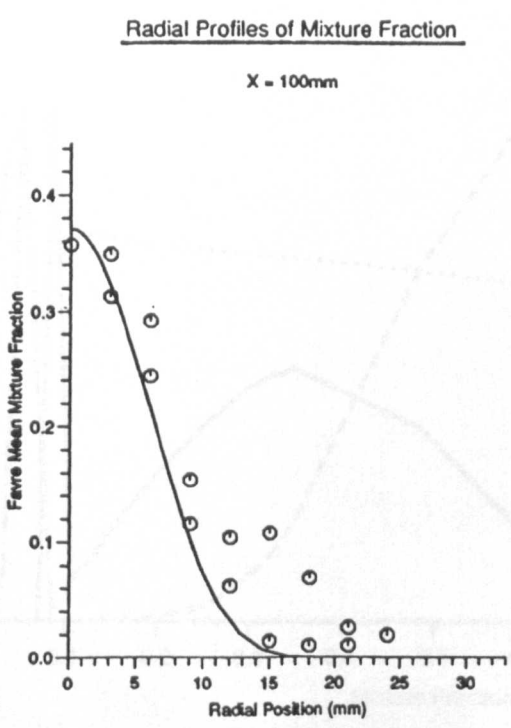

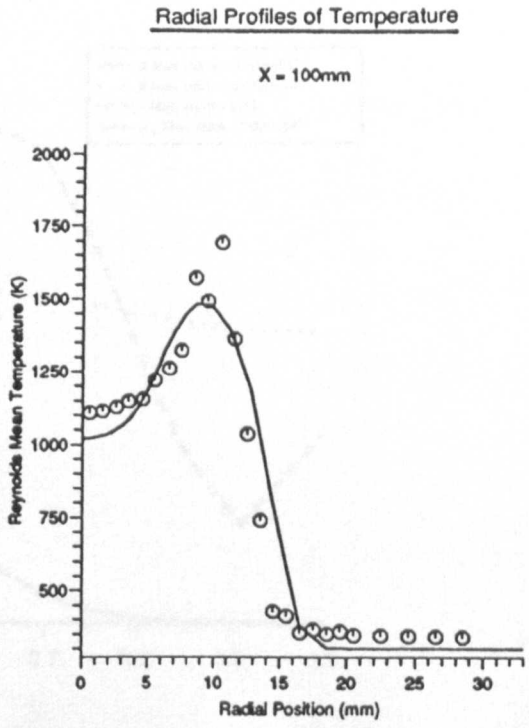

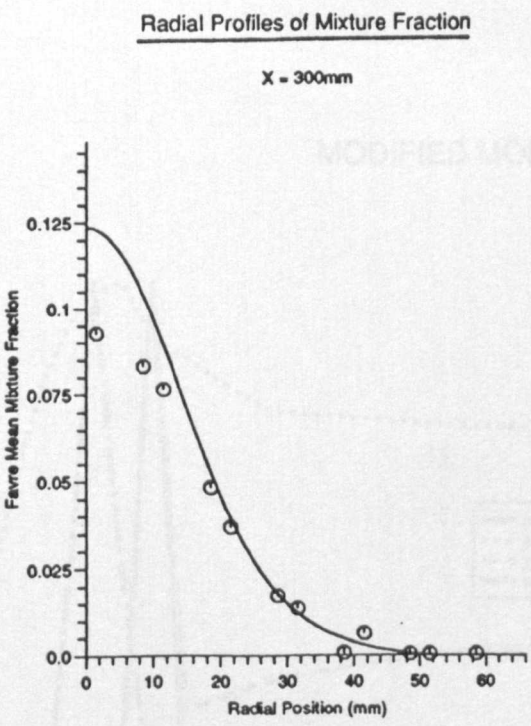

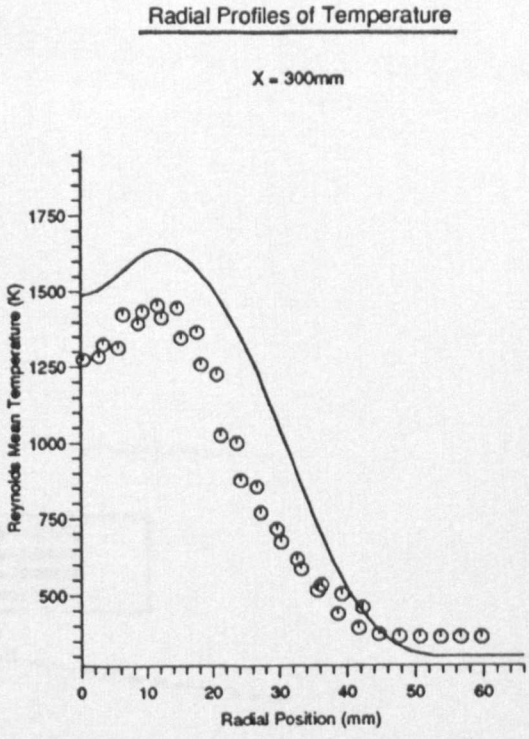

Fig(5.9) NORMALISED FLAMELETS OF THE SOOT SOURCE TERM PARAMETERS OF THE KEROSINE SOOT MODEL.

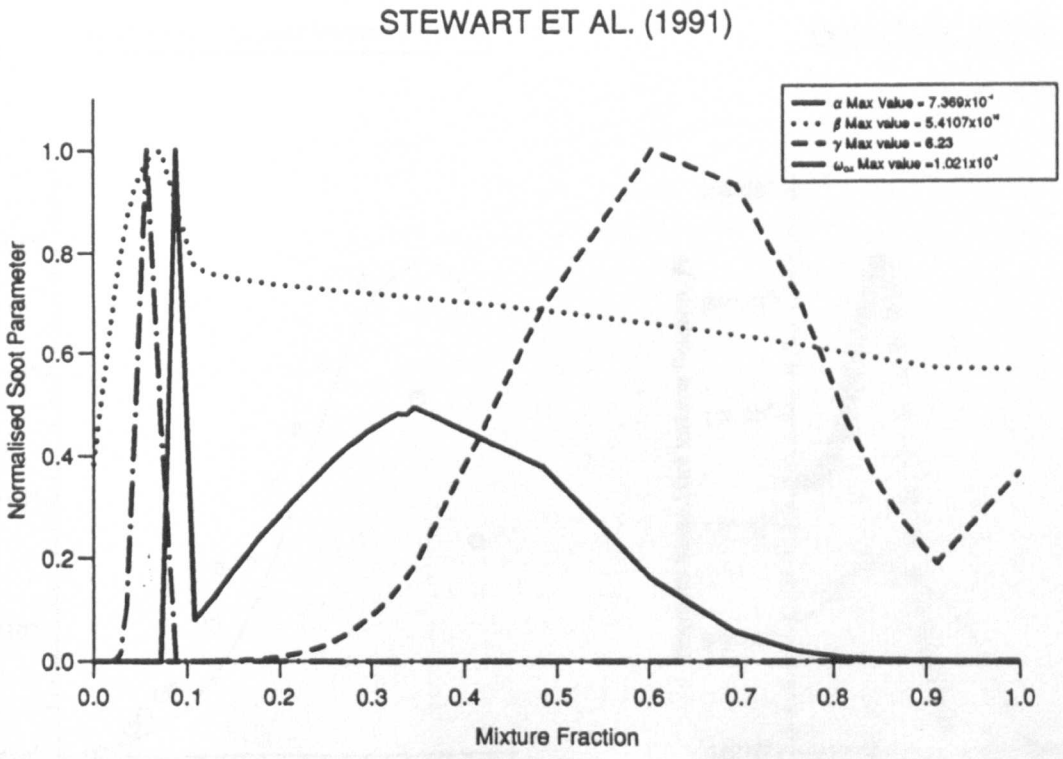

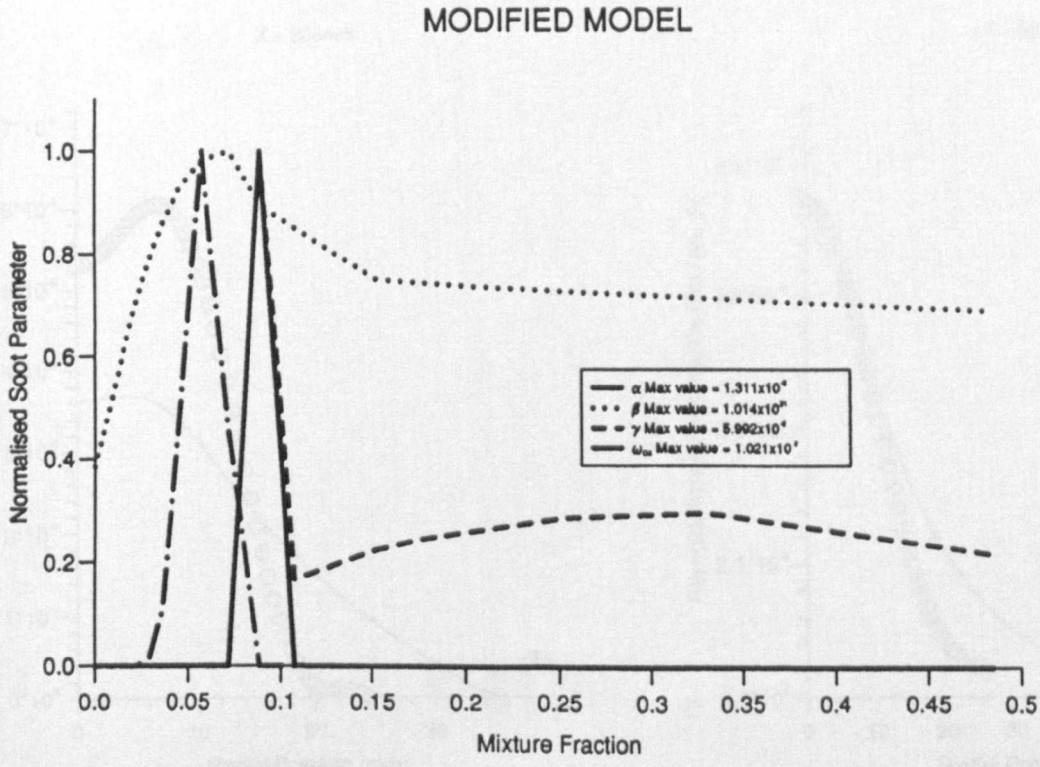

Fig(5.10) PREDICTION OF SOOT VOLUME FRACTION IN THE KEROSINE FLAME USING THE MODIFIED MODEL ASSUMING CARBON TO BE A PERTURBATION TO THE GASEOUS PHASE.

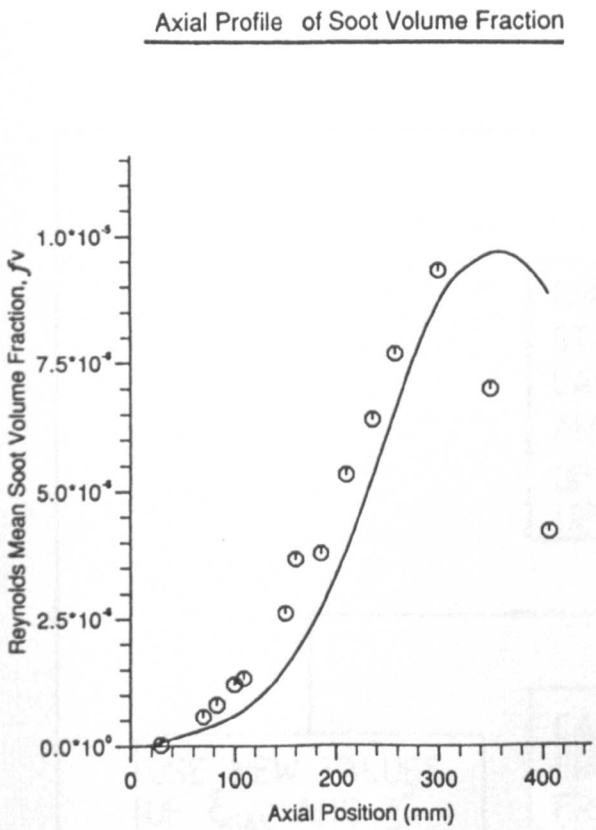

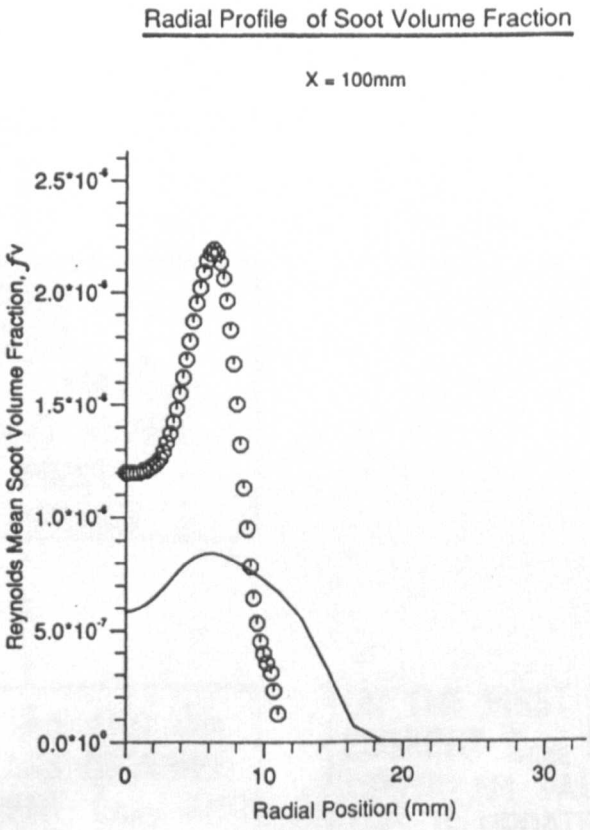

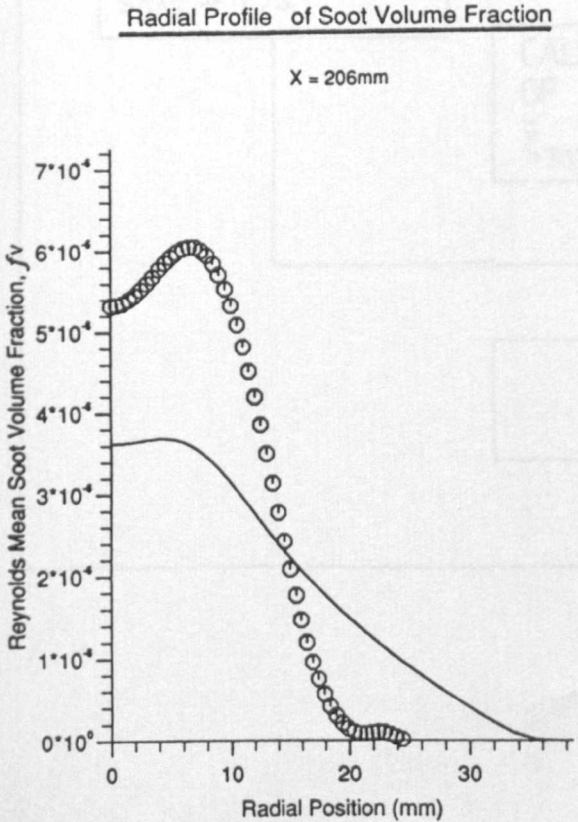

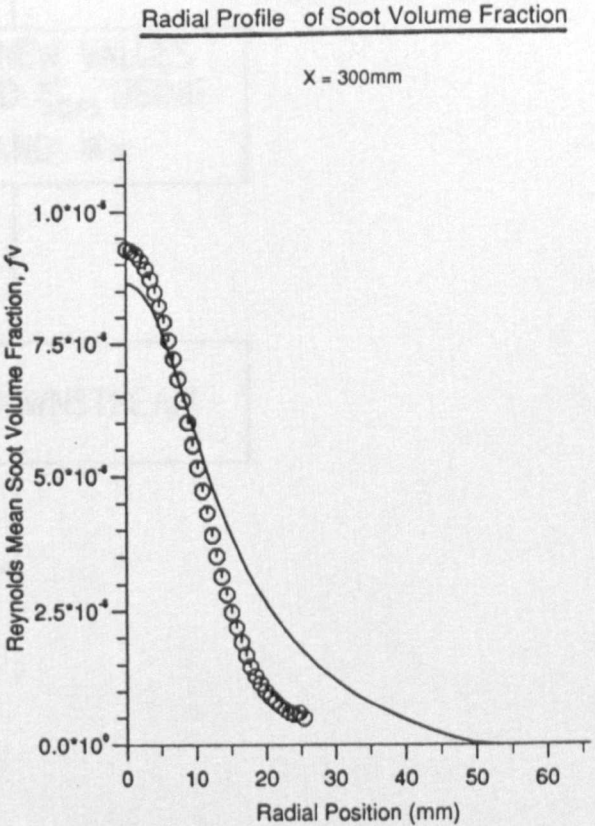

Fig(5.11) FLOWCHART OF SOOT FEEDBACK MECHANISM

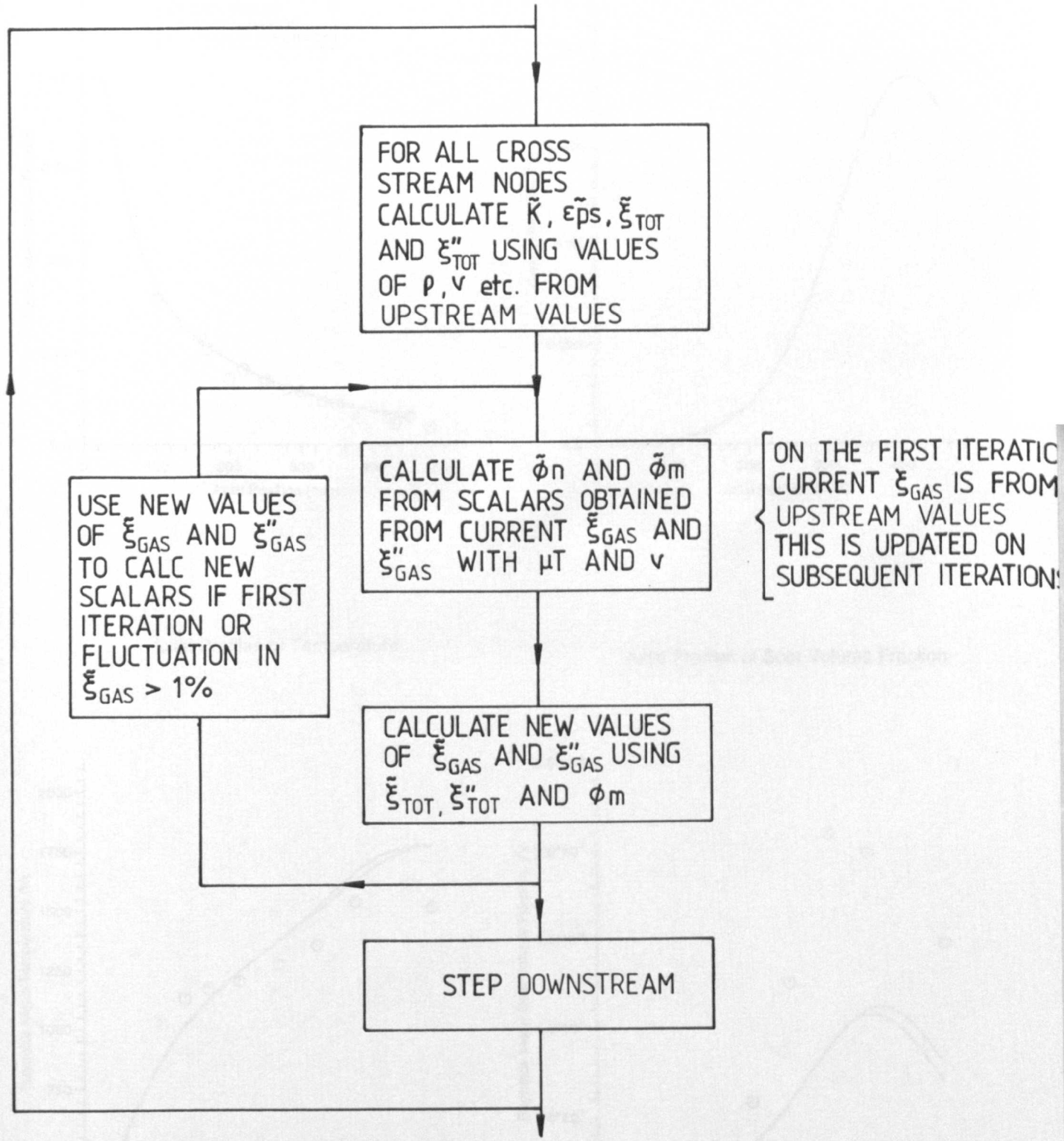

Fig(5.12) APPLICATION OF THE CARBON FEEDBACK SCHEME TO THE ETHYLENE FLAME SOOT SIMULATION AXIAL PROFILES

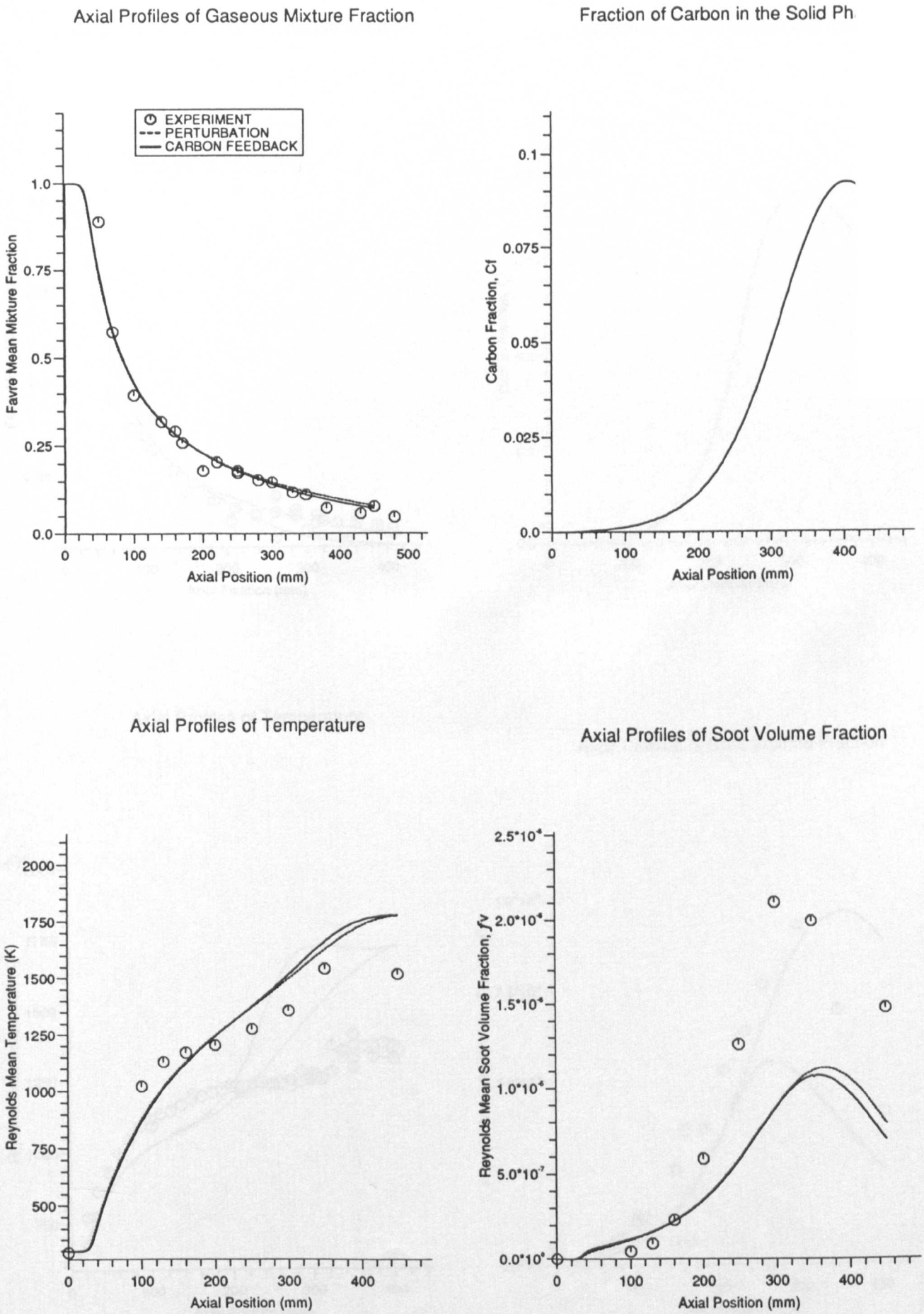

Fig(5.13) APPLICATION OF THE CARBON FEEDBACK SCHEME TO THE KEROSINE FLAME A SOOT SIMULATION - AXIAL PROFILES.

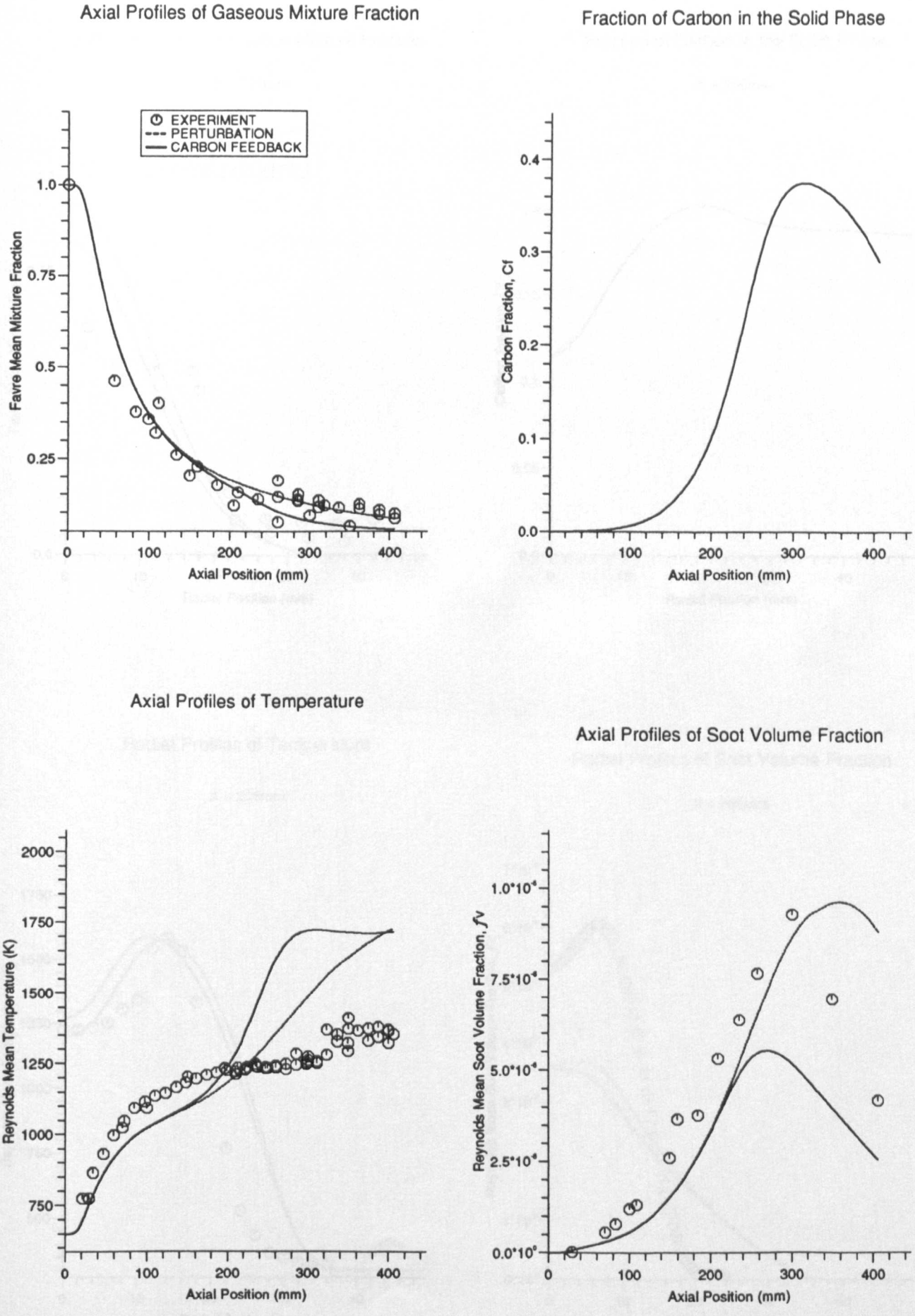

Fig(5.14) APPLICATION OF THE CARBON FEEDBACK MECHANISM TO THE KEROSINE FLAME A SOOT SIMULATION - RADIAL PROFILES.

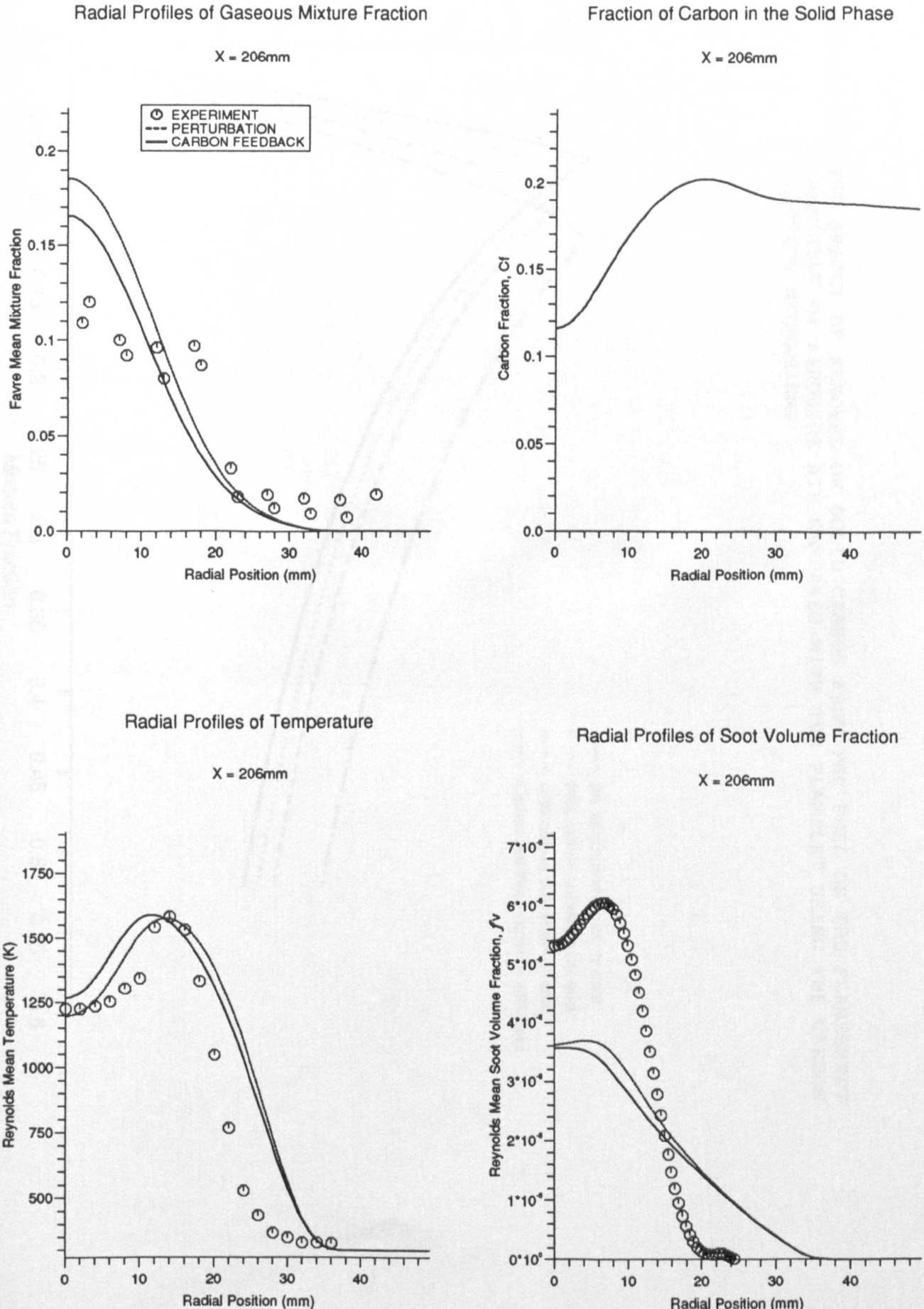

Fig(5.15) THE AFFECT OF REMOVAL OF SOLID CARBON FROM THE FUEL ON THE FLAMESHEET CHEMISTRY OF KEROSINE AIR COMPARED WITH THE FLAMELET USING THE CARBON FEEDBACK MECHANISM.

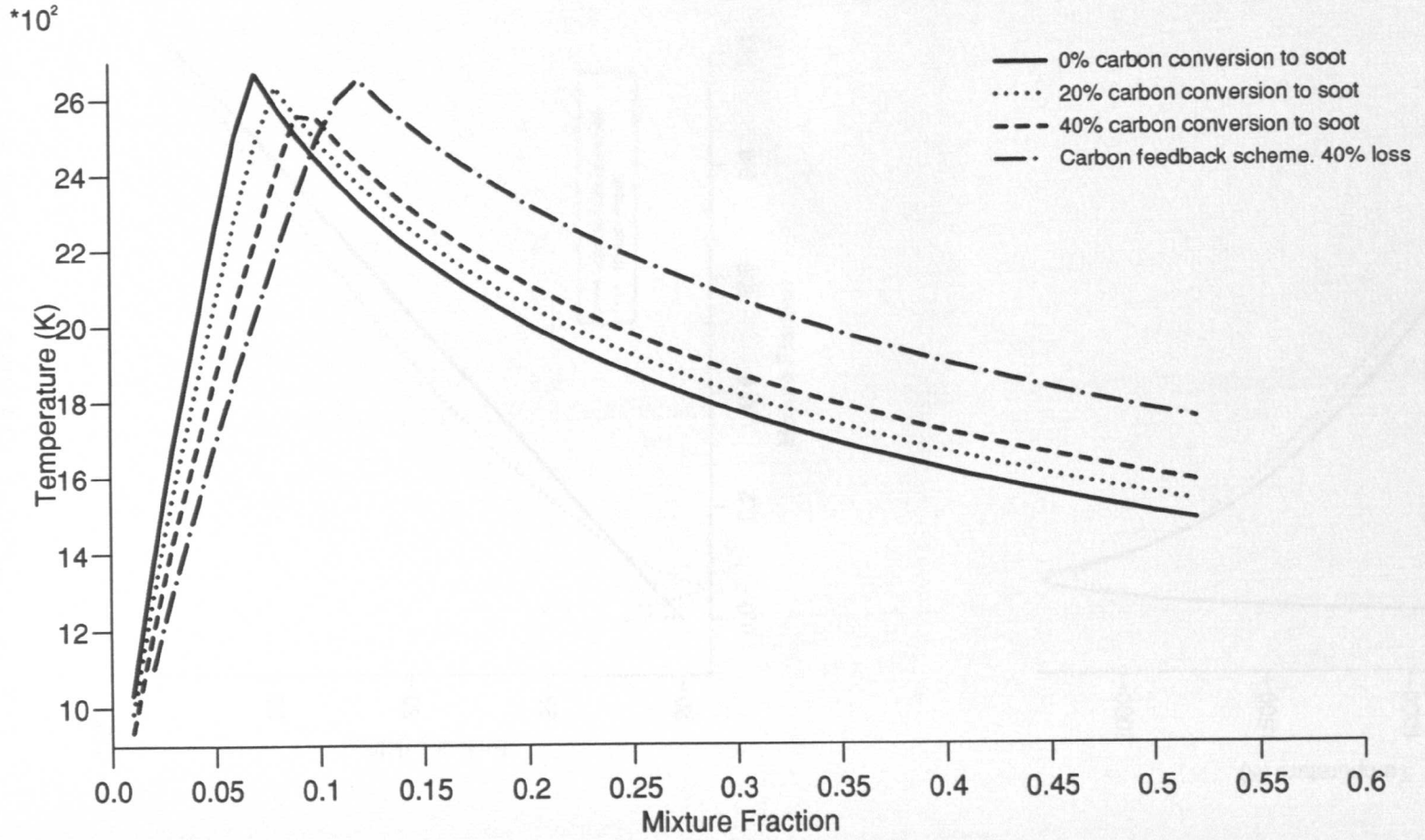

Fig(5.16) ADIABATIC MIXTURE ENTHALPY AND TEMPERATURE FOR THE ETHYLENE AIR SYSTEM WITH AND WITHOUT IMPOSING THE LINEAR ENTHALPY MIXTURE FRACTION RELATIONSHIP

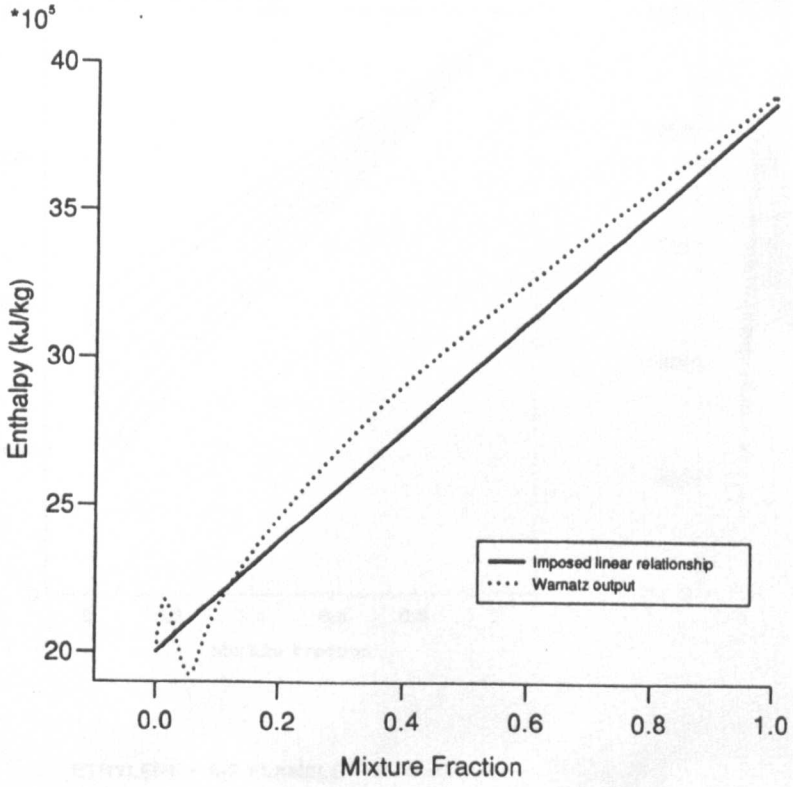

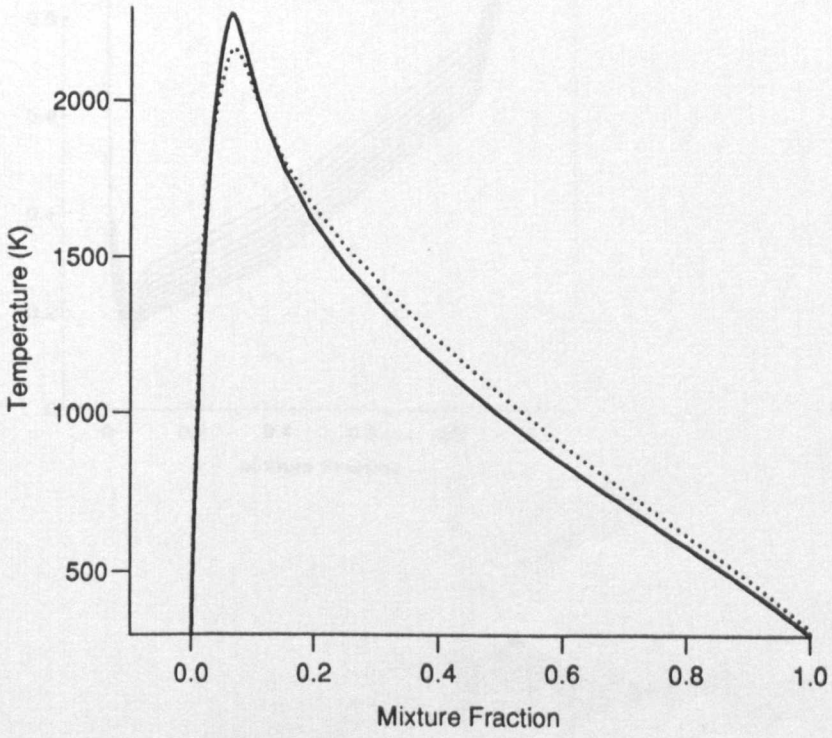

Fig(5.17) FLAMELETS OF THE MAIN THERMOCHEMICAL SCALARS FOR THE ETHYLENE AIR SYSTEM WITH VARYING DEGREES OF HEAT LOSS. 6% loss between flamelets.

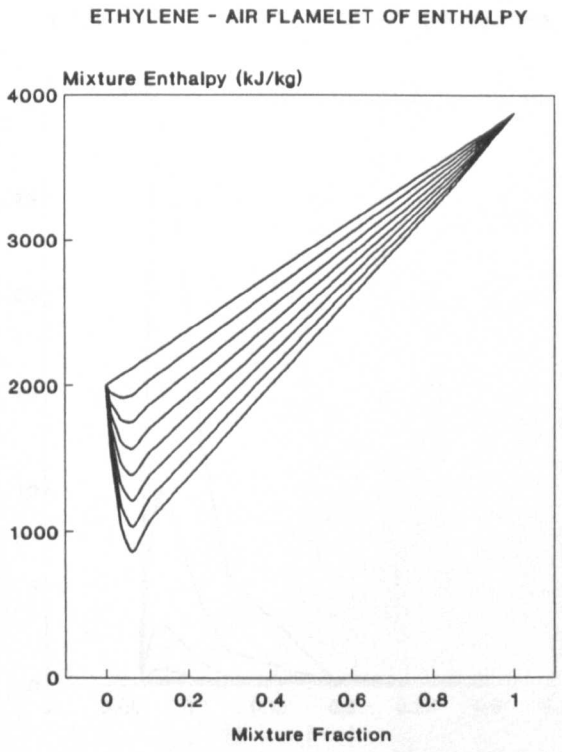

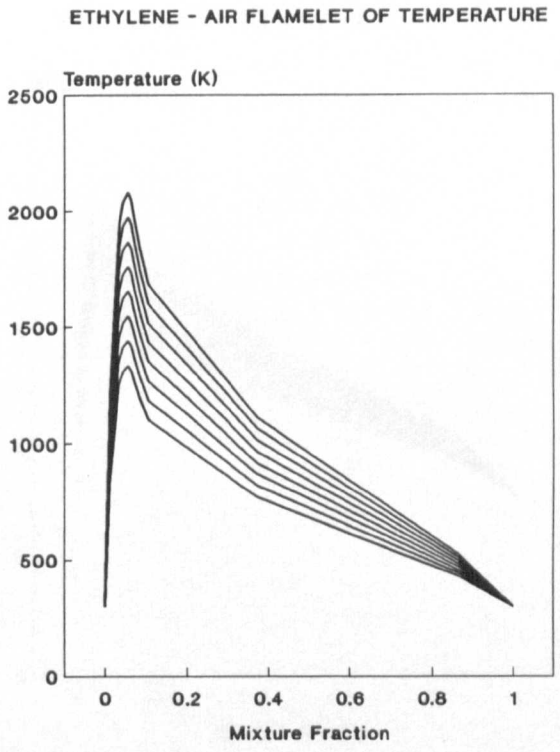

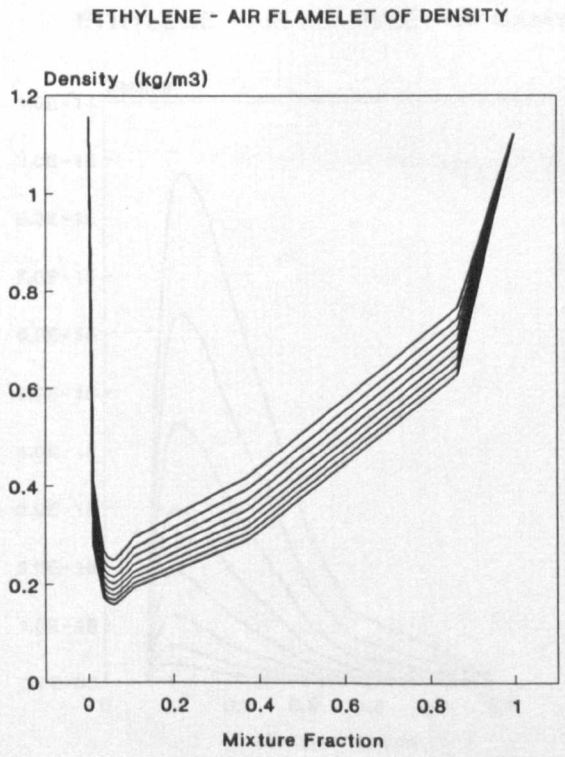

Fig(5.18) FLAMELETS OF THE SOOT SOURCE TERM SCALARS FOR THE ETHYLENE AIR SYSTEM WITH VARYING DEGREES OF HEAT LOSS. 6% loss between flamelets.

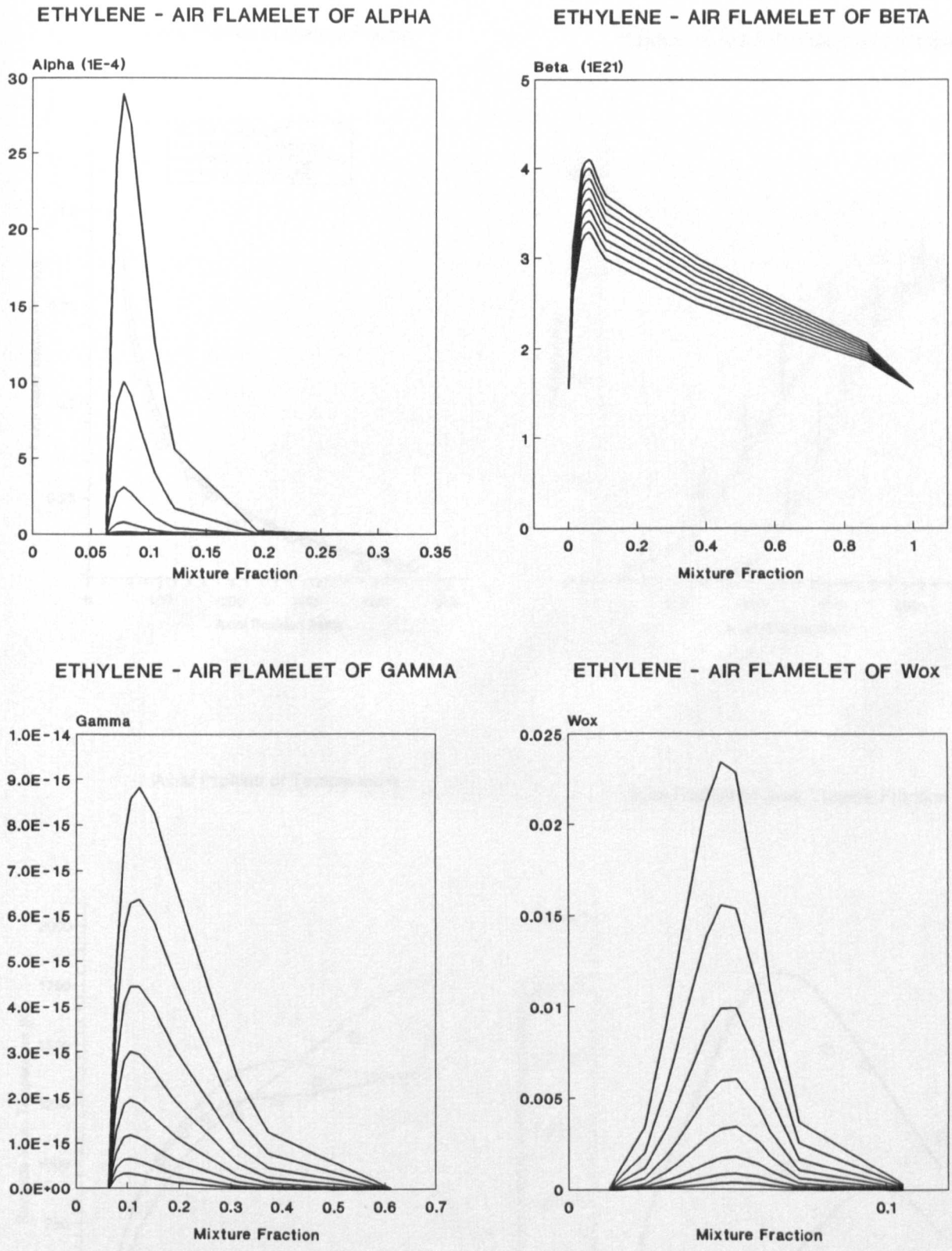

Fig(5.19) APPLICATION OF THE RADIATION LOSS MODEL TO THE ETHYLENE FLAME SIMULATION ALONG THE FLAME AXIS - SINGLE FLAMELET, PARTIALLY COUPLED AND FULLY COUPLED CALCULATIONS SHOWN

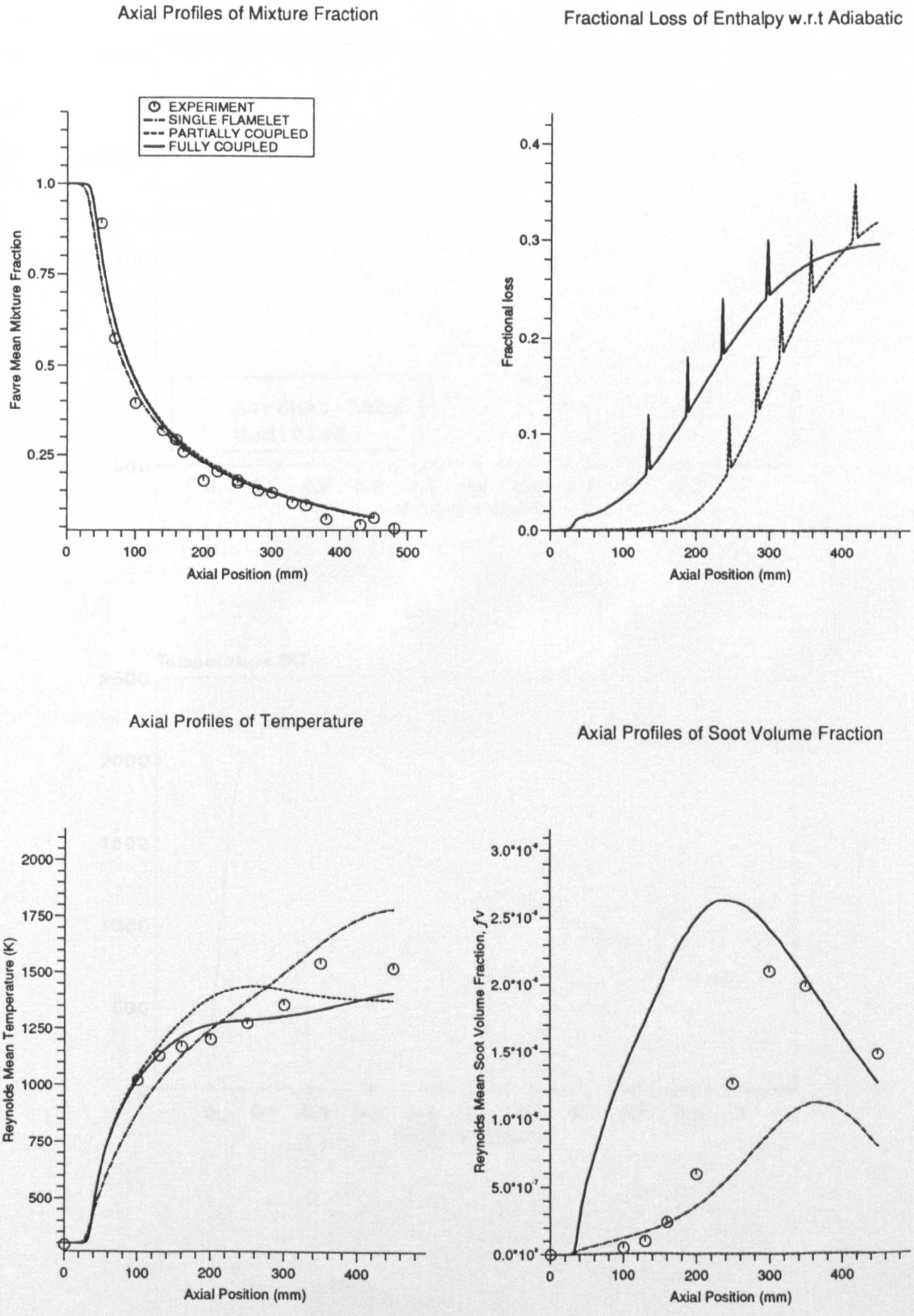

Fig(5.20) ADIABATIC MIXTURE ENTHALPY AND TEMPERATURE FOR THE KEROSINE AIR LAMINAR DIFFUSION FLAMELET WITH AND WITHOUT IMPOSING THE LINEAR ENTHALPY / MIXTURE FRACTION RELATIONSHIP.

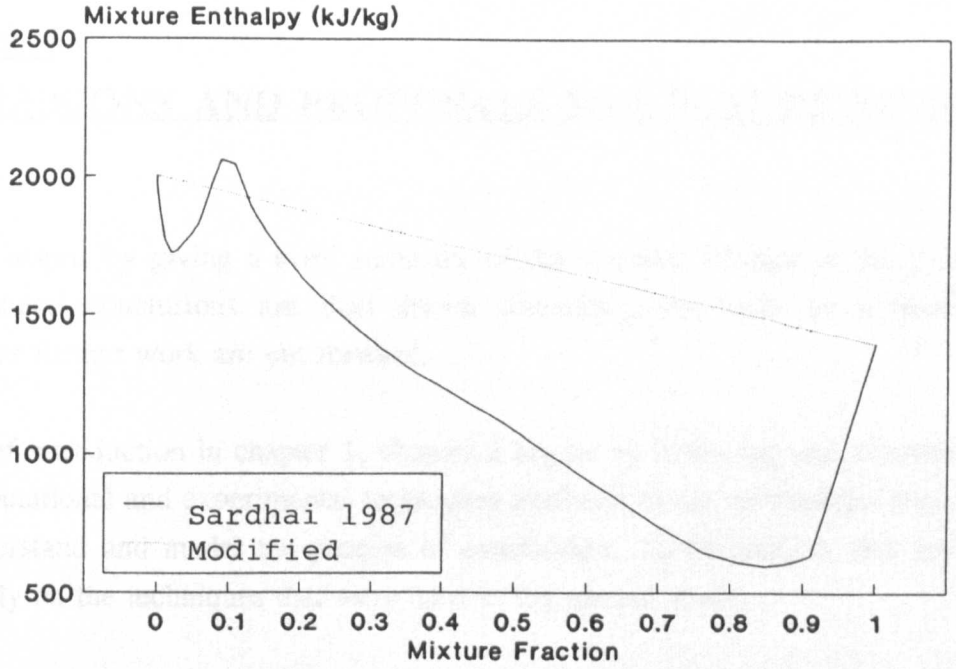

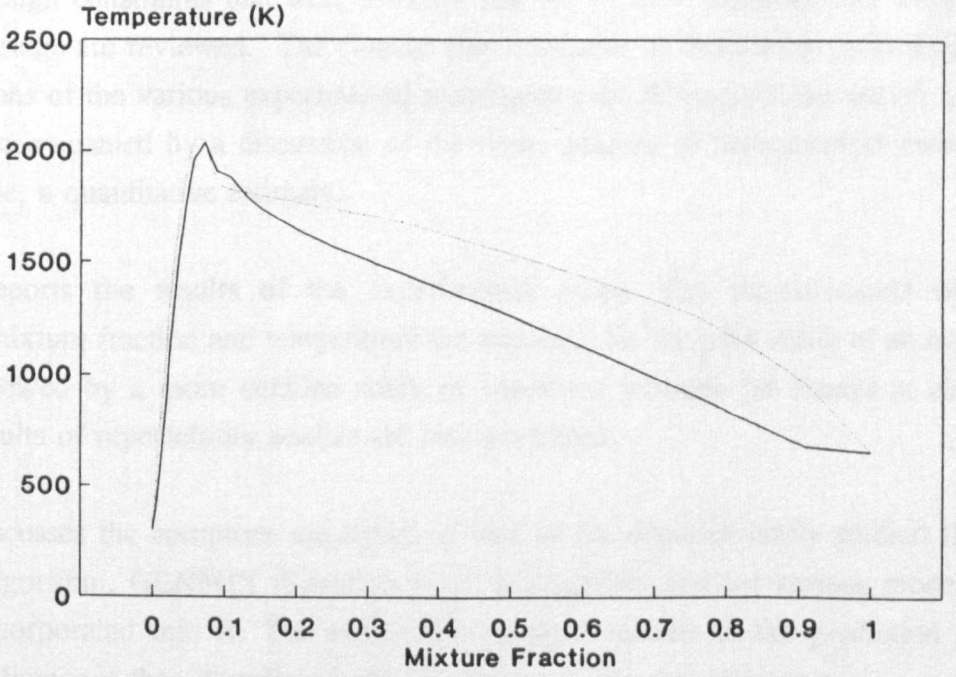

CHAPTER 6
CONCLUSIONS AND PROPOSALS FOR FUTURE WORK

This chapter begins by giving a brief summary of the contents of each of the preceding chapters. General conclusions are then drawn concerning the work as a whole and suggestions for further work are put forward.

After the brief introduction in chapter 1, chapter 2 begins by reviewing and discussing the various computational and experimental techniques available to the combustion engineer in order to understand and model the process of combustion. To be concise, this review is focused mainly on the techniques that were used in the present study.

Chapter 3 continues by describing in detail the configuration of the ethylene and vaporised kerosine jet flame experiments studied here. Particular attention is paid to the design and construction of the pressure vessel test rig which was manufactured especially for the present study. The design constraints that were imposed and the various decisions that were made at the design stage are reviewed. The chapter then continues by describing individually the implementations of the various experimental techniques used throughout the study. In each case this is accompanied by a discussion of the likely sources of measurement error and, where possible, a quantitative estimate.

Chapter 4 reports the results of the experimental study. The measurements of soot parameters, mixture fraction and temperature are reported for the pilot study of an ethylene jet flame followed by a more detailed study of vaporised kerosine jet flames at elevated pressure. Results of repeatability studies are also presented.

Chapter 5 discusses the computer simulation of two of the experimentally studied flames. Firstly, the algorithm, GENMIX (Spalding 1977) is described and the various models that have been incorporated into it. The application of these models to the prediction of the experimental flames is then described with comparison to the measurements.

The main achievement of this study has been the generation of an experimental dataset of mean soot volume fraction, mixture fraction and temperature for a variety of ethylene and

kerosine flames at differing pressures. Although the measurements of mixture fraction at elevated pressure are sparse, such a database is unique and extremely useful for the purposes of model validation in turbulent situations.

One of the most important discoveries was the amount of fuel carbon conversion to soot that was encountered in the kerosine flames. Previous experience of Stewart and Moss 1989 in laminar flames, demonstrated the high sooting propensity of kerosine, but the increased mixing and shorter timescales of the jet flame were expected to reduce this significantly. However, conversions of fuel carbon to soot of up to 60% were still measured resulting in a highly radiating optically thick environment.

Given the above experimental observations, the emphasis of the computational study was shifted towards the development of methods to incorporate solid / gaseous phase chemistry and radiation interaction into the computer simulation.

The computer analysis began with the pilot study of the ethylene jet flame in which soot loadings remained at a reasonable level (<20%). In this situation it was possible to circumvent the problems of radiation / chemistry interaction by assuming a single radiatively perturbed flamelet of temperature to prevail throughout the domain. Subsequent application of the soot model of Moss et al. 1988, which was based upon laminar experiment, gave very encouraging results and proved the technique to be a viable one.

The areas of the greatest concern with the model application lay in three areas. Firstly, in the assumptions necessary to implement the model, secondly the unknown particle size and, thirdly, the uncertain oxidation mechanism by which soot is destroyed. Gaps in the present knowledge of all these factors were evident in the data. More experimental information would be desirable including soot particle size and instantaneous soot parameter / mixture fraction information.

It is unfortunate that the two attempts at soot particle sizing had limited success in this study given the importance of these parameters on both the radiative nature of the soot and its chemistry. A further, more detailed study into the size of soot particles would augment the present dataset greatly. Further implementation of the multicolour extinction technique is suggested but using an infra red probe wavelength and simultaneous measurement. Alternatively, different techniques such as dynamic scattering (Charalampopoulous and Felske 1987) could be considered.

Regarding the instantaneous soot / mixture fraction measurement, although optical techniques potentially offer such information, their successful application in such an optically thick, soot laden environment is not guaranteed.

Further computer simulation of the atmospheric kerosine jet flame 'A' using the same strategy as above proved more problematic. It soon became clear that the description of this flame in terms of a single radiatively perturbed flamelet was close to the limits of acceptability. The quality of the temperature predictions was poor and the extrapolation of the soot model of Stewart et al. 1991 to these conditions unsuccessful. Further, the assumption that the soot may be treated as a mere perturbation to the gaseous phase chemistry was also doubtful given the measured conversions of gaseous to solid carbon of up to 40%.

A new soot model, based on that for the ethylene flame was therefore created in order to develop methods of modelling situations in which there are high soot and radiation loadings.

The effect of high carbon loadings was modelled using a development of the droplet combustion model of Jones and McGuirk 1979. A necessary assumption of this technique, if it is to be implemented in the same manner as in the original report, is that the effect of solid carbon on the gaseous phase chemistry is negligible. It was concluded that such an assumption was inappropriate for the heavily sooting kerosine flame case. The resulting movement of the local gaseous component of mixture fraction towards leaner values produced a predicted compression of the flame in physical space and substantially poorer predictions of measured temperature.

A flamesheet analysis of the kerosine air system with a variety of soot loadings showed that the thermal ballast of the soot to the gaseous phase must also be considered. A method is suggested of incorporating such a scheme with the laminar flamelet strategy which would require a library of flamelets with varying carbon loadings to be referenced depending on the local conversion. Such an strategy must be approached with caution, however, since high smoke levels in most situations are also accompanied with high radiation levels. The necessity of a three dimensional library of flamelets becomes apparent.

Further detailed chemical kinetic analysis of a laminar, heavily sooting flame -such as any of those reported by Stewart and Moss 1989 - is recommended to increase the fundamental understanding of the influence of solid carbon on the local flame structure by removing the confusing affects of turbulence.

Finally a first attempt at modelling the radiation / chemistry / soot interaction was attempted on the pilot study of the ethylene flame. A new model of laminar flamelet / radiation model coupling is proposed which removes some of the closure problems associated with similar techniques (eg.Kent and Honnery 1987, Lin 1992). Flamelet and conservation equation enthalpy are compared in order to decide which set, from a library of sets flamelets with varying radiative heat loss, is, locally, the most appropriate.

For this first application of the model, the enthalpy equation used had a simplified description of radiation loss assuming it to emanate solely from the soot in the optically thin limit. The resulting predictions demonstrate the extremely temperature sensitive nature of the soot model and also show an overprediction of centreline temperature at low heights in the flame where radiation levels must be small. A number of explanations are given but, again, the added uncertainties of the turbulence on all parameters acts to confuse the analysis. Once more, detailed laminar flame predictions would help remove this further uncertainty.

Regarding this work as a whole and considering its original aims, the study was subject to unexpected ambiguity. The aim of the experiment was to generate a detailed set of experimental data to aid the study of soot formation in kerosine jet flames at elevated pressure. The concept was to study a flame in which soot formation could be studied in isolation from other poorly understood processes in gas turbine combustion. Although, indeed, the aim was met and a formidable database was compiled, the combined effects of high soot and radiation levels served to obscure the analysis and prevented the process of soot formation from being studied exclusively. Rather, the modelling uncertainties of high soot and radiation levels were inextricably married to create a very difficult problem.

In the light of the findings, it is clear that the jet flame geometry is not ideally suited to this purpose. The poor mixing of this flame with relation to most practical devices and the longer timescales provide excessive opportunity for smoke production and dissallow the possibility of treating soot as a perturbation to the gas phase. Rather, in some locations, soot becomes the major carbon bearing species. Modification to the nature of the flame is clearly necessary. Two possible alternatives exist: to improve the mixing or to increase the effectiveness of the oxidation process.

The oxidation process could be augmented by either of two methods. The temperature or the level of oxygen in the air could be increased. Regarding both methods, however, the difficulty is that the mixing rates would remain roughly the same. Since both techniques would indirectly also increase the temperature of the oxygen starved, fuel rich core of the

jet, the likely effect would actually be an increase in soot levels. This is borne out by the study of Nishida and Mukohara 1982 on propane jet flames. An increase in air temperature from 300 - 600K resulted in an approximately twofold increase in peak soot levels although subsequent burnout was more affective.

Therefore, it is the second strategy of increasing the level of fuel / air mixing which is recommended. Methods available could either involve, the addition of a recirculation to entrain more air, the use of a lifted flame to promote partial premixing or the use of fuel in fine droplet form again to increase entrainment. The disadvantage of all such methods is that they increase the complexity of the flow field and hence the demands on the CFD and combustion model to varying degrees. However, it would appear that some complication is inevitable and the merits of each geometry should be weighed against their shortfalls.

An important consequence of the above difficulties is the further relevance of the present experiment and analysis to the field of fire hazard modelling. The spillage of liquefied natural gas (LNG) or liquefied petroleum gas (LPG) can result in large pool fires which, due to their underventilated nature and size, produce vast amounts of smoke and hence radiation. The result is a fire which is optically thick in nature and far from adiabatic with fuels which, under normal circumstances, would be regarded as relatively soot free.

Small scale laboratory based simulations of these flames have traditionally been extremely difficult since their optical path lengths and, hence radiative properties are very different from the real pool fires. This has led to very expensive field tests being undertaken on large scale simulations in order to assess radiation levels (ref. Mizner and Eyre 1982).

The present study, however, demonstrates that there are conditions in the laboratory under which a very small scale jet flame can exhibit many of the features of the large pool fire. This is, clearly, a very important discovery. The simple geometry and controlled conditions possible coupled with the detailed and repeatable measurements achievable admit great insight into such flames and, undoubtedly, will be very cost effective.

To further augment this data, a study of the emitted radiative energy from the flames at a variety of locations would also be very useful. This could be compared with predicted fluxes in order to assess the radiation model. Also, it would seem sensible to upgrade the radiation model, itself. A solution of the radiative transfer equation including re-absorption is probably a necessity in such an optically thick environment. As a first formulation of the problem a simple two flux description (Viskanta and Menguc 1987) would be a good starting point.

REFERENCES

Abbas A.S., Lockwood F.C. (1985) "Prediction of soot concentration in turbuelent diffusion flames". J.Inst.Energy, pp.112-115

Abramowitz M., Stegun I.A. (1964) "Handbook of Mathematical Functions", Constable and Company Ltd.

Adkins R.C. (1990). Private conversation. Senior lecturer, Cranfield Inst. of Tech., Beds.

Andrews S.A. (1962) "Thermocouples for gas temperatures up to 2000°C", Proceedings of symposium on some developments in techniques for temperature measurement, (Inst. Mech. Engrs.), paper 2, pp.10-19

Askari-Sardhai A. (1987) "Laminar flamelet modelling of turbulent combustion chemistry for practical fuels", Ph.D. thesis, Cranfield Inst. of Tech., England

Avva K.A., Smith C.E., Singhal A.K. (1990) "Comparative study of high and low Reynolds number versions of k-e models" AIAA - 90 - 0246, pp.1-9

Ballyantyne A., Boon D.J., Moss J.B. (1976) "Measurements of fluctuating temperature in open diffusion flames employing fine wire thermocouples", AASU Memo No. 76/3, Univ. Southampton.

Bard S., Pagni D.J. (1981), "Carbon Particulates in Small Pool Fire Flames". J.Heat.Trans, vol.103,pp.357-362.

Batten C.E. (1985), "Spectral Optical Constants of Soots from Polarized Angular Reflectance Measurements". App. Optics. Vol.24, No.8. 15 April

Becker H.A., Hottel H.C., Williams G.C. (1967) "The nozzle fluid concentration of the round, turbulent, free jet", J. Fluid Mech., 80, pp.285-303

Bilger R.W. (1976) "Turbulent jet diffusion flames", Prog. Energy Comb. Sci., Vol. 1, pp.87-109

Bilger (1980) - see Libby and Williams 1980.

Black J.D., Stewart C.D. (1989) "CARS temperature measurements in laminar sooting diffusion flames at Cranfield Institute of Technology", Rolls Royce internal report RR(OH)1060.

Blazowski W.S. (1979) "Dependence of soot production on fuel blend characteristics and combustion conditions." ASME 79-GT-155

Bockhorn H., Fetting F, Meyer U., Reck R., Wonnemecher G. (1981), "Measurement of soot concentration and soot particle sizes in propane oxygen flames" 18th Symp. (Int.) on Comb., Combustion Institute. pp.1137 - 1147

Bonczyk P.A., Hall R.J. (1991) "The fractal properties of soot agglomerates", Langmuir 1991, vol.7 No.6,pp.1274-1280

Bond N.R. (1990) "Introduction of feedback from the soot model of the flow field calculation in PACE", Rolls Royce Internal report J330/L39

Borghi R. (1975) - See Murthy 1975.

Boussinesq J. (1877) "Theorie de l'ecoulement tourbillant", Mem. Pre. par Div. Sav. 23, Paris.

Calcote H.F. (1981) "Mechanisms of soot nucleation in flames - A critical review", Comb. Flame, 42, pp.215-242.

Charalampopoulos T.T., Felske J.D. (1987) "Refractive indices of soot particles deduced from in-situ laser light scattering measurements", Comb. Flame, 68, pp.283-294

Chedaille J., Braud Y. (1972) "Measurements in flames", Edward Arnold Ltd., London, England.

Chippet S., Gray W.A. (1978), "The Size and Optical Properties of Soot Particles". Comb and Flame. 31, pp.149-159

Chen C.J., Rodi W. (1975) "A mathematical model for turbulent stratified flow and its

application to buoyant jets", 11th IAHR Congress, Sao Paulo, Brazil.

Chou P.Y. (1945) "On the velocity correlations and the solution of the equations of turbulent fluctuation", Quart. Appl. Math., 3, p.38.

Dalzell W.H., Sarofim A.F. (1969) "Optical constants of soot and their application to heat flux calculations", J. Heat Transf. 91 pp.100-104.

Dalzell W.H., Williams G.C., Hottel H.C. (1970), "A light scattering method for soot concentration measurement". Comb. and Flame, vol.14, no.2, p161-170.

DeRis J (1978) "Fire Radiation - a review", 17th Symp. (int.) on Comb., The Comb. Inst. pp.1003-1016

Durbin E.J. (1950) "Optical methods involving light scattering for measuring size and concentration of condensation particles in super cooled, hypersonic flow", NACA Tech note 2441.

Ebrahimi I., Kleine K. (1977) "The nozzle fluid concentration fluctuation fields in round, turbulent, free jets and jet diffusion flames", 16th Symp. (Int.) on Comb., The Comb. Inst., p.1711

Eckbreth A.C. (1990) - see Kalghatgi 1990

Eckbreth A.C., Bonczyk P.A., Verdieck J.F. (1979) "Combustion diabnostics by laser Raman and fluorescence techniques", Prog. Energy Comb. Sci., Vol.5, pp.253-322.

Edwards D.K., Balakrishnan A. (1973) "Thermal radiation by combustion gases", Int. J. Heat Mass Transf., 16, pp.25-40

Ewart P. (1990) - see Kalghatgi 1990

Faeth G.M., Gore J.P., Sivanathu Y.R. (1987) "Radiation from soot containing flames", AGARD-CP-422, 17.

Faeth G.M., Jeng S.M., Gore J. (1985) - see LAw et al. (1985)

Fairweather M., Jones W.P., Ledin H.S., Lindstedt R.P. (1992) "Predictions of soot formation in turbulent non-premixed propane flames", 24th Symp. (Int.) on Comb., The Comb. Inst., In publication.

Fennimore C.P., Jones G.W. (1967) "Oxidation of soot by hydroxl radicals", J. Phys. Chem., 71, pp.593-597.

Fissan H. "Sampling and Transport" Lecture notes, Loughborough University. Aerosol science short course. (unpublished)

Flower W.L. (1988), 'An investigation of soot formation in axisymmetric turbulent diffusion flames at elevated pressure', SAND 88-8627 Jan

Flower W.L., Bowman C.T. (1986), 'Soot Production in laminar diffusion flames at pressures from 1 to 10 atmospheres', 21st Symp. (Int.) on Comb., The Combustion Institute. pp.1115-1124

Friedel R.A., Orchin M. (1951), "Ultraviolet Spectra of Aromatic Compounds.", Wiley, New York.

Fristrom R.M., Westernberg A.A (1965) "Flame structure", McGraw Hill series in advanced chemistry, USA.

Garo A., Prado G., LaHaye J. (1990) "Chemical aspects of soot particles oxidation in a laminar methane air diffusion flame", Comb. Flame., 79, pp.226-233

Gilbert M., Lobdell J.H. (1953) "Resistance thermometer measurements in a low pressure flame", 4th Symp. (Int.) on Comb., The Comb. Inst., p.285

Giliatzedinov L.P. (1972) "The kinetics and formation mechanism of carbon black during the thermal decomposition of hydrocarbons in the gas phase", Khim. Tverd. Topl., 3, pp.103-111.

Givi P. (1989) "Model free simulations of turbulent reactive flows", Prog. Energy and Comb. Sci., 15, pp.1-107.

Glassman I. (1988) "Soot formation in combustion processes", 22nd Symp. (Int.) on Comb.,

The Comb. Inst. pp.295-311

Godoy S. (1982) "Turbulent diffusion flames", Ph.D. thesis, University of London, England.

Gordon S., McBride B.J. (1971) "Computer program for calculation of complex chemical equilibrium compositions, rocket performance, incident and reflected shocks, and Chapman Jouget detonations", NASA-SP-273

Gore J., Faeth G.M. (1988) "Structure of radiation properties of luminous turbulent acetylene / air diffusion flames", J. Heat. Transf., ASME, 110, pp.173-181

Greenhalgh D.A. (1990) - see Kalghatgi 1990

Guidt J.B., Gonsebert G., Toulouzon J.N. (1990) 'Accurate validation of visible, infra red double extinction simultaneous measurement of particle sizes and number densities using densely laden standard media", Appl. Opt., 29, No.7. pp.1011-1022

Hall R.J. (1988) "Computation of the radiative power loss in a sooting diffusion flame", Appl. Opt., Vol.27, No.5, pp.809-811

Hall R.J., Bonczyk P.A. (1990) "Sooting flame thermometry using emission / absorption tomography", Appl. Opt., Vol. 29, No. 31, pp.4590-4598

Hanson R.K. (1986) 'Combustion diagnostics: Planar Imaging Techniques', 21st Symp. (int.) on Combustion, The Comb. Inst., p.1677

Haynes B.S., Wagner H.Gg. (1981) "Soot formation", Prog. Energy and Comb. Sci., 7, pp.229-273.

Hirchfelder J.O., Curtiss C.F., Bird R.B. (1954) "The molecular theory of gases and liquids", John Wiley and sons Inc., New York.

Honnery.D (1991) "Surface Growth in Sooting Laminar Flames". Ph.D thesis, Univ. Sydney.

Hottel H.C., Sarofim A.F. (1967) "Radiative Heat Transfer", Mc.Graw Hill Book Co., New York.

Hurley C.D. (1982) "Carbon formation by the pyrolysis of gas turbine fuels in preflame regions of gas turbine combustors", ASME 82-GT-84

Jones W.P., Launder B.E. (1972) "The prediction of laminarization with a two-equation model of turbulence", Int. J. Heat and Mass Transf., 15, pp.301-314.

Jones W.P., McGuirk J.J. (1979) "Mathematical modelling of gas-turbine combustion chambers", The propulsion and energetics panel, 45th (B) specialists meeting DFVLR, Cologne, Germany AGARD-CP-275

Kalghatgi G.T. (1990) "Spectroscopy in Combustion Studies", I.O.P. short meeting series no. 27, Chester.

Keady P.B., Quant F.R., Sem G.J. (1983), "Differential Mobility Particle Size: A new instrument for high resolution aerosol size distribution measurement below 1 micron" T.S.I. Quarterly April/June.

Kent J.H., Honnery D. (1987), "Soot and Mixture Fraction in Turbulent Diffusion Flames". Comb. Sci. Tech., Vol.54, pp.383-397.

Kent J.H., Wagner H.Gg. (1982), "Soot Measurements in Laminar Ethylene Diffusion Flames". Comb.Flame 47 pp.53-65

Kent J.H., Wagner H.Gg. (1984), "Why do diffusion flames emit smoke?", Comb. Sci. Tech., 41, pp.245-269.

Kerker M. (1969), "The Scattering Of Light". Academic Press, London.

Khan I.M., Greeves G., (1974) "A method for calculating the formation and combustion of soot in Diesel engines", Afgan N.H., Beer J.M. (Eds.), Scripta Book Co.

Kreith.F, Black.W.E. (1980), "Basic Heat Transfer". Harper and Row.

Kunugi M., Jinno H. (1966), "Determination of Size and concentration of Soot Particles in Diffusion Flames by a Light-Scattering Technique". 11th Symp. (Int.) on Comb., Combustion Institute.

Langelle G., Verdier C. (1973) "Gas sampling and analysis in combustion phenomena", AGARD-AG-168

Launder B.E., Morse A.P., Rodi W., Spalding D.B. (1972) "The prediction of free shear flows - a comparison of six turbulence models", NASA SP-311

Launder B.E., Spalding D.B. (1972) " Lectures in mathematical models of turbulence", Academic Press, London.

Launder B.E., Spalding D.B. (1974) "The Numerical Computation of Turbulent Flows" Comp. Maths. in Appl. Sci. and Eng. 3 pp.269-289

Law, Jaluria, Yuen, Miyasaka (eds.) "Heat transfer in fire and combustion", New York ASME., pp.137-151

Lee K.B., Thring M.W., Beer J.M. (1962) "On the rate of combustion of soot in laminar flames", Comb. Flame, 6, p.137

Lee S.C., Tien C.L. (1981), "Optical Constants of Soot in Hydrocarbon Flames". 18th Symp. (Int) on Comb., The Combustion Institute, pp.1159-1166

Lefebvre A.W. (1983) "Gas Turbine Combustion", McGraw Hill series in Energy Combustion and Environment.

Leung K.M., Lindstedt R.P., Jones W.P. (1991) "A simplified reaction mechanism for soot formation in nonpremixed flames", Comb. and Flame, 87. pp.289-305.

Libby P.A., Williams F.A. (Ed.) (1980) "Fundamental aspects in: turbulent reacting flows', Topics in Applied Physics. Vol.44, Springer Verlag.

Libby P.A. , Bray K. (1980) "Counter gradient diffusion in premixed turbulent flames", AIAA-80-0013

Liew S.K. (1983) "Flamelet models of turbulent non-premixed combustion", Ph.D thesis, Univ. Southampton.

Liew S.K., Bray K.N.C., Moss J.B. (1981) "A flamelet model of turbulent non-premixed

combustion", Comb. Sci. Tech., 27, pp.69-73

Lin D.C. (1992) "Computational modelling of solid fuel combustion", Ph.D thesis, Cranfield Inst. of Tech., Beds.

Lockwood F., Naguib A.S. (1975) "Prediction of horizontal and vertical turbulent, buoyant wall jets", J.Heat Transf. 103, pp.343-349

McGuirk J.J., Rodi W. (1977) "The calculation of three dimensional free jets", Symp. on. Turb. Shear Flows, Pensylvania state university.

Megaridis C.M., Dobbins R.A. (1989) "Comparison of soot growth and oxidation in smoking and non-smoking ethylene diffusion flames", Comb. Sci. Tech., 66, pp.1-16.

Mithchell R.E., Sarofim A.F., Clomburg L.A. (1980), "Experimental and numerical investigation of confined laminar diffusion flames", Comb. Flame, 37, pp.227-244

Mizner G.A., Eyre J.A. (1982) "Large scale LNG and LPG pool fires", I.Chem. Symp. No. 71, pp.147-163

Morse A.P. (1977) "Axisymmetric turbulent shear flows with and without swirl", Ph.D. thesis, London University, England.

Moss J.B., Stewart C.D., Syed K.J. (1987), 'Flamlet Chemistry of Soot Formation for Radiation Prediction in Combustor Flowfields', AGARD-CP-422 pp.18-1,12

Moss J.B., Stewart C.D., Syed K.J. (1988), "Flowfield Modelling of soot formation at elevated pressure" 22nd Symp. (Int.) on Comb., Combustion Institute. pp.413-423

Mullins J., Simmons B., Williams A. (1987) "Rates of formation of soot from hydrocarbon flames and its destruction", AGARD-CP-422, 23

Mullins J., Williams A. (1987), "The Optical Properties of Soot: a comparison between Experimental and Theoretical Values". Fuel, Vol.66, Feb. pp.277-280

Murthy S.N.B. (Ed.) (1975) "Turbulent mixing in non-reactive and reactive flows", Plenum Press, New York

Nagle J., Strickland-Constable R.F. (1962) "Oxidation of carbon between 1000 and 2000$_0$C", Proc. 5th Carbon Conf., Vol. 1, pp.154-164

Nazih A. (1989) "Applications del la spectroscopie par correlation de photons a: 1) la granulometrie 2) la velocimetrie", Ph.D thesis, Universitie de Rouen.

Nishida O., Mukohara S. (1982), 'Characteristics of Soot Formation and Decomposition in Turbulent Diffusion Flames', Comb. and Flame., 47: pp.269-279

O'Brien 1980 - see Libby and Williams 1980.

Paczko G., Lefdal P.M., Peters N. (1986) "Reduced reaction schemes for methane, methanol and propane flames", 21st Symp. (Int.) on Comb., The Combustion Institute., pp.739-748.

Patankar S.V. (1980) "Numerical heat transfer and fluid flow",McGraw Hill.

Peters N. (1984) "Laminar diffusion flamelet models of non-premixed turbulent combustion", Prog. Energy Comb. Sci., 10, pp.319-339.

Pope S.B. (1978) "An explanation of the turbulent round jet / plane jet anomoly" AIAA-78 pp.279-281

Pope S.B. (1981) "A Monte Carlo method for the PDF equations of turbulent reactive flows", Comb. Sci. Tech., 25, pp.159-174.

Pope S.B. (1990) "Computations of Turbulent Combustion: Progress and Challenges" 23rd Symp. (Int.) on Comb., The Comb. Inst. pp.591-612.

Prado G., Jagoda J., Neoh K., Lahaye J. (1981), "A study of soot formation in premixed propane/oxygen flames by in-situ optical techniques and sampling probes" 18th Symp. (int.) on Comb., Combustion Institute. pp.1127-1136

Prandtl L. (1925) "Bericht uber Untersuchungen zur aus-gebildeten Turbulenz", ZAMM 5, 136.

Ramachandran G.N., Lakshminarayanan A.V. (1971), "Three-Dimensional Reconstruction from Radigraphs and Electron Micrographs: Application of Convolutions instead of Fourier

Transforms" Prof. Nat. Acad. Sci. USA. Vol 68, No 9, pp.2236-2240.

Rodi W. (1972) "The prediction of free turbulent boundary layers by use of a two - equation model of turbulence", Ph.D. thesis, London University, England.

Sentfleben H., Benedict E. (1917). Ann. Phys. 54, p.65

Shepp L.A. and Logan B.F. (1974) "The Fourier Reconstuction of a Head Section". IEEE Transactions on Nuclear Science, Vol.Ns-21, June. pp.21-43

Siegel R., Howell J.R. (1981) "Thermal Radiation Heat Transfer. 2nd Ed", Hemisphere Publishing Co, Washington D.C.

Sivanathu Y.R., Faeth G.M. (1990) "Temperature soot volume fraction correlations in the fuel rich region of buoyant turbulent diffusion flames", Comb. Flame, Vol.81, No.2, pp.150-165

Smooke M.D., Mitchell R.E., Keyes D.E. (1989) "Numerical solution of two dimensional axisymmetric diffsion flames", Comb. Sci. Tech. 67, pp.85-122

Smyth K.C., Miller J.H.,Dorfman R.C., Mallard W.G., Santoro R.J. (1985) "Soot inception in a methane / air diffusion flame as characterised by detailed species profiles", Comb. Flame, 62, pp.157-181

Spalding D.B. (1971) "Concentration fluctuations in a round turbulent jet", Chem. Eng. Sci., 110, pp.173-181.

Spalding D.B. (1977) "GENMIX: A general computer program for two dimensional parabolic phenomenon.", Pergamon press.

Steward F.R. Cannon P. (1971) "The calculation of radiative heat flux in a cylindrical furnace using the Monte Carlo method", Int. Jour. Heat Mass Transf., Vol.14, pp.245-262

Stewart C.D., Moss J.B. (1989) "Soot formation in kerosine air diffusion flames", CIT internal report No. 2028/0163RAE(P)

Stewart C.D., Syed K.J., Moss J.B. (1991) "Modelling soot formation in non-premixed

kerosine-air flames", Comb. Sci. Tech., Vol. 75, pp.211-226

Syed K.J. (1990) "Soot and radiation modelling in buoyant fires", Cranfield Institute of Technology Ph.D thesis.

Syed K.J., Stewart C.D., Moss J.B. (1990), "Modelling soot formation and thermal radiation in buoyant turbulent diffusion flames" 23rd Symp. (Int.) on Comb., Combustion Institute. pp.1533-1541

Tait N.P., Greenhalgh D.A. (1990) "Cold flow parent fuel concentration in a Rolls Royce plc. phase 5 model combustor", Cranfield Inst. Tech. internal report.

Tait N.P., Greenhalgh D.A. (1992) "2D laser induced fluorescence imaging of parent fuel fraction in non-premixed combustion", 24th Symp. (Int.) on Comb., The Comb. Inst.

Tait N.P., Greenhalgh D.A. (1992a) "2D soot field measurements by laser induced incandescence", Opt. Meth. in Heat and Fluid Flow, Inst. Mech. Eng., pp.185-195

Tennekes H., Lumley J.L., (1972) "A first course in turbulence", MIT press.

Tesner P.A., Snegiriova T.D, Knorre V.G. (1971) "Kinetics of dispersed carbon formation", Comb. Flame., 17, pp.253-260.

Tien C.L., Lee S.C. (1982) "Flame radiation", Prog. Energy. Comb. Sci., 8, pp.41-59

Viskanta R., Menguc M.P. (1987) "Radiation heat transfer in combustion systems", Prog. Energy Combust. Sci., Vol.13, pp.97-160

Warnatz J. (1981) "The structure of laminar alkane-, alkene- and acetylene flames", 18th Symp. (Int.) on Comb., The Comb. Inst. pp.369-384.

Weast R.C. ed.(1973), 'Handbook of Chemistry and Physics', 54th edition, Chemical Rubber Co. Press.

Williams F.A. (1985) "Combustion Theory. 2nd ed.", The Benjamin Cummings Publishing Co.

Wood C.P., Samuelson G.S. (1985), "Optical Measurements of Soot Size and Number Density in a Swirl-Stabilized Combustor". Trans. ASME 38. Vol.107, Jan.

Young K.J. (1992) "Measurements in jet flames of ethylene and vapourised kerosine at elevated pressure",Cranfield Internal Report.

Young K.J., Stewart C.D., Syed K.J., Moss J.B. (1991) "Soot formation in confined turbulent jet flames fuelled by pre-vapourised kerosine and ethylene" 10th Int. Symp. on Air Breathing Engines, ISABE 91-7023, pp.239-248

APPENDIX A: RADIATION LOSS SOURCE TERM

The absorptivity of an aerosol of soot may be approximated by the following expression when the particles are in the Rayleigh regime:

$$K_{a_\lambda} = \frac{C f_v}{\lambda} \tag{A.1}$$

Under the assumption that the flame is in the optically thin / emission dominated regime of radiation, the radiative transfer equation may be written:

$$(\Omega \cdot \nabla) I_\lambda(r,\Omega) = K_{a_\lambda} I_{b_\lambda}(r) \tag{A.2}$$

Where $I_{b\lambda}$ is the Plank black body function:

$$I_{b_\lambda} = \frac{2 C_1}{\lambda^5 (\exp(C_2/\lambda T) - 1)} \tag{A.3}$$

and: $C_1 = 0.59544 \times 10^{-16} \mathrm{Wm}^2$, $C_2 = 1.4388 \times 10^{-2}$ mK (Siegel and Howell 1981).

Integrating the RTE over the entire spectrum yields the emitted power per unit solid angle per unit volume. For an elemental solid angle, $d\Omega$ and volume dV:

$$\dot{Q}_{rad} = -\int_0^\infty \frac{C f_v}{\lambda} \cdot \frac{2 C_1}{\lambda^5 (\exp(C_2/\lambda T) - 1)} d\lambda \tag{A.4}$$

Making the substitution, $\phi = C_2/\lambda T$ and rearranging:

$$\dot{Q}_{rad} = -\frac{2 C_1 C f_v T^5}{C_2^5} \int_\infty^0 \frac{\phi^4}{(\exp\phi - 1)} d\phi \tag{A.5}$$

From Abramowitz and Stegun 1964, the value of the integral is 124.4. Evaluating the constant and integrating over the solid angle of 4π steradians yields:

$$\dot{Q}_{rad} = -6.04\times10^{-4} C f_v T^5 \quad (W/m^3) \tag{A.6}$$

(cf. Hall 1988). Due to the good agreement that Hall 1988 achieved using the above expression with C = 4.9m^{-1}, this value is used here.

APPENDIX B: MIXTURE FRACTION MEASUREMENT WITH THE MASS SPECTROMETER.

At the beginning of the traverse the oxygen and sample flowrates were balanced. The mass spectrometer was switched to the 'histogram display' mode in which a histogram of concentration against mass number is plotted. A qualitative inspection of the relative concentrations of all species is possible.

With the probe positioned in the region of maximum mixture fraction (centreline for radial traverses, closest to burner for axial traverses), flowrates of sample and oxygen were finely adjusted such that there was always a small excess of oxygen. This guaranteed complete conversion of the carbon bearing species in the sample to CO_2 and, hence, assured the same at all other location in that traverse since the carbon concentration there would be lower.

The spectrometer was then switched to the '16 channel peak select' mode. In this mode a maximum of 16 mass numbers may be inspected with much greater accuracy than any other mode but at the expense of speed. Four channels were selected: 14 (N), 44 (CO_2), 00 (pressure), and 32 (O_2). The values of [14], [44] and [00] were logged during the traverse, the value of 32 was checked to ensure excess oxygen.

Once the traverse was complete, without exiting the '16 channel peak select' mode, the mass spectrometer was connected to a bottle of calibration gas. For the range of spectrometer pressures seen during the traverse the values of [00], [14] and [44] were again measured in order to calculate the calibration factor, K.

$$K = \frac{\left[\frac{N_2}{CO_2}\right]_{mass}^{calibration\ gas}}{\frac{[14]}{[44]}}$$

The value of $[N2/CO_2]_{mass}$ of the calibration gas used in the present study was 2.5327, corresponding to a kerosine / air mixture fraction of 0.0862.

For each measurement point in the traverse the value of K corresponding to the spectrometer chamber pressure at that point was calculated by linear interpolation of the calibration results.

Multiplication of K with the measured value of [14/44] then gave the absolute value of $[N_2/CO_2]_{mass}$ at that location. This was then substituted into eq.(3.4) to calculate mixture fraction.

APPENDIX C: OPERATION SCHEDULES FOR THE KEROSINE JET FLAME PRESSURE VESSEL

Power Up and Normal Operation Schedule

1 - Check kerosene cut off valve is closed.
2 - Check all flowmeter valves are closed.
3 - Pressurize all gas lines and the kerosene line.
4 - Turn on the evaporator cooling water.
5 - Turn on extractor fan.
6 - Arm the spark igniter electrics.
7 - Purge the pressure vessel with air for a few minutes (to ensure all residual gases have been expelled)
8 - Introduce a small flow of co-flow air.
9 - Introduce a small flow of purge ethylene through the main burner and ignite.
10 - Increase both the ethylene and co-flow air simultaneously until the air flow is at the required level for the test and the ethylene flame is a reasonably strong jet.
11 - Turn on the power to both the evaporator and burner electrical heaters.
12 - Establish the premixed pilot and, if necessary, probe cleaner flames.
13 - When the evaporator temperature has reached $\simeq$ 400°C and the pilot flame is stable open the kerosene cut-off valve and introduce kerosene.
14 - Once the flow of kerosene reaches the evaporator turn off the ethylene purge.
14 - Adjust flow rates, voltages and rig pressure until the stable operating condition has been achieved. Check again at regular intervals.

Power Down Schedule

1 - Turn off the kerosene flow at the flowmeter and the cut off valve and turn on the ethylene purge flow immediately, to prevent flame extinction.
2 - Turn off the power supply to both the evaporator and burner heater.
3 - Turn off the premix flames, stopping the oxygen supply first.
4 - Allow enough time for the evaporator and burner to cool to below 200°C then stop the purge ethylene flow and reduce the air flow rate to a small value.
5 - Depressurize all gas lines and the kerosene supply.
6 - Turn off the extractor and leave the rig to stand with the small air flow and cooling water flow.
7 - Turn cooling water and air flow off after a few hours.

APPENDIX D: PLUG FLOW ANALYSIS OF SOOT SOURCE TERMS

NUMBER

Considering the source of soot number density, eq.(5.14), ignoring oxidation. If plug flow is assumed, then streamlines and lines of constant mixture fraction are coincident. For a given value of mixture fraction, α and β are constant. Then:

$$N = \frac{n}{N_o} = \sqrt{\alpha/\beta}\tanh\left(\sqrt{\alpha\,\beta}\,t\right) \qquad \text{(D.1)}$$

When $t = 0$, $dN/dt = \alpha$ and $n = N_o\alpha t$ - ie. Initial linear growth.

$t \to \infty$, $dN/dt \to 0$ and $n = N_o\sqrt{(\alpha/\beta)}$ - ie. Saturated constant value.

In practice, the residence time, t, for the number density to reach its saturated limit is short and depends upon the magnitudes of α and β. The time for number to reach 95% if its saturated value may be estimated using the following relationship: $t_{95} = 1.83\sqrt{(\alpha/\beta)}$.

MASS

Consider eq.(5.15). Since, initially, soot mass and number are 0, the nucleation term dominates. Hence a linear initial growth region results:

$$f_v = \frac{1}{\rho_s}\delta\, t \qquad \text{(D.2)}$$

At longer residence times, the nucleation term will become less significant in relation to the surface growth term which depends upon soot number and volume fraction. The two different surface growth formulations - area and number dependent, eq.(5.15) - must be treated individually. For either formulation, there are two limiting regimes of soot mass growth which must be considered:

(i) The surface growth term dominates before the number density has saturated and is still in its linear growth rate regime.

(ii) The surface growth term dominates when the number density has saturated.

Undoubtedly, the second of these two limiting conditions will occur in all cases. However, situations may arise when the former is not realised.

The resulting values of plug flow soot volume fraction are shown in table A1 for both formulations of the mass formation rate equation in these two limiting cases.

TABLE A1

Source term formulation	Linear growth region of soot number, $n = N_o \alpha t$	Soot number saturated $n = N_o\sqrt{(\alpha/\beta)}$
Number dependent	$\frac{dm}{dt} = \gamma N_o \alpha t$ (D.3) $\rightarrow f_v = 2\gamma N_o \alpha t^2/\rho_s$	$\frac{dm}{dt} = \gamma N_o\sqrt{\alpha/\beta}$ (D.4) $\rightarrow f_v = \gamma N_o\sqrt{\alpha/\beta}\, t/\rho_s$
Area dependent	$\frac{dm}{dt} = \gamma (\alpha N_o t)^{1/3} m^{2/3}$ $\rightarrow f_v = (3\gamma/4)^3 \alpha N_o t^4/\rho_s$ (D.5)	$\frac{dm}{dt} = \gamma (N_o\sqrt{\alpha/\beta}) m^{1/3}$ (D.6) $\rightarrow f_v = \gamma^3 N_o\sqrt{\alpha/\beta}\, t^3/\rho_s$

APPENDIX E: OXIDATION SOOT SOURCE TERMS

MASS

Specific mass reduction rate of soot, ω_{ox} ($kgm^{-2}s^{-1}$) is defined by the oxidation mechanism.

$$\frac{dm}{dt} = \omega_{ox} \times \textit{surface area} \quad (\textit{per unit volume}) \tag{E.1}$$

For a monodisperse aerosol of spherical soot particles:

$$\textit{surface area} = n\pi D^2 = N_o^{1/3} m^{2/3} N^{1/3} \sqrt[3]{\frac{36\pi}{\rho_s^2}} \tag{E.2}$$

and hence:

$$\frac{dm}{dt} = N_o^{1/3} \omega_{ox} \epsilon m^{2/3} N^{1/3} \tag{E.3}$$

where $\epsilon = \sqrt{(36\pi/\rho_s^2)}$

NUMBER

We have the rate of reduction of mass from equation E.3. Substituting the value soot volume fraction, m, with its expansion yields:

$$\frac{d}{dt}\left[\rho_s \cdot \frac{1}{6} n\pi D^3\right] = \frac{1}{6}\rho_s \pi D^3 \frac{dn}{dt} \tag{E.4}$$

Then:

$$\begin{aligned} \frac{m}{N}\frac{dN}{dt} &= N_o^{1/3} \epsilon \dot{\omega}_{ox} m^{2/3} N^{1/3} \\ \rightarrow \quad \frac{dN}{dt} &= N_o \epsilon \dot{\omega}_{ox} m^{-1/3} N^{4/3} \end{aligned} \tag{E.5}$$

The approximation, implicit in equation E.4 is that the particles removed by oxidation are of the mean size and hence, $dD^3/dt = 0$. This has no fundamental basis since in reality the removal of particles by oxidation will be a cascade process in which particles become progressively smaller until they are completely destroyed. However, no better approximation of this term is possible in this simplified model of a very complex process.

APPENDIX F: THE EFFECTS OF SOLID CARBON ON FLAME SHEET CHEMISTRY

For the kerosine air system, the general flamesheet reaction which includes the effects of solid carbon may be written:

$$C_{12}H_{24} + X(0.21O_2 + 0.79N_2) \rightarrow YC_s + aCO_2 + bC_{12}H_{24} + cO_2 + dH_2O + 0.79XN_2 \quad \text{(F.1)}$$

Carbon balance

$$(12 - Y) = a + 12b \quad \text{(F.2)}$$

Oxygen balance

$$0.42X = 2a + 2c + d \quad \text{(F.3)}$$

Hydrogen balance

$$12 = 12b + d \quad \text{(F.4)}$$

Mixture fraction based upon the original mixture:

$$\xi = 5.8252/X \quad \text{(F.5)}$$

The mass fraction of fuel in the solid phase, Fc

$$F_c = y/12 \quad \text{(F.6)}$$

For a stoichiometric mixture, b = c = 0.
Hence

$$X_{stoi} = \frac{18 - Y}{0.21} \quad \text{(F.7)}$$

If the mixture is rich: c = 0
Hence

$$
\begin{aligned}
a &= 7X/50 - Y/3 \\
b &= 1 - Y/18 - 7X/600 \\
d &= 7X/50 + 2Y/3
\end{aligned}
\qquad \text{(F.8)}
$$

If the mixture is lean: b = 0
Hence

$$
\begin{aligned}
a &= 12 - Y \\
c &= 0.21X - 18 + Y \\
d &= 12
\end{aligned}
\qquad \text{(F.9)}
$$

The adiabatic temperature at any mixture fraction is then calculated by equating reactant and product enthalpies.